BIODEGRADABLE HYDROGELS AND CRYOGELS FOR BIOMEDICAL APPLICATIONS, IN PARTICULAR BONE TISSUE ENGINEERING

by

Melek Naz Güven

B.S., Chemistry, Boğaziçi University, 2014

M.S., Chemistry, Boğaziçi University, 2016

Submitted to the Institute for Graduate Studies in

Science and Engineering in partial fulfillment of

the requirements for the degree of

Doctor of Philosophy

Graduate Program in Chemistry

Boğaziçi University

2023

ACKNOWLEDGEMENTS

When I first saw Boğaziçi University, it was in May 2006 during a university trip we took with our high school class. Like everyone else, I was impressed by the beauty of the south campus and the magnificent view, but choosing Boğaziçi was not on my mind at that time. In fact, I had no idea about what I would choose. However, through a series of coincidences, I ended up being settled to the Boğaziçi University Chemistry Department. When I started the department, I had no clue about what I would do in the future until I had the opportunity to intern at Prof. Avcı's lab. during my 3rd year. This choice I made in my 3rd year is the biggest reason why I am writing this thesis today.

I would like to express my gratitude to my thesis advisor Prof. Dr. Duygu Avcı Semiz, for providing me with this opportunity and for always encouraging my interest in research. Throughout all these years, I am thankful for her guidance and support. From her, I have learned not only the importance of conducting ethical and accurate research but also how to embody the qualities of an educator. I hope to carry all the knowledge I have gained from her with me throughout the rest of my career and keep it with me throughout my life.

I would like to extend my gratitude to Prof. Dr. Funda Havva Yağcı Acar for our valuable collaboration since the master's process and for her contributions and the recommendation to all the work we have undertaken together. I also want to extend my thanks to my examining committee Assoc. Prof. Ali Ersin Acar, Assist. Prof. Sesil Çınar and Assist. Prof. Fırat İlker for their constructive review of the final manuscript of the thesis.

I would also wish to express my thanks to Prof. Oğuz Okay for his valuable discussions and recommendations regarding my research, to Assist. Prof. Ümit Gülyüz for his help in uniaxial compression measurements and to Gözde Demirci for her contribution in all cytotoxicity and cell studies.

One of the things I have learned throughout all these years is the importance of our colleagues in the laboratory with whom we worked together. In this regard, I have always been fortunate, and I would like to express my heartfelt thanks to my current and former lab colleagues, Ece, Seçkin, Türkan, Betül, Tuğçe, Burcu, Neslihan, Simay and Miraç for their genuine friendship and the support we shared during both joyful and challenging times.

I would like to express my gratitude to Boğaziçi University for showing me the possibility of a free and just world. I know that what I have gained from this university is much more than diplomas and titles. This place, where I spent the most beautiful days of my life, has enriched me with a unique culture that will stay with me throughout my life, along with friendships that will last a lifetime. Additionally, I would like to convey my thanks to the entire Chemistry Department. This place, where I spent more than ten years, has become a second home to me, and I sincerely thank everyone who contributed in any way.

I would like to acknowledge The Scientific and Technological Research Council of Turkey (TÜBİTAK) for financial support for research and scientific activities through TÜBİTAK 1001 project (117Z330).

Last but not least, I would like to express my deepest gratitude to my family. Throughout this entire journey, they have stood behind me with unwavering support and encouragement in every decision I made. To my mother Asuman, my father Ömer, my sisters Şirin Nur and Elif Su and my brother-in-law Emre thank you for always being there for me. This thesis is dedicated to my beloved nephews, Emir and Mirza, who have shown me the capacity to love any living being so deeply in my heart.

ABSTRACT

BIODEGRADABLE HYDROGELS AND CRYOGELS FOR BIOMEDICAL APPLICATIONS, IN PARTICULAR BONE TISSUE ENGINEERING

This work consists of synthesis, characterization and evaluation of bisphosphonate, bisphosphonic acid or carboxylic acid functionalized polymers, macromers and their crosslinked network hydrogels and cryogels for various biomedical applications in particular bone tissue engineering. In the first project, poly(amido amine) (PAA) macromers functionalized using sodium alendronate, and their cryogels were synthesized and the effects of the macromer structure as well as bisphosphonic acid content on the cryogel properties such as swelling, degradation, mineralization, and mechanical properties were investigated. In the second project, novel PAA polymers and macromers functionalized using tetraethyl vinylidene bisphosphonate were synthesized. The polymers' rheological properties were investigated in the context of their interaction with cations such as Ca^{2+} and Fe^{3+}. Subsequently, both bisphosphonate-functionalized and control macromers were copolymerized with HEMA to prepare hydrogels. The swelling, degradation, mechanical, biocompatibility, cell adhesion and biomineralization characteristics of these hydrogels were thoroughly examined to assess their suitability for potential applications in tissue engineering and the effect of bisphosphonate functionalization. The third section reports the synthesis of four novel highly water soluble, carboxylated diacrylate and diacrylamide macromeric crosslinkers based on meso-2,3-dimercaptosuccinic acid and their hydrogels with 2-hydroxyethyl methacrylate. The study is focused on examining how macromer structure and amounts enable control of the swelling, degradation, mechanical properties, and metal adsorption capabilities of the hydrogels. In the last part, phosphate functionalized double network hydrogels were prepared using dual curing method, an aza-Michael reaction of 1,4-butanediamine with poly(ethylene glycol) diacrylate or N,N'-methylene bisacrylamide followed by radical photopolymerization of 10-methacryloyloxydecyl dihydrogen phosphate, and their potential use for tissue engineering applications were investigated.

ÖZET

BAŞTA KEMİK DOKU MÜHENDİSLİĞİ OLMAK ÜZERE BİYOMEDİKAL UYGULAMALAR İÇİN BİYOBOZUNUR HİDROJELLER VE KRİYOJELLER

Bu çalışma, başta kemik doku mühendisliği olmak üzere çeşitli biyomedikal uygulamalar için bisfosfonat, bisfosfonik asit veya karboksilik asit fonksiyonlu polimerlerin, makromerlerin ve bunların çapraz bağlı hidrojelleri ve kriyojellerinin sentezini, karakterizasyonunu ve değerlendirmesini içermektedir. İlk proje kapsamında sodyum alendronat kullanılarak fonksiyonlandırılmış poli(amido amin) (PAA) makromerler ve onların kriyojelleri sentezlenmiş ve makromer yapısı ile bisfosfonik asit içeriğinin kriyojellerin şişme, bozunma, mineralizasyon ve mekanik özellikleri üzerindeki etkileri incelenmiştir. İkinci proje kapsamında, tetraetil viniliden bisfosfonat kullanılarak fonksiyonlandırılmış yeni PAA polimerler ve makromerler sentezlenmiştir. Polimerlerin reolojik özellikleri, Ca^{2+} ve Fe^{3+} gibi katyonlarla etkileşimleri bağlamında incelenmiştir. Daha sonra, bisfosfonat fonksiyonlandırılmış ve kontrol makromerleri HEMA ile kopolimerleştirilerek hidrojeller hazırlanmıştır. Bu hidrojellerin şişme, bozunma, mekanik, biyouyumluluk, hücre yapışma ve biyomineralizasyon özellikleri, doku mühendisliği potansiyel uygulamaları için uygunluklarının ve bisfosfonat fonksiyonlandırılmasının etkisinin değerlendirilmeleri amacıyla detaylı bir şekilde incelenmiştir. Üçüncü bölümde meso-2,3-dimerkaptosüksinik asit temelli yüksek su çözünürlüklü, dört yeni karboksillenmiş diakrilat ve diakrilamid makromerik çapraz bağlayıcıların sentezi ve onların 2-hidroksietil metakrilat ile hidrojelleri raporlanmıştır. Bu çalışma, makromer yapısı ve miktarlarının hidrojel şişme, bozunma, mekanik özellikler ve metal adsorpsiyon yeteneklerini kontrol etmeyi nasıl mümkün kıldıldığının incelenmesine odaklanmıştır. Son bölümde fosfat fonksiyonlu çift ağlı hidrojeller ikili kürleme, 1,4-bütandiamin ile poli(etilen glikol) diakrilat veya N,N'-metilen bisakrilamid aza-Michael reaksiyonu ve takiben 10-metakriloiloksidesil dihidrojen fosfatın radikal fotopolimerizasyonu, yöntemleri ile gerçekleştirilmiş ve doku mühendisliği uygulamalarındaki potansiyel kullanımları incelenmiştir.

TABLE OF CONTENTS

ACKNOWLEDGEMENTS iii

ABSTRACT v

ÖZET vi

TABLE OF CONTENTS vii

LIST OF FIGURES xiii

LIST OF TABLES xxii

LIST OF SYMBOLS xxiii

LIST OF ACRONYMS/ABBREVIATIONS xxiv

1. INTRODUCTION 1

1.1. Biomaterials From Past to Present 1

1.1.1. Biodegradable Polymers Used as Biomaterials 3

1.2. Poly(amido amine)s as Biodegradable Polymers 8

1.2.1. Synthesis of PAAs 8

1.2.2. PAA Hydrogels in Tissue Engineering Applications 10

1.2.3. PAA Hydrogels in Gene Delivery Applications 11

1.3. Stimuli Responsive Hydrogels as Smart Biomaterials 14

1.3.1. Synthesis of Hydrogels 17

1.3.2. Temperature Responsive Hydrogels 19

1.3.3. pH- Responsive Hydrogels 20

1.4. Important Functional Groups for Biomaterials 22

1.4.1. Phosphorous Containing Materials 22

1.4.2. BPs for Bone Tissue Engineering 25

1.4.3. BPs for Drug Delivery Applications 29

2. OBJECTIVES AND SCOPE 31

3. ALENDRONATE-FUNCTIONALIZED POLY(AMIDO AMINE) CRYOGELS FOR BIOMEDICAL APPLICATIONS 32

3.1. Introduction 32

3.2. Experimental 33

3.2.1. Materials and Methods 33

3.2.2. Synthesis of PAA Macromers 34

3.2.3. pH Titration 35

3.2.4. Preparation of Cryogels 35

3.2.5. Swelling Studies 35

3.2.6. Degradation Studies 36

3.2.7. *In vitro* Mineralization 36

3.2.8. Mechanical Studies 37

3.2.9. *In vitro* Cytotoxicity Assay 38

3.2.10. Statistical Analysis 38

3.3. Results and Discussion 39

3.3.1. Synthesis and Characterization of PAA Macromers 39

3.3.2. Synthesis and Properties of Cryogels 44

3.3.3. Swelling of Networks 46

3.3.4. Degradation Studies 47

3.3.5. Mineralization of Cryogels 48

3.3.6. Mechanical Properties 51

3.3.7. *In vitro* Cytotoxicity of Cryogel Degradation Products 56

3.4. Conclusions 57

4. BISPHOSPHONATE-FUNCTIONALIZED POLY(AMIDO AMINE) POLYMERS, MACROMERS AND THEIR 2-HYDROXYETHYL METHACRYLATE HYDROGELS AS TISSUE ENGINEERING SCAFFOLDS 59

4.1. Introduction 59

4.2. Experimental 60

4.2.1. Materials and Methods 60

4.2.2. Synthesis of PAA Polymers (PAA1, PAA2 and PAA3) 62

4.2.3. Rheological Characterizations of Linear PAAs 63

4.2.4. Synthesis of PAA Macromers (PAA-NHBoc, PAA-NH_2 and PAA-BP) 63

4.2.5. Acid-Base Titration 64

4.2.6. Hydrogel Preparation 64

4.2.7. Swelling Studies 65

4.2.8. Degradation Studies 65

4.2.9. Water Contact Angle Measurements 66

4.2.10. Mineralization of the Hydrogels 66

4.2.11. Mechanical Studies 66

4.2.12. *In vitro* Cytotoxicity Assay 67

4.2.13. Cell Attachment Experiment 68

4.3. Results and Discussion 68

4.3.1. Synthesis and Characterization of Linear PAAs 68

4.3.2. Rheological Characterizations of Linear Polymers 72

4.3.3. Synthesis and Characterization of PAA Macromers 74

4.3.4. Synthesis and Characterization of Hydrogels 79

4.3.5. Swelling, Degradation and Wettability Behaviour 80

4.3.6. Mineralization of Hydrogels 83

4.3.7. Mechanical Properties 86

4.3.8. *In vitro* Cytotoxicity of Hydrogel Degradation Products 87

4.3.9. Cell Interaction Studies 87

4.4. Conclusions 89

5. MESO-2,3-DIMERCAPTOSUCCINIC ACID-BASED MACROMERS FOR PH-SENSITIVE DEGRADABLE HYDROGELS 91

5.1. Introduction 91

5.2. Experimental 93

5.2.1. Materials and Methods 93

5.2.2. Synthesis of Macromers 94

5.2.3. Photopolymerization Studies 95

5.2.4. Synthesis of Hydrogels 96

5.2.5. Swelling Studies 97

5.2.6. Degradation Studies 97

5.2.7. Determination of Fe^{3+} Adsorption of Hydrogels 97

5.2.8. Mechanical Studies 98

5.2.9. *In vitro* Cytotoxicity Assay 99

5.3. Results and Discussion 100

5.3.1. Synthesis and Characterization of Macromers 100

5.3.2. Photopolymerization of Macromers 104

5.3.3. Synthesis and Characterization of Hydrogels 107

5.3.4. Complexing Capacities with Fe^{3+} Ion 112

5.3.5. Mechanical Properties 113

5.3.6. *In vitro* Cytotoxicity of Macromers 114

5.4. Conclusion 115

6. PHOSPHATE-FUNCTIONALIZED INTERPENATRATING NETWORK HYDROGELS FOR TISSUE ENGINEERING APPLICATIONS 117

6.1. Introduction 117

6.2. Experimental 118

6.2.1. Materials and Methods 118

6.2.2. Hydrogel Preparation 119

6.2.3. Swelling Studies 119

6.2.4. Degradation Studies 120

6.2.5. Mechanical Studies 120

6.2.6. Mineralization of Hydrogels 121

6.3. Results and Discussion 121

6.3.1. Synthesis and Characterization of Hydrogels 121

6.3.2. Swelling and Degradation Studies 124

6.3.3. Mechanical Properties of Hydrogels 126

6.3.4. Mineralization of Hydrogels 127

6.4. Conclusion 132

7. CONCLUDING REMARKS 133

REFERENCES 136

APPENDIX A: SUPPLEMENTARY DATA 159

APPENDIX B: COPY RIGHT LICENCES 162

LIST OF FIGURES

Figure 1.1. Timeline of some key milestones in biomaterials. Reprinted from [6]. 2

Figure 1.2. Number of studies in years 2000 and 2020 for selected keywords. Reprinted from [6]. 3

Figure 1.3. Classification of biodegradable polymers. Reprinted from [16]. 5

Figure 1.4. Degradation sequence of bulk and surface degraded polymers. 8

Figure 1.5. Synthesis of PAAs. 9

Figure 1.6. Structure of RGD-mimicing PAA hydrogel and the cellular morphology. Reprinted from [40]. 11

Figure 1.7. Gene delivery mechanism for non-viral vectors of cationic polymers. Reprinted from [41]. 13

Figure 1.8. (Bis)phosphonic acid-functionalized poly(ethyleneimine) poly(amido amine)s for in vitro transfection. Reprinted from [50]. 14

Figure 1.9. Structural changes of a hydrogel based on environmental stimuli. Reprinted from [57]. 16

Figure 1.10. Classification of hydrogels based on the different characteristics. Reprinted from [61]. 17

Figure 1.11. Synthesis of interpenetrating network (IPN) and semi-interpenetrating network (SIPN) hydrogels. Reprinted from [68]. 18

Figure 1.12. Temperature responsive hydrogels transforming from sol to gel, from gel to sol when temperature drops below LCST, at LCST, and above LCST. Reprinted from [81]. 20

Figure 1.13. Schematic representation of a general behavior of pH-responsive hydrogel. Reprinted from [86]. 21

Figure 1.14. Adsorption mechanism of polymer. Reprinted from [96]. 24

Figure 1.15. Structure of pyrophosphate and bisphosphonate. 24

Figure 1.16. Some application areas of bisphosphonates. Reprinted from [105]. 26

Figure 1.17. Different strategies for incorporating BPs in scaffolds. Reprinted from [102]. 27

Figure 1.18. Bisphosphonated hyaluronan and calcium phosphate nanoparticles, hybrid HABP.CaP nanocomposite and its self-healing property. Reprinted from [116]. 29

Figure 1.19. Examples of bisphosphonate–drug conjugates for bone targeting. Reprinted from [105]. 30

Figure 3.1. Synthesis of PAA macromers. 39

Figure 3.2. ^{1}H NMR spectra of sodium alendronate, 5-amino-1-pentanol and MPAA1 macromer. 41

Figure 3.3. ^{1}H NMR spectra of MPAAc and MPAA2 macromers. 42

Figure 3.4. The integrated ^{1}H NMR spectrum of MPAA1. 42

Figure 3.5. FTIR spectra of MPAAc, MPAA1, MPAA2 macromers. 43

Figure 3.6. A) pH-responsive titration curves of MPAA1, MPAA2 and MPAAc in aqueous solutions and B) structures of alendronate units in macromers at different pH. 44

Figure 3.7. SEM images of A) PAAc, B) PAA1 and C) PAA2 cryogels. 45

Figure 3.8. Swelling percentages of PAA cryogels in water, buffer solutions (pH 9.0, 7.4, 6.0, 2.0) and $CaCl_2$ (0.5 M) after 24 h. All the experiments

were carried out in triplicates (n=3) and mean average values with standard error (±SD) are represented in the error bars. 47

Figure 3.9. A) Degradation behaviour of cryogels in PBS (pH 7.4) at 37 °C, B) SEM images of PAA1 cryogel before and C) after 4 w degradation. 48

Figure 3.10. A) TGA thermograms of PAA2 (before and after mineralization in 5xSBF) and PAAc (before mineralization) cryogels, B) XRD patterns of mineralized PAA2 and PAAc cryogels at 2 days in 5xSBF, C) FTIR spectra of PAA2 (before and after mineralization in 5xSBF and SBF) and PAAc (in 5xSBF) cryogels. 50

Figure 3.11. SEM images of A) PAA1 cryogel before mineralization, B) PAA1 cryogel after 4 weeks of mineralization in SBF, C) PAA2 cryogels after 2 days of mineralization in 5xSBF, D) PAAc cryogel after 2 days of mineralization in 5xSBF. 51

Figure 3.12. Stress – strain curves A) and the mechanical parameters E and σ_f A) of PAAc, PAA1, and PAA2 cryogels swollen in water. The inset in A) is zoom in to the data below 50 % strain to highlight the initial mechanical properties. 52

Figure 3.13. Stress – strain curves (A, B) and the mechanical parameters E and σ_f (C, D) of PAAc, PAA1, and PAA2 cryogels in dry (A, C) and swollen states (B, D). The inset in (A) and (B) are zoom in to the data below 50 % strain. 53

Figure 3.14. Stress – strain curves A) and the mechanical parameters E and σ_f B) of PAAc, PAA1, and PAA2 cryogels before and after mineralization in SBF and 5xSBF. 54

Figure 3.15. Stress – strain curves A) and the mechanical parameters E and σ_f B) of PAAc, PAA1, and PAA2 cryogels before and after immersion in aqueous $CaCl_2$ solution. 55

Figure 3.16. Viability of U-2 OS, Saos-2 and C2C12 cell lines treated with alendronate and degradation products of PAAc, PAA1 and PAA2 for 48 h. Viability was tested with MTT assay. Statistical significance: (*) p<0.0332, (**) p<0.021, (***) p<0.0002, (****) p<0.0001. 57

Figure 4.1. Synthesis of linear polymers PAA1, PAA2 and PAA3..... 69

Figure 4.2. ^{1}H NMR spectra of PAA1 and PAA2. 70

Figure 4.3. Synthesis of linear polymers PAA4, PAA5, PAA6 and PAA7..... 71

Figure 4.4. ^{1}H NMR spectra of PAA6 and PAA7. 72

Figure 4.5. A) The viscosities of the solutions of PAA1 at concentrations of 5%, 10%, and 22.5%. B) The viscosities of the solutions of PAA1, PAA2, and PAA3 polymers at a concentration of 10%. C) The viscosity of the solution of PAA2 and PAA2 in $CaCl_2$. D) The viscosity of the solution of PAA3 and PAA3 in $CaCl_2$. 733

Figure 4.6. Synthesis of poly(amido amine) macromer with BP side chains. 75

Figure 4.7. ^{1}H NMR spectra of products of each reaction step during synthesis of PAA-BP. 77

Figure 4.8. ^{13}C NMR spectra of PAA-NH_2 and PAA-BP macromers. 78

Figure 4.9. A) FTIR spectra and B) acid-base titration curves of PAA-NH_2 and PAA-BP macromers. 78

Figure 4.10. DSC profiles of PAA-NH_2 and PAA-BP. 79

Figure 4.11. The preparation of H: PAA-BP and its biomineralization in 5xSBF. 79

Figure 4.12. SEM images showing pore sizes of A) H:PAA-NH_2 and B) H:PAA-BP. 80

Figure 4.13. A) SEM image of H:PAA-BP, B) equilibrium swelling ratio (%) of hydrogels in water, various buffer and $CaCl_2$ solutions, C)

degradation (%) of hydrogels in PBS (pH 7.4) solution at 37 °C and D) water contact angles of the hydrogels. 82

Figure 4.14. FTIR spectra of hydrogels A) before and B) after mineralization in in 5xSBF. 84

Figure 4.15. SEM images and EDX spectra (inset) of hydrogels A) H:PAA-BP and B) H:PAA-NH_2, mineralized by immersion in 5xSBF. 85

Figure 4.16. A) XRD spectra for hydrogels H:PAA-BP and H:PAA-NH_2 before and after mineralization in 5xSBF, B) TGA thermograms of H:PAA-BP, before and after mineralization, and H:PAA-NH_2 after mineralization, in 5xSBF. 86

Figure 4.17. Stress – strain curves A) and Young's modulus E B) of H:PAA-NH_2 and H:PAA-BP before and after mineralization in 5xSBF. 87

Figure 4.18. Viability of Saos-2, U-2 OS, NIH 3T3 and C2C12 cell lines treated with degradation products of H:PAA-NH_2 and H:PAA-BP for 48 hours. Statistics were conducted by using an ordinary one-way ANOVA analysis of variance followed by multiple Dunnett's comparison test of GraphPad Prism 8 software. Data were presented as mean ± SD of independent experiments (n = 6 for Saos-2, U-2 OS and C2C12 cells, n = 4 for NIH 3T3 cells). $p < 0.05$ was accepted as a statistically significant difference. $p < 0.0332$(*) and $p < 0.0021$(**). Dashed lines show the 80% and 50% viability. 88

Figure 4.19. Attachment and spread of C2C12 myoblast muscle cells on the mineralized H-PAA-BP gel after 20 hours of incubation. Blue: Nuclear DAPI stain; Green: Phalloidin cytoskeleton stain. Filters: DAPI filter and FITC filter. Magnification: 10X. Scale: 200 µm. 89

Figure 5.1. Design of functional hydrogels. 93

Figure 5.2. Synthesis of macromers. 101

Figure 5.3. ^{1}H NMR spectra of PEG-DMSA/Na and MBA-DMSA/Na. 102

Figure 5.4. ^{13}C NMR spectrum of PEG-DMSA/Na. 102

Figure 5.5. ^{1}H NMR of MBA-DMSA/TEA and PEG-DMSA/TEA. 103

Figure 5.6. A) FTIR spectra of all macromers and B) Raman spectrum of PEG-DMSA/Na. 104

Figure 5.7. Rate–time and conversion–time plots for HEMA containing macromers (1 and 4 mol%). Photopolymerizations were carried out using Irgacure 2959 (2 wt%) under UV-vis light (320–500 nm) irradiation at 25 °C under nitrogen. 106

Figure 5.8. Rate–time and conversion–time plots for PEGDA containing macromers (1 and 4 mol%). Photopolymerizations were carried out using Irgacure 2959 (2 wt%) under UV-vis light (320–500 nm) irradiation at 25 °C under nitrogen. 106

Figure 5.9. FTIR spectra of all hydrogels. 107

Figure 5.10. A) swelling ratios of the hydrogels, B) swelling ratios of PEG-DMSA/Na homogels, C) swelling– shrinking behavior of H:PEG-DMSA/Na. 109

Figure 5.11. A) SEM image of H:PEG-DMSA/Na B) SEM image, C) EDX spectrum of H:PEG-DMSA/Na after swelling in 0.5 M $FeCl_3$ solution for 24 h. 110

Figure 5.12. A) Degradation of HEMA hydrogels, SEM images of H:PEG-DMSA/TEA B) before degradation, C) after degradation in PBS (magnification x1000). 111

Figure 5.13. Fe^{3+} adsorption capacities of hydrogels 112

Figure 5.14. A) Young's moduli E of the gels swollen in different solutions B) Stress – strain curves of hydrogels swollen in EtOH (solid curves) and $FeCl_3$ (dashed curves). 114

Figure 5.15. Viability of U-2 OS and C2C12 cell lines treated with macromers for 24 hours. Dashed lines show the 50 and 80% viabilities. Data were presented as mean ± SD of independent experiments (n = 5). $p < 0.0332$ (*), $p < 0.0021$ (**), $p < 0.0002$ (***). 115

Figure 6.1. Hydrogel preparation. 122

Figure 6.2. FTIR spectra of MDP and MDP containing hydrogels. 123

Figure 6.3. SEM images of A) PEGDA-MDP, B) MBA-MDP and C) EDX image of MBA-MDP hydrogels. 123

Figure 6.4. Swelling capacities of hydrogels. 125

Figure 6.5. Degradation (%) of hydrogels. 126

Figure 6.6. A) Stress – strain curves of hydrogels swollen in 0.5 M $CaCl_2$ (solid curves) and H_2O (dashed curves), The inset shows MBA-MDP hydrogel after being kept in H_2O and $CaCl_2$ solution, B) Young's moduli E of the hydrogels. 127

Figure 6.7. FTIR spectra of PEGDA-MDP and PEGDA-control hydrogels before and after mineralization. 128

Figure 6.8. FTIR spectra of MBA-MDP and MBA-control hydrogels before and after mineralization. 129

Figure 6.9. SEM images of PEG-MDP hydrogels A) after mineralization in 5xSBF, B) first immersing in $CaCl_2$ then mineralization in 5xSBF, C) EDX result of PEGDA-MDP-$CaCl_2$-5xSBF and MBA-MDP hydrogels D) after mineralization in 5xSBF, E) first immersing in

$CaCl_2$ then mineralization in 5xSBF, F) EDX result of MBA-MDP-$CaCl_2$-5xSBF 130

Figure 6.10. XRD spectra of mineralized hydrogels. 131

Figure A.1. ^1H NMR of PAA3 159

Figure A.2. FTIR spectrum of PAA2 159

Figure A.3. FTIR spectrum of PAA3 160

Figure A.4. FTIR spectra of PAA5, PAA6 and PAA7 160

Figure A.5. A) The viscosities of the solutions of PAA5, PAA6, and PAA7 polymers at a concentration of 10%. B) The viscosities of the original form of PAA5 and its solutions at pH 2. C) The viscosities of the solutions of PAA6 and PAA6 in $CaCl_2$ and $FeCl_3$. D) The viscosities of the solutions of PAA7 and PAA7 in $CaCl_2$ and $FeCl_3$ 161

Figure B.1. Permission from [6] Elsevier, Copyright (2013). 162

Figure B.2. Permission from [16] John Wiley and Sons, Copyright (2014). 162

Figure B.3. Permission from [40] Acta Materialia by Elsevier, Copyright (2013). . 163

Figure B.4. Permission from [41] Taylor & Francis Group, Copyright (2023). 163

Figure B.5. Permission from [50] American Chemical Society, Copyright (2021). 164

Figure B.6. Permission from [57] Royal Society of Chemistry, Copyright (2022). 164

Figure B.7. Permission from [61] IntechOpen, Copyright (2016). 165

Figure B.8. Permission from [68] Elsevier, Copyright (2020). 165

Figure B.9. Permission from [81] Elsevier, Copyright (2021). 166

Figure B.10. Permission from [86] MDPI, Copyright (2021). 166

Figure B.11. Permission from [96] Elsevier, Copyright (2021). 167

Figure B.12. Permission from [102] Mary Ann Liebert, Copyright (2012). 167

Figure B.13. Permission from [105] Elsevier, Copyright (2013). 168

Figure B.14. Permission from [116] Elsevier, Copyright (2014). 168

LIST OF TABLES

Table 3.1. Feed compositions during macromer synthesis, number average molecular weights (M_n) and and T_g of the macromers……..40

LIST OF SYMBOLS

λ	Compressive ratio
σ_f	Compressive strength
σ_{nom}	Compressive stress
ε	Extinction coefficient
E	Young's modulus
M_n	Number average molecular weight
pH	Power of hydrogen
pKa	Acid dissociation constant
pK_b	Base dissociation constant
Q	Degree of swelling
Rp	Rate of polymerization
T_g	Glass transition temperature

LIST OF ACRONYMS/ABBREVIATIONS

ABG	4-aminobutylguanidine
ALE	Alendronate
AP	5-amino-1-pentanol
BMP	Bone morphogenetic protein
BP	Bisphosphonate
BTE	Bone tissue engineering
CaP	Calcium phosphate
DAPI	4′,6-diamidino-2-phenylindole
DBC	Double bond conversion
DCM	Dichloromethane
DMEM	Dulbecco's modified eagle medium
DMSA	2,3-Dimercapto succinic acid
DMSO	Dimethyl sulfoxide
DNA	Deoxyribonucleic acid
DSC	Differential scanning calorimetry
DTT	Dithiothreitol
EDX	Energy-dispersive X-ray spectroscopy
EPR	Enhanced permeability and retention
FBS	Fetal bovine serum
FITC	Fluorescein isothiocyanate
FT-IR	Fourier transform infrared spectroscopy

GPC	Gel permeation chromatography
GSH	Glutathione
HAP	Hydroxyapatite
HEMA	2-Hydroxyethyl methacrylate
Irgacure 2959	2-Hydroxy-4′-(2-hydroxyethoxy)-2-methylpropiophenone
LCST	Lower critical solution temperature
LRP	Living radical polymerization
MBA	Methylene bisacrylamide
MDP	10-Methacryloyloxydecyl dihydrogen phosphate
MTT	Thiazolyl blue tetrazolium bromide
NIH 3T3	Mouse embryonic fibroblast cells
NMR	Nuclear magnetic resonance spectroscopy
PAA	Poly(amido amine)
PBAE	Poly(β-amino ester)
PBS	Phosphate buffered saline
PDI	Polydispersity index
PEG	Poly(ethylene) glycol
PEGDA	Poly(ethylene glycol) diacrylate
PEI	Polyethylene imine
RGD	Arginylglycylaspartic acid peptide
RPMI	Roswell Park Memorial Institute
Saos-2	Human osteogenic sarcoma cells
SBF	Simulated body fluid

SEC	Size exclusion chromatography
SEM	Scanning electron microscope
TEA	Triethylamine
TFA	Trifluoroacetic acid
TGA	Thermogravimetric analysis
THF	Tetrahydrofuran
TMS	Tetramethylsilane
TMSBr	Trimethylsilyl bromide
UV	Ultraviolet
U-2 OS	Human bone osteosarcoma epithelial cells
XRD	X-ray diffraction

1. INTRODUCTION

1.1. Biomaterials From Past to Present

The word “biomaterial”, which is an extremely common word today, was not used until 80 years ago, but it is known that the history of biomaterials dates back to ancient civilizations [1]. For example, it has been determined that biomaterials were used as parts such as artificial nose, ears, eyes, and teeth in Egyptian mummies. Since ancient times, it has been known that natural biomaterials such as glue and rubber, as well as materials such as iron, gold, silver and glass are used in defective or missing parts of the body. These raw biomaterials have been tried in many different areas such as dental implants, artificial organs, contact lenses and prostheses, but they have generally not been successful due to deficiencies such as biocompatibility, toxicity and sterilization. With today’s developing technology, biomaterials have become indispensable for humanity [2].

Broadly, biomaterials can be defined as natural or synthetic materials that are used to direct, supplement, or replace the functions of living tissues [3]. In order for biomaterials to be usable, they must be accepted by the body and also have some properties such as being non-toxic, non-carcinogenic and chemically inert. In addition, long-term usability, high corrosion and wear resistance and mechanical strength are other properties that most biomaterials should have according to their usage areas. Biocompatibility can be considered as a complementary definition with biomaterials to define biological performance of materials and it is defined as the ability of a material to perform the desired functions with an appropriate host response in a specific application. In other words, it refers to the compatibility of the biomaterial with living systems, i.e. is its ability to be in contact with the tissues of the human body without harming the body. It is associated not only with toxicity, but with all the possible negative effects of a material in a biological system [4].

In the recent past, especially during and after the second world war, the concept of biomaterials came to the forefront as a result of developing medical and surgical technology. In the 1950s, the first vascular prosthesis was performed by using vessels made of synthetic fabrics to replace some parts of the aorta. At the same time, the first pacemaker was developed and with these developments, great advances were made in the treatment of heart diseases. Again, in the 1950s, scientists discovered that the soft and hard tissues that make up the skeleton are composed of collagen together with hydroxyapatite, very important information for the development of implant technology. While the definition of biomaterials was originally used for implanted devices, the definition of nonviable is no longer applicable for biomaterials. Jonathan Cohen, an orthopedic surgeon, defined biomaterials in 1967 as all materials used as implants except drugs and soft biological tissues. This definition is appropriate for biomaterials as it focuses on hard materials used in orthopedic treatments. However, in today's modern world, biomaterials are used in many applications other than implanted devices, including drug delivery systems, imaging contrast agents, and tissue engineered constructs, so biomaterials have come to be considered synonymous with biomedical materials (Figure 1.1) [1,3,5].

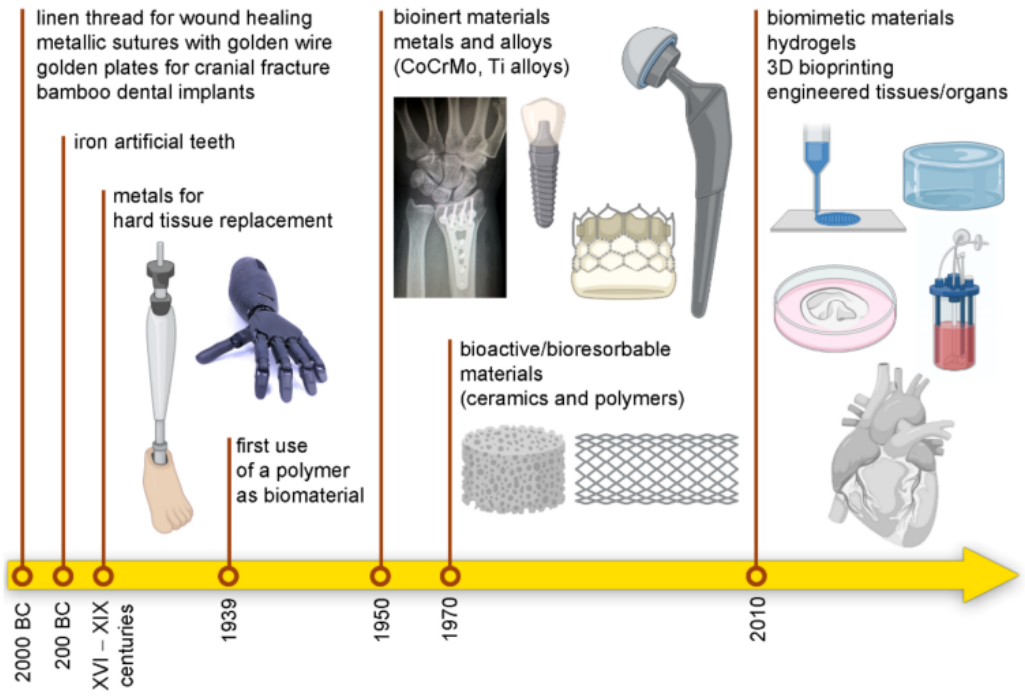

Figure 1.1. Timeline of some key milestones in biomaterials. Reprinted from [6].

Biomaterials, previously defined as materials placed in the locations of missing tissues, organs, or other body parts through surgical procedures, eventually transformed into more specifically designed and engineered materials, particularly with the advancement of polymer synthesis after the 1950s. Especially in the last 20 years, studies about smart and stimuli-responsive polymers, functionalized in various ways, as biomaterials, has tremendously increased, thanks to the ability to design polymers with desired properties. Additionally, polymeric hydrogels, due to their structural similarities to the extracellular matrix (ECM), have garnered even more specific interest for biomedical applications. The comparison of the numbers of studies on selected topics can be seen in Figure 1.2 [6].

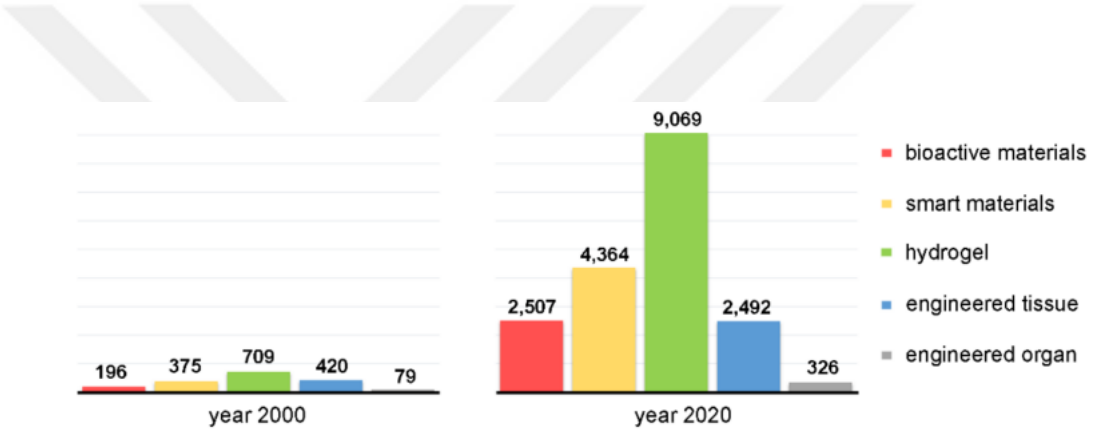

Figure 1.2. Number of studies in years 2000 and 2020 for selected keywords. Reprinted from [6].

1.1.1. Biodegradable Polymers Used as Biomaterials

When we look at the history of biomaterials, we can observe the utilization of natural polymers dating back to ancient times. However, it was in the 1940s, with the advancement of polymer synthesis, that polymer-based biomaterials rapidly evolved. In the early 1940s, nylon sutures were introduced for the first time. In the mid-1940s, prominent medical journals began to publish review articles about the surgical applications of various polymers like nylon, poly(methyl methacrylate) (PMMA), Dacron polyester, and polyvinyl chloride. In addition to these polymers, materials such as Teflon, polyurethane, and high-density polypropylene have also played a crucial role in the field of clinical medicine. They have

been utilized as integral components of perpetual artificial implants such as hip prostheses, synthetic lenses, wide-bore vascular grafts, and similar items [7,8]. However, especially in the last 20 years, the concept of biomaterials has transitioned from being permanent materials implanted into the body to materials that interact with biological systems to assess, treat, augment, or replace any tissue, organ, or function of the body. This transition has significantly increased the importance of polymer-based biomaterials. Polymer-based biomaterials find extensive applications in various biomedical fields, such as controlled drug delivery and new implantable polymers for gene therapy. Additionally, they are widely used in tissue engineering applications to aid in the regeneration of three-dimensional tissue and organ structures [9].

One of the most crucial properties that polymers must possess to be suitable for such applications is biodegradability. Nowadays, the importance of being biodegradable has replaced the previous emphasis on being biostable as a significant feature for biomaterials [10-12]. Biodegradable polymers, while extensively studied as biomaterials for medical use, have also become an important focus in the industrial sector. They are increasingly used as alternatives to products like plastic packaging, construction materials, agricultural and hygiene products, which cause waste disposal issues and can persist in the environment for years, causing significant harm. This shift towards using biodegradable polymers in various applications is currently a highly emphasized area of research [13].

Biodegradable polymers can be divided into two primary categories according to their source: natural and synthetic. Natural polymers are a logical selection for biomedical uses owing to their exceptional biocompatibility. These polymers closely resemble natural cellular surroundings, showcase distinctive mechanical traits, and are capable of biological degradation through enzymatic or hydrolytic pathways. Nonetheless, despite these benefits, the extensive application of natural polymers in the biomedical domain has been hindered by certain inherent drawbacks. These include the potential for viral infections, antigenicity, difficulties in sourcing materials, and variations in properties across different batches. In the context of material usage, the primary polysaccharides of relevance are cellulose and starch. However, there is increasing interest in more complex carbohydrate polymers produced by

bacteria and fungi, especially polysaccharides such as hyaluronic acid [14,15]. On the other hand, synthetic polymers offer significant advantages over natural polymers in terms of material properties. Synthetic polymers are reproducible, and desired functional groups can be easily incorporated into their structures. Additionally, their degradation rates and mechanical strength can be tailored according to specific requirements [14,16]. Poly(α-hydroxy acids), known for their remarkable biocompatibility and customizable degradation characteristics, stand as one of the most extensively explored synthetic polymer categories in the realm of biomedical applications. This grouping encompasses poly(glycolic acid), poly(lactic acid), and their diverse copolymers like poly(lactic-co-glycolic acid).

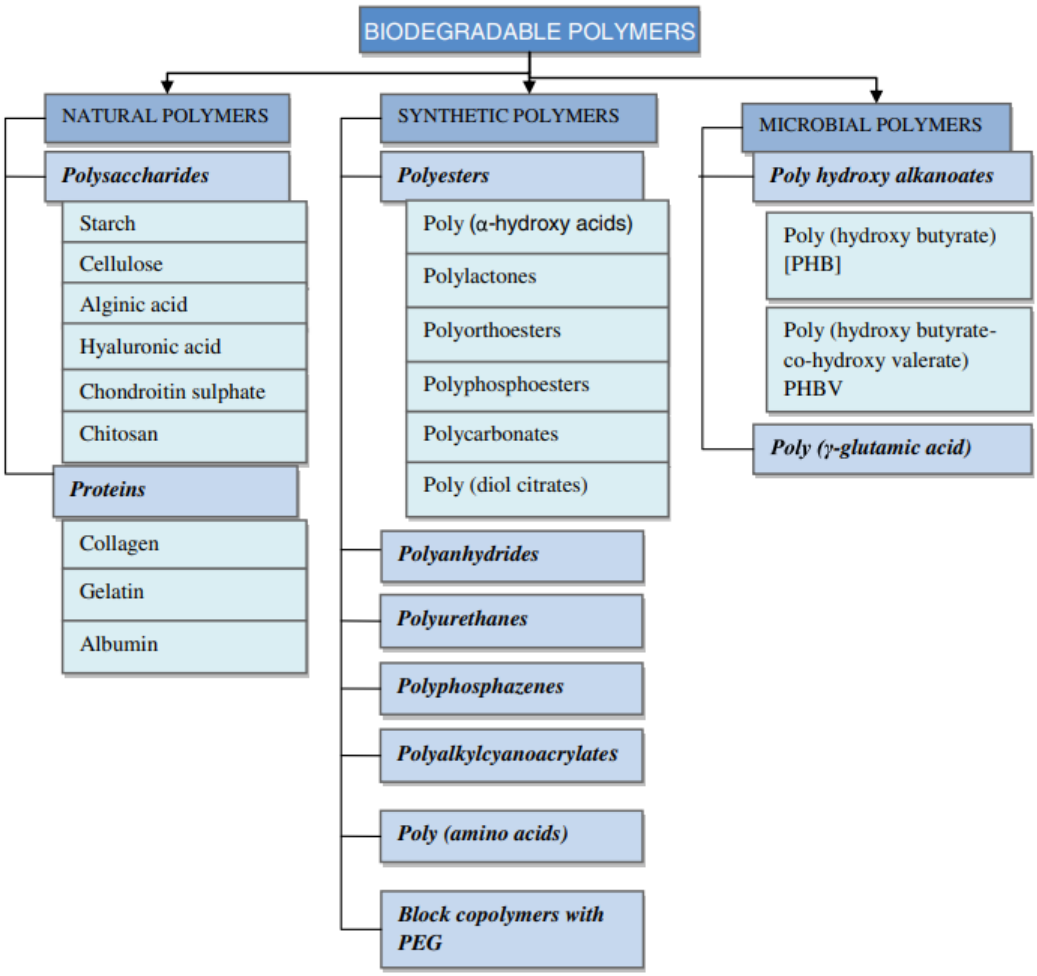

Figure 1.3. Classification of biodegradable polymers. Reprinted from [16].

Based on the mode of degradation, polymeric biomaterials can be categorized as hydrolytically degradable polymers and enzymatically degradable polymers. The degradation process in polymeric biomaterials can involve an active mechanism, often driven by enzymes present in bodily fluids, as well as passive hydrolytic cleavage, resulting in polymer erosion across all degradation types.

Enzymatic degradation is typical for natural polymers, with fungal enzymes holding particular importance in breaking down these materials. For instance, extracellular enzymes contribute to the enzymatic hydrolysis of cellulose and starch into glucose, while chitosan undergoes decomposition through various enzymes, including lysozyme, yielding non-toxic oligosaccharides that can be assimilated into glycosaminoglycans and glycoproteins [9,17,18]. On the other hand, hydrolytically degradable polymers are those that have hydrolytically sensitive chemical bonds in their backbones.

Synthetic polymers with functional groups such as esters, orthoesters, anhydrides, carbonates, amides, urethanes, and ureas degrade in this manner. Poly(α-ester)s are among the most biodegradable synthetic polymers due to the presence of hydrolytically unstable aliphatic ester linkages in their backbones.

Polylactic acid (PLA), polyglycolic acid (PGA), polycaprolactone (PCL), and polyhydroxybutyrate (PHB) stand out as some of the prominent polymers within this category that exhibit the ability to undergo degradation under physiological conditions, yielding non-harmful byproducts. For example, the synthetic polymer PGA (polyglycolic acid) degrades by breaking down its carbonyl groups in hydrolytic environments, resulting in the production of L-lactic acid as a degradation product. While PGA experiences complete biological degradation within approximately 4 months, its mechanical properties tend to diminish significantly after around 6 weeks [19,20].

Poly(β-amino ester)s (PBAEs) and poly(amido amine)s (PAAs) are another important classes of biodegradable synthetic polymers which are synthesized by the Michael addition reaction. PBAEs can be easily synthesized from the reaction of diacrylates with primary alkyl amine or secondary diamine. In the thiol Michael addition reaction, thiol group is used instead of the amine. PAAs are synthesized from the reaction of acrylamides with primary alkyl amine or secondary diamine instead of acrylate. Ease of synthesis and lack of by-products make these synthetic polymers desirable for various biomedical applications [21]. PBAE and PAA hydrogels are also well suited for use in biomedical applications. They can be easily modified structurally, have adjustable degradability, and features such as biodegradability, biocompatibility, and water-solubility enable them to be used in many different biomedical applications, from drug release to gene transfer, from being used as a scaffold for tissue engineering to being used as bioimaging agents [22].

Polymers can undergo degradation in two ways: bulk erosion and surface erosion (Figure 1.4). When polymers are exposed to bulk hydrolysis, the material absorbs water or body fluid and breaks down, leading to a sudden decrease in its mechanical properties as the material is lost from the entire polymer volume simultaneously. In this case, the rate of degradation depends on the total amount of the material. After liquid diffusion, oligomers having acidic terminal groups catalyze the process of hydrolysis, subsequently dispersing from the polymer and giving rise to a profoundly porous structure. Consequently, the degradation pace of polymers undergoing bulk erosion is not uniform. The majority of synthetic polymers, such as poly(α-ester)s, generally experience bulk erosion.

Conversely, surface erosion entails material loss exclusively from the external layer of the polymer matrix. This phenomenon is typically observed in hydrophobic polymers or those comprising a hydrophobic component, where water encounters difficulty in penetrating into the core. Ideally, the rate of surface erosion will be directly linked to the polymer's surface area. Polyanhydrides, classified as highly hydrophobic synthetic polymers, undergo surface erosion, whereby the degradation speed on the surface surpasses the bulk erosion rate within the matrix [23-25].

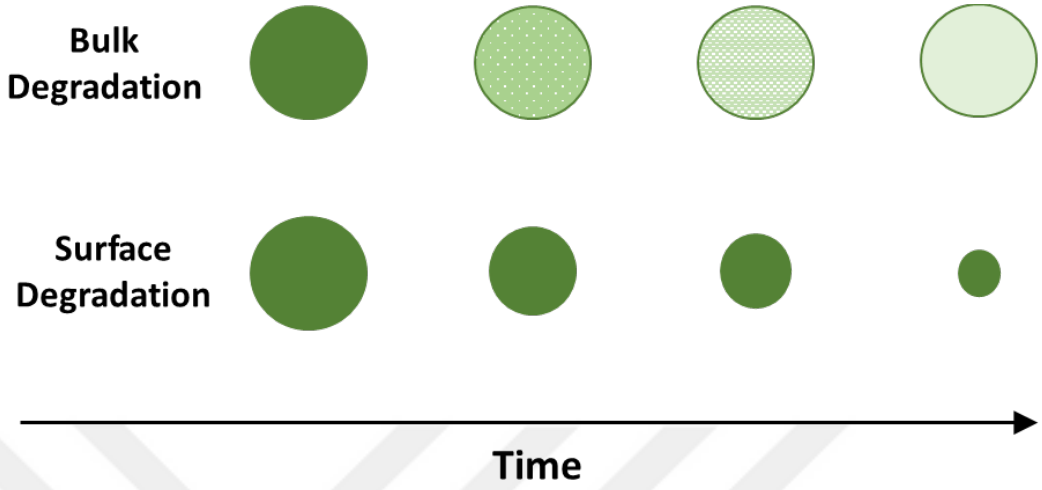

Figure 1.4. Degradation sequence of bulk and surface degraded polymers.

1.2. Poly(amido amine)s as Biodegradable Polymers

1.2.1. Synthesis of PAAs

Poly(amido-amine)s (PAAs) are one of the significant group of synthetic functional polymers widely utilized in various biomedical applications. PAAs are originally obtained by stepwise Michael-type polyaddition of primary or secondary aliphatic amines to bis(acrylamide)s [26]. A wide variety of amine and bisacrylamide monomers can be used in the polymerization reaction, providing considerable flexibility in the chemical functionalities of both the main chain and side chain of the resulting polymers (Figure 1.5) [27]. Michael addition which is also called conjugate addition has become an important polymer synthesis method. This reaction takes place in mild and environmetally friendly reaction conditions between an enolate-type nucleophile in the presence of a catalyst with an activated α,β-unsaturated carbonyl. In Michael type addition reactions, non-enolate nucleophiles such as amines, thiols and phosphines can be used as Michael donors [28].

The most effective way to synthesize PAAs through the Michael addition reaction involves conducting the process in aqueous media or, alternatively, in alcohols. This preference is due to the necessity of a proton source to accelerate the reaction and attain high molecular weight products within a reasonable timeframe. The polymerization reaction can proceed at temperatures exceeding 10°C without the requirement for supplementary catalysts. The best outcomes are achieved by employing high concentrations of monomers and maintaining relatively lower reaction temperatures. Even though aprotic solvents might possess significant polarity, they are unsuitable as reaction media due to their tendency to yield products of low molecular weight. During PAA synthesis, amino groups react solely when they exist as free bases. To address concerns regarding solubility, other substances such as methanol, ethanol, hydroxyethyl amine can also serve as viable alternatives [29,30].

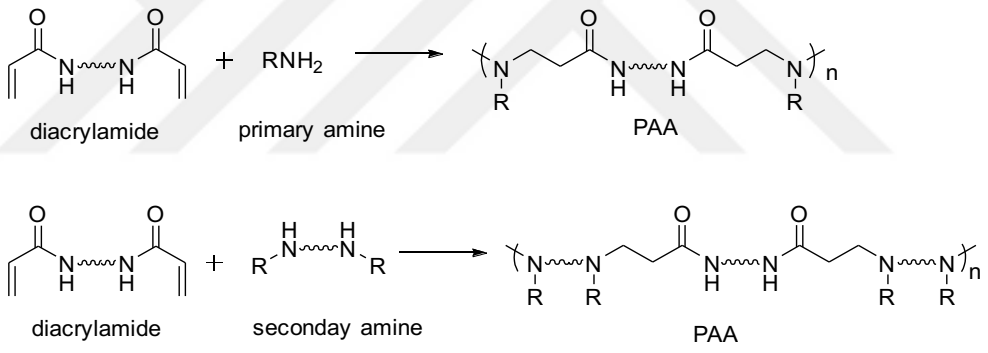

Figure 1.5. Synthesis of PAAs.

In the synthesis of PAAs, primary monoamines and secondary diamines lead to linear polymers. While under non-selective conditions, primary diamines typically result in cross-linked products with bisacrylamides. However, under specific conditions with low reactant concentrations, low initial temperatures, and excess diamines, it has been reported that linear PAAs with secondary amino groups in the main chains can be obtained instead of tertiary ones. PAAs are naturally highly functional polymers, and they are also amenable to further functionalization. Monomers containing groups like hydroxyl, tertiary amine, and allyl can be used in PAA synthesis, and groups like free amines on the polymer can be functionalized later [31]. Another well-studied approach for PAA synthesis involves using bisacrylamides

or amine groups with disulfide linkages in their backbones. Amphoteric PAAs are a subgroup of PAAs that carry acidic functionalities, mostly carboxyl groups, as side substituents. They can be obtained using carboxylated bisacrylamides or amino acids as monomers. Additionally, PAMAM dendrimers are extensively used hydrophilic and highly branched PAA derivatives. Due to their highly adjustable and controlled synthesis, PAMAM dendrimers have the unique advantage of having very low polydispersity [29,32].

1.2.2. PAA Hydrogels in Tissue Engineering Applications

The basic requirements for hydrogels to be used as scaffolds for tissue engineering; in addition to properties such as being biocompatible, biodegradable and non-toxic, are that they should also have appropriate mechanical properties, cell adhesion, cell permeability and diffusion properties. Using PAA macromers functionalized with various chemical groups, such as carboxyl groups, hydroxyl groups, and allyl groups, hydrogels can be easily obtained. Furthermore, important properties for tissue engineering, such as the rate of degradation, can be tuned by functionalization of hydrogels. Besides these properties, PAAs are biodegradable and despite their polycationic nature, most are virtually non-toxic. These highly functional, non-toxic, and highly water retaining PAA hydrogels have the potential to be used as scaffolds for tissue engineering [33-37].

It is known that the addition of bioactive functional groups to synthetic materials increases the cell adhesion of these materials. For example, the synthesis of RGD (arginine-glycine-aspartic acid)-containing hydrogels has been extensively studied, as grafting of the RGD to materials provides strong cell adhesion [38]. For example, pure PEG hydrogels do not have cell adhesion properties, while RGD modified PEG hydrogels have the ability to promote cell adhesion [39]. However, the use of the RGD-mimic structure of the guanidine side group instead of RGD is a widely studied topic due to the complex synthesis procedure and high production cost. Martello et al. synthesized the RGD-mimicking structure with 4-aminobutylguanidine (ABG) and used it in the synthesis of PAA hydrogels to produce

hydrogels with potential for use in tissue engineering, demonstrating significant cell growth on these gels [40].

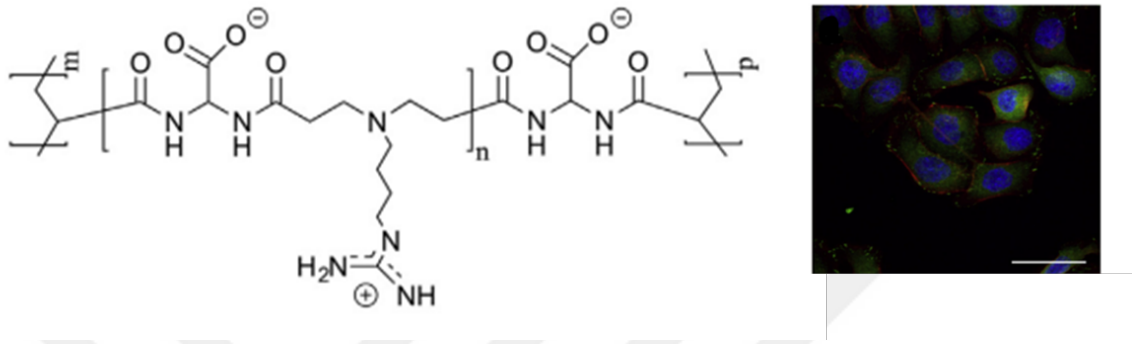

Figure 1.6. Structure of RGD-mimicing PAA hydrogel and the cellular morphology. Reprinted from [40].

1.2.3. PAA Hydrogels in Gene Delivery Applications

Gene therapy has emerged as a novel and effective strategy in addressing both hereditary or acquired disorders, including genetic anomalies, cancer, cardiovascular issues, and neurological conditions. Within this therapeutic approach, therapeutic gene molecules such as deoxyribonucleic acid (DNA) and ribonucleic acid (RNA) play crucial roles in altering faulty genes, replacing missing ones, and silencing mutated ones. As our understanding of disease-causing genes improves, gene therapy holds great promise as a potential treatment for a wide range of currently incurable diseases. However, therapeutic genes encounter challenges stemming from their negative charge, hydrophilic characteristics, and high molecular weight, leading to limited cellular membrane permeability, low cellular uptake, and reduced stability during circulation in the bloodstream [41-43].

Despite these cell permeability challenges, gene delivery vectors have been designed to effectively deliver therapeutic genes to target cells, release genes within cells and facilitate

eventual transfection processes. Gene delivery vectors can be broadly divided into two main types: viral and non-viral vectors. While viral vectors exhibit high gene delivery efficacy, their progress is limited due to important safety concerns such as immune responses, inflammatory reactions, toxicity issues, and potential mutagenesis associated with their use. In contrast, non-viral vectors that are immune-compatible, cost-effective, have enhanced loading capacities, and offer high chemical versatility have attracted great interest in gene delivery applications in recent years.

Cationic polymers are among the most studied non-viral vector types in gene delivery applications [29,44]. Cationic polymers can form polyplexes with negatively charged siRNA and plasmid DNA (pDNA) through electrostatic interaction. These polyplexes, which are about a few hundred nanometers in size, can be taken up by cells. Then these polyplexes taken into the cell are degraded and release their cargo into the cell from acidic intracellular compartments such as lysosome and endosome via proton-sponge mechanism or swelling and local mechanical breakdown mechanism (Figure 1.7). Many cationic polymers have been extensively studied for their potential use in gene delivery applications, with the most popular ones being polyethyleneimine (PEI), poly(L-lysine) (PLL), and polyamidoamine dendrimers (PAMAM) [45].

To investigate the impact of polymeric functionalities on the physicochemical and colloidal properties of polyplexes, Garnett explored linear poly(amino acids) (PAAs) with varying charge density and chain stiffness for DNA binding, colloidal stability, and transfection activity. The results showed that these PAAs demonstrated structure-dependent DNA binding behavior [46].

Furthermore, the utilization of disulfide bonds as degradable linkages has garnered significant attention in recent years due to their potential for enzymatic cleavage within cellular environments, facilitated by enzymes like glutathione. Building on the promising results observed in gene delivery studies involving disulfide-containing biodegradable poly(amido amine)s (SS-PAAs), researchers have conducted comprehensive investigations

into the influence of various pendant functional groups within SS-PAAs on their gene delivery characteristics.

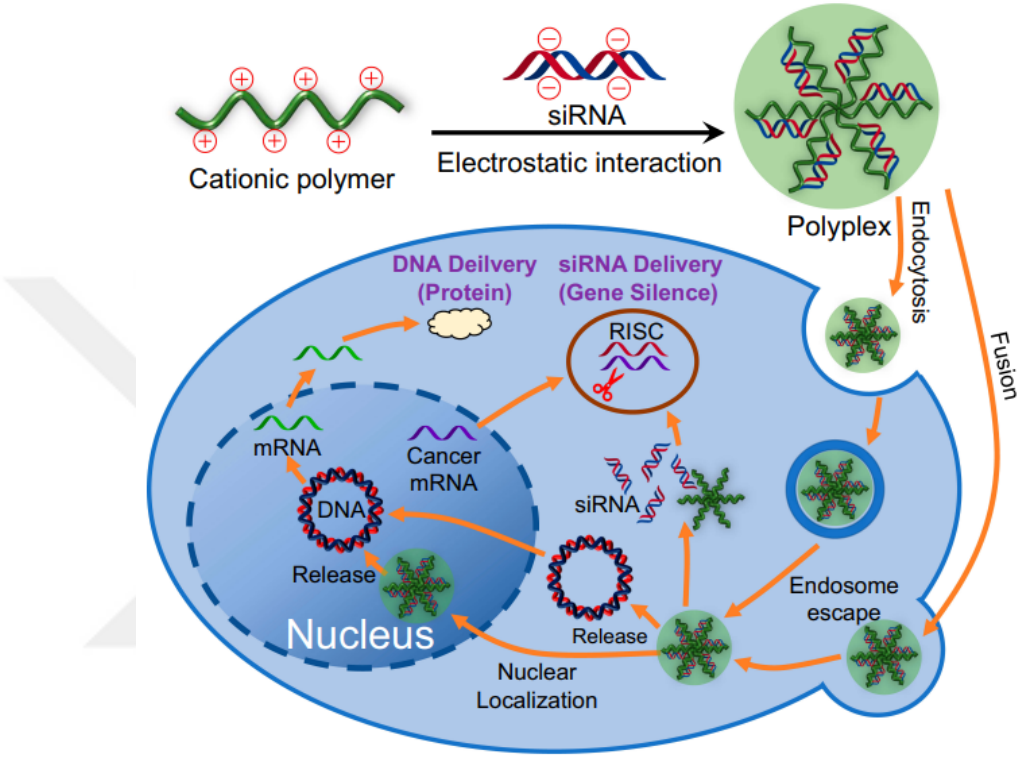

Figure 1.7. Gene delivery mechanism for non-viral vectors of cationic polymers. Reprinted from [41].

Research conducted by Lee et al. has suggested that disulfide-containing PEIs exhibited improved gene vector attributes in comparison to 25 kDa branched PEI. This enhancement was attributed to similar levels of transfection efficacy achieved with notably reduced cytotoxicity [47].

Ferruti and Duncan documented that an amphiprotic PAA featuring carboxylic acid side groups demonstrates transfection effectiveness similar to that of 25 kDa branched polyethyleneimine (PEI). Furthermore, it has been suggested that the polymer undergoes a conformational shift upon protonation within endosomes, potentially aiding in the escape

from endosomal compartments [48,49]. The buffer capacities and DNA carrying properties of bone-targeting cationic polymers obtained as a result of the binding of bis (phosphonic acid)-functionalized PAAs with PEI were investigated in a study in which our group was also collaborator (Figure 1.8) [50].

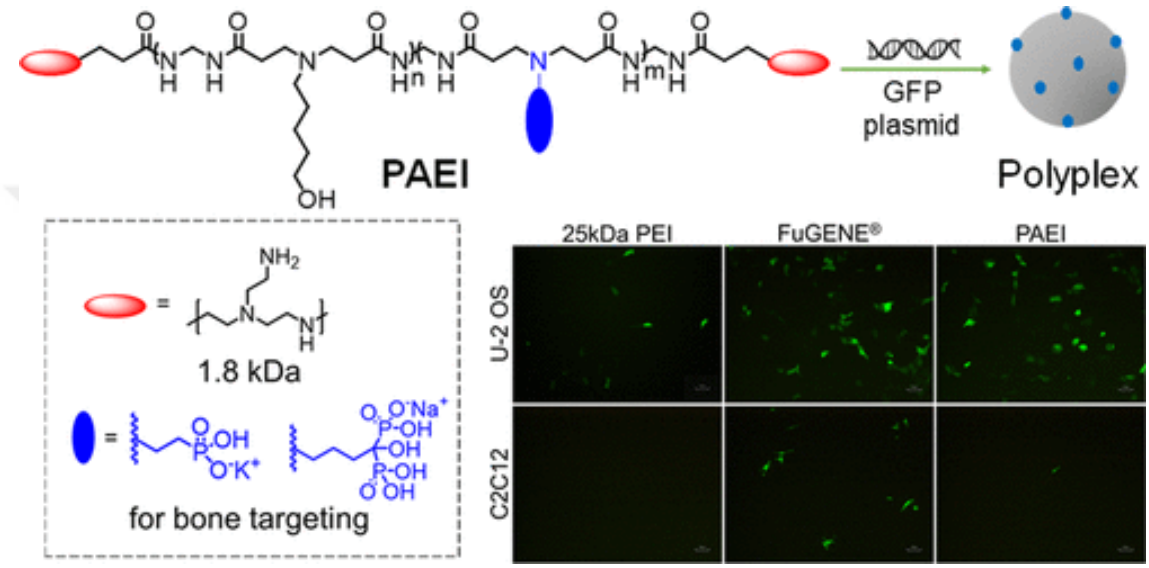

Figure 1.8. (Bis)phosphonic acid-functionalized poly(ethyleneimine)−poly(amido amine)s for in vitro transfection. Reprinted from [50].

1.3. Stimuli Responsive Hydrogels as Smart Biomaterials

Hydrogels represent hydrophilic, three-dimensional polymeric networks capable of absorbing and retaining substantial quantities of water or biological fluids. These structures are created using natural or synthetic polymers and are structured into three-dimensional (3D) forms via physical or chemical cross-linking processes. For a substance to be classified as a hydrogel, it must contain a minimum of 10% water relative to its weight (or volume).

In cases where crosslinking points are absent, hydrophilic linear polymer chains readily dissolve in water due to the favorable thermodynamic interaction between the

polymer chains and the aqueous environment. Conversely, the presence of crosslinking points counteracts solubility by introducing an elastic retractive force initiated by the network's crosslinks.

Hydrogels, notable for their substantial biocompatibility and resemblance to bodily tissues, have emerged as an immensely promising category of biomaterials. The capacity of hydrogels to absorb water is correlated with the presence of specific functional groups like –COOH, –OH, $–CONH_2$, –CONH–, and $–SO_3H$. Other factors such as capillary effect and osmotic pressure also play a role in determining the water uptake equilibrium of hydrogels [51,52].

Various studies are being conducted to design "smart" or "intelligent" hydrogels by modifying their physical and chemical properties. Traditional hydrogels can change their swelling behavior depending on the presence of water and their environment [53]. In contrast, stimuli-responsive hydrogels can sharply alter their swelling performance, mechanical strength, sol-gel transitions, permeability, and network structures in response to external stimuli.

Physical stimuli such as temperature, electric and magnetic fields, solvent composition, light intensity, and pressure, as well as chemical or biochemical stimuli involving pH, ions, and specific chemical compositions, can affect hydrogels (Figure 1.9). These conformational changes are usually reversible, allowing hydrogels to revert to their original state after the stimulus is removed [53-57]. Hydrogels can be categorized based on different characteristics they exhibit. One classification is according to their origin, which distinguishes hydrogels produced from natural polymers and those derived from synthetic polymers. Depending on the presence of ionic charges in their bonded groups, hydrogels can be classified as cationic, anionic, or neutral.

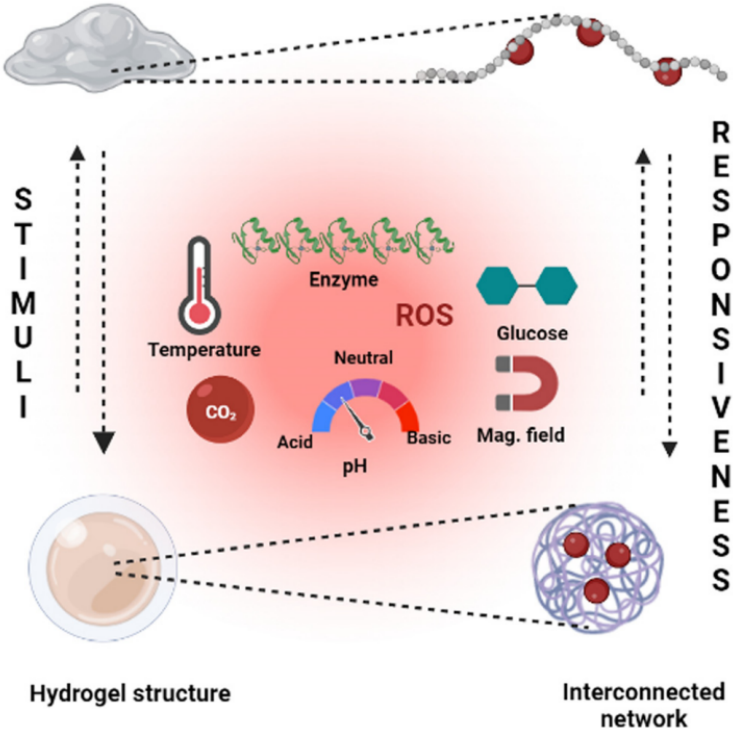

Figure 1.9. Structural changes of a hydrogel based on environmental stimuli. Reprinted from [57].

Another classification is based on their crosslinking patterns, which can be physical, chemical, or biochemical. Physical gels undergo a transition from liquid to gel phase in response to changes in environmental conditions such as temperature, ionic concentration, pH, or the mixing of two components. Chemical gels form covalent bonds, providing enhanced mechanical integrity and resistance to degradation compared to weaker materials [57-59].

Biochemical hydrogels involve biological substances like enzymes or amino acids in the gelation process. Additionally, hydrogels can be grouped according to their structure, distinguishing them as amorphous, semi-crystalline, crystalline, or hydrocolloid aggregates [60,61]. Classification of hydrogels according to their different characteristics is seen in the Figure 1.10.

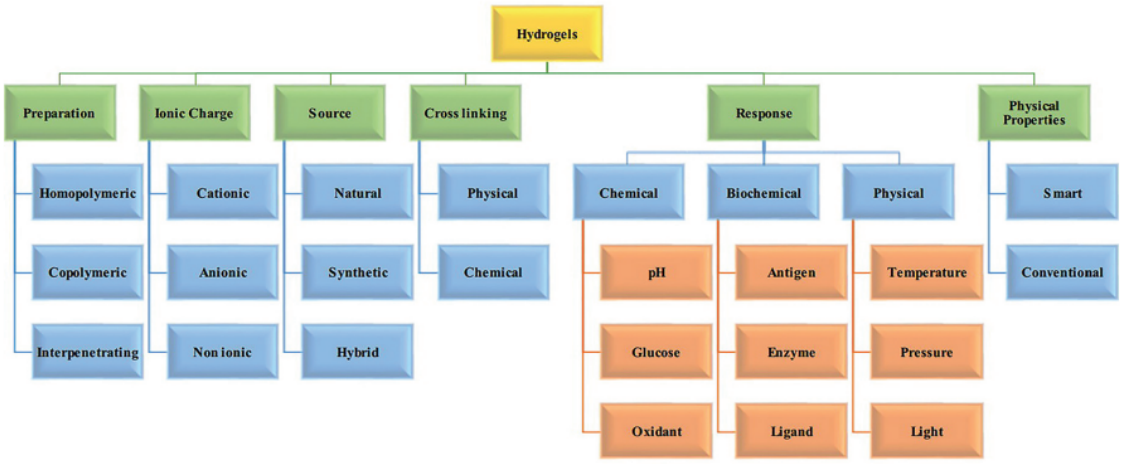

Figure 1.10. Classification of hydrogels based on the different characteristics. Reprinted from [61].

Due to their mechanical similarity to biological tissues, hydrogels derived from both natural and synthetic polymers have been suggested as highly promising materials for a wide range of biomedical applications. In particular, smart hydrogels have shown great potential in bioscience applications. They can play an essential role in remote-controlled therapies (e.g. targeted drug delivery) [62], tissue engineering [63], injectable systems (e.g. cell delivery)[64], regenerative medicine [65], biosensors [66], wastewater treatment [67] and so on. The response of hydrogels to external stimuli primarily depends on factors such as the nature of the monomer, charge density, pendant chains, and cross-linking degree. Additionally, the magnitude of the response is directly related to the intensity of the applied external stimulus.

1.3.1. Synthesis of Hydrogels

Based on the methods of preparation, hydrogels may be classified as homopolymer, copolymer, semi-interpenetrating network (semi-IPN) and interpenetrating network (IPN). Polymer blends and composite hydrogels are structures that improve the physical properties of hydrogels, especially their mechanical properties. However, these materials can often

undergo phase separation, which can lead to the deterioration of hydrogel properties over time. Especially for biopolymer hydrogels, there is an increasing interest in designing and incorporating secondary interpenetrating networks to obtain and further enhance the desired properties [68].

To produce interpenetrating Networks (IPN), at least one polymer is synthesized and/or crosslinked immediately adjacent to another, and they are crosslinked polymers that cannot be separated as long as their chemical bonds remain intact. IPNs are a subgroup of "Double Network" (DN) hydrogels and were first defined by Gong and colleagues. Despite their high water content (60-90%), IPNs are characterized by extremely high tensile strengths [69,70]. Semi interpenetrating network (SIPN) hydrogels consist of two polymers where one polymer is crosslinked in intimate presence of the other. In SIPN one linear polymer penetrates network of another crosslinked polymer without any chemical bond formation between these two polymers (Figure 1.11). In many cases, polysaccharide chains are used to create SIPNs [71,72].

The interpenetrating networks (IPNs) and semi-interpenetrating networks (SIPNs) have been shown to have significantly improved mechanical strength and greater capacity to immobilize drugs which appear because of the synergy between the two polymers. Therefore, IPN and SIPN hydrogels are preferred in many applications due to their improved mechanical strength, efficient drug loading capacity, and controlled swelling behavior [73-76].

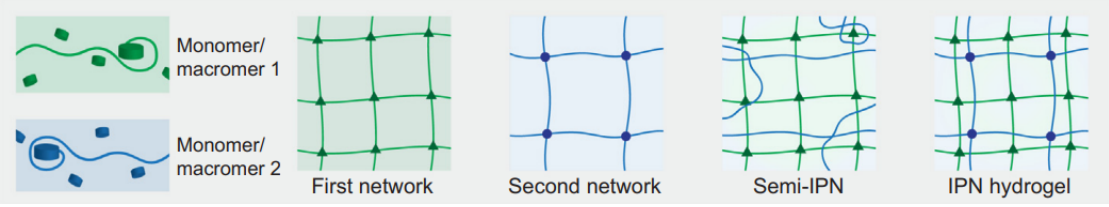

Figure 1.11. Synthesis of interpenetrating network (IPN) and semi- interpenetrating network (SIPN) hydrogels. Reprinted from [68].

1.3.2. Temperature Responsive Hydrogels

Temperature-responsive hydrogels are aqueous monomer/polymer solutions which undergo reversible volume-phase transition upon temperature change. Among all stimuli-responsive hydrogels, temperature sensitive ones are one of the most studied groups. The temperature-responsive shape change of these hydrogels relies on the balance between hydrophilic and hydrophobic region present within the polymer network. These hydrogels primarily exhibit hydrophobic groups, like methyl, ethyl, and propyl groups and hydrophilic segments like amine and carboxyl, which tend to interact favorably with water molecules through hydrogen bonding, resulting in the swelling of the hydrogel [59,77].

In most cases, the water solubility of polymers tends to increase as the temperature rises. However, there are instances where water solubility decreases with increasing temperature. This phenomenon is particularly observed in thermo-responsive hydrogels with a lower critical solution temperature (LCST). At lower temperatures, water molecules prefer to form hydrogen bonds with polar groups in the polymer, leading to enhanced dissolution in water due to hydrogen bonding interactions.

Conversely, at higher temperatures, the increase in Gibbs free energy (ΔG) makes hydrogen bonding between water molecules and polymer chains less favorable compared to interactions between polymer-polymer and water-water. As a result, water moves into the bulk solution, and the polymer chains collapse onto themselves, forming hydrophobic interactions (Figure 1.12). This reversible volume phase transition at the LCST is a characteristic feature of thermoresponsive hydrogels [78-80].

Among the various hydrogels exhibiting thermos responsive characteristics, one of the extensively studied gels is poly(N-isopropylacrylamide) (PNIPAm). When the temperature rises above its lower critical solution temperature (LCST) of 32 °C, P(NIPAAm) polymers undergo a distinct coil-to-globuli conformational transition, leading to the dehydration and

collapse of the P(NIPAAm)-based polymer networks. The remarkable phase transition behavior of P(NIPAAm) occurring around physiological temperatures makes it a widely utilized material for in situ forming sol gels [82,83].

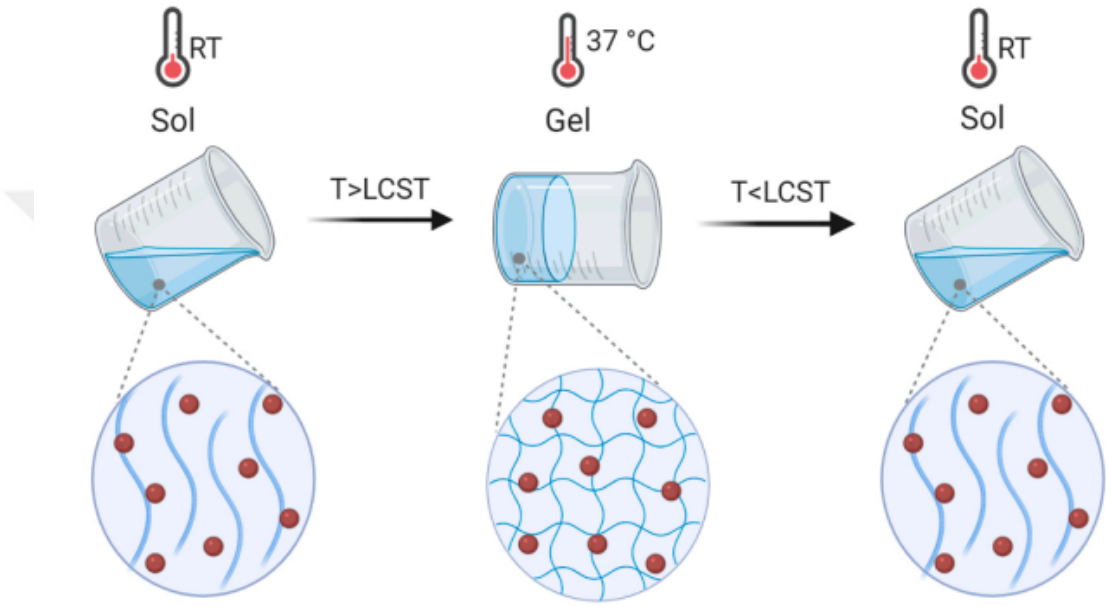

Figure 1.12. Temperature responsive hydrogels transforming from sol to gel, from gel to sol when temperature drops below LCST, at LCST, and above LCST. Reprinted from [81].

1.3.3. pH- Responsive Hydrogels

For the design of pH-responsive hydrogels, ionic pendant groups (e.g., COO- and -NH) can be incorporated into their structures. These groups can accept or donate a proton depending on their pKa values and the environmental pH changes [84]. Any modification in the external pH level induces a proportional shift in the extent of ionizable group dissociation, consequently causing variations in internal and external ion concentrations. Cationic hydrogels, when exposed to low pH conditions (pH < pKa), experience swelling owing to the protonation of amino/imine groups. This leads to the repulsion of positively charged segments present on the polymer chains. Conversely, anionic hydrogels display

swelling tendencies at elevated pH levels (pH > pKa) due to the ionization of acidic groups, which subsequently prompts chain repulsion (Figure 1.13) [85].

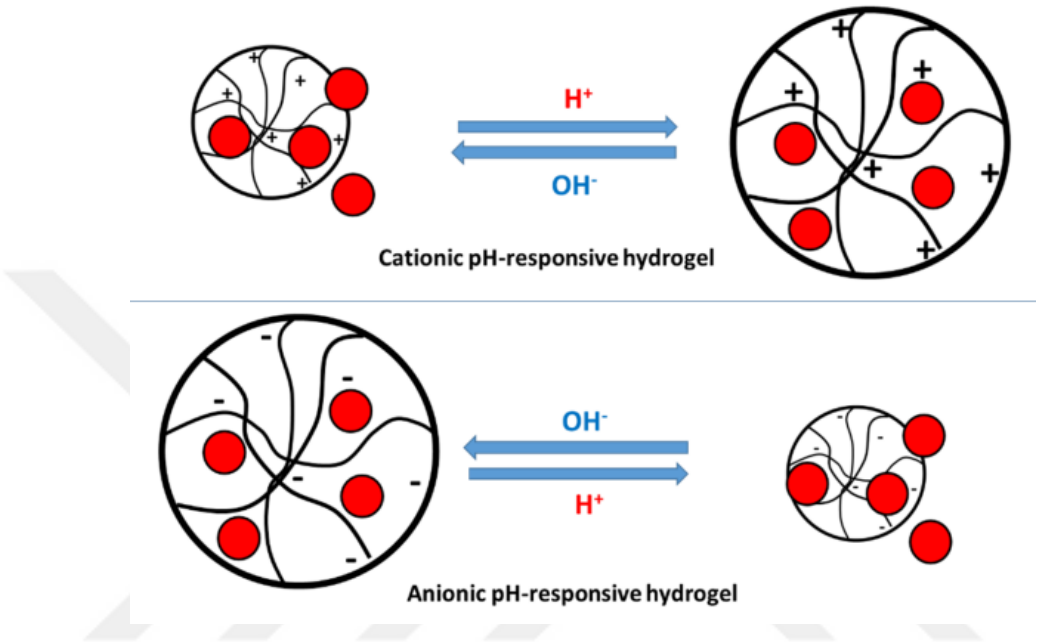

Figure 1.13. Schematic representation of a general behavior of pH-responsive hydrogel. Reprinted from [86].

Polymeric materials like poly(acrylic acid) (PAA), polyacrylamide (PAAm), poly(methacrylic acid) (PMAA), and poly(diethylaminoethyl methacrylate) (PDEAEMA) with weak polyelectrolyte characteristics are commonly employed for the formulation of pH-sensitive hydrogels. These polymers encompass hydrophobic segments and exhibit swelling behavior contingent on the pH of their environment when immersed in water. Furthermore, pH-responsive swelling behavior is also observed in a range of natural polymers including anionic chitosan, cationic alginate, albumin, and gelatin. The integration of pH-responsive features from these polysaccharides with thermosensitive materials allows the creation of dual-stimulus responsive polymeric hydrogels capable of reacting to specific pH and temperature changes within the human body. This unique combination renders them highly suitable for targeted drug delivery applications [87].

By modifying the polymer structures, it is possible to conveniently regulate the release kinetics of pH-responsive gels. For instance, cationic hydrogels release drugs when they swell at low pH levels, whereas anionic hydrogels release drugs at higher pH values. As a result, anionic hydrogels are favored for controlled intracellular drug release in tumor cells, while cationic hydrogels are preferred for drug release in the extracellular matrix of tumor tissues. Beyond drug delivery applications, pH-responsive gels show significant potential in tissue engineering endeavors [88-90].

1.4. Important Functional Groups for Biomaterials

1.4.1. Phosphorous Containing Materials

Phosphorus-containing materials are of great interest because of their broad application areas. For example, they are widely used in industry due to their ability to bind metals, and they are also used as protective coatings that prevent any oxygen transport towards the burning area and extinguish the fire, since the flame-retardant effect of phosphorus is known. Polymeric materials with phosphonic moieties are also used in alternative energy production because they are located in proton-conducting fuel cell membranes [91,92]. Moreover, the utilization of polymers containing phosphorus groups, including polyphosphates, polyphosphonates, polyphosphoesters, and phosphonated polymethacrylates, is widely prevalent in biomedical applications. These polymers have demonstrated biodegradability and compatibility with blood, exhibit minimal protein adsorption, and display strong interactions with dentin, enamel, or bones [93].

The advancement of controlled radical polymerization techniques has facilitated the production of uniformly functionalized macromolecules with precisely controlled molecular weights. Utilizing this approach, various well-defined phosphorus-based materials have been successfully synthesized. Monge et al. demonstrated the RAFT synthesis of a diblock copolymer using a phosphorus-containing acrylamide monomer. Initially, diethyl-2-

(acrylamido) ethyl phosphonate was homopolymerized with RAFT to serve as a macro chain transfer agent, allowing for controlled polymerization of N-n-propylacrylamide. Subsequent hydrolysis of phosphorylated esters resulted in the formation of phosphonic acid groups [94].

Heavy metal ions are generally hazardous and have a propensity to accumulate within organisms. These metals can lead to diverse diseases as they infiltrate the human body via drinking water and the food chain. Numerous techniques are under development to eliminate heavy metals. For instance, activated carbon, while possessing strong adsorption capabilities, is cost-prohibitive due to its limited operational lifespan. This has prompted researchers to explore natural or synthetic polymer materials. Polymers incorporating functional groups such as amino and hydroxyl groups, which exhibit the ability to capture heavy metal ions from water through chelation or ion exchange, are employed for heavy metal removal purposes. The utilization of adsorption materials containing anionic groups for heavy metal removal is a heavily researched avenue [95].

Polymers containing groups such as carboxylic acid are widely used in these studies, and the addition of phosphoric acid groups can effectively improve the adsorption capacity of adsorption materials. Therefore, Tang et al. synthesized a new chitosan-based adsorbent polymer with adsorption properties by the simultaneous addition of amidoxime and phosphonic acid groups into chitosan and showed that Cu(II) and Ni(II) accumulated on this adsorption material according to the results of FTIR and XPS analysis (Figure 1.14) [96].

Among all these phosphorus-containing materials, the importance of bisphosphonate is quite high. Bisphosphonates (BPs) first appeared as anti-osteoporotic drugs 55 years ago. In recent years, they have been used as bone targeting groups, especially in the treatment of bone diseases because of the affinity of BPs to bone mineral hydroxyapatite (HA) is the basis for their use as inhibitors of bone resorption [97].

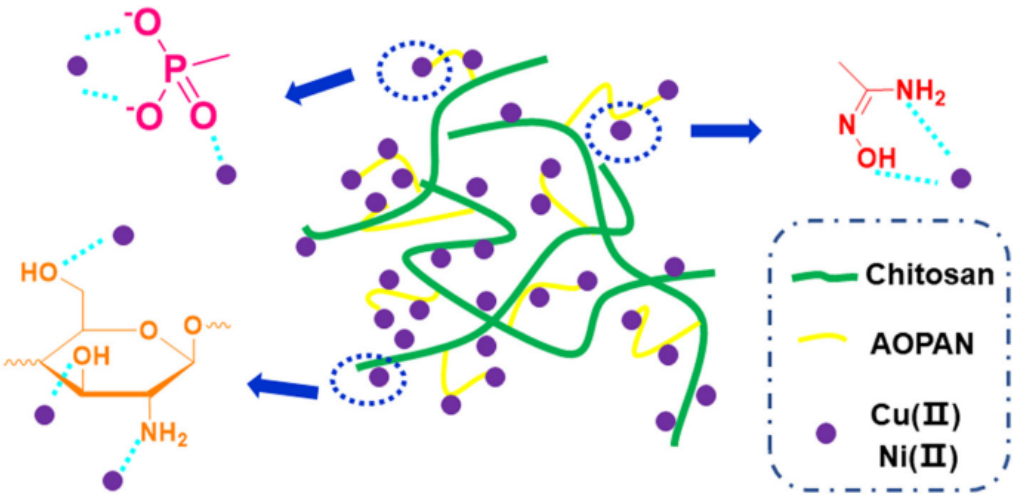

Figure 1.14. Adsorption mechanism of polymer. Reprinted from [96].

Pyrophosphate in plasma firstly found by Fleish et al. which has an inhibiting effect on calcification [98]. However, pyrophosphate is very weak against enzymatic hydrolysis due to its P-O-P bond. BPs are more stable and hydrolysis-resistant analogs of pyrophospate that have a P-C-P bond instead of a P-O-P bond (Figure 1.15). In addition, the R1 and R2 side chain groups that BPs have are the groups that determine the bone affinity and potency of BPs [99].

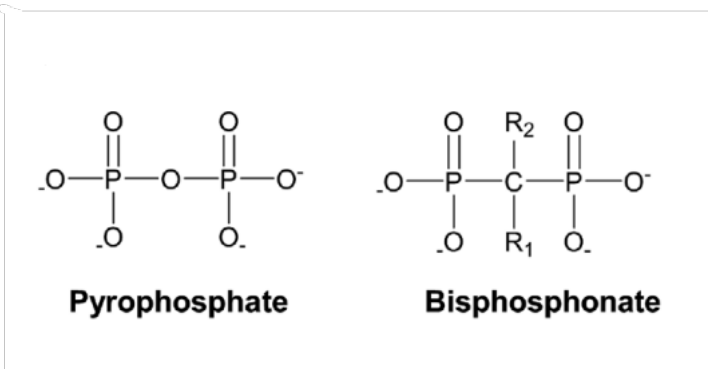

Figure 1.15. Structure of pyrophosphate and bisphosphonate.

BPs are used for a wide range of purposes, taking advantage of their unique structures and properties (Figure 1.16). BPs are preferred for treating various bone diseases by their

excessive osteoclast activity, including Paget's disease, bone metastasis, and hypercalcemia. Furthermore, besides their bone resorption inhibition effects, BPs also demonstrate direct antitumor effects [100,101]. Furthermore, when BPs are used as a covering material for prosthetics, they can increase the amount of bone adjacent to the implant, resulting in better fixation of the implant. Bp-containing drugs target bone, concentrating the therapeutic agent at the desired site of activity, providing high specific bone response and optimum bioavailability [102]. Additionally, BPs are utilized as flame retardant materials since they create a coating that restricts the passage of oxygen to the burning area [103].

Beyond all these applications, BPs have the ability to bind with divalent ions of the alkaline earth metals (Mg^{2+}, Ca^{2+}, Sr^{2+}, and Ba^{2+}) [104]. BP-containing materials can be used as dental materials due to the strong interaction between BPs with Ca^{2+} in hydroxyapatite, for the same reason, incorporating BPs in scaffolds functionalized scaffolds have great potential for using in bone tissue engineering applications.

1.4.2. BPs for Bone Tissue Engineering

Bone is a crucial tissue with vital functions such as protection, support and storing calcium and other essential inorganic ions, in addition to serving as a location for the generation of white blood cells in the body. It is a special connective tissue composed of organic part (collagen1) and inorganic part (HAP crystals), which makes it a composite material. Collagen and HAP combined at the nanoscale contribute to both the compressive strength and stiffness of bone [102].

Bone tissue engineering (BTE) is an emerging multidisciplinary field aimed at restoring or replacing damaged native tissues. While bone possesses some self-healing abilities, significant bone defects often require external intervention or treatment for proper healing. Bone tissue engineering, an innovative approach that integrates materials engineering with biological technology, holds promise as a strategy to enhance bone graft

materials. Utilizing genes, cells, growth factors, and bioactive drugs, these products create a conducive environment for bone defect healing [106].

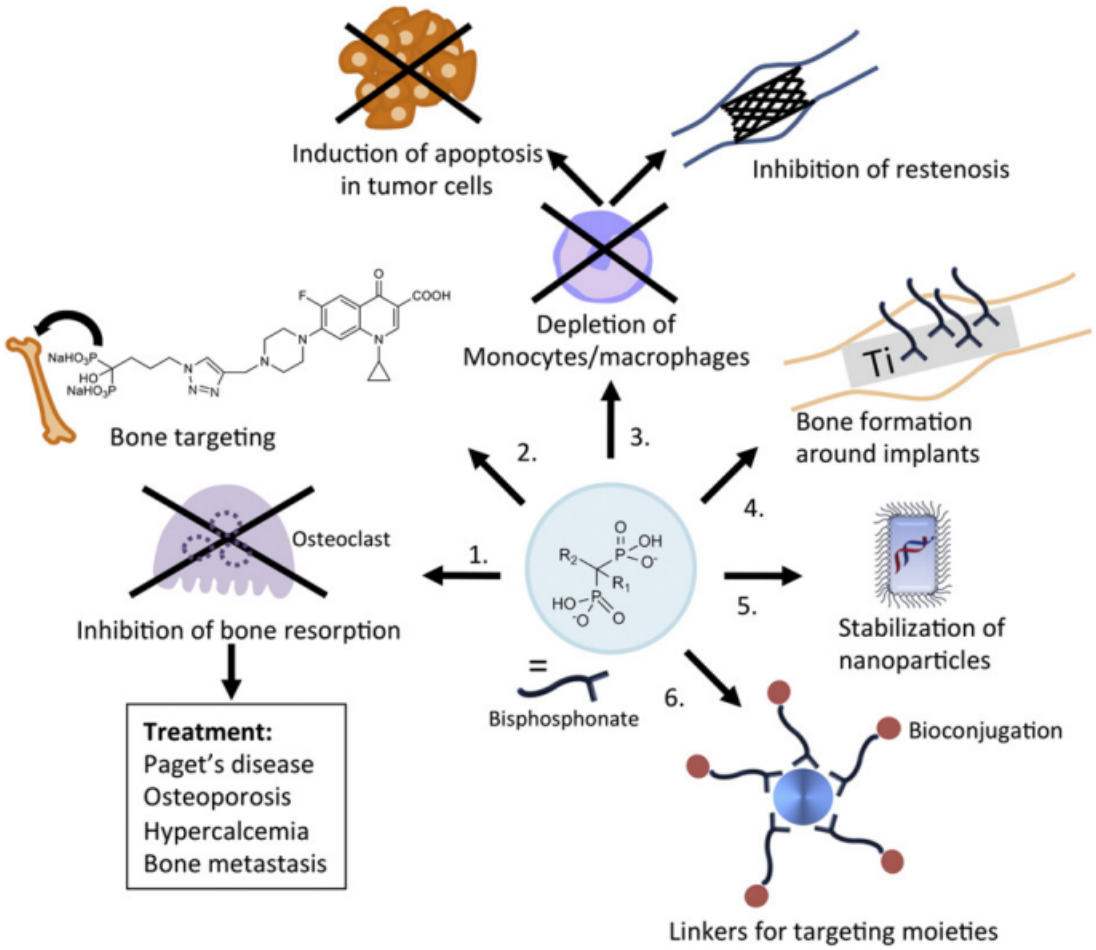

Figure 1.16. Some application areas of bisphosphonates. Reprinted from [105].

One of the most important requirements of bone tissue engineering (BTE) is the design and processing of a three-dimensional biodegradable scaffold with high interconnected porous structure. These scaffolds should provide cellular adhesion, proliferation and differentiation in order to promote bone regeneration [107]. A wide variety of materials have been used in the preparation of 3D scaffolds for BTE, such as calcium phosphates (CaP), mesoporous silica, bioactive glasses, and mostly natural or synthetic polymers. Hydrogels

are an appealing scaffold material because their structures are similar to the extracellular matrix (ECM) [108].

The bone's extracellular matrix comprises proteins abundant in polyaspartic acid and polyglutamic acid, making them possess an anionic nature. These negatively charged functional groups are thought to play an important role in the mineralization process by acting as Ca^{2+} binding agents and creating nucleating sites that promote mineralization. [109]. BPs have exceptionally high affinity to Ca^{2+} ions as well as to the bone mineral hydroxyapatite (HAP). Also, BPs have been shown to enhance the proliferation, differentiation, and bone-forming activity of osteoblasts directly. Therefore, adding BPs to scaffolds for BTE is a topic of study. Methods such as adding BP to scaffolds with inorganic structures such as CaP to which it can bind well, or inflating the scaffold in a solution containing BP are some of the methods that have been tried before (Figure 1.17) [102].

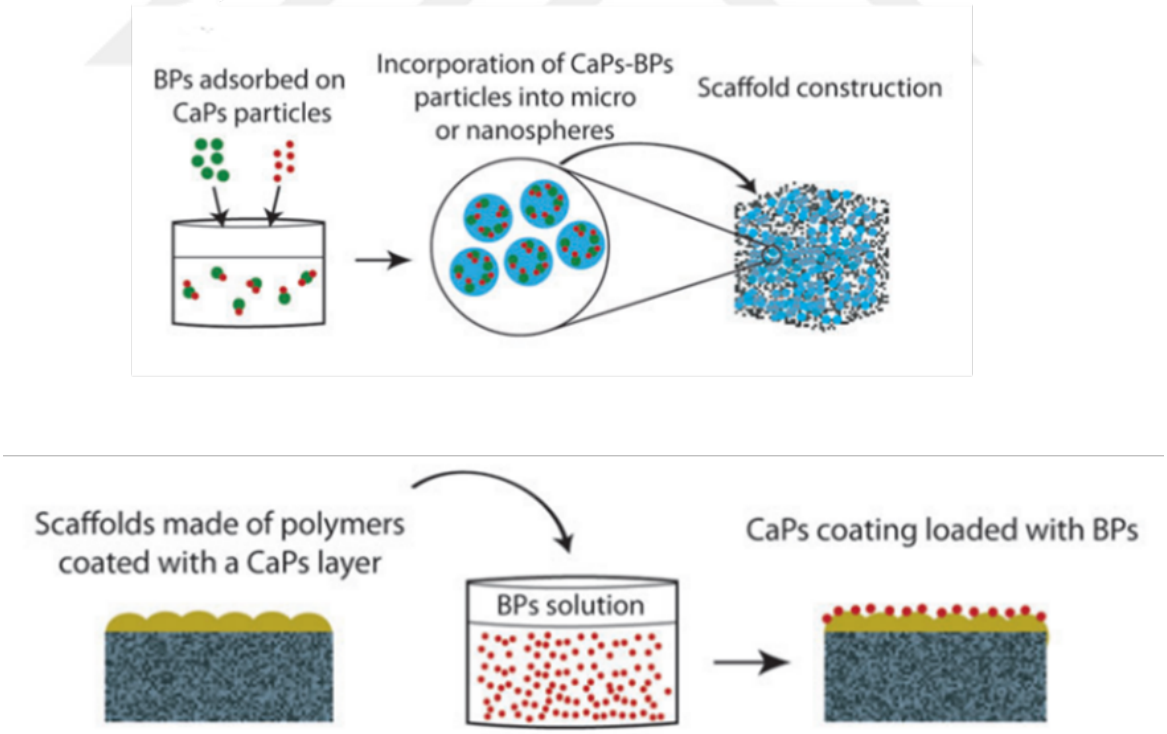

Figure 1.17. Different strategies for incorporating BPs in scaffolds. Reprinted from [102].

Another approach involves creating hydrogel scaffolds from polymers that incorporate BP groups into their backbones [110,111]. For instance, Ossipov et al. utilized a click reaction to synthesize a BP-functionalized hyaluronic acid polymer and examined its biomineralization characteristics. To investigate the biomineralization property, they immersed the hydrogel matrix in a $CaCl_2$ solution and synthesized biodegradable scaffolds containing nanosized Ca-BP coprecipitation, which incorporated both inorganic and organic functional groups [112].

While natural polymers such as chitosan (CS) can be used to function with BP in hydrogel scaffolds, there have also been those that BP- functionalize degradable synthetic polymers such as poly(lactic-co-glycolic acid) (PLGA) [113]. There are also studies using different divalent ions such as Mg^{2+} instead of calcium. Zhang et al. Composite hydrogels were obtained by combining bisphosphonate-modified hyaluronic acid (HA-BP) macromers with different divalent ions such as Mg^{2+}, Ca^{2+}, Co^{2+}, and Ni^{2+}, and examined in terms of mechanical and cell proliferation [114]

One of the most studied subjects is the construction of hybrid hydrogel scaffolds with BP containing polymers using CaP nanoparticles [115]. Nejadnik et al., reported a nanocomposite hydrogel formed using BP functionalized hyaluronan and calcium phosphate (CaP) showing good self-healing properties and biomineralization properties. They noted that the incorporation of BP groups into polymer backbones significantly increases the storage modulus of the hydrogels and self-healing properties to the hydrogels (Figure 1.18) [116].

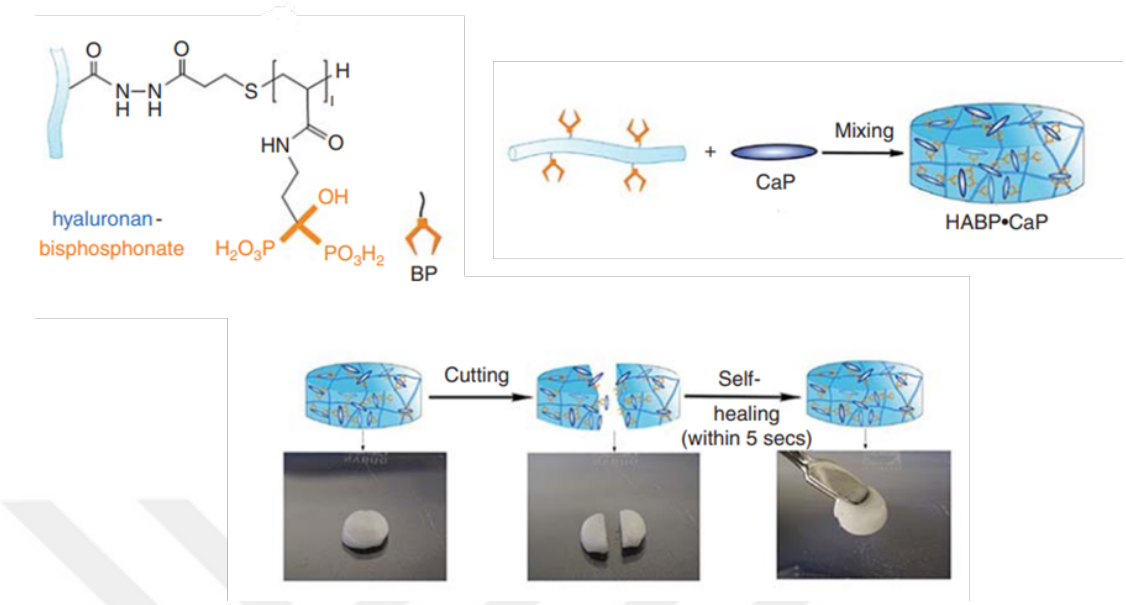

Figure 1.18. Bisphosphonated hyaluronan and calcium phosphate nanoparticles, hybrid HABP.CaP nanocomposite and its self-healing property. Reprinted from [116].

1.4.3. BPs for Drug Delivery Applications

Age-related conditions like osteoporosis, osteoarthritis, and bone cancer are significant health concerns. Various therapeutic substances have been formulated to address these bone diseases. However, given the widespread distribution of bones within the body, it is imperative to maintain a systemic drug concentration that enables the pharmacological effectiveness of the drug in the specific peripheral area [117]. As a result, adverse reactions frequently arise. Due to this factor, drugs designed to target bones specifically prove to be suitable agents for managing bone-related disorders. Compounds such as bisphosphonates, phosphonates, tetracyclines, and alizarin red exhibit a strong attraction to hydroxyapatite [118,119].

Much research is being conducted into the use of BP ligands for targeted delivery in a variety of applications, including therapeutic drug delivery, imaging probes, and radiotherapy [120,121]. Among the initial applications of bisphosphonate-conjugated drugs,

there is the incorporation of bisphosphonates with estradiol. Estradiol holds antiresorptive attributes and encourages bone generation. In rodent studies, linking estradiol to a bisphosphonate through an ester bond has demonstrated a decrease in bone loss without inducing a notable rise in uterine weight [122]. Subsequent to this, bisphosphonates have been linked with diverse medications for bone-specific targeting (Figure 1.19). Morioka and colleagues formulated distinct esterase or protease responsive conjugates, singling out one containing a phenolic carbamate group which exhibited enhanced efficiency compared to free estradiol [123]. Pan et al. demonstrated that bisphosphonates have been conjugated with large-scale drug carriers, like poly[N-(2-hydroxypropyl) methacrylamide] (PHPMA). In this context, alendronate was explored as a directing agent to transport the hydrophobic chemotherapeutic agent paclitaxel to bone tissues. PHPMA was employed as the foundational macromolecule to prolong circulation duration, prevent paclitaxel permeation across the blood-brain barrier, and facilitate accumulation at the tumor location via the enhanced permeability and retention (EPR) phenomenon. [124].

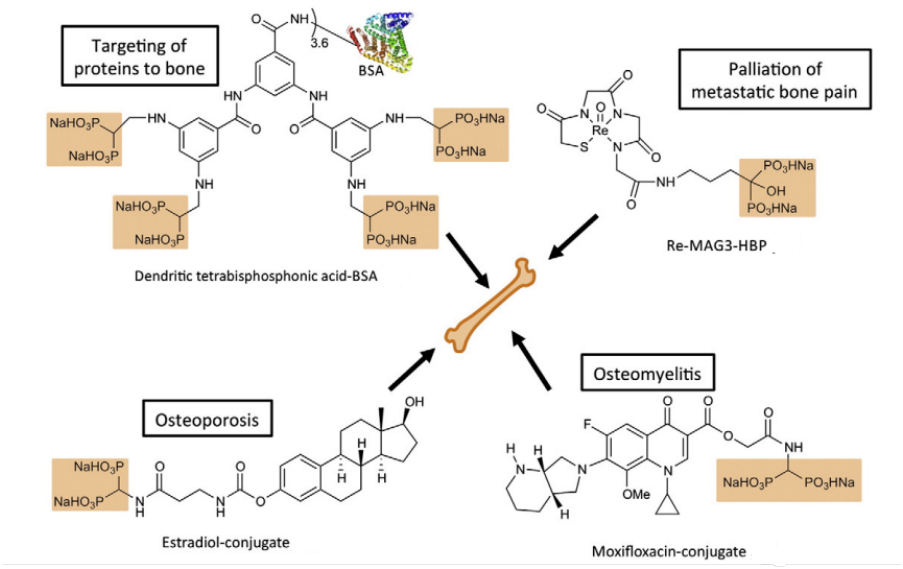

Figure 1.19. Examples of bisphosphonate–drug conjugates for bone targeting. Reprinted from [105].

2. OBJECTIVES AND SCOPE

Our work is focused on design of novel structural templates to produce biomaterials, especially to produce biomimetic materials on organic matrices for bone-related applications. In this study, pH sensitive and degradable hydrogels and cryogels based on poly(amido amine)s and poly(β-amino ester)s and functionalized with bisphosphonate, bisphosphonic acid, phosphate or carboxylate groups were synthesized and their properties were evaluated.

The biomaterials functionalized with bisphosphonate, bisphosphonic acid, phosphate or carboxylate groups are analogous to nucleation proteins in biological systems and provide apatite nucleation. Poly(amido amine)s and poly(β-amino ester)s are pH responsive, biodegradable and biocompatible polymers and can be used as organic matrices on design of structural templates for tissue scaffolds.

In the first two parts, poly (amido amine) macromers containing adjustable amount of bisphosphonate/bisphosphonic acid are synthesized and homo- and copolymerized with HEMA to prepare hydrogels/cryogels as potential materials for bone tissue engineering applications. In the third part, synthesis of four novel carboxylated diacrylate and diacrylamide macromeric crosslinkers based on meso-2,3-dimercaptosuccinic acid and their hydrogels with 2-hydroxyethyl methacrylate are reported. In the last chapter 10-Methacryloyloxydecyl dihydrogen phosphate (MDP) containing interpenetrating network hydrogels are synthesized.

The swelling, degradation, mechanical, biocompatibility, cell adhesion, metal binding and biomineralization characteristics of these hydrogels/cryogels were investigated to assess their suitability for potential applications in tissue engineering and the effect of functionalization.

3. ALENDRONATE-FUNCTIONALIZED POLY(AMIDO AMINE) CRYOGELS FOR BIOMEDICAL APPLICATIONS

The work described in this section has been published as [125]: Guven, M. N., G. Demirci, S. Altuncu, U. Gulyuz, O. Okay, H. Yagci Acar, and D. Avci, "Alendronate-functionalized Poly(amido amine) Cryogels of High-toughness for Biomedical Applications", *Polymer*, Vol.190, p. 122248, 2020.

3.1. Introduction

Cryogels, a subset of gels produced through cryopolymerization, offer the ability to incorporate, cultivate, or provide support to biological entities such as plasmids, viruses, cell organelles, and notably, cells. These gels are characterized by a microscale macroporous structure and exhibit greater elasticity, resilience, and adaptability when compared to nanoporous hydrogels. As a result, they find diverse applications across biotechnology, bioseparation, and biomedicine domains. These applications encompass tasks such as purifying and immobilizing proteins, nucleic acids, and polysaccharides; separating whole cells; facilitating environmental separations including heavy metal removal; and playing a role in tissue engineering endeavors.

Poly(amido amine)s (PAAs) are a class of synthetic polymers mainly obtained by Michael-type polyaddition of primary amines or bissecondary amines to bisacrylamides. They have biomedically important properties such as biocompatibility, biodegradability and non-toxicity. Synthetic flexibility of the polymerization reaction by using different bisacrylamides and amines enables incorporation of additional functionalities such as side chain substituents. PAA hydrogels and cryogels functionalized with bioactive and biomimetic compounds can be designed as scaffolds for tissue engineering.

In this part we reported, for the first time to our knowledge, synthesis of PAA macromers functionalized with alendronate as a BP, and their cryogels for potential bone tissue scaffold applications. We also investigated the effects of the macromer structure as well as BP content on the cryogel properties. We use two different alendronate concentrations to highlight the effect of BP functionalization on the swelling, degradation, mineralization, and mechanical properties of the cryogels.

3.2. Experimental

3.2.1. Materials and Methods

N,N′-methylene bisacrylamide, 5-amino-1-pentanol, 2-hydroxy-4′-(2-hydroxyethoxy)-2-methylpropiophenone (Irgacure 2959) and all solvents were purchased from Sigma-Aldrich and used as received. Phosphate buffered saline (PBS) was obtained from Biomatik Corporation (Canada). Sodium alendronate (ALE) was a kind gift from DEVA A.Ş. Dulbecco's Modified Eagle Medium (DMEM) (with l-glutamine and high glucose (4.5g/l)), penicillin/streptomycin (pen-strep), fetal bovine serum (FBS) and trypsin-EDTA were purchased from Diagnovum, Ebsdorfergrund (Germany). Thiazolyl blue tetrazolium bromide (MTT) was provided Gold Biotechnology (USA) and phosphate buffered saline (PBS) tablets was obtained from BBI Life Sciences (China). 96-Well plates were purchased from Nest Biotechnology (China). Saos-2 human osteosarcoma cells were a kind gift of Dr. Halil Kavakli (Department of Molecular Biology and Genetics, Koc University, Istanbul, Turkey). U-2 OS human bone osteosarcoma epithelial cells were a kind gift of Prof. Devrim Gozuacık (Department of Molecular Biology, Genetics and Bioengineering, Sabancı University, Istanbul, Turkey). C2C12 mouse myoblast muscle cells were obtained from ATCC, Manassas (USA).

The chemical structures of PAA macromers were confirmed by ^{1}H NMR and FTIR spectroscopies. ^{1}H NMR spectra were recorded on a Varian Gemini 400 MHz spectrometer

using deuterated water (D_2O) as solvent. FTIR spectra were collected between 400 cm^{-1} and 4000 cm^{-1} by a Thermo Scientific Nicolet 380 spectrometer. Potentiometric titrations of macromers were carried out using a WTW Inolab 720 pH meter and WTW SenTix 41 epoxy pH electrode at room temperature. Differential scanning calorimetry (DSC) (TA Instruments Q100) was used to determine the glass transition temperatures (Tg) of the macromers. All samples (5-10 mg) were sealed in aluminium pans and heated under nitrogen atmosphere from −80 °C to 80 °C with a scanning rate of 10 °C min^{-1}. The morphologies of the cryogel samples were examined with scanning electron microscopy (SEM) (FEI-Philips XL30) with an accelerating voltage of 7.0 kV. The lyophilized hydrogel samples were sputter coated with a platinum layer and their internal fracture surface was examined. The X-ray powder diffraction (XRD) analysis (Rigaku-D/MAX-Ultima diffractometer) was used to identify the mineral phase of materials. Degradation studies were done using an incubator shaker (VWR) operating at 37 °C and 200 rpm. The mineral content of the cryogels was determined from thermogravimetric measurements (TGA). TGA studies were performed using a Perkin Elmer STA 6000 machine. Samples were heated up to 700°C at a rate of 10 °C/min under nitrogen atmosphere.

3.2.2. Synthesis of PAA Macromers

PAA macromers were synthesized from N,N'-methylene bisacrylamide (MBA), 5-amino-1-pentanol (AP) and sodium alendronate (ALE) at a total concentration of 0.4 M in water/methanol mixture (v/v = 1/1) at 50 °C for 4 days. The macromers were prepared at two different molar ratios of MBA: AP: ALE, namely 1.1:0.9:0.1 and 1.1:0.7:0.3, which where denoted as MPAA1 and MPAA2, respectively. Typically, to prepare MPAA1 macromer, MBA (308 mg, 2 mmol), AP (171 mg, 1.66 mmol) and ALE (50 mg, 0.18 mmol) were dissolved in water/methanol mixture (v/v = 1/1, 9.6 mL in total) and stirred at 50 °C for 4 days under nitrogen. The solution was then diluted with water and dialyzed using a membrane with a molecular weight cut-off of 1000 in distilled water to remove the unreacted components. The product was obtained as a white solid after lyophilization.

A control macromer without ALE, denoted by MAAc, was also synthesized from MBA and AP at 1.1:1 molar ratio as described above. The yields of the products MPAA1, MPAA2, and MPAAc were 60, 50, and 65%, respectively.

3.2.3. pH Titration

PAA macromers, 50 mg of each macromer was dissolved in deionized water at a concentration of 1.0 mg/mL and the pH was adjusted to 2.0 using 2 M HCl solution. The macromer solution was titrated with 0.1 M NaOH with increments of 0.05 mL until pH 11.0. The increase in pH was recorded with a pH meter (WTW Inolab pH 720) at room temperature. The pK_b value was determined from the inflection point of the titration curve which responds to the pH value where 50% of protonated amine groups are neutralized.

3.2.4. Preparation of Cryogels

0.1 g PAA macromer and the photoinitiator Irgacure 2959 (5 wt %) were dissolved in 0.9 mL distilled water and placed into glass vials (diameter: 9 mm, thickness: 5 mm). The solutions were cooled to -18 ºC and held at this temperature for 6-8 hours. They were then exposed to UV light (365 nm, approximately 248 W/m^2) for 15 min in a photoreactor (Kerman UV/18, inner radius 15 cm, height 30 cm) containing 12 Philips TL 8 W BLB lamps on the perimeter. The cryogels were thawed at room temperature, lyophilized and weighed (W_i). Then, they were washed with ethanol and distilled water to remove unreacted macromers, dried under vacuum and weighed again (W_f). The percent gelation was calculated as

$$Gelation(\%) = \frac{W_f}{W_i} \times 100. \quad (3.1)$$

3.2.5. Swelling Studies

Dry cryogel samples were immersed in water, buffer solutions (pH 9, 7.4, 6.0, 2.0), and $CaCl_2$ (0.5 M) solution at 37 °C to reach equilibrium swelling. Then the samples were removed from the solutions, the excess solution was removed with a tissue paper and the swollen weight was measured. The samples were removed from the solution at pre-determined time intervals, blotted on filter paper and the swollen weight was measured. The increase in the weight of the samples was recorded as a function of time until equilibrium was reached. The degree of swelling (Q) was calculated using the equation:

$$Q = \frac{Ws-Wd}{Wd}\ x\ 100, \tag{3.2}$$

where W_s and W_d refer to the weight of swollen and dry samples respectively. The average data obtained from triplicate measurements were reported.

3.2.6. Degradation Studies

Each lyophilized cryogel was weighed as w_i and then immersed in PBS (pH 7.4) at 37 °C. After incubation at 37 °C for 1, 2 and 4 weeks, the samples were taken out, rinsed with water, freeze-dried and re-weighed as w_f. The degradation % was calculated as

$$Degradation\ (\%) = \frac{W_i-W_f}{W_i} \times 100. \tag{3.3}$$

3.2.7. *In vitro* Mineralization

Simulated Body Fluid (SBF) was prepared as described by Kokubo and Takadama [126]. A buffer solution (2 L, pH 7.4) containing 142 mM Na^+, 5 mM K^+, 1.5 mM Mg^{2+}, 2.5 mM Ca^{2+}, 147.8 mM Cl^-, 4.2 mM HCO_3^-, 1 mM HPO_4^{2-}, and 0.5 mM SO_4^{2-} was prepared in ultrapure water. 5 times concentrated SBF (5xSBF) was prepared as described by Chou

et al [127]. $CaCl_2$, $MgCl_2$, $NaHCO_3$ and $K_2HPO_4.3H_2O$ were dissolved in ultrapure water. Solution pH was lowered to 6 by adding 1M HCl to increase the solubility. Then Na_2SO_4, KCl and NaCl were added until the solution become clear. The final pH was adjusted to 6.0 with 1M HCl or 1M NaOH. Both solutions were filter sterilized (Millipore, sterivex filter unit, 0.22 μm) and stored at +4 °C.

Biomimetic mineralization of cryogels were carried out by two different methods. In the first method, cryogel samples were immersed in 0.2 M $CaCl_2$ solution for one day, then washed with deionized water 3 times, then placed in 15 mL falcon tubes containing 10 mL of freshly prepared and filtered SBF solution and incubated at 37 °C while shaking gently (50 rpm). The SBF was changed every two days. After 4 weeks the cryogel samples were taken out of the solution, rinsed with ultrapure water, and then freeze-dried to constant weight. In the other method, to accelerate the biomineralization process from 4 weeks to 2 days, the cryogels were immersed in 10 mL of 5xSBF and incubated at 37 °C for two days, during which 5xSBF being changed every day. The cryogels were then taken out of the solution, rinsed with ultrapure water and then freeze-dried to constant weight. The characterization of mineralized hydrogels was carried out by using TGA, FTIR, SEM and XRD analyses.

3.2.8. Mechanical Studies

Mechanical properties of cryogels in dry and equilibrium swollen states in water were investigated in a thermostated room at 23 ± 2 °C using uniaxial compression measurements on a Zwick Roell test machine with a 500 N load cell. The tests were carried out at a constant cross-head speed of 1 mm min^{-1}. The nominal σ_{nom} and true stresses σ_{true} ($= \lambda\sigma_{nom}$) were recorded, which are the forces acting per unit area of the undeformed and deformed gel specimens, respectively, and λ is the compression ratio. The strain was calculated as ε, the change in the length of the specimen with respect to its initial length, i.e., $\varepsilon = 1 - \lambda$. The compressive strength and strain at break of the cryogels were calculated from the maxima in

σ_{true} versus ε curves as detailed before [128]. Young's modulus *E* of the cryogels was calculated from the slope of stress−strain curves between 5 and 10% compression.

3.2.9. *In vitro* Cytotoxicity Assay

Impact of the degradation products of prepared gels on the viability of Saos-2, U-2 OS and C2Cl2 cell lines was evaluated using the standard MTT assay. The Saos-2 and U-2 OS cells were cultured in McCoy and DMEM complete medium, respectively, supplemented with 10% (v/v) FBS and 1% (v/v) pen-strep in a 5% CO_2-humidified incubator at 37 °C and passaged every 2-3 days. C2C12 cells were cultured in the same way using phenol red free-DMEM. For viability test, 100 µl degradation product in cell culture medium was added to each well of a 96 well-plate at a concentration between 12.5-200 µg/mL. Then, cells were seeded at a density of $15x10^3$ cells in 100 µl DMEM complete medium in each well and incubated at 37 °C in 5% CO_2 atmosphere. After 48 h incubation, the cell viability was assessed using MTT colorimetric assay. First, 50 µl of MTT solution (5 mg/mL in PBS) was added into each well with 150 µL of culture medium and incubated for 4 h. Then, the purple formazan crystals formed as a result of mitochondrial activity in viable cells were dissolved with ethanol:DMSO (1:1 v/v) mixture. Absorbance at 570 nm with a reference reading at 630 nm was recorded for each well using a Synergy-H1 microplate reader (BioTek Instruments Inc., Winooski, VT, USA). Cells which were not exposed to degradation products of gels were used as controls. 100% viability is assumed for the control cells. The relative cell viability was calculated by

$$Cell\ viability\ (\%) = \frac{Absorbance_{sample}}{Absorbance_{control}} \text{x } 100. \quad (3.4)$$

3.2.10. Statistical Analysis

Statistical analyses of the degradation products were conducted by using ordinary one-way ANOVA analysis of variance followed by multiple Dunnett's comparison test of

GraphPad Prism 8.3.0 software package (GraphPad Software, Inc., USA). All measurements were expressed as mean values ± standard deviation (SD) based on 8, 7 and 5 replicas for U-2 OS, Saos-2 and C2C12 cells, respectively. Significance between different alendronate concentrations was conducted by using non-parametric Mann-Whitney test of GraphPad Prism 8 software. All results were two tailed. $p < 0.05$ was accepted as statistically significant difference.

3.3. Results and Discussion

3.3.1. Synthesis and Characterization of PAA Macromers

Two novel bisphosphonic acid functionalized PAA macromers, MPAA1 and MPAA2, were synthesized by aza-Michael reaction of MBA with AP and ALE at a fixed MBA:amines feed molar ratio of 1.1:1 (Figure 3.1). AP serves as a hydrophilic diluent, as also used before in the preparation of many biomaterials, in particular for gene delivery applications [129]. We prepared PAA macromers at two different molar ratios of AP to ALE, namely 90:10 and 70:30 which are denoted as MPAA1 and MPAA2, respectively. The molar ratio of AP:ALE in macromers controls the bisphosphonic acid functionality and hence tunes the hydrophilicity, degradability, mineralization and mechanical properties of the resulting PAA cryogels. In the literature, PAAs are mainly prepared in methanol or methanol:water mixtures because these protic solvents facilitate the reaction by activating both the amine and the acrylate through hydrogen bonding [130,131].

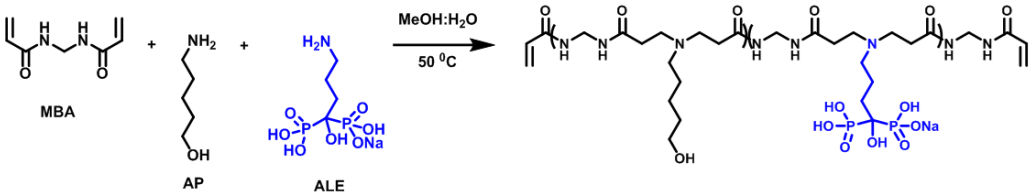

Figure 3.1. Synthesis of PAA macromers.

Here, we used equivolume mixture of methanol and water as the solvent because while sodium alendronate is soluble only in water, and MBA is slightly soluble in water but soluble in methanol, the resulting macromers are only soluble in this mixture. The total concentration of the reactants was fixed at 0.4 M which was the maximum reachable concentration in the solvent. A control macromer denoted by MPAAc was also synthesized under the same conditions in the absence of ALE in order to investigate effect of bisphosphonic acid functionality on the cryogel properties. The macromers were obtained as white solids in 50-65% yields after dialysis. The composition and properties of macromers are summarized in Table 3.1.

Table 3.1. Feed compositions during macromer synthesis, number average molecular weights (M_n) and and T_g of the macromers.

Macromer	**MBA (mol)**	**AP (mol)**	**ALE (mol)**	**Yield (%)**	**M_n[a] (g/mol)**	**T_g (°C)**
MPAA1	1.1	0.9	0.1	60	1365	4
MPAA2	1.1	0.7	0.3	55	1150	12
MPAAc	1.1	1.0	0	65	1900	-1

[a)]Calculated from ^{1}H NMR spectra

The structures of the macromers were confirmed using ^{1}H NMR (Figure 3.2, Figure 3.3, Figure 3.4) and FTIR (Figure 3.5) spectroscopies. The peaks at 6.26 and 5.83 ppm indicate the end-capping acrylamide protons. The characteristic peaks of methylene protons of ALE appear at 1.42 (y), 1.69 (z), 3.04 (x) and 3.27 (f) ppm. The peaks at 1.33 (o), 1.50

(p), 1.57 (n), 3.59 (r) and 2.54 (m) are due to methylene protons of AP. The average number of ALE repeating units was calculated via comparison of the areas of the double bond protons (6 protons) to methylene protons of ALE at 1.69 ppm (2 protons). The double bond protons (6 protons) were also integrated with respect to methylene protons of AP at 1.57 or 3.59 ppm (2 protons) to find average number of AP repeating units. From the total number of ALE and AP repeating units and the formula weights of ALE and AP repeat units, and the formula weight of the end group (MBA), number-average molecular weights M_n of ALE-functionalized macromers MPAA1 and MPAA2 were calculated as 1365 and 1150 g/mol, respectively, which are lower than the control macromer MPAAc prepared without ALE, 1900 g/mol. Moreover, yield of gelation decreased with increasing ALE content of the macromers. These all suggest higher steric hindrance of ALE as compared to AP, decreasing both the molecular weight and macromer yield. Degree of ALE substitution to macromers were found as 8 and 15 mol % for MPAA1 and MPAA2, respectively.

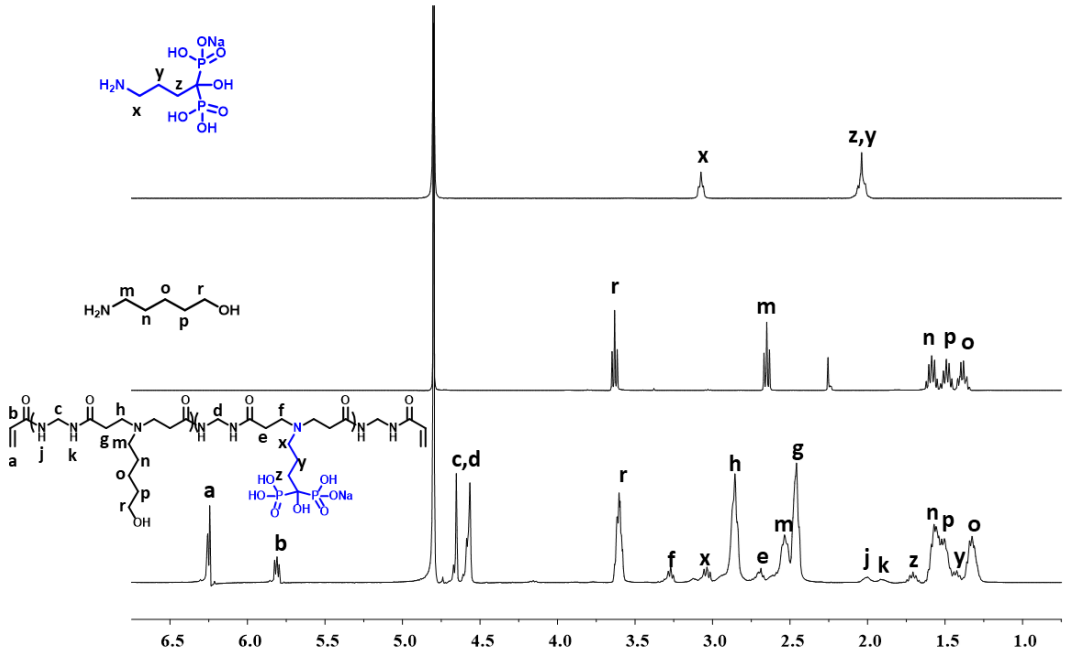

Figure 3.2. ^{1}H NMR spectra of sodium alendronate, 5-amino-1-pentanol and MPAA1 macromer.

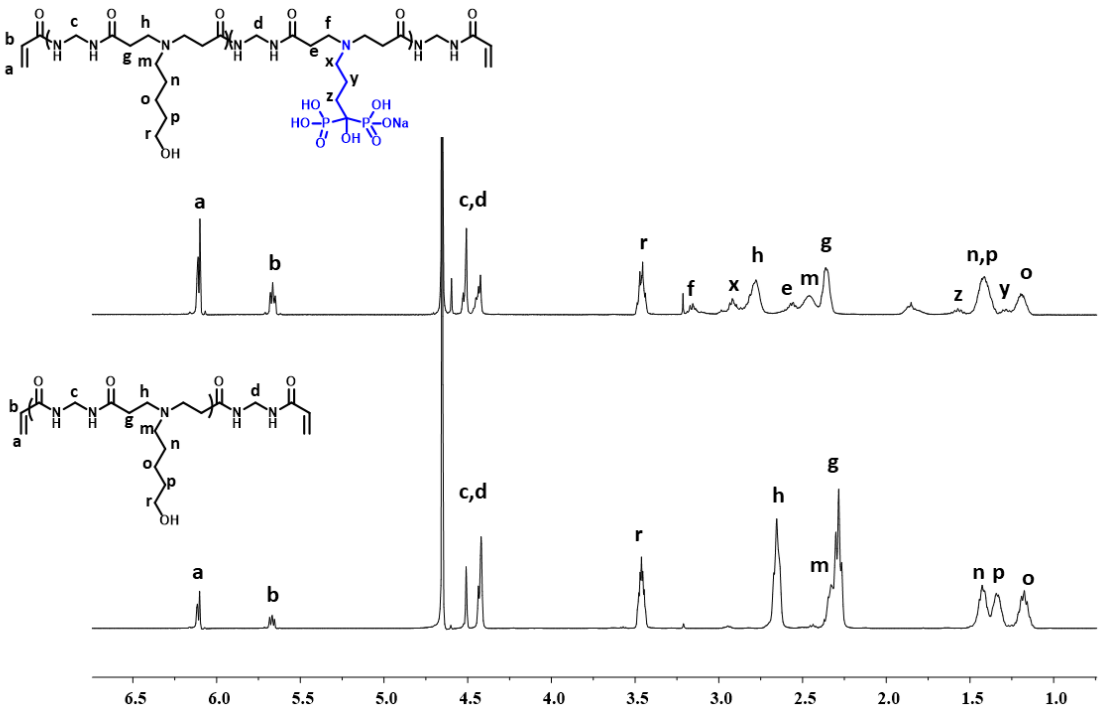

Figure 3.3. ^{1}H NMR spectra of MPAAc and MPAA2 macromers.

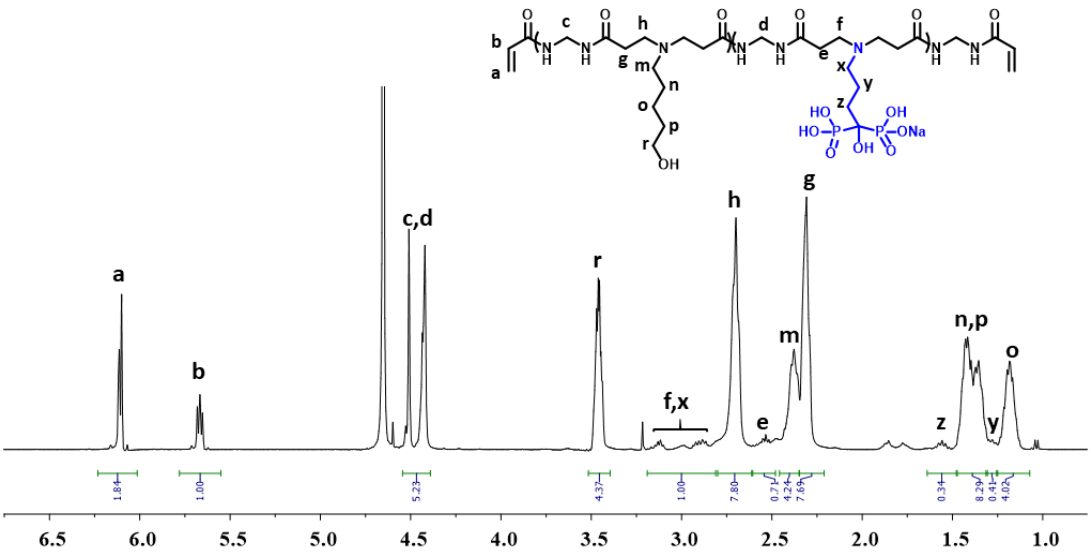

Figure 3.4. The integrated ^{1}H NMR spectrum of MPAA1.

The FTIR spectra of the macromers show broad peaks in the region of 3500−3100 and 3000−2800 cm^{-1} due to OH and NH stretching and strong peaks at 1712 cm^{-1} due to C=O stretching. Moreover, the strong bands at 1070 and 1020 cm^{-1} correspond to the symmetric and asymmetric vibration of P−O. The thermal properties of the macromers investigated by DSC revealed that their glass transition temperatures (T_g) well-correlate with their chemical structures (Table 3.1). The ALE functionalized and hence bisphosphonic acid salt-containing macromers exhibit a higher T_g as compared to the reference macromer, MPAAc, and T_g increases with increasing amount of ALE, i.e., -1, 4 and 12 °C for 0, 10, and 30 mol % ALE, respectively, due to the presence of steric hindrance of bulky side group and polar interaction.

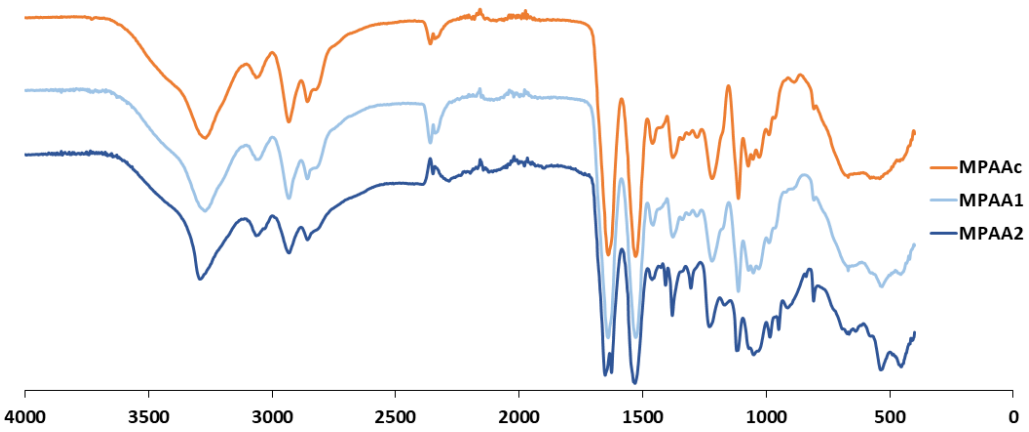

Figure 3.5. FTIR spectra of MPAAc, MPAA1, MPAA2 macromers.

PAAs are pH-responsive cationic polymers because of the tertiary amine functionality in their structures, i.e., the tertiary amines are unprotonated at a high pH (~9-10) and they become protonated at a low pH (~4). They have buffer capacity (usually defined as the percentage of amino groups that becomes protonated in the pH range 7.4 to 5.1) indicated by a relatively flat slope. The pH-responsiveness of the synthesized macromers was determined by titration method, results shown in Figure 3.6a, which is typical of the pH sensitivities of poly (amido amine)s as seen in the literature [132,133]. We found that the pH sensitivity of the present PAAs depends on the chemical structure and can be tuned by

changing components such as MBA and amines used in the macromer preparation. For example, when the hydrophilic alendronate groups were introduced, the pK_b values shifted to higher regions (7.01, 7.22 and 7.39 for MPAAc, MPAA1 and MPAA2). A similar structure effect was also reported for poly (β-amino esters) in the literature [134]. It was observed that for the macromers with longer alkyl chains, a higher proton concentration was needed to protonate the tertiary amine chains, thus pK_b values were shifted to lower regions. The effect of macromer structure was more significant on the pH-responsiveness plateau. The wider plateau of MPAAc indicates its better pH-responsive performance, whereas MPAA2 with higher hydrophilicity does not show a distinct plateau region. This can be explained by continuous deprotonation of bisphosphonic acid groups in the alendronate with an increase in pH as given in Figure 3.6B [135].

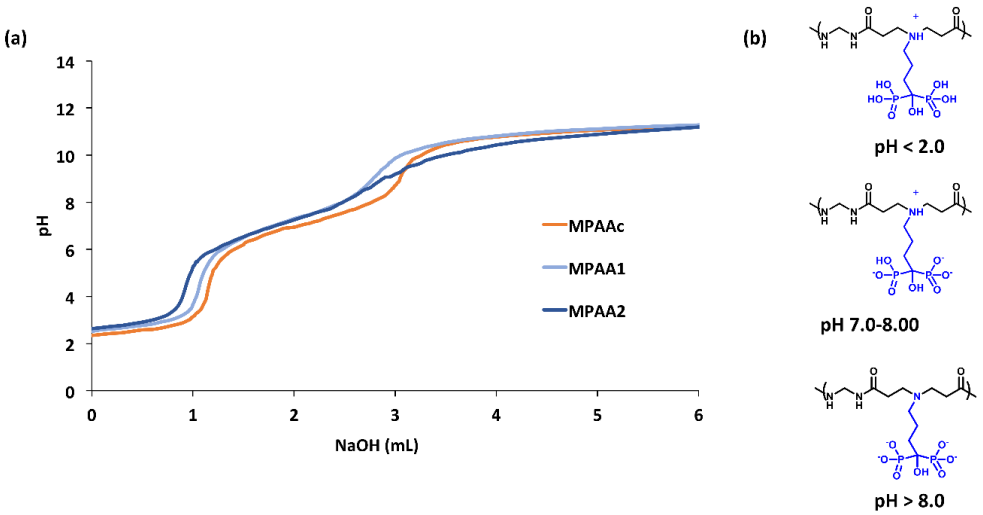

Figure 3.6. A) pH-responsive titration curves of MPAA1, MPAA2 and MPAAc in aqueous solutions and B) structures of alendronate units in macromers at different pH.

3.3.2. Synthesis and Properties of Cryogels

Cryogels were fabricated at a subzero temperature by free radical photopolymerization of aqueous 10 wt % macromer solutions. Because of the freezing of water in the reaction

solution, the macromers and initiator are concentrated in the nonfrozen liquid microphase. The gelation reactions thus occur in this unfrozen microphase surrounded by ice crystals acting as a template to produce the macroporous structure. As reported before, this technique allows fabrication of scaffolds with an interconnected macroporous structure. After around 15 min of the reaction, cryogels were thawed at room temperature and subsequently washed to remove unreacted macromeric precursors and the initiator. After drying, the gelation percentages were found to be in the range from 65% to 72%. The thermal properties of the cryogels were also studied using DSC. The glass transition temperatures T_g of the PAAc, PAA1 and PAA2 cryogels were found to be 37, 52 and 64 °C, respectively, well correlated with those of their macromers. There are many factors affecting properties of cryogels. The temperature at which cryogelation occurs, polymerization time, type of crosslinking, contents of monomers used, and freezing rate are variables determine physical properties of cryogels. In our work most of the synthesis parameters (temperature, time rate of freezing, etc.) were constant, giving cryogels with similar pore sizes of 38, 44 and 43 µm for PAAc, PAA1 and PAA2, obtained from SEM images (Figure 3.7); this qualifies them as supermacroporous.

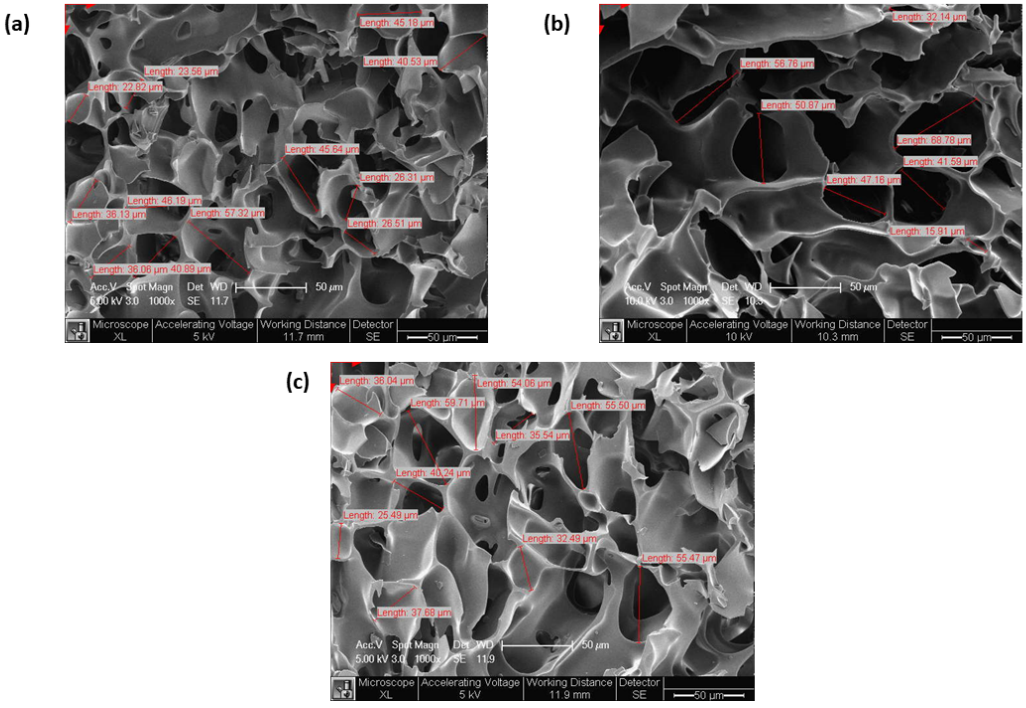

Figure 3.7. SEM images of A) PAAc, B) PAA1 and C) PAA2 cryogels.

3.3.3. Swelling of Networks

Cryogels were subjected to swelling measurements in distilled water, $CaCl_2$ solution (0.5 M) and different buffers with pH 2, pH 6, pH 7.4 and pH 9. For all cryogels, equilibrium swelling is reached very fast, within 5 min, as expected due to their macroporous structures facilitating the diffusion of water though the pores into the 3D cryogel network. Swelling percentages of the cryogels after 24 h (Fig. 3.8) show that the swelling percentages of cryogels are similar in water, pH 7.4 and pH 9; however, the swelling gets higher as the medium becomes more acidic. At each pH and in $CaCl_2$, the swelling of PAA1 is highest.

The swelling is affected by both the molecular structure and molecular weight of the macromer precursors. The difference in the swelling behavior of the control cryogel (PAAc) and the others can be explained by hydrophilic/hydrophobic properties of the cryogels. Although the PAAc control has the highest molecular weight which leads to the lowest crosslink density, ALE containing PAA1 cryogel shows a higher water uptake because of its ionic bisphosphonic acid groups at the side chain of polymer backbone. The higher ionic strength in the cryogel can cause a higher degree of swelling of PAA1 cryogel than the non-ionic PAAc cryogel. Although MPAA2 possesses a higher amount of ALE at the backbone, its cryogels swelled less at pH 2 because the molecular weight of MPAA2 is lower than MPAA1 and MPAAc. The protonation of the amino groups creates positively charged groups, giving rise to stronger swelling. The lower swelling at higher ALE concentrations can be explained by a decrease in total charge due to the ALE functionality, whose effect is attracting the chains together electrostatically. As the pH increases ionization of four hydroxyl groups of ALE occurs, creating also negative charge density on the polymer, while deprotonation of amine groups decreases the positive charge on the polymer. The magnitude of the total charge of the hydrogel stays nearly the same for a comparatively wide range of pH, leading to almost constant swelling between pH 7 and 9. When the hydrogels were immersed in 0.5 M $CaCl_2$ solution, exchange of sodium ions with calcium is expected. The interaction between bisphosphonic acid groups and Ca^{2+} ions may form physical crosslinking. Therefore, PAA2 gels with higher ALE content swelled less in $CaCl_2$ solution compared to PBS.

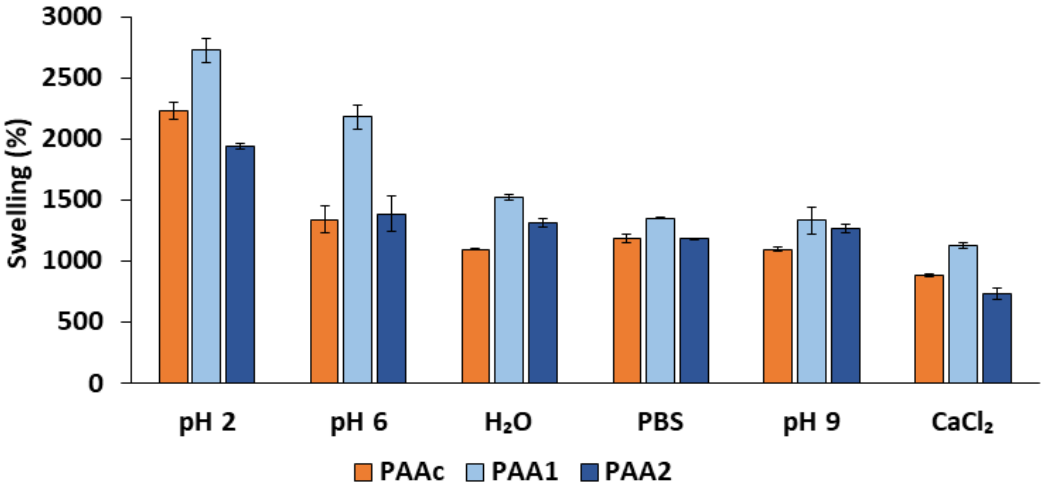

Figure 3.8. Swelling percentages of PAA cryogels in water, buffer solutions (pH 9.0, 7.4, 6.0, 2.0) and $CaCl_2$ (0.5 M) after 24 h. All the experiments were carried out in triplicates (n=3) and mean average values with standard error (±SD) are represented in the error bars.

3.3.4. Degradation Studies

The degradation behavior of the cryogels was investigated in PBS (pH 7.4) at 37 °C (Figure 3.9a). The mass loss of the gels was found to change between 5 to 38% in four weeks, and it decreases as the molecular weight of the precursor macromer is decreased, the effect of which dominates over other possible effects of the chemical structure such as hydrophilicity coming from incorporation of sodium alendronate. For example, the mass loss of gels made from MPAAc was found to be 38% in 4 weeks whereas for MPAA1 and MPAA2 gels the respective weight losses were 30 and 14%. This might be explained by the higher number of hydrolytically susceptible linkages between the crosslinks for higher molecular weight macromers. During degradation in PBS, pore size of the gels increased significantly. For example, after 4 weeks in PBS, the pore size of PAA1 increased from 44 µm to 54 µm (Figure 3.9C).

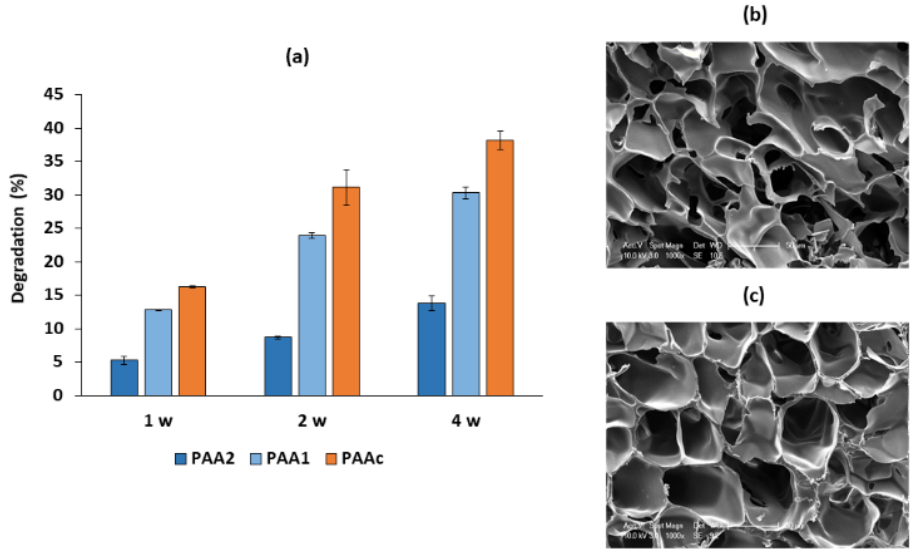

Figure 3.9. A) Degradation behaviour of cryogels in PBS (pH 7.4) at 37 °C, B) SEM images of PAA1 cryogel before and C) after 4 w degradation.

3.3.5. Mineralization of Cryogels

The synthesized cryogels were evaluated for their ability to mineralize apatite. It is expected that binding of Ca^{2+} to the ALE groups of the cryogels will lead to the initial nucleation for the mineralization of the cryogels. According to Hamai et al., Ca^{2+} incorporation into the polymer may accelerate apatite formation in SBF because of increase in Ca^{2+} release from the polymer [136]. Therefore, increasing ALE concentration of the cryogels may promote mineralization. The studies by Phadke et al. also showed that small changes in matrix interfacial hydrophobicity independent of functionality can profoundly influence the Ca^{2+} binding and formation of hydroxyapatite-like mineral phases on hydrogel matrices [137]. The synthesized cryogels were mineralized using two methods: (a) immersion in SBF, (b) immersion in 5xSBF. SBF was chosen because it closely mimics the ionic concentrations and pH typically observed in plasma [138]. Because the biomimetic mineralization occurs slowly, the experiments were also conducted at high SBF concentrations (5xSBF) in order to increase the rate of mineralization [139]. Before soaking

in SBF for 4 weeks or 5xSBF for 2 days, the cryogels were immersed in 0.2 M $CaCl_2$ solution to exchange sodium with calcium. Mineralization of the cryogels was studied by using SEM, FTIR, XRD and TGA.

In order to observe the level of mineral deposition, we performed TGA measurements. The TGA thermograms of PAA2 cryogels before and after mineralization and the control cryogel before mineralization are shown in Figure 3.10a. They all show an initial weight loss starting from room temperature up to 100 °C due to removal of adsorbed water. The main weight loss occurred between ca. 250 and 400 °C due to degradation of the main chain. The PAA2 cryogel had higher residual weight (43%) than the control cryogel (18%) at 500 °C and above. The difference in the residual weight was due to ALE amount in the cryogel. In case of mineralized PAA2 cryogels the residual weights were highest (55%) due to the amount of deposited mineral. Additionally, the main weight loss was shifted to higher temperature (from ca. 230 to 254 °C) probably due to the higher thermal stability of the hybrid material.

Mineralization of cryogels were also investigated by FTIR and XRD analysis. FTIR spectra of calcium phosphate materials are dominated by the two orthophosphate (P-O) absorption bands at 1130-1030 cm^{-1} and 600-560 cm^{-1}. In HAP, two major and one minor bands corresponding to phosphate were observed: 1016 (ν_3PO mode), 559, 600 (ν_4PO mode) and 964 cm^{-1} (ν_1PO mode) [140]. The FTIR spectra of the cryogels contained two broad peaks at around 1017-1050 and 530 (P-O) cm^{-1}. When the cryogels were mineralized, we observed an increase and slight shift in both bands and the appearance of a new band at 965 cm^{-1} which is related to the HAP spectrum (Figure 3.10C). These changes become clearer with increase in alendronate concentration; PAA2 was found to mineralize faster compared to PAA1. Here, we suggest the formation of a calcium phosphate precursor such as dicalcium phosphate dehydrate (DCPD) within the cryogel which can hydrolyzes to apatite subsequently [141]. Surprisingly, the IR spectrum of mineralized PAAc was found to be similar to that of HAP. In the literature it was observed that not only polyanions, but also polycations such as linear PEI have a strong influence on CaP mineralization [142]. LPEI accelerates the transformation brushite ($CaHPO_4,2H_2O$) (DCPD) to HAP by acting as a

proton acceptor, which takes up the protons released from either the calcium phosphate precipitate during the phase transformation or from ions present in solution during a presumed, but so far not directly observed, dissolution–reprecipitation process [143]. XRD spectra of mineralized cryogels also indicated that the mineral grown via incubation in was apatitic (Figure 3.10B), as seen from the peaks at 27 and 32° [144].

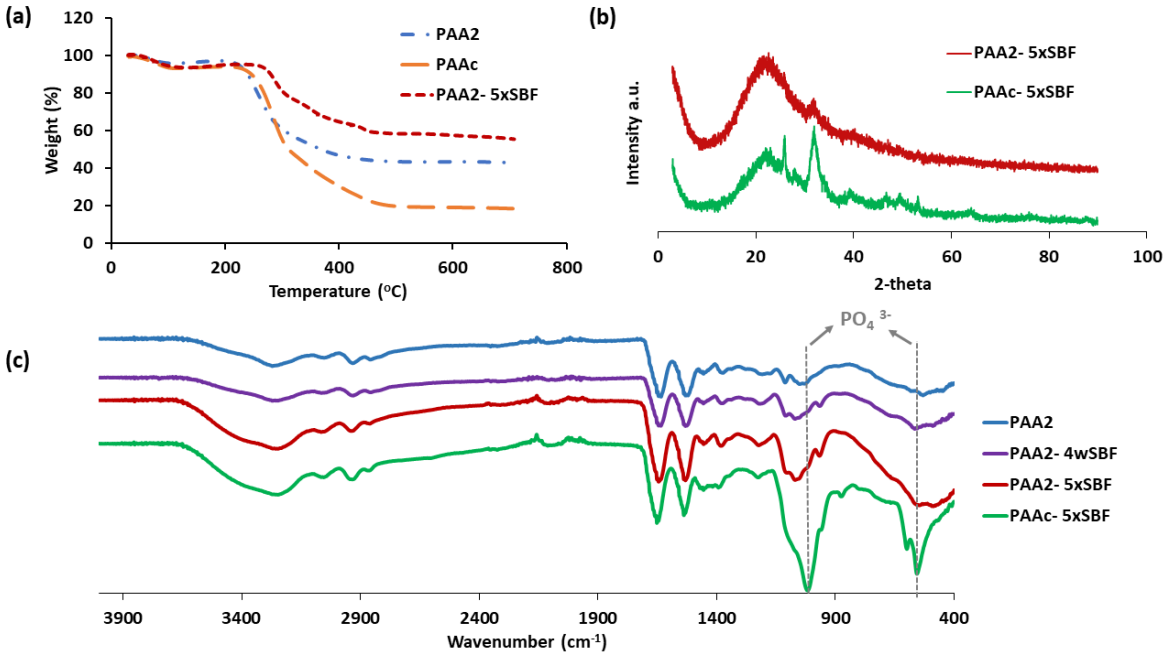

Figure 3.10. A) TGA thermograms of PAA2 (before and after mineralization in 5xSBF) and PAAc (before mineralization) cryogels, B) XRD patterns of mineralized PAA2 and PAAc cryogels at 2 days in 5xSBF, C) FTIR spectra of PAA2 (before and after mineralization in 5xSBF and SBF) and PAAc (in 5xSBF) cryogels.

Although FTIR spectroscopy is a non-invasive technique for molecular characterization of the mineralized samples, it does not provide morphological information. Therefore, we used SEM images to study the morphology of the minerals (Figure 3.11). The freeze-dried cryogel samples were used for SEM analysis. The samples were opaque before mineralization and did not change their appearance after mineralization. SEM images of PAA1 cryogels after 4 weeks of mineralization in SBF showed mineral layers (Figure 3.11B). The amount of mineral deposited was more significant for PAA2 cryogels after 2

days of mineralization in 5xSBF (Figure 3.11C). The control sample displayed plate like crystalline morphology (Figure 3.11D).

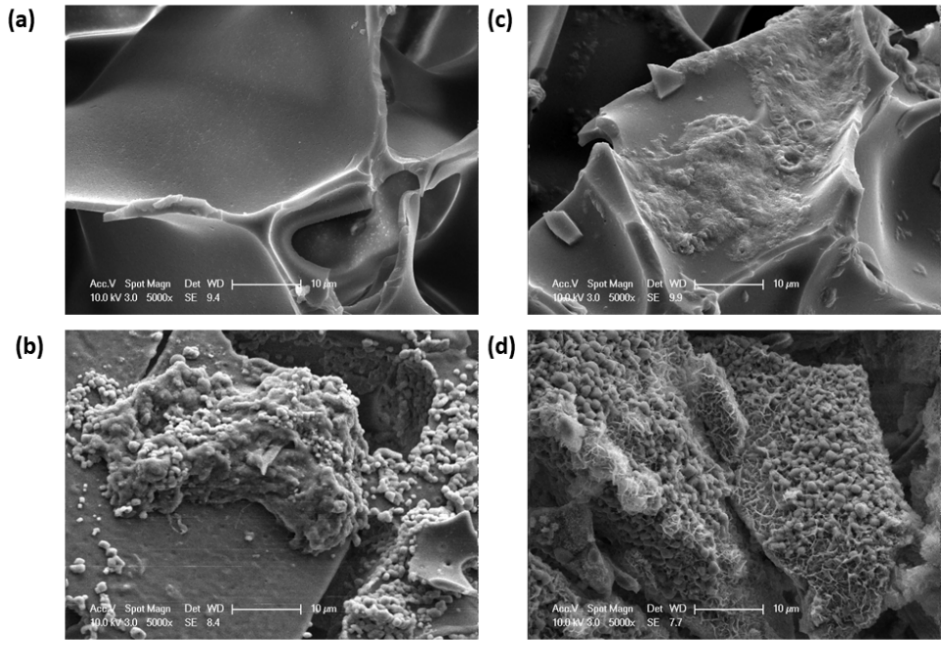

Figure 3.11. SEM images of A) PAA1 cryogel before mineralization, B) PAA1 cryogel after 4 weeks of mineralization in SBF, C) PAA2 cryogels after 2 days of mineralization in 5xSBF, D) PAAc cryogel after 2 days of mineralization in 5xSBF.

3.3.6. Mechanical Properties

The effect of BP content of the cryogels on their mechanical strength was investigated by uniaxial compression tests. Figures 3.12 A,B show nominal stress (σ_{nom})–strain (ε) curves and the mechanical parameters of water-swollen cryogels, respectively. All cryogels without (PAAc) or with BP (PAA1 and PAA2) sustain up to around 97% strain without any crack development reflecting their high toughness under compression load. Increasing BP content also increases both Young's modulus E and compressive strength σ_f of the cryogels. For instance, the modulus E of the reference BP-free PAAc cryogel is 5±1 kPa whereas it

increases to 10±1 and 9±1 kPa for ALE-functionalized PAA1 and PAA2 cryogels, respectively. Their compressive strengths σ_f are 1.1±0.3, 1.6±0.2, and 2.2±0.4 MPa for PAAc, PAA1, and PAA2, respectively, revealing that σ_f increases in the order of PAAc < PAA1 < PAA2, i.e., in the order of increasing ALE content of the cryogels. Thus, the results show increasing stiffness and strength of the cryogels after their functionalization with ALE. The inset to Figure 3.12 which is zoom in to the stress-strain data below 50 % strain reveals the appearance of a plateau-like regime above 20% strain. Such a behavior was previously reported in silk fibroin cryogels and reflects squeezing out pore water from cryogels and hence, the plateau stress corresponds to the mechanical strength of the cryogel network [145,146]. Because the mechanical strength of the present cryogels increases after their functionalization with ALE, the plateau stress also increases with increasing ALE content (Figure 3.12A).

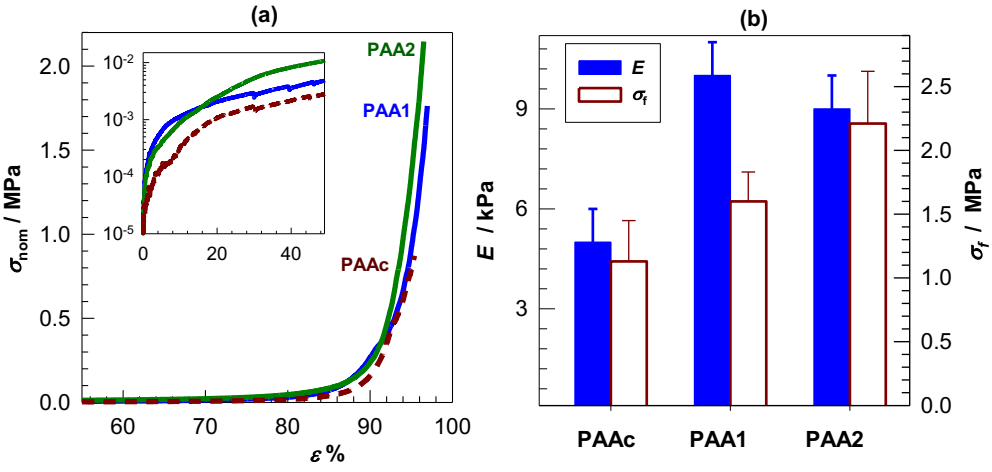

Figure 3.12. Stress – strain curves A) and the mechanical parameters E and σ_f A) of PAAc, PAA1, and PAA2 cryogels swollen in water. The inset in A) is zoom in to the data below 50 % strain to highlight the initial mechanical properties.

The mechanical tests were also conducted on dry cryogels. Similar results were obtained except that both Young's modulus E and compressive strength σ_f attained much higher values. For instance, the modulus E of BP-free PAAc cryogel in dried state is 19±8 kPa whereas it increases to 47±7 and 327±63 kPa for ALE functionalized PAA1 and PAA2

cryogels, respectively (Figure 3.13). A similar trend was observed for the compressive strength σ_f of dried cryogels; σ_f was found to be 9.6±0.6, 12±2, and 11±1 MPa for PAAc, PAA1 and PAA2 cryogels, respectively.

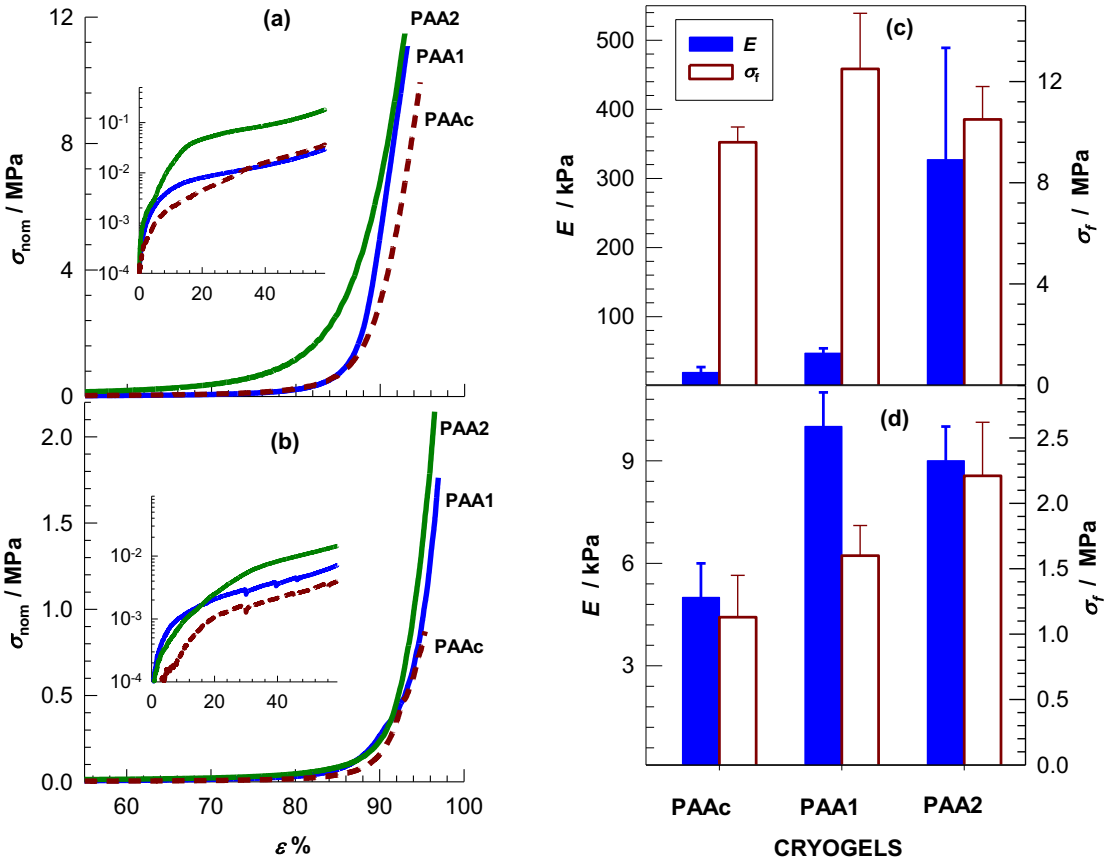

Figure 3.13. Stress – strain curves (A, B) and the mechanical parameters E and σ_f (C, D) of PAAc, PAA1, and PAA2 cryogels in dry (A, C) and swollen states (B, D). The inset in (A) and (B) are zoom in to the data below 50 % strain.

To highlight the effect of mineralization, mechanical tests were also conducted on cryogel specimens immersed in SBF and 5xSBF solutions corresponding to slow and fast mineralization procedures, respectively. The results are shown in Figures 3.14 a,b where the stress-strain curves and the mechanical parameters of the reference PAAc and ALE-functionalized cryogels PAA1 and PAA2 are presented. As expected, the mechanical properties of the reference PAAc hardly changed within the limits of experimental error after

mineralization. However, mineralization significantly affects the mechanical performances of both ALE-functionalized cryogels. For instance, the modulus *E* of PAA2 cryogel increases from 9±1 kPa to 41±2 and 54±21 kPa after mineralization in SBF and 5xSBF, respectively.

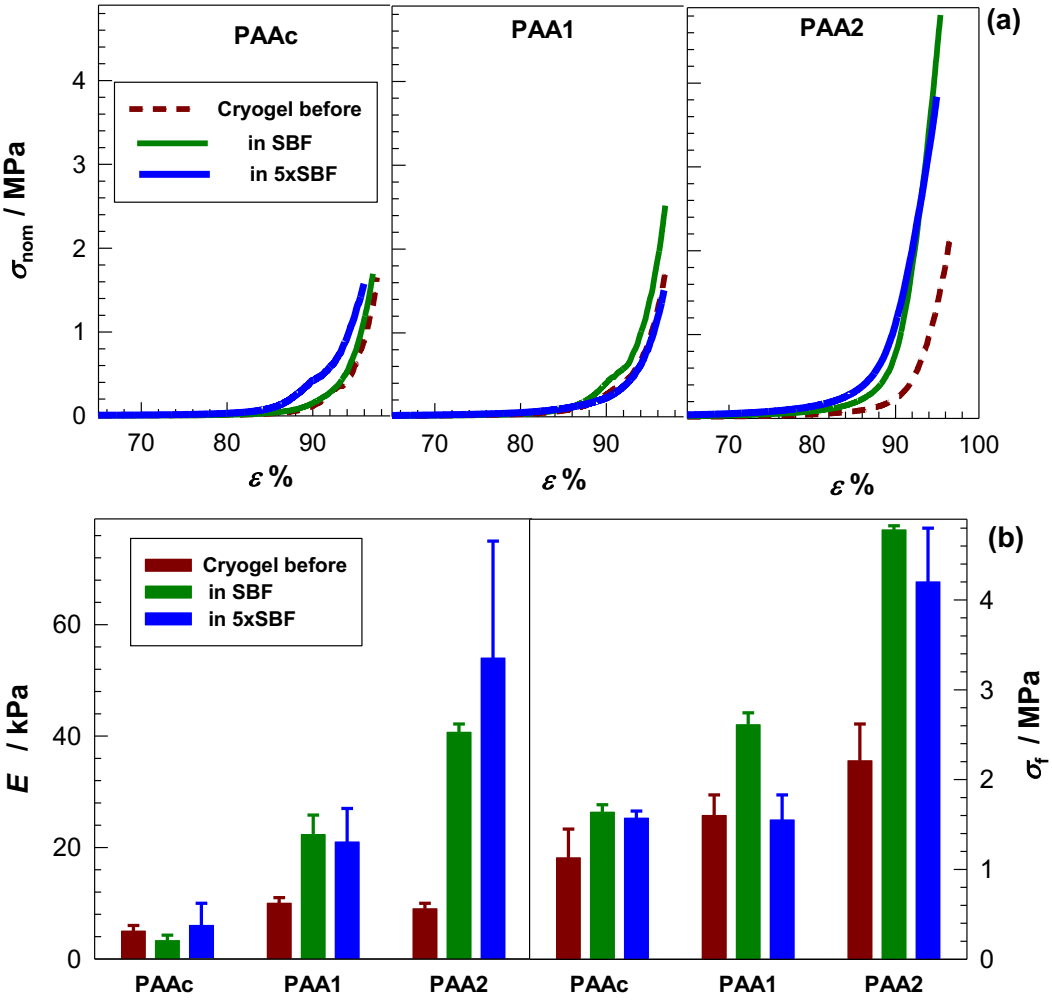

Figure 3.14. Stress – strain curves A) and the mechanical parameters *E* and σ_f B) of PAAc, PAA1, and PAA2 cryogels before and after mineralization in SBF and 5xSBF.

The significant increase of the modulus indicates formation of additional cross-links within the cryogel network due to the binding of Ca^{2+} to the ALE groups and hence acting as cross-links. Indeed, similar results were obtained when cryogels were immersed in

aqueous $CaCl_2$ solution (Figure 3.15). The modulus E of ALE-functionalized PAA2 increases from 9±1 to 25±8 kPa in $CaCl_2$ solution reflecting formation of ionic cross-links. The compressive strength σ_f of the cryogels also increases after mineralization or in $CaCl_2$ solution but at much lesser extent (Figures 3.14, 3.15). For instance, σ_f of PAA2 cryogel is 2.2±0.4 and 4.2±0.6 MPa before and after mineralization in 5xSBF, respectively.

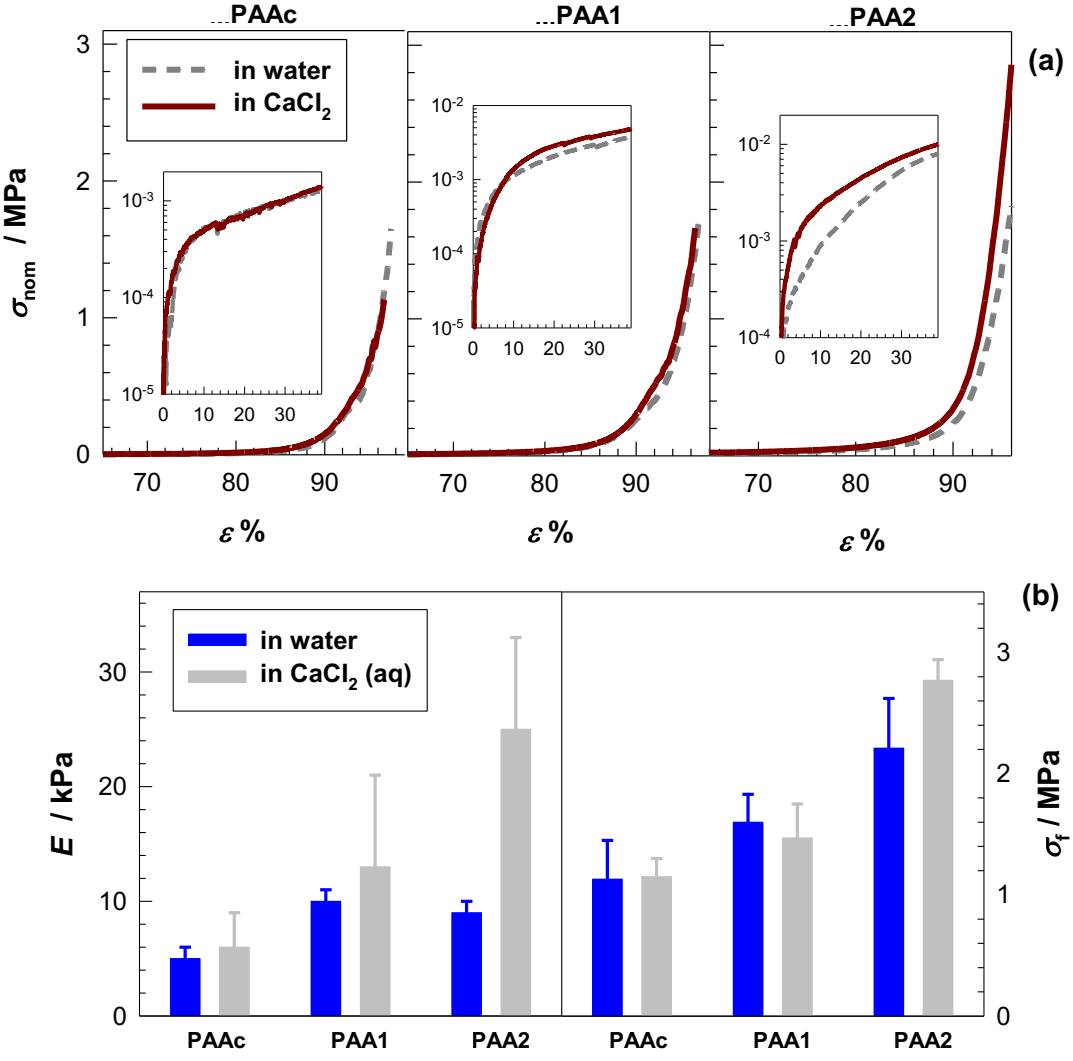

Figure 3.15. Stress – strain curves A) and the mechanical parameters E and σ_f B) of PAAc, PAA1, and PAA2 cryogels before and after immersion in aqueous $CaCl_2$ solution.

3.3.7. *In vitro* Cytotoxicity of Cryogel Degradation Products

Potential dose (12.5-100 µg/mL) dependent cytotoxicity of the PAA cryogel degradation products was evaluated on Saos-2, U-2 OS and C2Cl2 cells using the standard MTT assay, which indicates cell viability (Figure 3.16). Cell viability above 80% is assumed as noncytotoxic according to ISO 10993–5 [147]. Since these cryogels have ALE in their composition, we also studied the influence of free ALE on the cell viability. PAAc lacks ALE and used as a control. Degradation products of PAAc did not reduce the viability of the cancer cell lines in a significant amount after 48 h exposure. Degradation products of PAA2, which has 30% ALE in its feed composition, reduced the viability of U-2 OS cells in a dose dependent manner in a greater extent compared to PAA1 with 10% ALE in the feed. Viability of U-2 OS was 77% at the lowest dose and then 66-68% for the rest of the doses in case of PAA2. This toxicity is mostly due to ALE component since PAAc did not exert any toxicity. Indeed, ALE caused a significant reduction in cell viability in all three cell lines. For example, viability of U-2 OS was 68% when treated with 100 µg/mL PAA2 and 44% when treated with 25 µg/mL free ALE. Viability of U-2 OS cells treated with PAA1 degradation products were all above 89 % with no significant difference between doses due to lower content of ALE. ALE is not as toxic to SaOS-2 but still viability was dropped to 70-78% in the whole dose range. Parallel to this, viability of Saos-2 cells were above 90% when treated with PAA1 and significant reduction was observed with 50-100 µg/mL PAA2 degradation products. It was reported that ALE has an anti-invasive effect on some cancer cell lines including Saos-2 and U-2 OS [148]. This effect of bisphosphonates is usually attributed to inhibition of matrix metalloproteinases [148,149]. It was also reported that ALE induces apoptotic cell death, more in U-2 OS than Saos-2 in a study performed with 50-100 µM ALE with maximum cell death of 13.5% with 150 µM ALE after 48 h. Concentration of ALE in our study is between 50-400 µM, hence reduction in cell viability that we observe as a function of ALE agrees with these reports. Interestingly in C2C12, healthy muscle cells, 100 µg/mL PAAc degradation products reduced the viability to 80% and PAA1 showed more toxicity than PAA2 (78% versus 95% at 100 µg/mL). Indeed, PAA2 treated cells were not different than control cells and PAA1 did not show significant difference from the control at the doses lower than 100 µg/mL. ALE reduced the viability from 76 % to 57 % in

a dose dependent manner. It may be possible to say that PAAc component causes some toxicity in C2C12 cells while it was completely safe in the cancer cell lines in this study.

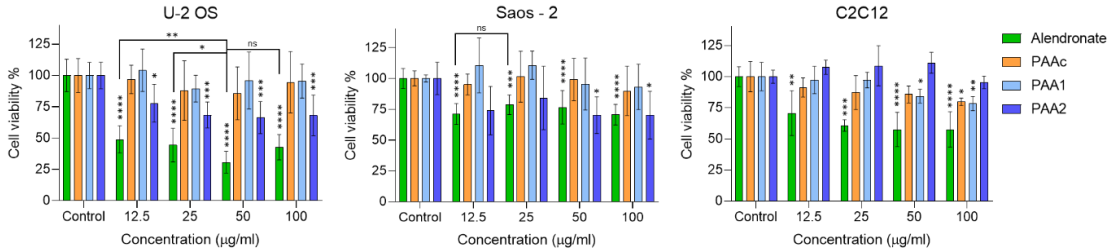

Figure 3.16 Viability of U-2 OS, Saos-2 and C2C12 cell lines treated with alendronate and degradation products of PAAc, PAA1 and PAA2 for 48 h. Viability was tested with MTT assay. Statistical significance: (*) p<0.0332, (**) p<0.021, (***) p<0.0002, (****) p<0.0001.

3.4. Conclusions

Two novel ALE and AP functionalized macromers with different compositions and a control macromer functionalized only with AP were synthesized and photopolymerized under cryogenic conditions to form cryogels to control the cryogel swelling, degradation, mechanical properties and their ability to support mineralization for biomedical applications. The swelling behavior of the cryogels is influenced both by molecular weight of the macromers and by the ion content determined by the ALE content and pH. The degradation percentages of the gels (5 to 38% in four weeks) are mostly affected by the molecular weight of the precursor macromer and overcome other possible effects of the chemical structure such as hydrophilicity coming from incorporation of sodium alendronate. The ALE functionalized cryogels have the ability *in vitro* growth of apatite, mostly DCPD and the extent of mineralization is influenced by the ALE content in the cryogel. Surprisingly the control cryogel, without ALE functionality, allows nucleation of HAP.

Mechanical tests reveal that all cryogels are very tough and sustain up to around 97% compression without any crack development. The stiffness and strength of the cryogels increase after their functionalization with ALE groups. Both Young's modulus and compressive fracture stress of the cryogels increase with increasing ALE content and they attain maximum values of around 10 kPa and 2.2±0.4 MPa, respectively. A significant increase in the modulus was also observed after mineralization of the cryogels in SBF due to the binding of Ca^{2+} to the ALE groups acting as physical cross-links. Safety of the degradation products seems to be dose, composition and cell type dependent. Most importantly, ALE between 12.5-100 μg/mL range reduces the viability of both U-2 OS and Saos-2 cancer cell lines and healthy C2C12 muscle cells and the major contributor to toxicity of cryogels seems to be the ALE component. However, degradation products of all cryogels are safe at 25 μg/mL and below. Above this dose, PAA2 with high ALE content is safe for C2C12 but toxic to cancer cells. Such cryogels may allocate toxic doses of ALE at the cancerous bone tissue and at the same time may provide new bone generation. Alternatively, cryogels with safe ALE content may be solely used for mineralization. Overall, these three PAA macromers and their cryogels have potential to be used as scaffolds for tissue engineering applications.

4. BISPHOSPHONATE-FUNCTIONALIZED POLY(AMIDO AMINE) POLYMERS, MACROMERS AND THEIR 2-HYDROXYETHYL METHACRYLATE HYDROGELS AS TISSUE ENGINEERING SCAFFOLDS

The work described in this section has been published as [150]: Guven, M. N., B. Balaban, G. Demirci, H. Yagci Acar, O. Okay, and D. Avci, "Bisphosphonate-functionalized Poly(amido amine) Crosslinked 2-Hydroxyethyl Methacrylate Hydrogel as Tissue Engineering Scaffold", *European Polymer Journal,* Vol.159, p. 110732, 2021.

4.1. Introduction

Bone tissue engineering (BTE) requires 3D porous scaffolds which mimic bone structure, providing a system for cells to attach, proliferate, and form an extracellular matrix (ECM). Biocompatibility, biodegradability, mechanical strength, adjustable pore size, facility of cell adhesion and proliferation are essential properties for suitable scaffolds. Polymer-based bone scaffolds possess most of these properties, which can be controlled by composition and preparation of the materials, e.g. modifying their functional groups.

One of the frequent method for achieving bone mineralization via polymers or hydrogels in BTE applications is to functionalize the backbone of polymers with anionic groups such as phosphoric acid (PO_4), phosphonic acid (PO_3H_2), bisphosphonic acid ($(OH)_2$-(O)P-C-P(O)-$(OH)_2$) or carboxylic acid (COOH). These negatively charged groups act as nucleation points to Ca cations and enhance HAP crystal deposition. Among these anionic groups, bisphosphonic acids (BPAc) stand out. In the literature, the term bisphosphonate is usually used as shorthand for bisphosphonic acid and is abbreviated as BP. Since in this work we have to distinguish between the bisphosphonate and bisphosphonic acid functional groups we will abbreviate them as BP and BPAc, respectively.

The objective of this work is to evaluate for the first time the effect of bisphosphonate (BP) functional group with the aim of developing biomimetic systems for bone tissue engineering. Therefore, a group of polymers containing bisphosphonate was synthesized with the aim of creating physically crosslinked gels using CaP and similar substances. However, successful formation of physically crosslinked gels could not be achieved. Instead of physically crosslinked gel, BP-functionalized poly(amido amine) (PAA) - based crosslinker was used in the synthesis of a 2-hydroxyethyl methacrylate (HEMA)-based hydrogel. The choice of a poly-HEMA-based hydrogel is motivated by the fact that its water content is similar to living tissues and it has hemocompatibility, shows resistance to degradation and has micro porous structure which is an advantageous morphology for tissue engineering scaffolds. After synthesis of the BP-functionalized PAA-crosslinked HEMA hydrogel, we investigated its swelling, degradation, mechanical, toxicity and cell interaction properties. We demonstrated its mineralization ability and compared it with the gels prepared by using the intermediate versions of macromers as crosslinkers where the functionalization is -NH_2 and -NHBoc respectively, instead of BP.

4.2. Experimental

4.2.1. Materials and Methods

N,N′-methylene bisacrylamide (MBA), *N*-Boc-1,6-hexanediamine, trifluoroacetic acid (TFA), 2-hydroxyethyl methacrylate (HEMA), 2-hydroxy-4′-(2-hydroxyethoxy)-2-methylpropiophenone (Irgacure 2959), all other chemicals and solvents were purchased at the highest quality from Sigma-Aldrich and used as received. Tetraethyl vinylidene bisphosphonate was prepared by the method of Degenhardt and Burdsall [151]. Dulbecco's Modified Eagle Medium (DMEM) (with l-glutamine and high glucose (4.5 g/l)) with and without phenol red, McCoy 5A modified cell medium, penicillin/streptomycin (pen-strep), fetal bovine serum (FBS) and trypsin-EDTA were purchased from Diagnovum, Ebsdorfergrund (Germany). Thiazolyl blue tetrazolium bromide (MTT) was provided by Gold Biotechnology (USA) and phosphate buffered saline (PBS) tablets were provided by

BBI Life Sciences (China). 48 and 96-Well cell culture plates were obtained from Nest Biotechnology (China). 4% Paraformaldehyde solution was obtained from Santa Cruz Biotechnology, Inc (USA). 4′,6-diamidino-2-phenylindole (DAPI) and fluorescein isothiocyanate (FITC)-labelled phalloidin were purchased from Sigma (USA). Saos-2 human osteosarcoma cells and NIH 3T3 mouse embryonic fibroblast cells were a kind gift of Prof. Dr. Halil Kavakli (Department of Molecular Biology and Genetics, Koc University, Istanbul, Turkey). U-2 OS human bone osteosarcoma epithelial cells were a kind gift of Prof. Dr. Devrim Gozuacık (Department of Molecular Biology, Genetics and Bioengineering, Sabanci University, Istanbul, Turkey). C2C12 (mouse myoblast muscle) cells were purchased from ATCC (USA).

^{1}H and ^{13}C NMR spectra were taken in deuterated methanol (MeOD) or deuterated water (D_2O) on a Varian Gemini 400 MHz spectrometer at ambient temperature and chemical shifts δ are given in ppm with respect to the residual water peak, δ = 4.80 ppm. A Fourier transform infrared spectrometer (FTIR) (Thermo Scientific Nicolet 380) equipped with a diamond ATR was used to characterize the macromers and analyze the mineralization of hydrogels. Differential scanning calorimetry (DSC) (TA Instruments Q100) was used to determine the glass transition temperatures (T_g) of the macromers. The morphologies of the hydrogel samples were examined with scanning electron microscopy (SEM) (FEI-Philips XL30) with an accelerating voltage of 10.0 kV after sputter coating of the lyophilized samples with a platinum layer. The energy-dispersive X-ray spectroscopy (EDX) analysis was used to identify the elemental composition of materials. Degradation studies were done using an incubator shaker (VWR) operating at 37 °C and 200 rpm. The mineral content of the cryogels was determined from thermogravimetric measurements (TGA). TGA studies were performed using a Perkin Elmer STA 6000 machine. Samples were heated up to 700 °C at a rate of 10 °C/min under nitrogen atmosphere. Also, crystallographic properties of the apatite formed were analyzed by using X-ray powder diffraction (XRD) analysis (Rigaku-D/MAX-Ultima diffractometer).

4.2.2. Synthesis of PAA Polymers (PAA1, PAA2 and PAA3)

7 novel linear poly amido amines (PAAs) were synthesized.

PAA1: The reaction of MBA (400 mg, 2.6 mmol) with 1,4-butanediamine (255.6 mg, 2.9 mmol) was carried out in MeOH (1.5 mL) for 12 h at 40 °C and the resulting polymer was purified by precipitation into diethyl ether. The pure product was obtained in 55% yield.

PAA2: The reaction of the PAA1 (186 mg, 0.078 mmol) with tetraethylvinylidene bisphosphonate (232 mg, 0.78 mmol) was carried out in MeOH (0.5 mL) for 5 days at room temperature and the polymer was purified by precipitation into diethyl ether. The pure polymer was obtained as a white solid in 54% yield.

PAA3: PAA2 (760 mg, 0.1 mmol) was reacted with TMSBr (0.2 mL) in dry DCM (0.2 mL) for 2 days at 30 °C. Purification of the polymer was carried out using a 1 kDa cellulose membrane.

PAA4: MBA (293 mg, 1.90 mmol) was reacted with *N*-Boc-1,6-hexanediamine (411 mg, 1.90 mmol) in water/methanol mixture (v/v = 3/1, 3.8 mL in total) (1 M) for 4 days at 50 °C under N_2. After the removal of the solvents under vacuum, the residue was washed three times with diethyl ether (5 mL). A white precipitate was filtered off and dried under vacuum to give pure product (PAA4) in 90% yield.

PAA5: To a solution of PAA4 (849 mg, 0.15 mmol) in dichloromethane (DCM) (10 mL), TFA (0.15 mL, 1.54 mmol) was added slowly at 0 °C under N_2 and the reaction mixture was stirred overnight at room temperature. After the removal of the volatiles under vacuum, the residue was dissolved in water and the pH of the aqueous solution was adjusted to 8.0 with 2.5 M NaOH solution. Then the solution was lyophilized, the remaining solid was dissolved in a small amount of methanol and added dropwise into diethyl ether (50 mL) under stirring.

The precipitate was filtered off to give the pure product (PAA5) as a white solid in 80% yield.

PAA6: PAA5 (250 mg, 1 equiv.) and tetraethyl vinylidene bisphosphonate (300 mg, 15 equiv.) were stirred in DCM (2 mL) at room temperature for 2 days. After the removal of DCM, the residue was washed with petroleum ether (2 x 5 mL) to remove unreacted tetraethyl vinylidene bisphosphonate and the pure product (PAA6) was obtained as a yellowish solid in 75% yield.

PAA7: PAA7 was synthesized by the reaction of PAA6 (155 mg, 0.03 mmol) with excess TMSBr (0.2 mL) in 0.2 mL dry DCM for 2 days at 30 °C. PAA7 was obtained as yellowish solid.

4.2.3. Rheological Characterizations of Linear PAAs

The rheological properties of linear polymers were investigated by rotational cylinder viscometer (Gemini 150 Rheometer, Bohlin Instruments). The viscosities of the polymers were measured at 25 ^{o}C and the shear rate was measured in the range of 50-500 cm^{-1}. After the aqueous solutions of the polymers were prepared, 3 mL was taken and the measurements were taken by placing them between the two cylinders of the instrument. While this instrument applies a torque (buckling force) to the wire attached to the inner cylinder, it causes the liquid to rotate in the outer cylinder and measures the viscosity from the flow rate of the rotating liquid.

4.2.4. Synthesis of PAA Macromers (PAA-NHBoc, PAA-NH_2 and PAA-BP)

Synthesis of PAA-BP macromer was carried out in three steps. In the first step, MBA (293 mg, 1.90 mmol) and *N*-Boc-1,6-hexanediamine (342.5 mg, 1.58 mmol) were dissolved

in water/methanol mixture (v/v = 3/1, 3.48 mL in total) (1 M) and the mixture was stirred about 4 days at 50 °C under N_2. After the removal of the solvents under vacuum, the residue was washed three times with diethyl ether (5 mL). A white precipitate was filtered off and dried under vacuum to give pure product (PAA-NHBoc) in 90% yield. In the second step, to a solution of the product from the first step (613 mg, 0.13 mmol) in dichloromethane (DCM) (1.5 mL), TFA (0.1 mL, 1.3 mmol) was added slowly at 0 °C under N_2 and the reaction mixture was stirred overnight at room temperature. After the removal of the volatiles under vacuum, the residue was dissolved in water and the pH of the aqueous solution was adjusted to 8.0 with 2.5 M NaOH solution. Then the solution was lyophilized, the remaining solid was dissolved in a small amount of methanol and added dropwise into diethyl ether (50 mL) under stirring. The precipitate was filtered off to give the pure product (PAA- NH_2) as a white solid in 80% yield. In the third step, PAA-NH_2 (250 mg, 1 equiv.) and tetraethyl vinylidene bisphosphonate (300 mg, 15 equiv.) were stirred in DCM (2 mL) at room temperature for 2 days. After the removal of DCM, the residue was washed with petroleum ether (2 x 5 mL) to remove unreacted tetraethyl vinylidene bisphosphonate and the pure product (PAA-BP) was obtained as a yellowish solid in 75% yield.

4.2.5. Acid-Base Titration

50 mg of each macromer was dissolved in deionized water with a concentration of 1 mg mL^{-1}. pH of the solution was first adjusted to 2.5 by use of 1 M HCl, and then the solution was titrated against 0.1 M NaOH with increments of 50 μL. The increase in pH was recorded with a pH meter (WTW Inolab pH 720) at room temperature.

4.2.6. Hydrogel Preparation

PAA-NHBoc, PAA-NH_2 or PAA-BP crosslinked HEMA hydrogels were prepared by dissolving macromers (100 mg) and HEMA (900 mg) at the 10:90 wt% ratio in 3 mL distilled water. The photoinitiator (Irgacure 2959) (2 wt% of total monomer weight) was added and

the mixture was placed into 2 mL syringes with inner diameter 4 mm. Then, the mixtures were exposed to UV light (365 nm) for 30 min in a photoreactor (Kerman UV/18) containing 12 Philips TL 8 W BLB lamps. The hydrogel samples were cut into pieces of length: 7 mm, thawed at room temperature, lyophilized and weighed (W_i). Then, unreacted gel precursors were removed by washing with ethanol (12 h) and distilled water (12 h), lyophilized and weighed again (W_f). The percent gelations were calculated as

$$Gelation(\%) = \frac{W_f}{W_i} \times 100. \quad (4.1)$$

4.2.7. Swelling Studies

Swelling ratios of dry hydrogel samples (45 mg ± 5 mg) (W_d) were studied by immersing them in water, 0.5 M $CaCl_2$ solution and PBS (7.4 and 3) solutions at 37 °C to reach equilibrium swelling. The hydrogel samples were removed from the solutions, the excess solution was removed with tissue paper and the swollen weight (W_s) was measured. The degree of swelling (Q) was calculated using the following equation where W_s and W_d refer to the weight of swollen and dry gel samples, respectively. The average data obtained from triplicate measurements were reported.

$$Q = \frac{W_s - W_d}{W_d} \times 100, \quad (4.2)$$

4.2.8. Degradation Studies

In vitro degradation studies of the hydrogels were conducted by immersing dry hydrogel samples (45 mg ± 5 mg) (W_i) in PBS solution (5 mL) at 37 °C and pH 7.4. At predetermined time intervals (1, 2 and 4 weeks) samples were taken out, rinsed with water, freeze-dried and re-weighed (W_f). The measurements were made in triplicate and the average data were reported. The degradation % was calculated as

$$Degradation\ (\%) = \frac{W_i - W_f}{W_i} \times 100. \quad (4.3)$$

4.2.9. Water Contact Angle Measurements

Freeze-dried hydrogel samples were allowed to swell in water and then air-dried at 25 °C. To obtain flat surfaced hydrogels at their semidried state, hydrogels were placed between two glass slides and allowed to dry further. Water contact angle values of hydrogels were measured in air via the sessile-drop method using a goniometer (CAM 101 KSV instruments). The side profiles of deionized water drops (approximately 3-5 μL) were recorded by an integrated digital camera for image analysis. The dynamic contact angle values were measured by the shape of the drop recorded in a time range of 0–10 s, collecting images every 1 s. Every contact angle value of the hydrogel was determined at five different spots on the sample and average contact angle values were reported.

4.2.10. Mineralization of the Hydrogels

Hydrogel samples were immersed into 5 times concentrated simulated body fluid (5xSBF) solution, prepared as described by Chou et al [126] and incubated at 37 °C for two days during which 5xSBF was changed every day. Then hydrogels were taken out of the solution, kept overnight in deionized water and freeze-dried to constant weight. The characterization of mineralized hydrogels was carried out by using TGA, FTIR, SEM, EDX and XRD analyses.

4.2.11. Mechanical Studies

Mechanical properties of hydrogels in equilibrium swollen states were investigated by uniaxial compression measurements on a Zwick Roell test machine with a 500 N load cell in a thermostated room at 25 °C. The tests were carried out at a constant cross-head speed of 5 mm min^{-1}. Before the tests, a complete contact between the gel specimen and the metal plate was provided by applying an initial compressive force of 0.05 N. The compressive

stress is calculated as its nominal σ_{nom}, which is the force per cross-sectional area of the undeformed gel specimen, while strain is given by ε which is the change in the specimen length with respect to its initial length. Young's modulus E of the hydrogels was calculated from the slope of stress–strain curves between 5 and 15% compressions. Measurements were made with at least 3 hydrogels and the results were averaged.

4.2.12. *In vitro* Cytotoxicity Assay

Impact of the degradation products of the prepared gels on the viability of Saos-2, U-2 OS, NIH 3T3 and C2C12 cell lines was evaluated using the standard MTT assay. The NIH 3T3 and U-2 OS cells were cultured in phenol red containing DMEM complete medium, and C2C12 cells were cultured in DMEM without containing phenol red, supplemented with 10% (v/v) FBS and 1% (v/v) pen-strep in a 5% CO_2-humidified incubator at 37 °C and passaged every 2-3 days. Saos-2 cells were cultured in the same way using McCoy 5A complete medium. For viability test, cells were seeded at a density of $37.5x10^3$ cells/mL for C2C12 cells and $75x10^3$ cells/mL for other cells in each well of a 96-well plate and incubated at 37 °C in 5% CO_2 atmosphere.

The degradation product was added at a concentration between 5-100 µg/mL. After 48 h incubation, the cell viability was assessed using MTT colorimetric assay. First, 50 µl of MTT solution (5 mg/mL in PBS) was added into each well with 150 µL of culture medium and incubated for 4 h. Then, the purple formazan crystals formed as a result of mitochondrial activity in viable cells were dissolved with ethanol: dimethyl sulfoxide (1:1 v/v) mixture. Absorbance at 570 nm with a reference reading at 630 nm was recorded for each well using a Synergy – H1 microplate reader (BioTek Instruments Inc., Winooski, VT, USA). Cells which were not exposed to degradation products of gels were used as controls which were assumed as 100% viability. The relative cell viability was calculated as

$$Cell\ viability\ (\%) = \frac{Absorbance_{sample}}{Absorbance_{control}} \text{x } 100. \quad (4.4)$$

4.2.13. Cell Attachment Experiment

To investigate cell interaction of the mineralized hydrogels, PAA-BP crosslinked HEMA hydrogels were prepared as described in section 2.5 on treated polystyrene 48-well plates. 5xSBF was added onto the hydrogel samples to initiate mineralization and the plates were kept at 37 °C for two days during which 5xSBF was changed every 12 hours. The mineralized hydrogels were washed with PBS and sterilized under UV light. Then, C2C12 cells at a density of 66.7×10^3 cells/mL in complete medium were seeded to 48 well plate and incubated for 20 hours. After washing twice with PBS, cells were fixed with 4% paraformaldehyde solution for 20 min and washed again twice with PBS. Cells were stained with DAPI and phalloidin solution (both 4 μg/mL in PBS) for 20 min, washed twice with PBS and stored at 4 °C in 0.2 mL PBS to prevent the cells from drying out. Then, the fixed cells were visualized under Zeiss Axio Observer Z1 Fluorescence Microscope (Germany) equipped with DAPI filter for nucleus staining and FTIC filter for cytoskeleton staining with phalloidin. Images were colored and merged using the ZEN 3.1 (Blue version) software.

4.3. Results and Discussion

4.3.1. Synthesis and Characterization of Linear PAAs

The first polymer of the first set of linear polymers PAA1 was obtained by the Michael addition reaction of MBA with 1,4-butanediamine (Figure 4.1). The obtained white solid polymer dissolves in water, methanol and THF. The molecular weight of the polymer was determined by GPC as Mn =2400 g/mol. In the second step, the reaction of the PAA1 with tetraethyl vinylidene bisphosphonate was carried out at room temperature and when the polymer was purified by precipitation into diethyl ether, a linear polymer with bisphosphonate function PAA2 was obtained as a white solid.

The bisphosphonate groups in the structure of these polymers can be controlled by changing the polymer: tetraethyl vinylidene bisphosphonate molar ratios. PAA2 is soluble in water and methanol. The molecular weight of the polymer was determined by ^{1}H NMR as Mn =7600 g/mol. Third polymer, PAA3, was synthesized from the cleavage reaction of phosphonate ester groups of bisphosphonate-functionalized polymer (PAA2) with TMSBr (Figure 4.1). PAA3 was obtained as yellowish solid and the molecular weight of the polymer was determined by ^{1}H NMR as Mn =5700 g/mol.

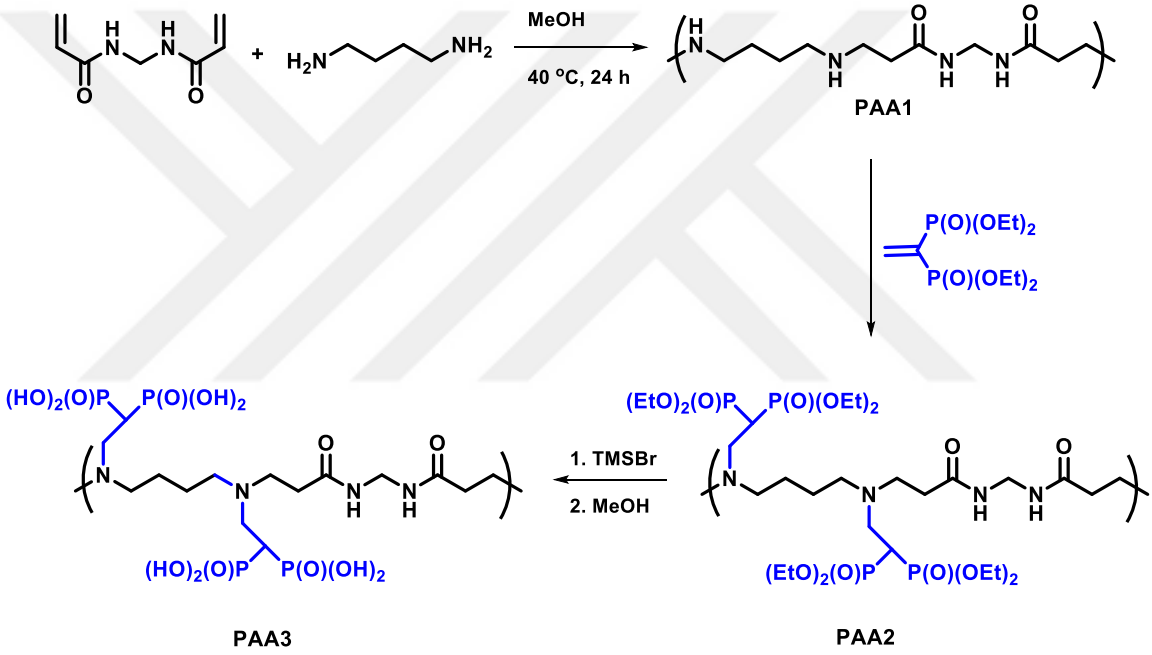

Figure 4.1. Synthesis of linear polymers PAA1, PAA2 and PAA3.

The ^{1}H NMR spectra of the polymers are shown in Figure 4.2 and Figure A.1. In the ^{1}H NMR spectrum of PAA1 methylene protons of MBA are seen at 4.52 ppm, the peak due to the methylenes attached to carbonyls is seen at 2.27 ppm. In the ^{1}H NMR spectrum of PAA2 the ethyl protons (m and n) of the bisphosphonate ester are seen at 4.24 and 1.36 ppm which is proof that the functionalization of the polymer with BP is successful (Figure 4.2).

^{1}H NMR of PAA3 shows that the ethyl peaks of the bisphosphonate decrease but do not completely disappear, which means that this reaction did not occur in 100% yield, resulting in a polymer containing both bisphosphonate and bisphosphonic acid groups on the polymer (Figure A.1). It was found that the diffraction reaction from the integrals of the ethyl peaks of the bisphosphonate groups on the polymer against the acrylamide protons occurred with 30% yield. FTIR spectra of PAA2 and PAA3 can be seen in Figure A.2. and Figure A.3. In the FTIR spectrum of PAA2, P=O stretching peak are seen at around 1200 cm^{-1}. FTIR spectra of PAA3 show broad peaks in the region of 3000–2600 cm^{-1} due to OH stretching of bisphosphonic acid group.

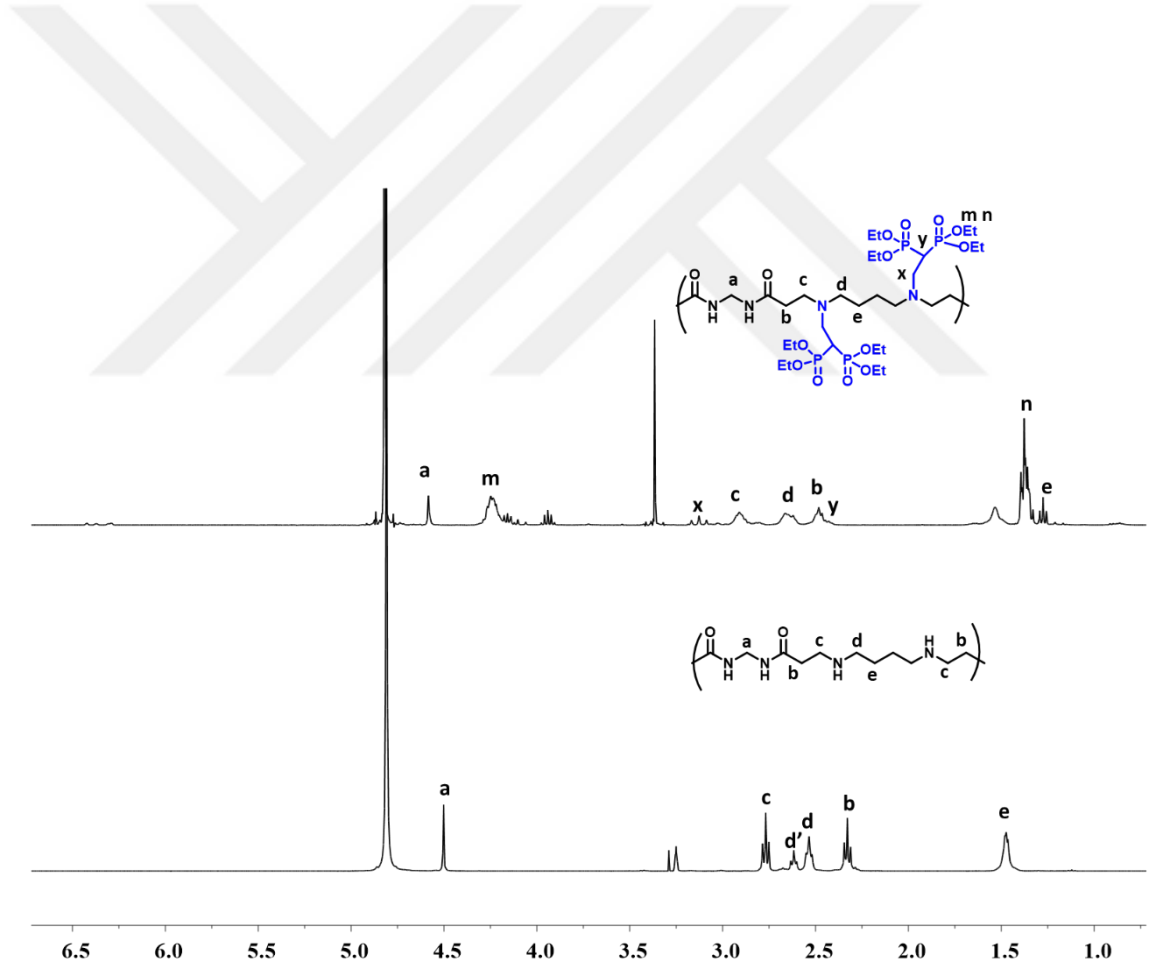

Figure 4.2. ^{1}H NMR spectra of PAA1 and PAA2.

The steps in the synthesis of the second set of linear polymers are as follows: i) Reaction of MBA with N-Boc-1,6-diaminohexane in a 1:1 molar ratio (PAA4), ii) Removal

of N-Boc protecting groups with TFA (PAA5), iii) Reaction of the polymer with tetraethyl vinylidene bisphosphonate (PAA6), iv) Cleavage of the ethyl groups of bisphosphonate with TMSBr and methanol (PAA7). These steps are shown in Figure 4.3.

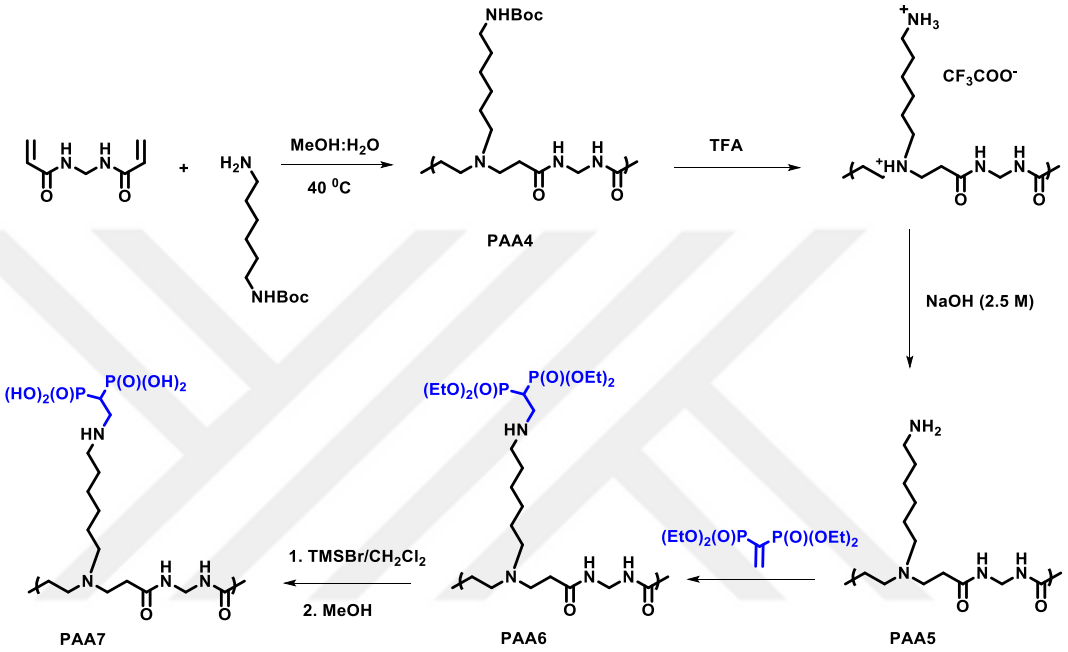

Figure 4.3. Synthesis of linear polymers PAA4, PAA5, PAA6 and PAA7.

Characterization of the products at the end of each step was carried out using ^{1}H NMR and FTIR. In the ^{1}H spectrum of PAA7, a decrease in the ethyl protons from PAA6 was observed (Figure 4.4). Additionally, it was observed that the peaks corresponding to the methylene protons attached to nitrogen shifted to the left due to the formation of quaternary amines.

In the FTIR spectra of PAA5, PAA6, and PAA7, the C=O peaks are observed around 1710 cm^{-1}, while the P=O peak originating from the bisphosphonate is absent in PAA5 and appears around 1215 cm^{-1} in PAA6 and PAA7. Similarly, the P-O peaks are observed around 1070 cm^{-1} and 950 cm^{-1} in the spectra of PAA6 and PAA7. The broad peak observed between 3100-3200 cm^{-1} in the FTIR spectra of all three polymers is attributed to NH stretching,

while the broad peak around 3000 cm^{-1} observed in PAA7 corresponds to the OH stretching of the bisphosphonic acid (Figure A. 4).

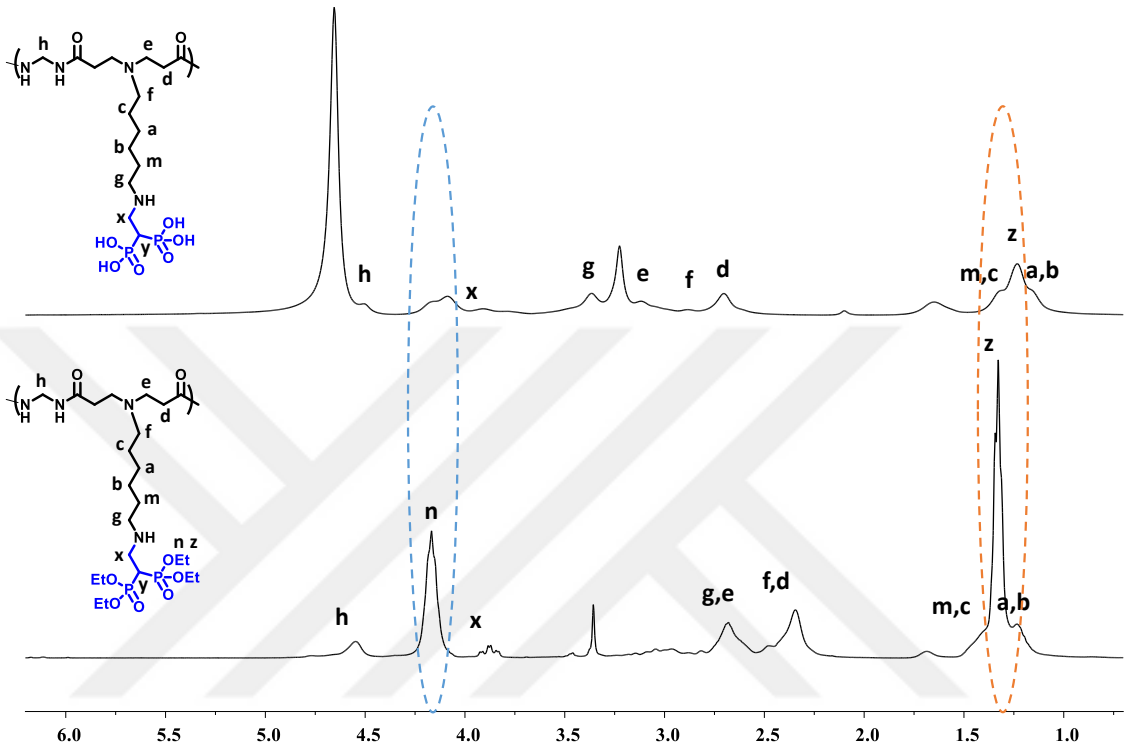

Figure 4.4. ^{1}H NMR spectra of PAA6 and PAA7.

4.3.2. Rheological Characterizations of Linear Polymers

The rheological properties of linear polymers were investigated with a rotary cylinder viscometer (Gemini 150 Rheometer, Bohlin Instruments). Since the measurement was made with a 3 mL solution in a rotary cylinder viscometer, 5 wt%, 10 wt% and 22.5 wt% dilute solutions of PAA1 were prepared and their viscosities were measured at 25 °C, and the shear rate was measured in the range of 50-500 cm^{-1} (Figure 4.5A). As expected, the viscosity increased as the concentration increased. The viscosity (η) of the 5% PAA1 solution was found to be 3.5, the 10% solution to 5, and the 22.5% PAA1 solution to be 11. For all other measurements, the polymers were prepared as 10 % solutions. A solution of PAA2, which is the bisphosphonate-functionalized form of PAA1, was prepared at a concentration of 10% by weight, and a solution of PAA3 polymer, which represents the state of PAA2 where

bisphosphonate groups have been cleaved into bisphosphonic acid, was also prepared at a concentration of 10% by weight. Their viscosities were then compared. Viscosities of PAA2 and PAA3 solutions were found to be 4 and 12, respectively. (Figure 4.5B). The physical crosslinking properties of polymers with $CaCl_2$ were investigated. When $CaCl_2$ was added separately to polymer solutions with a total salt concentration of 100 µM and their viscosities were measured, it was observed that the viscosity of the PAA2 polymer increased from 4 to 12 (Figure 4.5C). While the viscosity of PAA3 was 12, it was measured as 17 after $CaCl_2$ (Figure 4.5D).

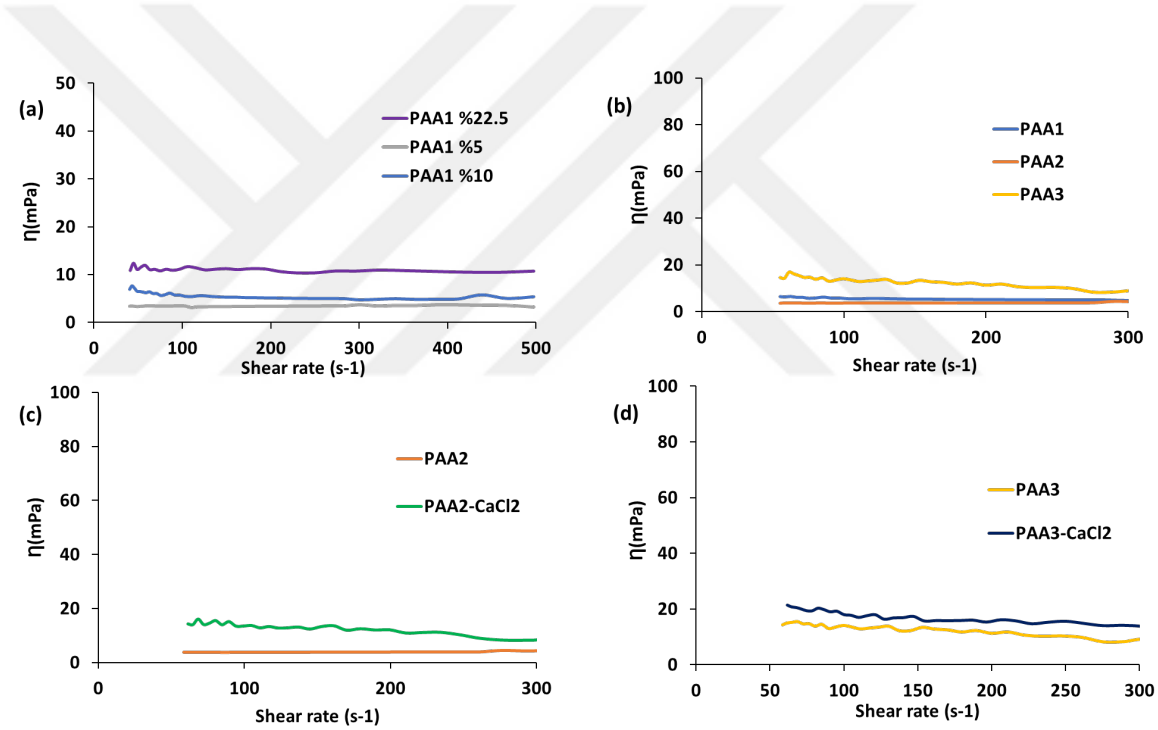

Figure 4.5. A) The viscosities of the solutions of PAA1 at concentrations of 5%, 10%, and 22.5%. B) The viscosities of the solutions of PAA1, PAA2, and PAA3 polymers at a concentration of 10%. C) The viscosity of the solution of PAA2 and PAA2 in $CaCl_2$. D) The viscosity of the solution of PAA3 and PAA3 in $CaCl_2$.

Likewise, the viscosity (η) of 10 wt% solutions of polymers PAA5, PAA6 and PAA7 were measured and found to be 10, 13 and 10, respectively (Figure A.5A). In addition, to see the changes in viscosity of the amines on the PAA5 polymer when protonated, the pH of

the solution was adjusted to 2 with HCl and the measurement was repeated. Viscosity was measured as 10 for both solutions (Figure A.5B). In order to examine the physical cross-linking properties of polymers with $CaCl_2$ and $FeCl_3$ salts, $CaCl_2$ and $FeCl_3$ salts were added separately to the polymer solutions at a concentration of 100 μM and their viscosities were measured. It was observed that the viscosity of the PAA6 polymer increased from 13 to 25 with the $CaCl_2$ salt, and the viscosity increased from 13 to 40 in the $FeCl_3$ salt solution (Figure A.5C). It was observed that the viscosity of the PAA7 polymer did not change with $CaCl_2$ and $FeCl_3$ salt, and the viscosity was measured around 10 in all three cases (Figure A.5D).

4.3.3. Synthesis and Characterization of PAA Macromers

A novel bisphosphonate-functionalized PAA macromer (PAA-BP) was synthesized in three steps as shown in Figure 4.6. The first step involves aza-Michael reaction of MBA and *N*-Boc-1,6-hexanediamine (1.2:1 bisacrylamide to amine mol ratio) at 50 °C for 4 days in methanol:water (1/3 v/v), mixture. A macromer (PAA-NHBoc) with the *N-tert*-butyloxycarbonyl (*N*-Boc)-protected amine group in the side chain was obtained as a white solid in 90% yield. This macromer was used as a control macromer to examine the effect of BP functionality on mineralization properties of the hydrogels. In the second step, the selective deprotection of the *N*-Boc group was performed by acidic cleavage using TFA to obtain a macromer (PAA-NH_2) in its CF_3COOH-salt form.

In the literature, linear polymer of the same macromer with the pendant primary amine HCl salt was synthesized by Michael polyaddition of the bisacylamide and protected amine in 1:1 mol ratio without solvent at 140 °C for about 12 h, followed by deprotection using HCl [152]. In another study, the deprotection of the amino groups of bioreducible PAAs with oligoamine side chains was carried out in a mixture of methanol/TFA and HCl for 4–6 h [153].

The deprotonation of the ammonium groups to neutral primary amines was performed using sodium hydroxide solution to give PAA-NH_2 as a white solid in 80% yield. This macromer was also used as a control macromer to compare the effect of BP and NH_2 functionality on hydrogel properties such as mineralization.

In the third step, post-modification of primary amines on the macromer was carried out: PAA-NH_2 was reacted with excess amount of tetraethyl vinylidene bisphosphonate by aza-Michael addition to give the novel macromer (PAA-BP) with side chain bisphosphonate groups, as a yellowish solid in 75% yield. PAA-NH_2 and PAA-BP showed good solubility in water.

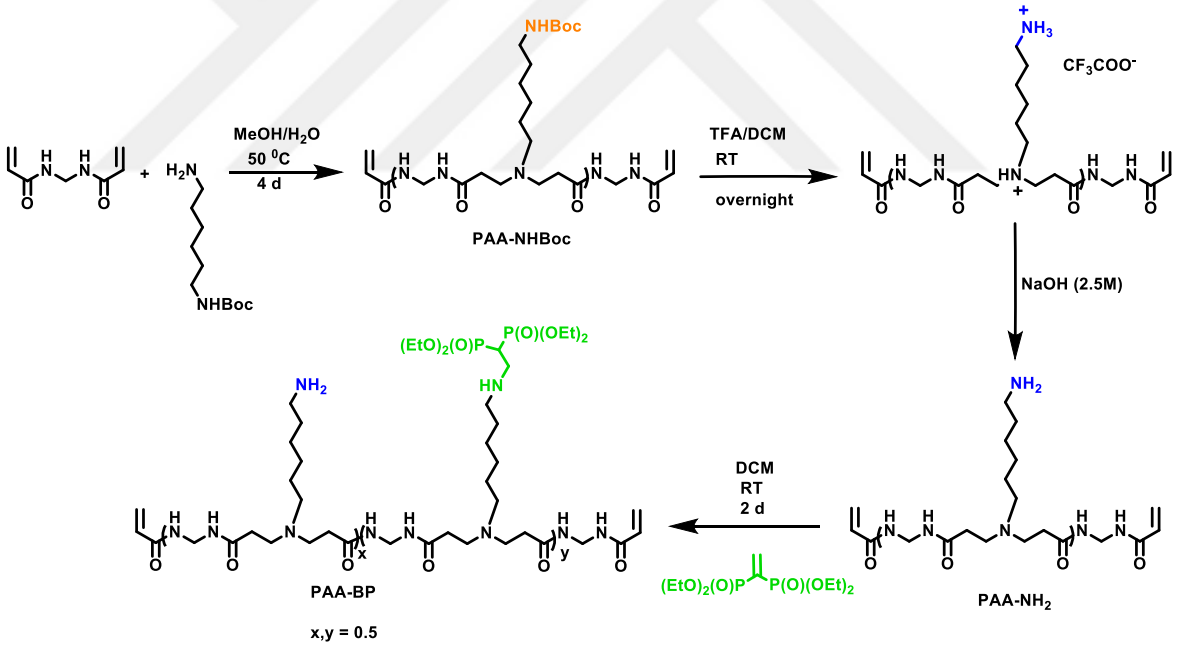

Figure 4.6. Synthesis of poly(amido amine) macromer with BP side chains.

The chemical structure of the macromers synthesized in each reaction step was verified by the ^{1}H NMR spectroscopy and FTIR. ^{1}H NMR of the product of the first step shows Boc groups at 1.36 ppm, acrylamide end groups at 5.62 and 6.19 ppm and methylene protons of MBA at 4.49 ppm. The number of repeating unit (*n*) of this macromer

was calculated by the ratio of the integrals of acrylamide double bond protons to the Boc protons and found to be 11. From the number of repeating units, the number-average molecular weight was calculated using M_n = (FW end groups) + (FW repeating unit)(*n*) as 4250 g/mol. After the second step, no peak was present around 1.36 ppm, corresponding to Boc group, indicating that the deprotection is complete. Also, we observe a downfield shift of most of the peaks (except k, i, h). This effect is due to decreased shielding of the protons due to positively charged ammonium ions relative to neutral amine (Figure 4.7). ^{13}C NMR spectrum of this product also confirmed its structure (Figure 4.8).

The M_n of this PAA macromer (PAA-NH_2) was calculated as 3150 g/mol. In the last step, ethyl protons of bisphosphonate group showed two splitted peaks at 4.24 and 1.39 ppm in ^{1}H NMR spectrum due to the coupling of the phosphorus signals to the protons in the compound. The average degree of substitution of the bisphosphonate group, determined from the ^{1}H-NMR spectrum by integrating bisphosphonate protons z or n with respect to double bond peaks (k, i), was found to be 50%, although excess amount of tetraethyl vinylidene bisphosphonate was used. This may be explained by the fact that BP groups are bulky groups, they cause steric hindrance as they are added to the structure. Also, because BP functionalization occurs via Michael addition reaction, retro-Michael reaction could occur, decreasing the degree of substitution [154]. Although this macromer was abbreviated as PAA-BP it has a copolymeric structure, having 50% of PAA-NH_2 units. M_n value of this macromer was calculated as 4800 g/mol.

The FTIR spectra of PAA-NH_2 and PAA-BP show broad peaks in the region of 3500−3150 cm^{-1} due to NH stretching and strong peaks at 1712 cm^{-1} because of C=O stretching (Figure 4.9A). Moreover, the strong bands at 1017 and 980 cm^{-1} in the FTIR spectra of PAA-BP correspond to the symmetric and asymmetric vibration of P−O, which are absent in PAA-NH_2 spectrum.

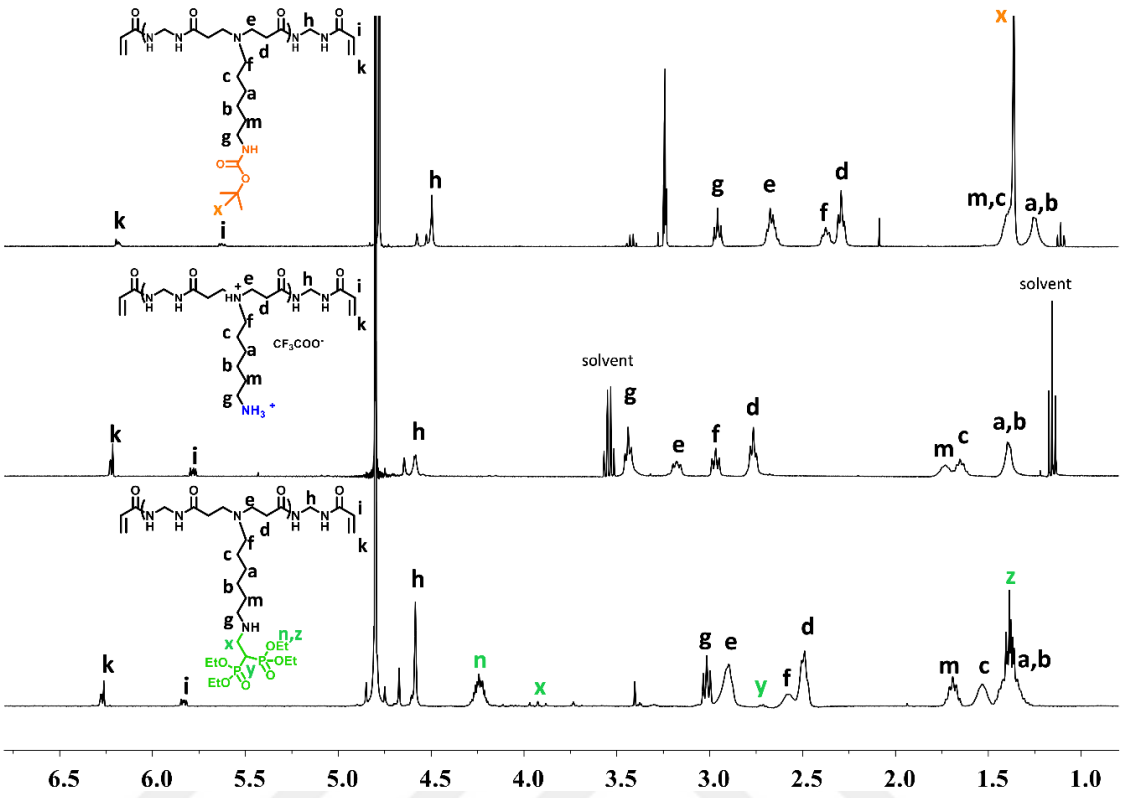

Figure 4.7. ^{1}H NMR spectra of products of each reaction step during synthesis of PAA-BP.

The pH sensitivities of PAA-NH_2 and PAA-BP macromers were evaluated by acid-base titration (Figure 4.9B). For both macromers a plateau region was observed in the pH range of about 6-8, which is characteristic for poly(amido amine)s [152,155]. The plateau is wider for PAA-BP compared to PAA-NH_2, indicating its better pH-responsive performance. PAA-NH_2 with higher hydrophilicity at low pH deprotonates continuously with an increase in pH, thus it does not show as distinct a plateau as PAA-BP.

The thermal properties of the PAA-NH_2 and PAA-BP macromers investigated by DSC showed their glass transition temperatures (T_g) as 27 °C and 38 °C (Figure 4.10). The higher T_g value of PAA-BP can be explained by the steric hindrance of bulky BP groups and their polar interaction.

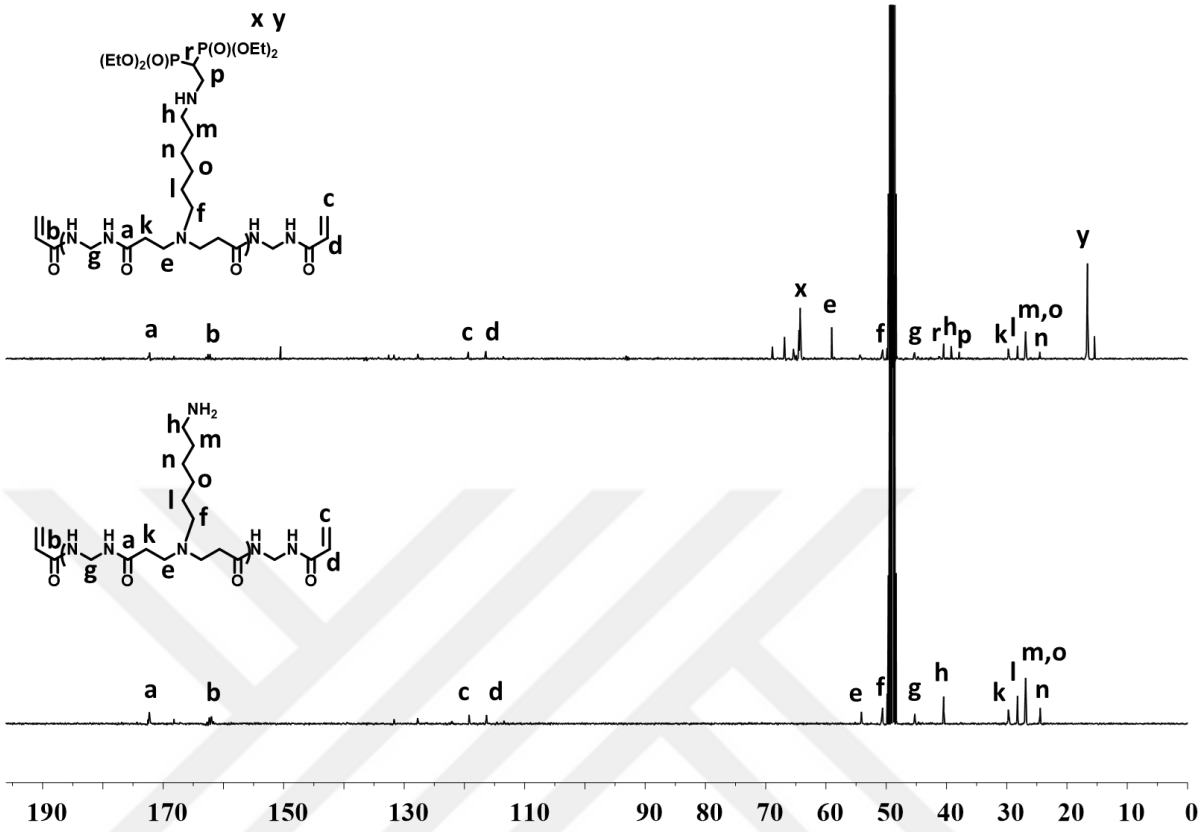

Figure 4.8. ^{13}C NMR spectra of PAA-NH_2 and PAA-BP macromers.

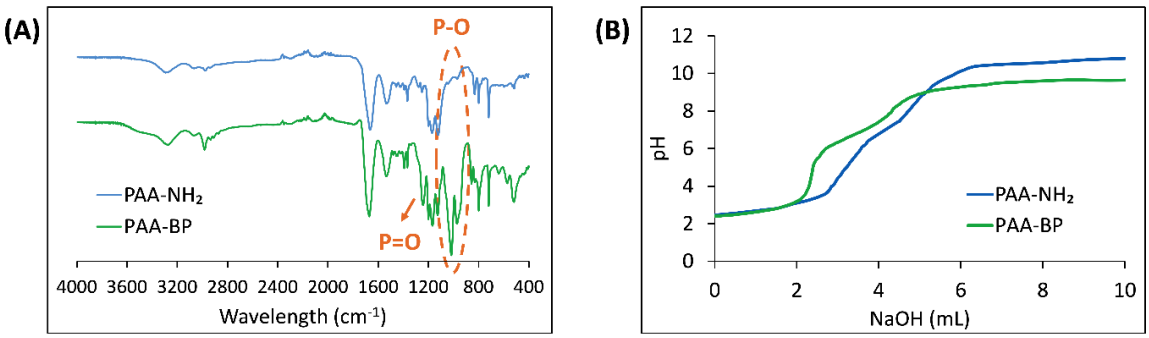

Figure 4.9. A) FTIR spectra and B) acid-base titration curves of PAA-NH_2 and PAA-BP macromers.

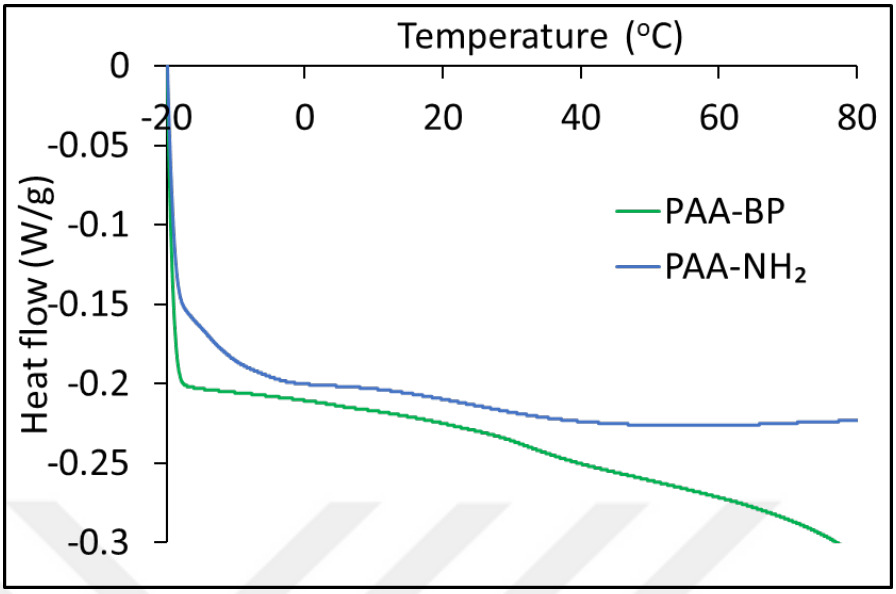

Figure 4.10. DSC profiles of PAA-NH_2 and PAA-BP.

4.3.4. Synthesis and Characterization of Hydrogels

To understand the effect of the bisphosphonate group on hydrogel properties, two of the macromers (PAA-NH_2 and PAA-BP) (10 wt%) were copolymerized with HEMA (90 wt%) by free radical photopolymerization using Irgacure 2959 as photoinitiator (Figure 4.11). The hydrogels are named as H:PAA-NH_2 and H:PAA-BP where "H" stands for hydrogel and PAA-x indicates the crosslinker. Gelation percentages of the hydrogels were found as 80 and 85% for PAA-NH_2 and PAA-BP, respectively.

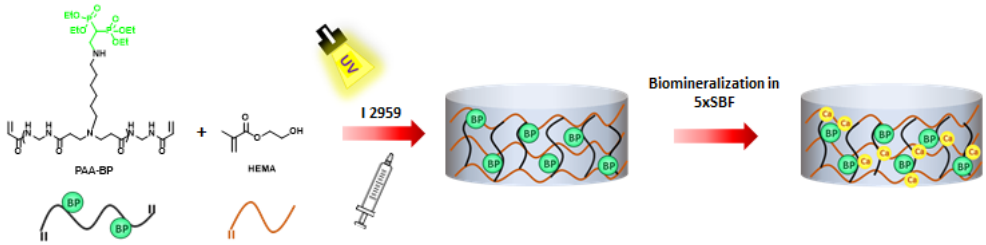

Figure 4.11. The preparation of H: PAA-BP and its biomineralization in 5xSBF.

SEM micrographs of synthesized hydrogels showed that hydrogels have macroporous (pore size > 100 µm) morphology which is one of the essential requirements for the tissue engineering scaffolds and directly affects bone formation [156]. The pore size of hydrogels were found as around 170 µm for H:PAA-NH_2 and 275 µm for H:PAA-BP (Figure 4.12). This difference can be explained by different crosslink density and/or hydrophilicity of the crosslinkers. H:PAA-BP hydrogel with lower mol% of crosslinker (since hydrogels are prepared by using same weight percentages of crosslinkers having different molecular weights) is expected to have lower crosslinking density than that of H:PAA-NH_2. Besides, the more hydrophilic crosslinker PAA-BP may also increase the pore size.

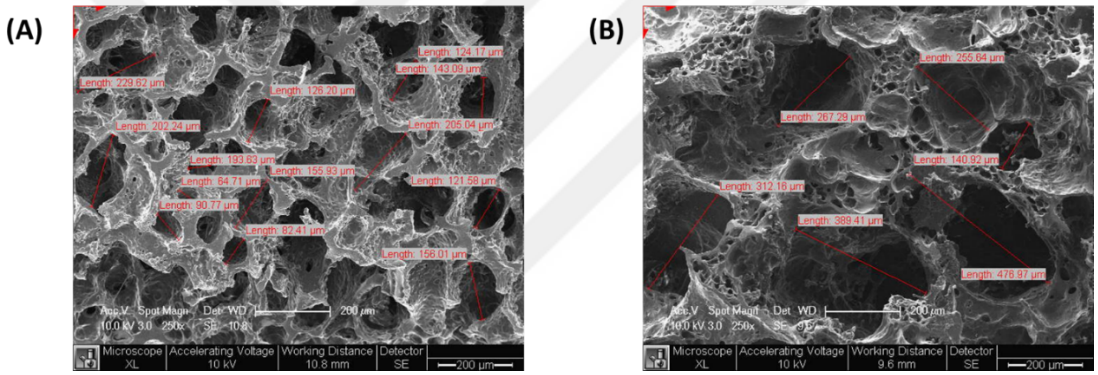

Figure 4.12. SEM images showing pore sizes of A) H:PAA-NH_2 and B) H:PAA-BP.

4.3.5. Swelling, Degradation and Wettability Behaviour

In general, the structural properties of hydrogels such as the hydrophilic/hydrophobic balance, the degree of cross-linking and the degree of ionization are the important parameters which control the equilibrium swelling. The swelling ratios of the synthesized hydrogel samples with two different PAA crosslinkers, PAA-BP and PAA-NH_2, in distilled water, $CaCl_2$ solution (0.5 M) and buffer solutions (pH 3.0 and 7.4) are shown in Figure 4.13. It was observed that after 120 min equilibrium swelling was reached in all solutions.

The swelling capacity of the PAA-BP crosslinked hydrogels was found to be higher than those of the PAA-NH_2 crosslinked ones in water and in pH 7.4. This can be explained by two factors: i) lower crosslink density (as explained above) and ii) the more hydrophilic nature of PAA-BP due to pendant secondary amine groups and BP groups: The pendant secondary amine groups may be already protonated at pH 7.4 and water in addition to tertiary amine (pK_a = 6-8) groups at the backbone. The protonated amines cause more electrostatic repulsion between chains and lead to the expansion of the network, hence diffusion of water into the network. However the NH_2 groups on the H:PAA-NH_2 hydrogel are not protonated at neutral pH because the pK_a value of the pendant primary amine group is approximately 6.5 [157] and stronger hydrogen bonding ability of these groups compared to in H:PAA-BP causes more crosslinking sites and therefore more compact structure. The swelling ratios of both hydrogels were found to be lower at pH 7.4 than in water, indicating high ion concentration preventing electrostatic repulsion which is more effective in PAA-BP crosslinked hydrogels.

The effect of acidic pH on the swelling ratios of the hydrogels is also measured at pH 3.0 and illustrated in Fig. 5B. The hydrogels showed different swelling behaviors in acidic solutions. It can be seen that the swelling ratio of H:PAA-NH_2 increased with decreasing the pH. The NH_2 groups on the hydrogel are protonated at acidic pH, the electrostatic repulsion causes breaking of hydrogen bonding between the chains, leading to the expansion of the network. We also expected an increase in swelling ratio of H:PAA-BP due to protonation of NH_2 groups in its structure. However, we observed a decrease compared to those of H:PAA-NH_2. This unexpected behavior can be explained by the presence of ionic groups at the side chain of PAA-BP crosslinker under neutral conditions which decrease the effect of hydrogen bonding due to NH_2 groups. Therefore, increase in ion concentration at low pH decreases the electrostatic repulsion already present in neutral form and thus swelling decreases compared to in water.

The swelling ratios of both hydrogels decreased in $CaCl_2$ solution compared to in water, more so for H:PAA-BP than for H:PAA-NH_2 (Figure 4.13B) which indicates interaction of BP groups with Ca^{2+} ions forming physical crosslinking. The degradation

behavior of the hydrogels was investigated in PBS (pH 7.4) at 37 °C (Figure 4.13C). The mass loss of the gels was found to change between 1 to 8% in four weeks, the main reason for the difference being differences in chemical structure such as hydrophilicity (coming from PAA-BP), the extent of secondary interactions (hydrogen bonding between NH_2 groups) and crosslink density. While H:PAA-BP hydrogels showed higher mass loss, H:PAA-NH_2 hydrogels which do not possess BP groups and have higher crosslink density showed lower degradation rate.

The contact angle of water droplet on the gel surface was determined using static water contact angle measurement at ambient temperature. The contact angle decreased from 79° (H:PAA- NH_2) to 41° (H:PAA-BP) with the increasing hydrophilicity arising from the PAA-BP crosslinker (Figure 4.13D).

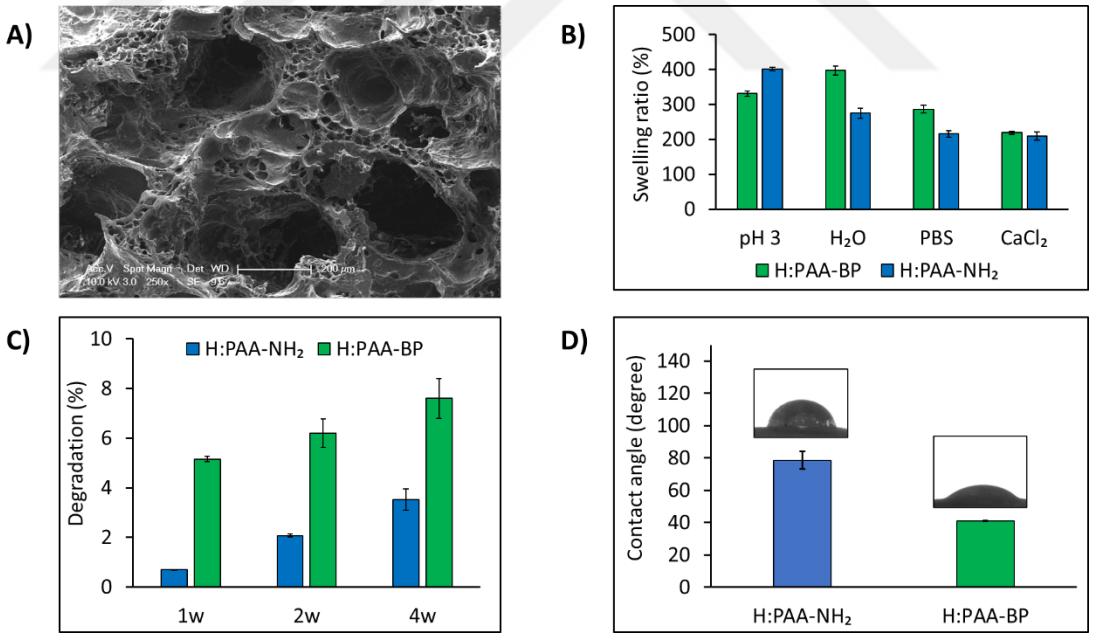

Figure 4.13. A) SEM image of H:PAA-BP, B) equilibrium swelling ratio (%) of hydrogels in water, various buffer and $CaCl_2$ solutions, C) degradation (%) of hydrogels in PBS (pH 7.4) solution at 37 °C and D) water contact angles of the hydrogels.

4.3.6. Mineralization of Hydrogels

The ability of materials to form calcium phosphate (CaP) phases at their surface similar to bone mineral is tested by immersing them in SBF, which mimics the ionic concentrations and pH typically observed in plasma. In the literature, the different types of SBF solutions have been developed with varying compositions [158]. In this study, we used high SBF concentrations (5xSBF) in order to increase the rate of biomimetic mineralization. In order to assess the role of NH_2 and NH_2/BP functional groups in the mineralization properties of the synthesized hydrogels, a H:PAA-NHBoc hydrogel was also prepared and used as control. After hydrogels (H:PAA-NHBoc, H:PAA-NH_2 and H:PAA-BP) were immersed in 5xSBF for 2 days and washed with deionized water overnight, they were freeze-dried. CaP minerals deposited were characterized by SEM, EDX, XRD, FTIR and TGA.

The FTIR spectra of all the hydrogels before mineralization mainly show absorption peaks of HEMA due to its high concentration, the broad OH stretching peak at around 3400 cm^{-1} and the C=O stretching at 1712 cm^{-1} (Figure 4.14A). The FTIR spectra obtained for mineralized H:PAA-NHBoc, H:PAA-NH_2 and H:PAA-BP hydrogels were used to characterize mineral phases in the samples (Figure 4.14B). As is known, there are four Raman and IR active vibrational modes for phosphate ions. O-P-O bending vibrations were indicated by the very intense ν_3PO mode between 1190-976 cm^{-1} and ν_4PO mode between 660-520 cm^{-1}. Also, phosphate ν_1PO band is observed at 962 cm^{-1} and ν_2PO band is observed in the region of 475 and 440 cm^{-1} as weak bands [159].

The spectra of mineralized H:PAA-NH_2 and H:PAA-BP are dominated by these peaks, similar to HAP. These observations, together with a significant decrease (complete disappearance for H:PAA-BP) in polymer peaks indicates a large amount of mineral on H:PAA-NH_2 and H:PAA-BP hydrogels. However, no major change in spectrum of H:PAA-NHBoc was observed, indicating that mineralization is not occurring. Furthermore, the mineralization performance of H:PAA-NH_2 can be explained by the fact that polycations such as linear PEI also have a strong effect on CaP mineralization [142].

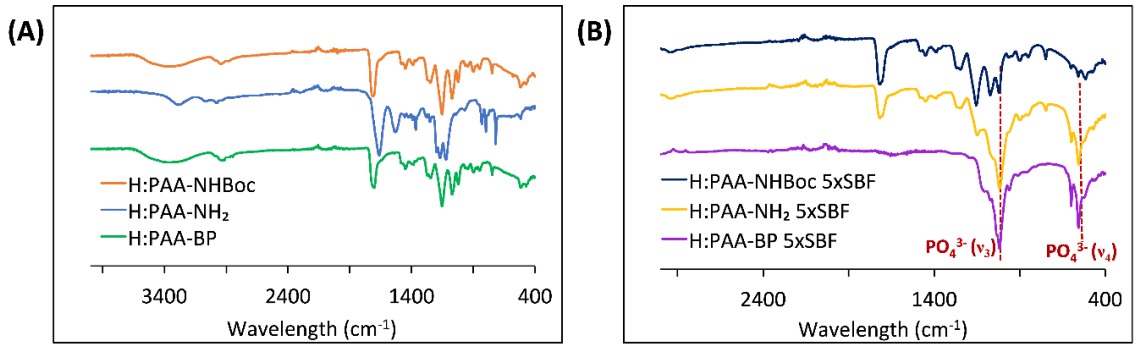

Figure 4.14. FTIR spectra of hydrogels A) before and B) after mineralization in in 5xSBF.

Formation of mineral phase was also confirmed by scanning electron microscopic (SEM) analysis of mineralized and freeze-dried hydrogels H:PAA-NH_2 and H:PAA-BP. Both showed needle-like crystals similar to HAP covering their whole surface when immersed in 5xSBF (Figure 4.15A and 4.15B). However, at one order of magnitude larger scale H:PAA-BP features are more or less uniform, but for H:PAA-NH_2 the needles occasionally aggregate into roughly spherical particles on the calcium phosphate layer.

Energy Dispersive X-ray Spectroscopy (EDS) is a method employed in the fields of materials science and chemistry for assessing the elemental makeup of a specimen. This technique involves inducing the generation of X-rays within the sample through targeted electron beam bombardment. Subsequently, the emitted X-rays are captured, and their energy is utilized to discern and measure the elemental constituents within the sample. In the current investigation, EDX was applied to scrutinize the elemental composition of the inorganic complex, revealing the existence of carbon, oxygen, phosphorus, calcium, and magnesium in the mineralized samples (Figure 4.15A and 4.15B). The Ca/P ratios was found to be 1.5 for both hydrogels. This ratio is known to be 1.67, 1.5, 1.0 and 1.33 in HAP [$Ca_{10}(PO_4)_6(OH)_2$], calcium phosphate [$Ca_3(PO_4)_2$] (amorphous), brushite [$(CaHPO_4)_3$-H_2O], and octacalcium phosphate [$Ca_8(PO_4)_6H_2$] [160,161]. These results suggest the formation of an apatite-like mineral, nonstoichiometric HAP.

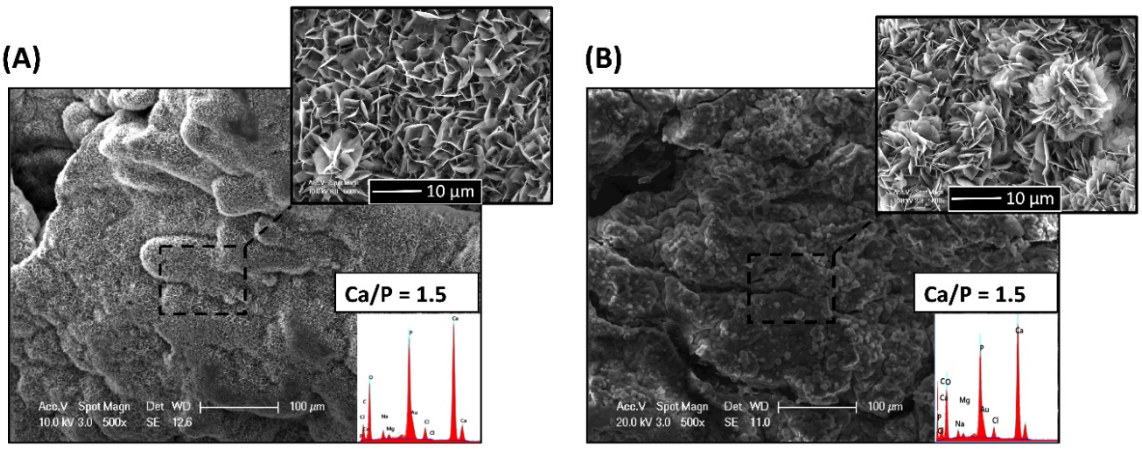

Figure 4.15. SEM images and EDX spectra (inset) of hydrogels A) H:PAA-BP and B) H:PAA-NH_2, mineralized by immersion in 5xSBF.

The crystal properties of the deposited minerals were analyzed by XRD measurements. In general, two XRD reflection peaks are used to monitor the HAP formation; one at 2θ = 26 and the other group is ranging from 2θ = 30 to 2θ = 34-36 [162,163]. We also observed peaks at about 2θ = 26 and 2θ = 32° indicating apatitic minerals (Figure 4.16A).

The TGA thermograms which indicate the degree of mineralization were investigated for H:PAA-BP hydrogel before and after mineralization and compared with the mineralization of H:PAA-NH_2 hydrogel (Figure 4.16B). For all hydrogels the first weight loss at ca. 100 °C is due to dehydration processes. The unmineralized H:PAA-BP hydrogel started to degrade at ca. 200 °C, whereas for the mineralized ones this temperature was shifted to ca. 300 °C probably due higher thermal stability of the hybrid materials. The weight loss continued until ca. 500 °C due to degradation of the main chain. The final amount of inorganics are 23 and 12% for H:PAA-BP and H:PAA-NH_2 hydrogels, compared to 0.9% for unmineralized H:PAA-BP hydrogel. This indicates that both the BP and amine groups contribute to mineralization but the performance of the former is better.

.

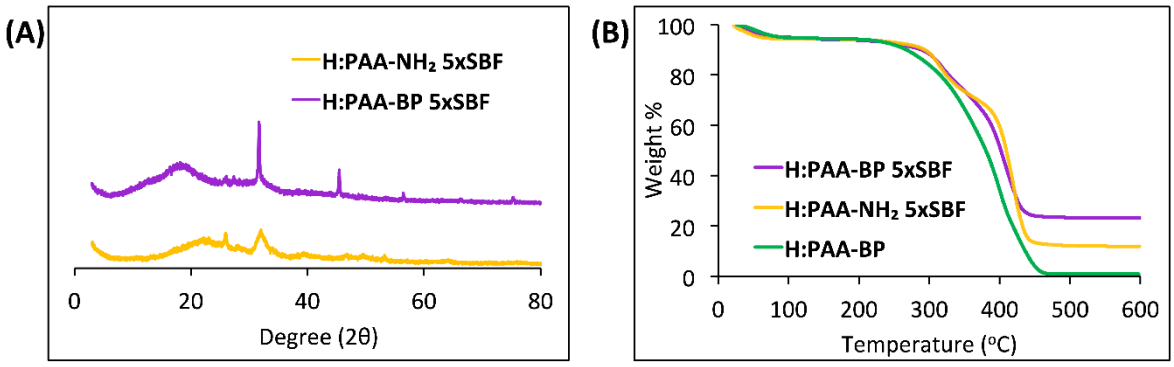

Figure 4.16. A) XRD spectra for hydrogels H:PAA-BP and H:PAA-NH_2 before and after mineralization in 5xSBF, B) TGA thermograms of H:PAA-BP, before and after mineralization, and H:PAA-NH_2 after mineralization, in 5xSBF.

4.3.7. Mechanical Properties

Mechanical properties of the gels in their equilibrium swollen states were investigated by uniaxial compression tests. Figure 4.17 shows nominal stress (σ_{nom})–strain (ε) curves and Young's modulus E of hydrogels before and after mineralization in 5xSBF. It is seen that both Young's modulus E and compressive strength of the BP containing hydrogel (H:PAA-BP) is higher than that of the control hydrogel (H:PAA-NH_2). For example, the modulus E of the H:PAA-BP hydrogel is 42±2 kPa compared to H:PAA-NH_2 hydrogel with a value of 34±2 kPa.

Mechanical tests were also conducted on mineralized hydrogels. It was observed that mineralization significantly affects the mechanical performances of both hydrogels, the modulus E increasing from 34±2 kPa to 54±3 kPa for H:PAA-NH_2 hydrogel and from 42±2 kPa to 83±1 kPa for the H:PAA-BP hydrogel. As expected, higher increase on mechanical properties was seen for the BP containing H:PAA-BP hydrogel after mineralization due to the physical interaction between polymer and HAP like minerals forming on hydrogels.

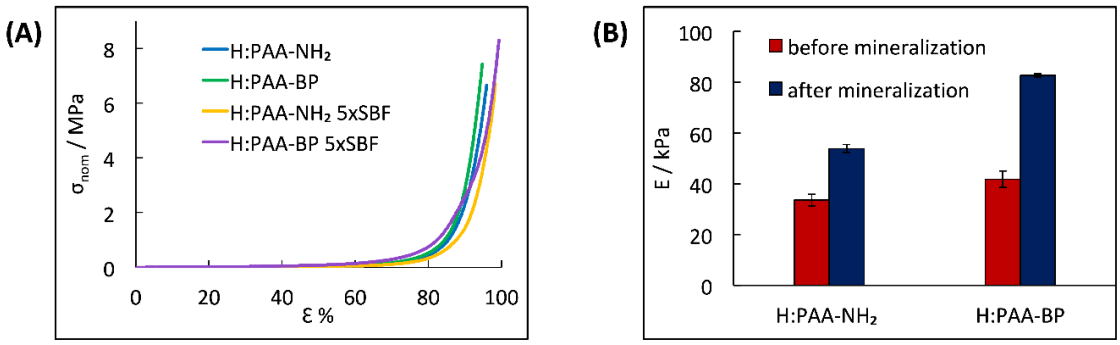

Figure 4.17. Stress – strain curves A) and Young's modulus E B) of H:PAA-NH_2 and H:PAA-BP before and after mineralization in 5xSBF.

4.3.8. *In vitro* Cytotoxicity of Hydrogel Degradation Products

Cytocompatibility of hydrogels was determined by extracting degradation products from the hydrogels and then exposing Saos-2, U-2 OS, NIH 3T3 and C2C12 cells to the extracts. A cell type and dose-dependent (5-100 µg/ml) study was performed in order to evaluate the influence of concentration of the degradation products as well as their composition on the viability of the cell lines (Figure 4.18). Cell viability above 80% is assumed as noncytotoxic according to ISO 10993–5 [147]. It was observed that both hydrogels' degradation products did not cause significant cytotoxicity in osteosarcoma cells (Saos-2 and U-2 OS cells) and muscle cells (C2C12 cells); and a low cytotoxicity (75% viability) of the degradation products of the control hydrogel was detected for NIH 3T3 cells at the highest tested concentration, 100 µg/ml due to more vulnerable nature of these cells.

4.3.9. Cell Interaction Studies

The ability to support cell proliferation is an essential requirement for tissue engineering scaffolds. Bisphosphonic acid, phosphate and phosphonic acid functional groups are known to positively affect cell adhesion, proliferation and spread [164-166].

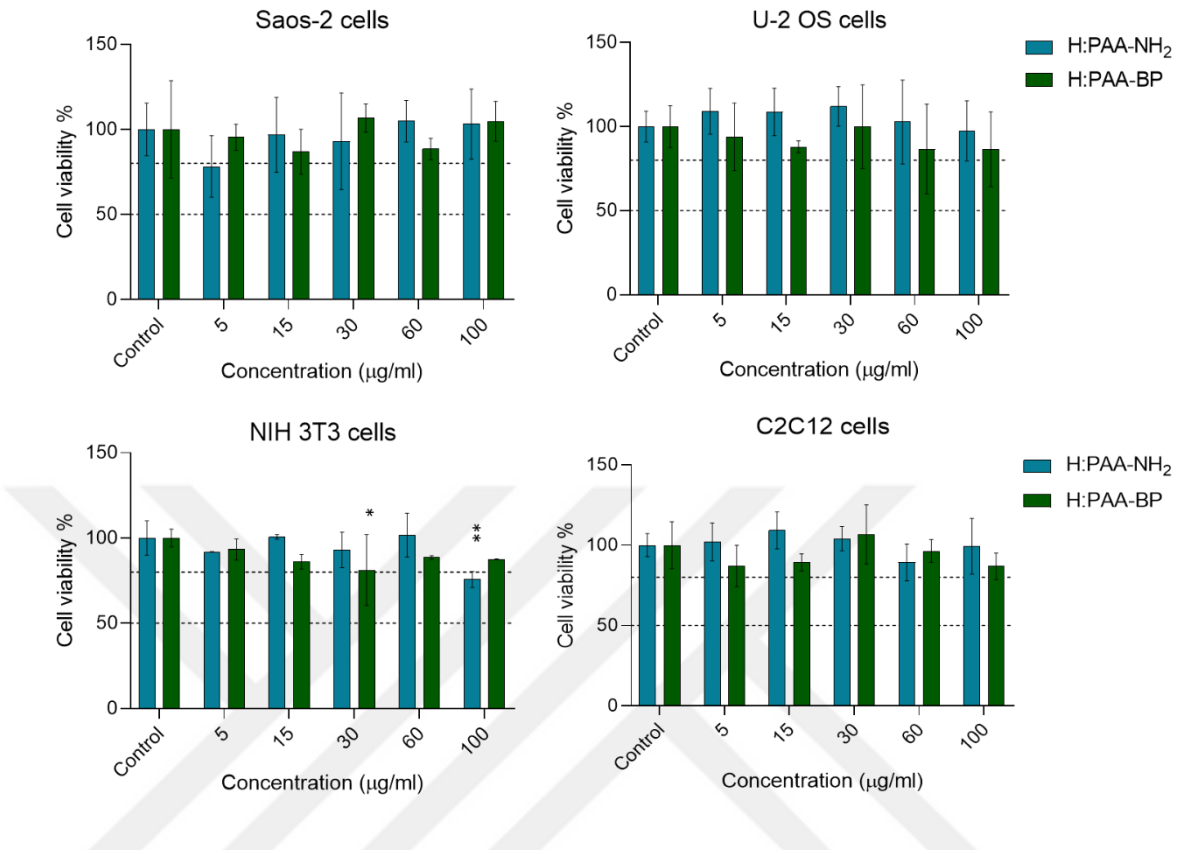

Figure 4.18. Viability of Saos-2, U-2 OS, NIH 3T3 and C2C12 cell lines treated with degradation products of H:PAA-NH_2 and H:PAA-BP for 48 hours. Statistics were conducted by using an ordinary one-way ANOVA analysis of variance followed by multiple Dunnett's comparison test of GraphPad Prism 8 software. Data were presented as mean ± SD of independent experiments (n = 6 for Saos-2, U-2 OS and C2C12 cells, n = 4 for NIH 3T3 cells). $p < 0.05$ was accepted as a statistically significant difference. $p < 0.0332$(*) and $p < 0.0021$(**). Dashed lines show the 80% and 50% viability.

Likewise, mineralized HAP or similar mineral layers on the gel layer leads to improved cell viability [167,168]. Here, we also observed successful attachment of C2C12 mouse myoblast muscle cells on mineralized H:PAA-BP hydrogels. Fluorescence images (Figure 4.19) obtained from cells stained with nuclear stain DAPI (blue) and cytoskeleton stain phalloidin (Green) show that attachment, spread, density, and the health of cells on mineralized hydrogels are comparable to those seen in control cells which were directly seeded on culture plates. Cytoskeleton staining with phalloidin (Green) interacted with the

gel but still shows the cytoskeleton around nuclei. These suggest that mineralized gels are suitable for attachment and proliferation of cells with no specific toxicity.

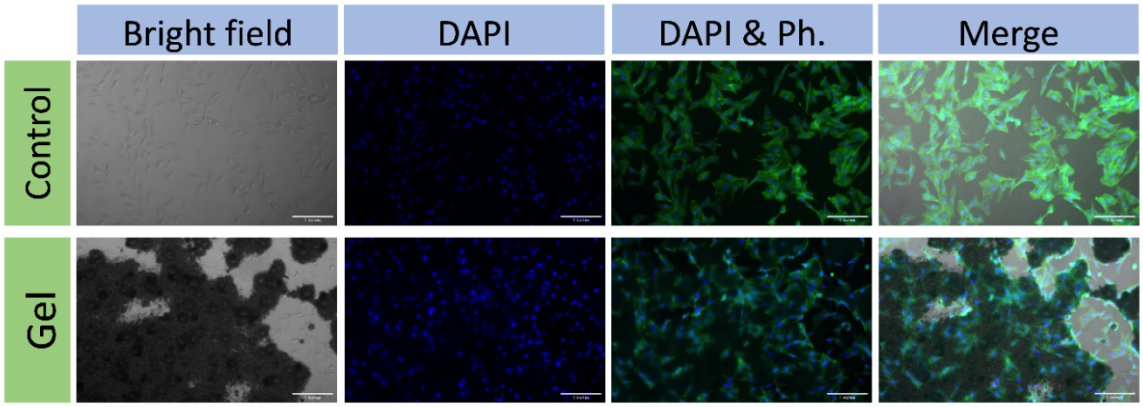

Figure 4.19. Attachment and spread of C2C12 myoblast muscle cells on the mineralized H-PAA-BP gel after 20 hours of incubation. Blue: Nuclear DAPI stain; Green: Phalloidin cytoskeleton stain. Filters: DAPI filter and FITC filter. Magnification: 10X. Scale: 200 µm.

4.4. Conclusions

A HEMA-based hydrogel bearing BP groups was shown to be an effective biomaterial for biomineralization. The hydrogel was synthesized by copolymerization of HEMA and a PAA macromer, where BP groups were incorporated into about half of the primary amine groups present at the side chains of the macromer in the previous step of the synthesis. This novel hydrogel was compared with one produced from the PAA macromer with no BP functionalization, i.e. featuring NH_2 only (control hydrogel). The macromers were found to enhance degradability of HEMA hydrogels (H:PAA-BP and H:PAA-NH_2), controlled by their hydrophilicity and hydrogen bonding interactions due to BP and NH_2 groups. The equilibrium swelling of both hydrogels were highly sensitive to pH of the swelling medium. In addition, H:PAA-BP's swelling is also positively affected by the presence of $CaCl_2$, which indicates the formation of physical crosslinks between BP groups and Ca^{2+} ions. Both hydrogels showed HAP like mineral layers in 5xSBF, with mineral contents of 23 and 12%

for H:PAA-BP and H:PAA-NH_2 hydrogels respectively, indicating better performance of the former. These results show that for purposes of adding mineralization ability to hydrogel biomaterials, the BP groups constitute an alternative to the bisphosphonic acid groups previously investigated in the literature. The mineralization significantly affects the mechanical performances of both H:PAA-BP and H:PAA-NH_2 hydrogels, as expected PAA-BP forming stronger hydrogel-apatite composites compared to PAA-NH_2. The cell experiments showed that H:PAA-BP hydrogel facilitates cell attachment, spread and proliferation after mineralization. Therefore these materials, especially the novel H:PAA-BP hydrogel, have great potential for use in tissue engineering applications.

5. MESO-2,3-DIMERCAPTOSUCCINIC ACID-BASED MACROMERS FOR PH-SENSITIVE DEGRADABLE HYDROGELS

The work described in this section has been published as [169]: Guven, M.N., G. Demirci, H. Yagci. Acar, and D. Avci, "Meso-2,3-dimercaptosuccinic Acid-Based Macromers for pH-Sensitive Degradable Hydrogels", *ACS Applied Polymer Journal,* Vol. 5, No. 11, pp. 9147-9158, 2023.

5.1. Introduction

Hydrogels are physically or chemically crosslinked three-dimensional polymer networks which are capable of containing significant amounts of water. Due to their tailorable mechanical properties and structural similarity to extracellular matrix (ECM), hydrogels have been attracting great interest for use in biomedical applications. Properties of hydrogels can be controlled by using different functional groups and preparation methods. For example, hydrogels can be designed to respond to different external stimuli such as temperature, pH, solvent, electric field, magnetic field, light, enzymes and redox state based on their chemical structure.

In particular, pH-responsive hydrogels have become very popular and were highly studied, especially in the biomedical field, since the pH of inflamed or cancerous tissue is slightly different from that of healthy tissue. An important subgroup of pH-responsive hydrogels is comprised by anionic ones. Their tunable pH dependent swelling behaviors make them excellent materials for use in drug delivery systems, while their heavy metal complexing ability makes them important for metal chelation studies.

Since hydrogels generally do not have sufficient mechanical strength for desired biomedical applications, producing hydrogels with high mechanical performance such as

nanocomposite hydrogels and double-network hydrogels has become a subject of much research recently [170-172]. In the hybrid double-network hydrogels chemical crosslinking can be achieved by covalent bonds, while physical crosslinking can be achieved by various methods such as ionic interaction, hydrogen bonds and hydrophobic association [173]. Metal coordination interaction can be used to form the second network in the presence of anionic pendant groups such as carboxylic acid groups of the polymer networks and the divalent or trivalent cations such as Ca^{2+} or Fe^{3+} [174,175].

In this study, we report the design of four DMSA-based macromers containing acid-sensitive functional groups with diverse properties and use of them for pH sensitive and degradable hydrogel formation. The macromers were synthesized via thiol-Michel addition reaction of DMSA by using two different ene-containing groups (MBA and PEGDA) and two different base catalysts (NaOH and triethyl amine). The characterizations of macromers with different backbone structures and different counterions of acid groups were investigated, as well as the effects of their structures on photopolymerization properties.

The hydrogels were prepared by radical photopolymerization of a mixture of the macromers and HEMA (2-hydroxyethyl methacrylate), since poly(HEMA) is one of the widely used polymers for various biomedical applications due to its biocompatibility. Swelling of the hydrogels can be modulated by crosslinker structure and environmental conditions. In the physiological environment, carboxylic acid/carboxylate anions can form hydrogen bonds with water molecules, increasing stability of the network structure. These macromers are expected to enhance degradation of HEMA hydrogels which degrade very slowly under physiological conditions. The carboxylate functional groups in hydrogel structures can provide the necessary chelating sites for the metal ions. Mechanical properties of hydrogels before and after complexing with Fe^{3+} were investigated.

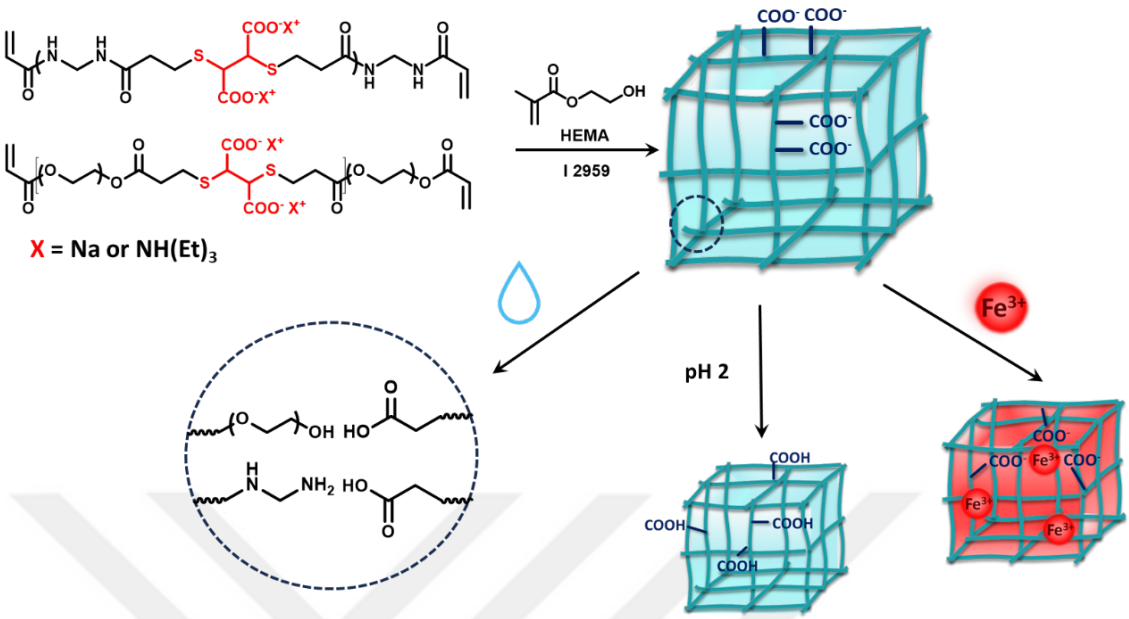

Figure 5.1. Design of functional hydrogels.

5.2. Experimental

5.2.1. Materials and Methods

DMSA, PEGDA (M_n = 575 g/mol), MBA, HEMA, 2-hydroxy-4′-(2-hydroxyethoxy)-2 methylpropiophenone (Irgacure 2959), triethylamine (TEA), calcium chloride, iron(III) chloride and all other chemicals and solvents were purchased in the highest quality from Sigma-Aldrich and used as received. Phosphate buffered saline (PBS) was obtained from Biomatik Corporation (Canada). Dulbecco's Modified Eagle's Medium (DMEM, with L-glutamine and high glucose (4.5 g L^{-1})), penicillin/streptomycin (pen–strep), fetal bovine serum (FBS) and trypsin–EDTA were purchased from Diagnovum, Ebsdorfergrund (Germany). Thiazolyl blue tetrazolium bromide (MTT) was provided by Gold Biotechnology (USA) and phosphate buffered saline (PBS) tablets were provided by BBI Life Sciences (China). 96-Well plates were obtained from Nest Biotechnology (China). U-2 OS human bone osteosarcoma epithelial cells were a kind gift from Prof. Dr. Devrim

Gozuacik (KUTTAM, Koc University, Istanbul, Turkey). C2C12 mouse myoblast cells were obtained from ATCC (USA).

The ^{1}H and ^{13}C NMR spectra of macromers were recorded at ambient temperature on a Varian Gemini (400 MHz) spectrometer. IR spectra were obtained using a Nicolet 380 spectrophotometer equipped with a diamond ATR. Raman spectra were recorded using a Renishaw InVia Raman Microscope. Photopolymerizations were performed on a Discovery DSC 250 (TA Instruments). Swelling and degradation studies of hydrogels were done by using an orbital shaker at 37 °C and 120 rpm. Degradation studies were carried out at 37 °C using a VWR Incubating Mini Shaker operating at 120 rpm. Scanning electron microscope (SEM) (FEI-Philips XL30) was used to assess the morphology of hydrogel samples after sputter-coating with a platinum layer.

5.2.2. Synthesis of Macromers

Four DMSA-based macromers (PEG-DMSA/Na, PEG-DMSA/TEA, MBA-DMSA/Na and MBA-DMSA/TEA) were synthesized via thiol-Michel addition reaction of DMSA with PEGDA or MBA using 1:1.4 mol ratio and NaOH or TEA as catalyst (PEGDA-DMSA/TEA using 1:1.8 mol ratio).

PEG-DMSA/Na

DMSA (110 mg, 0.6 mmol) was dissolved in H_2O and 10 wt% NaOH solution. Then PEGDA (483 mg, 0.84 mmol) was added to the solution and the total monomer concentration was adjusted as 0.5 M and the pH as 11 by adding H_2O (1.6 mL total) and 10 wt% NaOH solution (1 mL total). The solution was stirred at room temperature for 4 days and then dialyzed in water using a membrane with a molecular weight cut-off of 1000 Da. The pure product was obtained after lyophilization as a white solid in 85% yield.

MBA-DMSA/Na

MBA-DMSA/Na was synthesized using same method from reaction of DMSA (151 mg, 0.83 mmol) and MBA (179 mg, 1.16 mmol) in aq. NaOH solution. The reaction mixture was stirred for 3 days at room temperature and then dialyzed in water using a membrane with a molecular weight cut-off of 1000 Da. The pure product was obtained after lyophilization as white solid in 80% yield.

PEG-DMSA/TEA

PEG-DMSA/TEA was synthesized from reaction of DMSA (101 mg, 0.56 mmol), PEGDA (448mg, 0.78 mmol) and TEA (225 mg, 2.2 mmol) in H_2O. The mole ratios of PEGDA: DMSA: TEA were used as 1.8:1:3. The total concentration was adjusted as 0.5 M and pH 11. The reaction mixture was stirred for 3 days at room temperature and then dialyzed in water using a membrane with a molecular weight cut-off of 1000 Da. The pure product was obtained after lyophilization as colorless viscous liquid in 76% yield.

MBA-DMSA/TEA

MBA-DMSA/TEA was synthesized by the reaction of MBA (101 mg, 0.56 mmol), DMSA (448 mg, 0.78 mmol) and TEA (225 mg, 2.2 mmol) in H_2O (total concentration 0.5 M, pH 11). The reaction mixture was stirred for 3 days at room temperature and then dialyzed in water using a membrane with a molecular weight cut-off of 1000 Da. The pure product was obtained after lyophilization as white solid in 79% yield.

.

5.2.3. Photopolymerization Studies

The photo reactivities of the synthesized macromers were analyzed during their copolymerizations with both HEMA and PEGDA using photo-DSC, equipped with a UV-VIS light (320-500 nm) source (Omnicure 2000 with dual-quartz light guide). Formulations (3±0.5 mg) containing HEMA:macromer or PEGDA:macromer (96:4 mol% and 99:1

mol%), water (5 wt%) and Irgacure 2959 (2 wt% of total monomer amount) were exposed to irradiation at 25 °C under nitrogen for 5 min.

The heat flow of the polymerization reaction was recorded as a function of time. Total double bond conversion (DBC) was calculated by

$$DBC = \frac{\Delta Hp}{\Delta H_{0p}}, \tag{5.1}$$

where ΔH_p is the overall heat evolved and ΔH_{0p} is the theoretical heat obtained for 100% conversion. Polymerization rates (s^{-1}) were calculated by

$$Rate = \frac{\left(Q/_s\right)M}{n(\Delta H_{op})m}, \tag{5.2}$$

where *Q/s* is the heat flow per second, *M* is the molar mass of the monomer, *n* is the number of double bonds per monomer molecule, ΔH_{0p} (86 kJ/mol for acrylate and 82 kJ/mol for acrylamide double bonds) is the heat released per mole of double bonds reacted, and *m* is the mass of monomer in the sample.

5.2.4. Synthesis of Hydrogels

The macromer (PEG-DMSA/Na, PEG-DMSA/TEA, MBA-DMSA/Na and MBA-DMSA/TEA) crosslinked HEMA hydrogels were prepared using solutions of HEMA (96 mol%), macromer (4 mol%), Irgacure 2959 (2 wt% of total monomer) and distilled water (2 times the total monomer by weight). The solutions were placed into 2 mL syringes and exposed to UV light (365 nm) for 30 min in a photoreactor (Kerman UV/18) containing 12 Philips TL 8 W BLB lamps. The hydrogel samples were cut into cylindrical pieces (diameter: 4 mm, length: 7 mm) and immersed in ethanol and subsequently in distilled water for 12 h each to remove unreacted gel precursors and then lyophilized and weighed. Also, homogel of the macromer PEG-DMSA/Na was prepared by the same method. The percent gelation was calculated by

$$\text{Gelation (\%)} = \frac{\boldsymbol{weight\ of\ dried\ hydrogel}}{\boldsymbol{weight\ of\ initial\ (monomer+macromer)}} \times 100. \tag{5.3}$$

5.2.5. Swelling Studies

Swelling studies were carried out by immersing dry hydrogel samples into water, 0.5 M $FeCl_3$, 0.5 M $CaCl_2$, and phosphate buffer solutions (pH 2, pH 7.4 and pH 11) in an orbital shaker operating at 120 rpm at 37 °C. The hydrogel samples were taken out of the solutions at predetermined time intervals and the excess solution was removed with tissue paper and the swollen weights were measured. The swelling ratio (Q) was calculated by

$$Q = \frac{W_s - W_d}{W_d} \times 100, \quad (5.4)$$

where W_s and W_d refer to the weight of swollen and dry gel samples, respectively. The average data obtained from triplicate measurements were reported.

5.2.6. Degradation Studies

Degradation studies of the hydrogels were conducted by immersing dry hydrogel samples (W_i) in 15 mL of degradation solutions used in swelling study, at 37 °C. After 4 weeks, the samples were taken out, rinsed with water, freeze-dried and re-weighed (W_f). The degradation % was calculated according to

$$Degradation\ (\%) = \frac{W_i - W_f}{W_i} \times 100, \quad (5.5)$$

The average values from triplicate measurements were reported.

5.2.7. Determination of Fe^{3+} Adsorption of Hydrogels

Ferric ion adsorption properties of the hydrogels were determined by Ultraviolet-visible spectrophotometric method. The reduction of Fe(III) ion by hydroquinone in the presence of 1,10-phenanthroline yields an orange-red complex (ferrous tris(1,10-phenanthroline) iron(II)) with a maximum absorption at 512 nm [176]. First, a stock $FeCl_3$

solution was prepared by dissolving 138.61 mg of it in 1000 mL distilled water (total Fe^{3+} amount is 47.72 mg in 1000 mL). Calibration standard solutions were prepared by taking 5, 10, 15, 20 mL of the stock solution and adding 5 mL of 1,10-phenanthroline (2.5 g/L) and 15 mL of hydroquinone (10 g/L). The solutions were diluted to 100 mL with distilled water. Then a calibration curve of absorbance versus concentration was constructed at 512 nm.

The hydrogels disks were placed into 20 mL of stock $FeCl_3$ solution for 24 hours, then 10 mL of the solution was taken, hydroquinone (15 mL) and 1,10-phenanthroline (5 mL) were added. The amount of Fe^{2+} in the solution was determined using the calibration curve and the amount of Fe^{3+} adsorbed by the hydrogels was calculated [177]. The equilibrium adsorption capacity, q_e (mg g^{-1}), was calculated by

$$q_e = \frac{(C_o - C_e) \times V}{m}, \tag{5.6}$$

where C_0 (mg.L^{-1}) is the initial concentration, C_e (mg.L^{-1}) is the equilibrium concentration, m (g) is the weight of the dry sample and V (L) is the volume of the ionic solution [178].

5.2.8. Mechanical Studies

For compression tests, the macromer and HEMA mixture was prepared in the same way as above and polymerized in 1 mL syringes and washed in ethanol for 24 hours without cutting. Then hydrogels were placed in EtOH, pH2 buffer, 0.5 M $FeCl_3$ solution and water for 12 hours. Mechanical properties of hydrogels in equilibrium swollen states in these solutions were measured by uniaxial compression measurements on a Zwick Roell test machine with a 500 N load cell. After applying an initial compressive force of 0.05 N, tests were carried out at a constant crosshead speed of 5 mm min^{-1}. The stress was calculated as its nominal σ_{nom} and true values σ_{true} ($=\lambda\ \sigma_{nom}$), which are the forces per cross-sectional area of the undeformed and deformed gel samples, respectively, and λ is the compression ratio. The strain is given by ε which is the change in the specimen length with respect to its initial length, that is, $\varepsilon = 1 - \lambda$. The compressive strength and strain at break of the hydrogels were calculated from the maxima in σ_{true} versus ε curves as detailed before [128]. Young's

modulus E of the hydrogels was calculated from the slope of stress−strain curves between 5 and 15% compressions.

5.2.9. *In vitro* Cytotoxicity Assay

Cytotoxicity of the macromers was tested on U-2 OS and C2C12 cell lines using the standard MTT viability assay. The cells were cultured in DMEM complete medium with and without phenol red, respectively, supplemented with 10% (v/v) FBS and 1% (v/v) pen-strep in a 5% CO_2-humidified incubator at 37 °C and passaged regularly. For viability test, cells were seeded at a density of $75x10^3$ cells/mL in each well of a 96 well-plate and incubated at 37 °C in 5% CO_2 atmosphere. The macromer was added at concentrations between 5-100 µg/mL. After 24 h incubation, the cell viability was assessed using MTT colorimetric assay. 150 µL of culture medium and 50 µl of MTT solution (5 mg/mL in PBS) was added into each well and incubated for 4 h. Then, the purple formazan crystals formed as a result of mitochondrial activity in viable cells were dissolved with ethanol: DMSO (1:1 v/v) mixture. The absorbance at 570 nm with a reference reading at 630 nm was recorded for each well using a Synergy – H1 microplate reader (BioTek Instruments Inc., Winooski, VT, USA). Cells which were not exposed to macromers were used as controls which were assumed to have 100% viability. The relative cell viability was calculated by

$$Cell\ viability\ (\%) = \frac{Absorbance_{sample}}{Absorbance_{control}} \text{x } 100. \tag{5.7}$$

For statistical analysis of the MTT results, the one-way analysis of variance (ANOVA) analysis of variance followed by the multiple Dunnett's comparison test of GraphPad Prism 8.3 software package (GraphPad Software, Inc.) was used. All measurements were expressed as mean values ± standard deviation (SD). $p < 0.05$ was accepted as a statistically significant difference.

5.3. Results and Discussion

5.3.1. Synthesis and Characterization of Macromers

Four novel macromers PEG-DMSA/Na, PEG-DMSA/TEA, MBA-DMSA/Na and MBA-DMSA/TEA were synthesized by thiol Michael addition reactions of DMSA with MBA or PEGDA by setting the mol ratio of DMSA to acrylate or acrylamide to 1:1.4. For macromer PEG-DMSA/TEA, this ratio has been changed to 1:1.8 to get shorter macromer chain. In general, the thiol Michael addition reactions can be carried out under base catalysis with reagents such as primary and tertiary amines and phosphines to generate thiolate anion and conjugate acid. The thiolate anion attacks the double bond carbon, forming carbon-centered anion as an intermediate which is then protonated using the conjugate acid [179,180].

In our reactions NaOH or TEA was used as a base to generate anionic and strongly nucleophilic thiolates and the reactions were carried out in aqueous solution at room temperature for 3-4 days. After formation of the thioether products, regenerated base catalyst was also used to neutralize carboxylic acid groups of the products. The total concentration of the reactants was fixed at 0.5 M and the macromers were obtained in 75-85% yields after purification by dialysis. PEG-DMSA/TEA was obtained as a colorless liquid, while the other three were white solids (Figure 5.2).

The chemical structure of the macromers was verified by ^{1}H NMR, ^{13}C NMR, FTIR and Raman spectroscopy ^{1}H NMR of the macromer PEG-DMSA/Na shows acrylate end groups at around 5.95 and 6.45 ppm, methine protons of DMSA at 3.29 ppm and newly formed methylene protons at 2.71 and 2.87 ppm. Furthermore, small symmetrical peaks seen at 2.43 and 2.79 ppm in the spectrum of PEG functional macromers are due to the meso conformation of DMSA (Figure 5.3) [181].

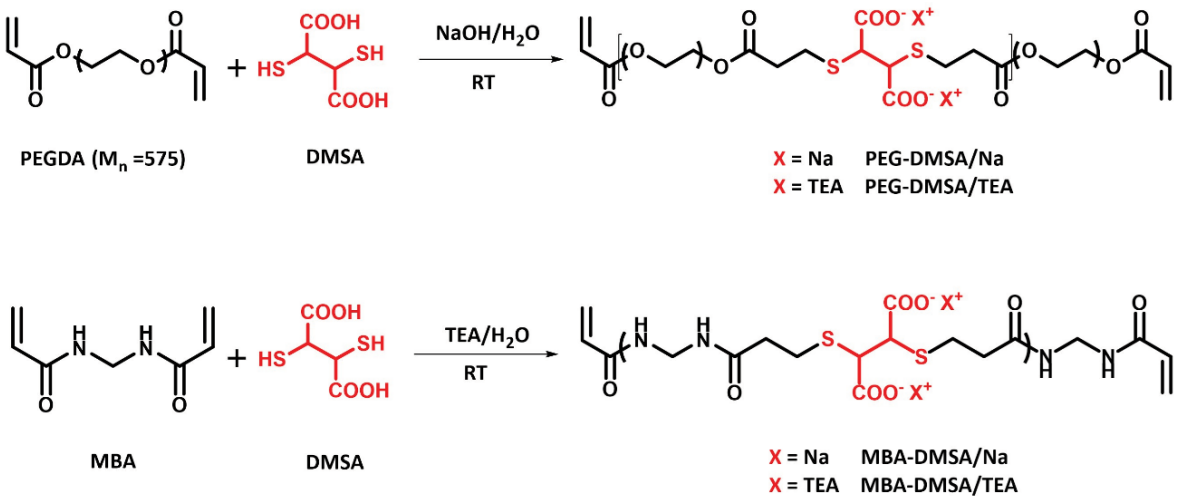

Figure 5.2. Synthesis of macromers.

^{13}C NMR spectrum of this macromer also confirmed its structure (Figure 5.4). The small symmetrical peaks were also seen in carbon NMR resulting from the meso conformation of DMSA. ^{1}H NMR spectrum of MBA-DMSA/Na shows the characteristic methylene (at the end and middle of the macromer) peaks of the MBA at 4.61 and 4.69 ppm. ^{1}H NMR of MBA-DMSA/TEA and PEG-DMSA/TEA show three peaks due to triethylammonium counterion at 3.3, 3.23 and 1.29 ppm, as a result of meso conformation (Figure 5.5).

The average number of repeating units (n) was calculated via comparison of the areas of the double bond protons to methylene protons attached to C=O. This value was found to be 4 for PEG-DMSA/Na and 5 for MBA-DMSA/Na; and used to determine the number-average molecular weights using the equation: M_n = (formula weight of end groups) + (formula weight of repeating unit)(n). The corresponding M_n values was calculated as 3630 and 1900 g/mol for PEG-DMSA/Na and MBA-DMSA/Na. The molecular weights of the macromers synthesized using TEA were higher, indicating better initiating activity of this amine. For PEG-DMSA/TEA n and M_n values were found to be 11 and 12340 g/mol, even at 1:1.8 DMSA: acrylate mol ratio. M_n value of MBA-DMSA/TEA was found as 3100 g/mol.

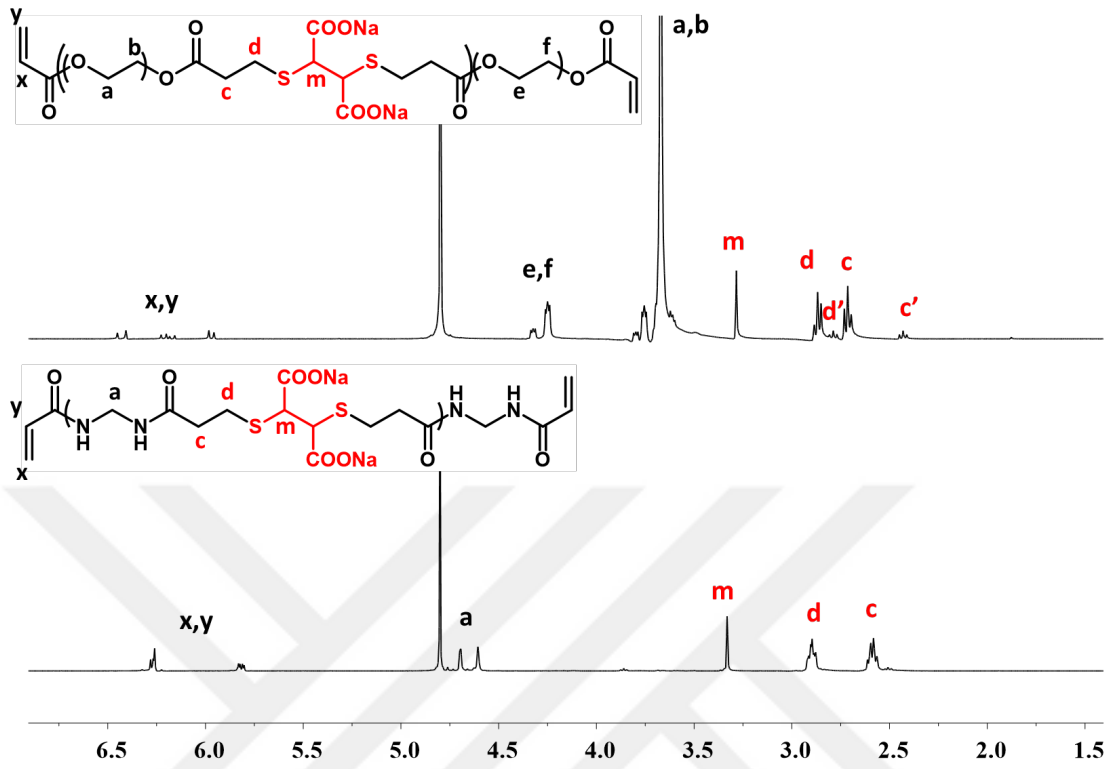

Figure 5.3. ^{1}H NMR spectra of PEG-DMSA/Na and MBA-DMSA/Na.

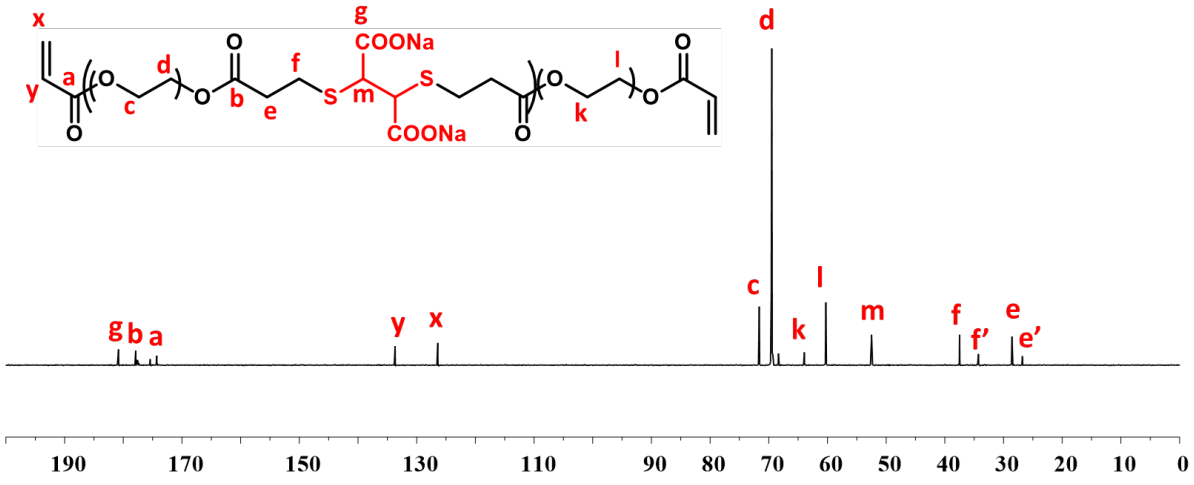

Figure 5.4. ^{13}C NMR spectrum of PEG-DMSA/Na.

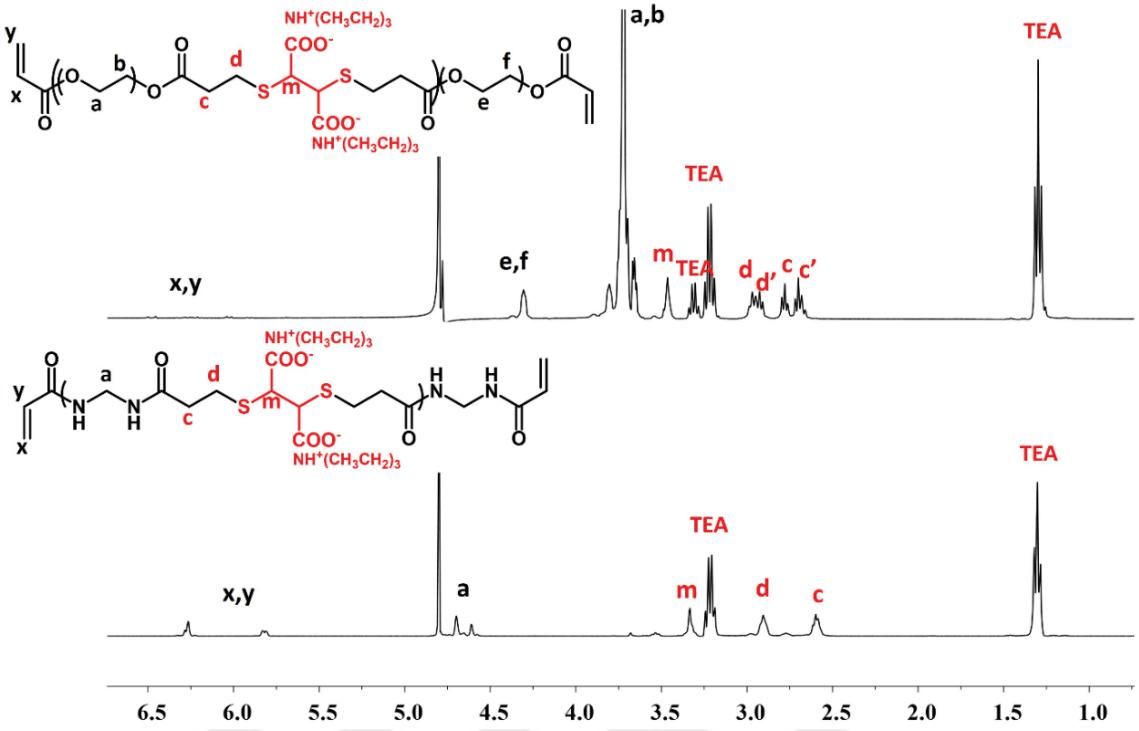

Figure 5.5. ^{1}H NMR of MBA-DMSA/TEA and PEG-DMSA/TEA.

The FTIR spectra of the MBA functional macromers exhibited two major absorption peaks in the range of 1651-1680 cm^{-1} and 1500-1590 cm^{-1} for C=O stretching of amide and carboxylate groups; and 1550-1560 cm^{-1} for N-H bending vibration (Figure 5.6A). On the other hand, PEG functional macromers showed a sharp C=O stretching in the range of 1722-1730 cm^{-1} for ester groups. Besides, characteristic asymmetric vibration bands for carboxylate groups were seen at 1560-1530 cm^{-1}.

Raman spectroscopy was used to observe the presence of -SH and -CS. It was expected that peaks belonging to -SH group would not be seen as a result of the reaction but -CS peaks would be seen. This was confirmed by the Raman spectrum of PEG-DMSA/Na (Figure 5.6B).

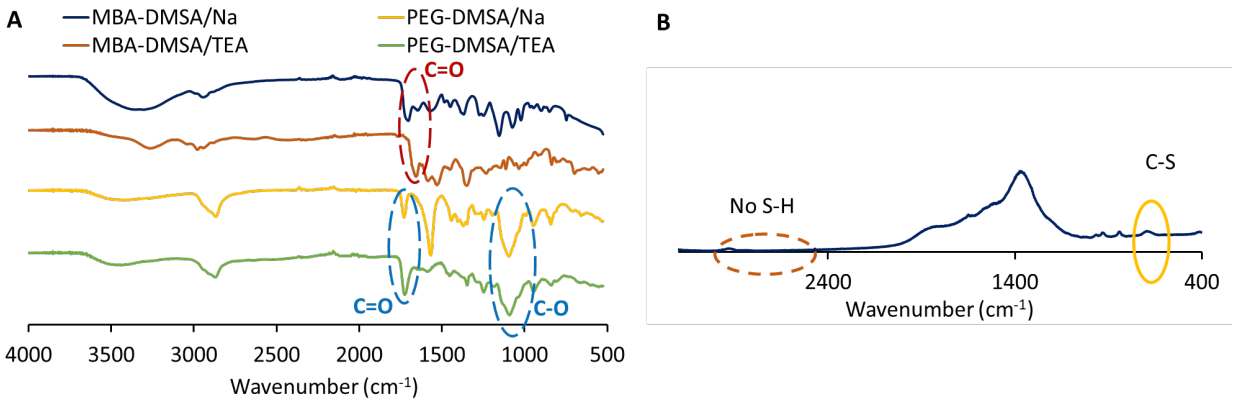

Figure 5.6. A) FTIR spectra of all macromers and B) Raman spectrum of PEG-DMSA/Na.

5.3.2. Photopolymerization of Macromers

The macromers have different functional groups (acrylate/acrylamide), polarity, counterion (Na/TEA), concentration of double bonds (different molecular weights) and flexibility, which may lead to different polymerization reactivities. In order to check their structure-reactivity relationship polymerization kinetics of three of the synthesized macromers (PEG-DMSA/Na, PEG-DMSA/TEA and MBA-DMSA/Na) were investigated during copolymerization with HEMA and PEGDA using photo-DSC. The macromer MBA-DMSA/Na could not be tested due to its low solubility in HEMA and PEGDA. Because the molecular weights of the macromers are different, formulations containing same mole percentages (1 and 4 mol %) of macromers in HEMA or PEGDA were prepared. Since two of the macromers were solid, 5 wt% of water was added to all formulations to prevent dissolution problem, including the reference formulations, HEMA and PEGDA alone.

First, the influence of the macromer structure and its concentration on the polymerization (rate of polymerization, double bond conversion and time to to achieve the maximum polymerization rate) of HEMA were analyzed (Figure 5.7). Dashed lines refer to formulations having 1 mol% of macromer while the solid lines belong to the mixtures prepared with 4 mol% macromer. When a small amount (1 or 4 mol%) of macromer is added to HEMA, we observe a significant increase in the polymerization rate (4 mol% gives a

somewhat higher rate than 1 mol%). The final conversions of the double bonds were in the range 50–70%, much lower than HEMA alone. In general, the formulations having higher marcomer amount (4 mol%) have lower conversions compared to those of having 1 mol% due to their higher crosslinking tendency which reduces the flexibility of the system, leading to a highly rigid network. A dramatic decrease in t_{max} was observed for all formulations compared to HEMA. For example, the t_{max} values of PEG-DMSA/TEA (96:4mol%) and PEG-DMSA/Na (96:4mol%)-containing formulations were 3.0 and 8.4 s, respectively, and hence much lower than HEMA (64.6 s). The increase in polymerization rate, decrease in t_{max} and conversion values were due to the difunctionality of the macromers.

Although it was difficult to correlate the macromers' photopolymerization properties to their structures, it is seen that the crosslinker MBA-DMSA/TEA has the lowest polymerization rate, similar conversions and higher t_{max} values compared to the other macromers at the same concentration. This can be explained by its more rigid structure due to lower molecular weight (smaller distance between functional groups) and amide functionality, both decreasing the mobility of the macromer. PEG-functionalized macromers showed similar polymerization behavior, independent of their counterions and very different molecular weigths.

Contrary to HEMA formulations, when macromers (1 or 4 mol%) were added to PEGDA, we observe a slightly lower polymerization rate, similar t_{max} and conversion values compared to those of PEGDA (Figure 5.8). This behavior can be expected due to difunctional nature of both PEGDA and the macromers. The change in concentration of the macromer from 1 to 4 mol% did not significantly influence the polymerization kinetics. Among the macromers the most reactive one was found to be MBA-DMSA/TEA.

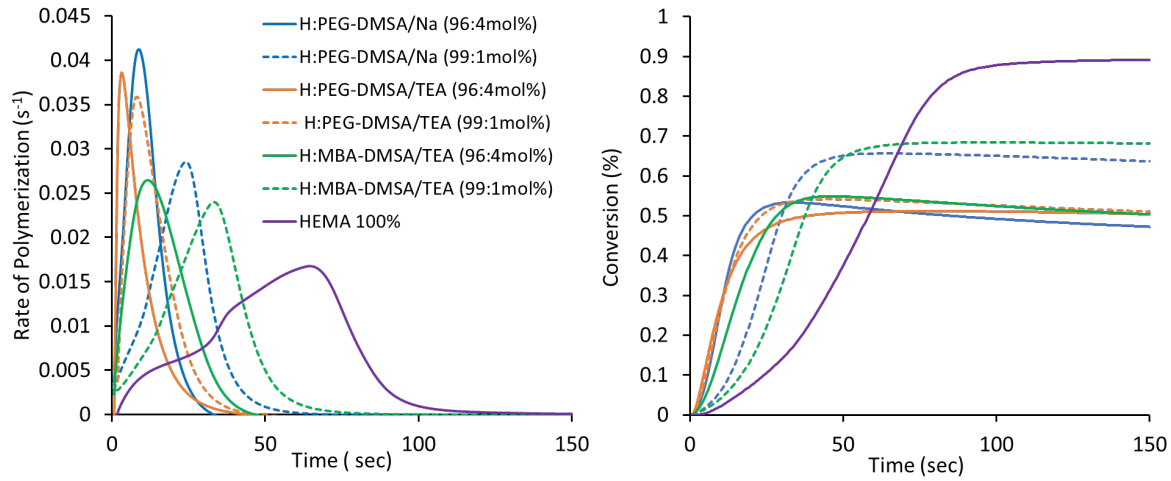

Figure 5.7. Rate–time and conversion–time plots for HEMA containing macromers (1 and 4 mol%). Photopolymerizations were carried out using Irgacure 2959 (2 wt%) under UV-vis light (320–500 nm) irradiation at 25 °C under nitrogen.

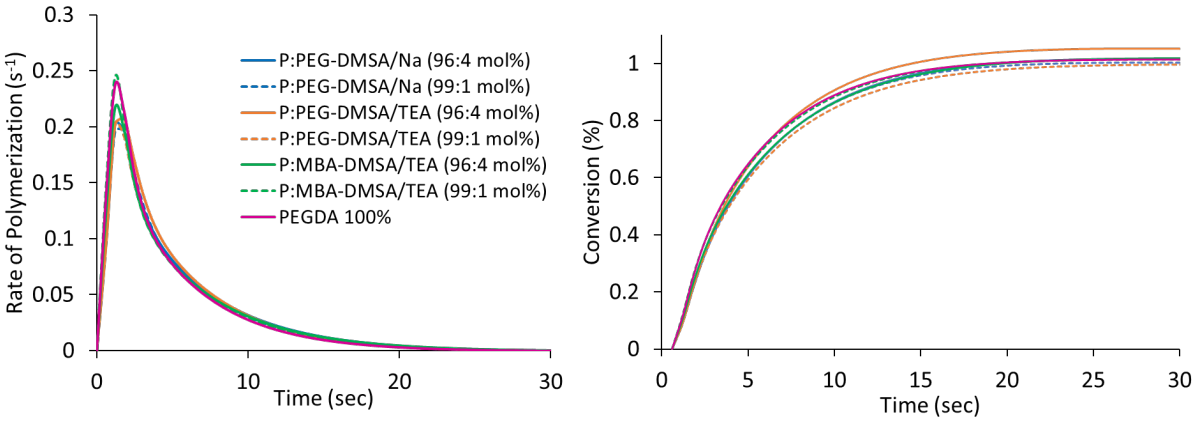

Figure 5.8. Rate–time and conversion–time plots for PEGDA containing macromers (1 and 4 mol%). Photopolymerizations were carried out using Irgacure 2959 (2 wt%) under UV-vis light (320–500 nm) irradiation at 25 °C under nitrogen.

5.3.3. Synthesis and Characterization of Hydrogels

To examine the effect of four macromers with different structures (PEG-DMSA/Na, PEG-DMSA/TEA, MBA-DMSA/Na and MBA-DMSA/TEA) on hydrogel properties, macromers (4 mol%) were separately copolymerized with HEMA by free radical photopolymerization. The hydrogels are named by prefixing the name of the macromer with "H", for example H:PEG-DMSA/Na. Gelation percentages of the hydrogels were found between 80 and 85%. In the FTIR spectra of the hydrogels prepared with PEG-DMSA/Na and PEG-DMSA/TEA, carbonyl stretching peaks both from HEMA and the macromers overlap in the range of 1720-1730 cm^{-1}, while those prepared with MBA-DMSA/Na and MBA-DMSA/TEA show two peaks due to the ester carbonyl of HEMA and the amide carbonyl of the macromers at 1715 cm^{-1} and 1650 cm^{-1} (Figure 5.9). For PEG-DMSA/Na and PEG-DMSA/TEA crosslinked hydrogels, strong C-O stretching peaks were observed between 1000-1100 cm^{-1}.

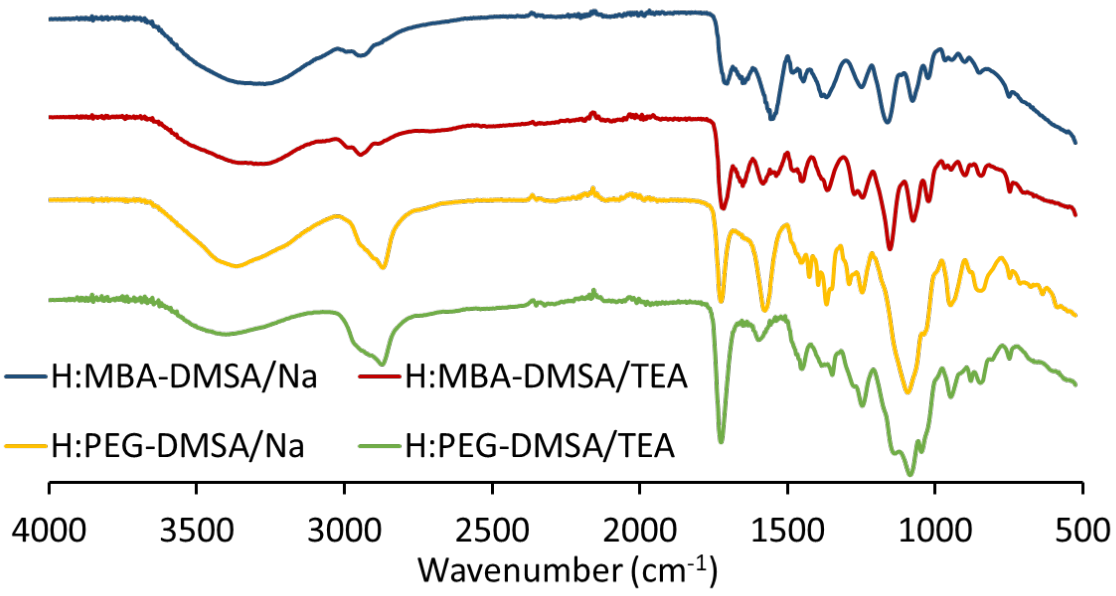

Figure 5.9. FTIR spectra of all hydrogels.

It is known that swelling behavior of hydrogels depends on the structure of the crosslinked polymer, molecular weight of the crosslinker as well as the solvent. First, the swelling properties of the synthesized hydrogels were investigated in different mediums: water, 0.5 M $FeCl_3$, and buffer solutions (pH 2, pH 7.4) at physiological temperature (37 ^oC). (Figure 5.10A). The swelling behavior of homogels of macromer PEG-DMSA/Na was also investigated under the same conditions (Figure 5.10B).

As expected, the swelling degree of hydrogels was higher in water and pH 7.4, due to charge repulsion of the deprotonated carboxylic acid groups, compared to those at pH 2 [182]. At pH 2, strong hydrogen bonding between the carboxylic acid groups increases the degree of crosslinking, reducing free volume and leads to shrinkage of the hydrogel network. The hydrogels soaked in 0.5 M $FeCl_3$ displayed the lowest equilibrium swelling ratio due to strong $Fe^{3+}COO^-$ interactions leading to a double network.

Homogels of PEG-DMSA/Na showed higher swelling ratio than H:PEG-DMSA/Na due to greater charge density and hydrophilicity. Then, the hydrogels are compared among themselves to investigate the effect of crosslinker structure on swelling behavior. The PEG-DMSA/TEA crosslinked hydrogels showed the highest percentage of equilibrium swelling in all solutions. This can possibly be attributed to the highest molecular weight of the crosslinker, reducing the crosslink density and increasing charge density. When the MBA-DMSA/TEA and PEG-DMSA/Na crosslinked hydrogels were compared, the hydrogels containing more hydrophilic PEG group were found to have higher swelling properties, although they have similar molecular weights.

When the swelling properties of the MBA-DMSA/TEA and MBA-DMSA/Na crosslinked hydrogels were compared, the gels containing Na^+ as counter ion had swelling properties close to those containing TEA, although there were large differences in molecular weights, thus in crosslink densities. The negative effect of containing TEA as a counter ion on the swelling properties of gels can be explained by the steric hindrance that TEA adds to the macromer chain, as well as the ionic feature that Na^+ provides to the macromer. To

observe the stability of the hydrogels against cyclic swelling in buffers with different pHs, the H:PEG-DMSA/Na gels were repeatedly immersed in neutral pH (PBS buffer) and acidic pH (pH 2 buffer) solutions, sequentially and it was found that the continuous swelling and shrinking in these solutions did not cause any damage to the hydrogel network (Figure 5.10C).

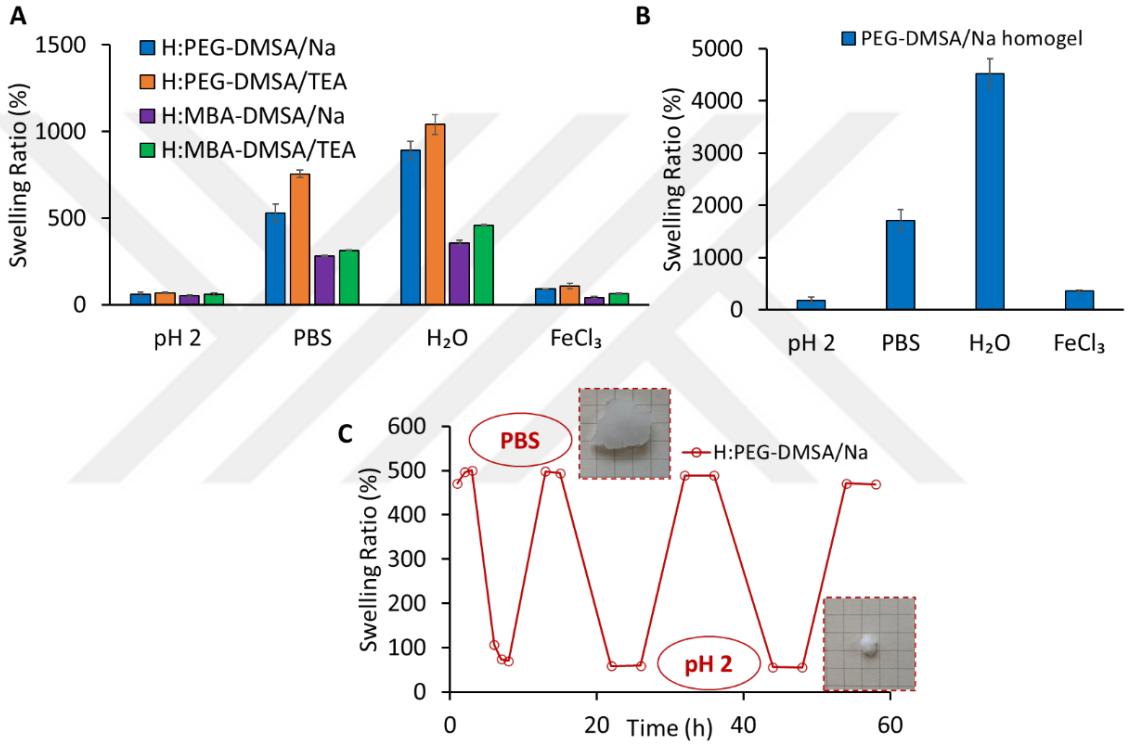

Figure 5.10. A) swelling ratios of the hydrogels, B) swelling ratios of PEG-DMSA/Na homogels, C) swelling– shrinking behavior of H:PEG-DMSA/Na.

The surface morphology of the hydrogels was also investigated by SEM. Figure 5.11A shows the surface cross-sectional SEM image of H:PEG-DMSA/Na. The average pore size of H:PEG-DMSA/Na, H:PEG-DMSA/TEA and H:MBA-DMSA/TEA were found to be similar, 50, 55 and 42 µm, while H:MBA-DMSA/Na gels shows smaller pore sizes (11 µm). Although hydrogels are close to each other in pore sizes except for H:MBA-DMSA/Na, it was observed by SEM images that gels containing Na^+ as counter ion had more porous structure. The SEM image of H:PEG-DMSA/Na hydrogels swollen in 0.5 M $FeCl_3$ was also

recorded and are shown in Figure 5.11B. In the SEM image, adsorption of metal ions was observed on the surfaces and in the pores. Furthermore, a decrease in pore size from 50 µm to 10 µm was observed due to $Fe^{3+}COO^-$ interactions, leading to a denser morphology. All these results support the swelling behavior of the hydrogels. EDX spectrum shows that the crystal structures deposited on the surface belonged to the Fe^{3+} ions (Figure 5.11C).

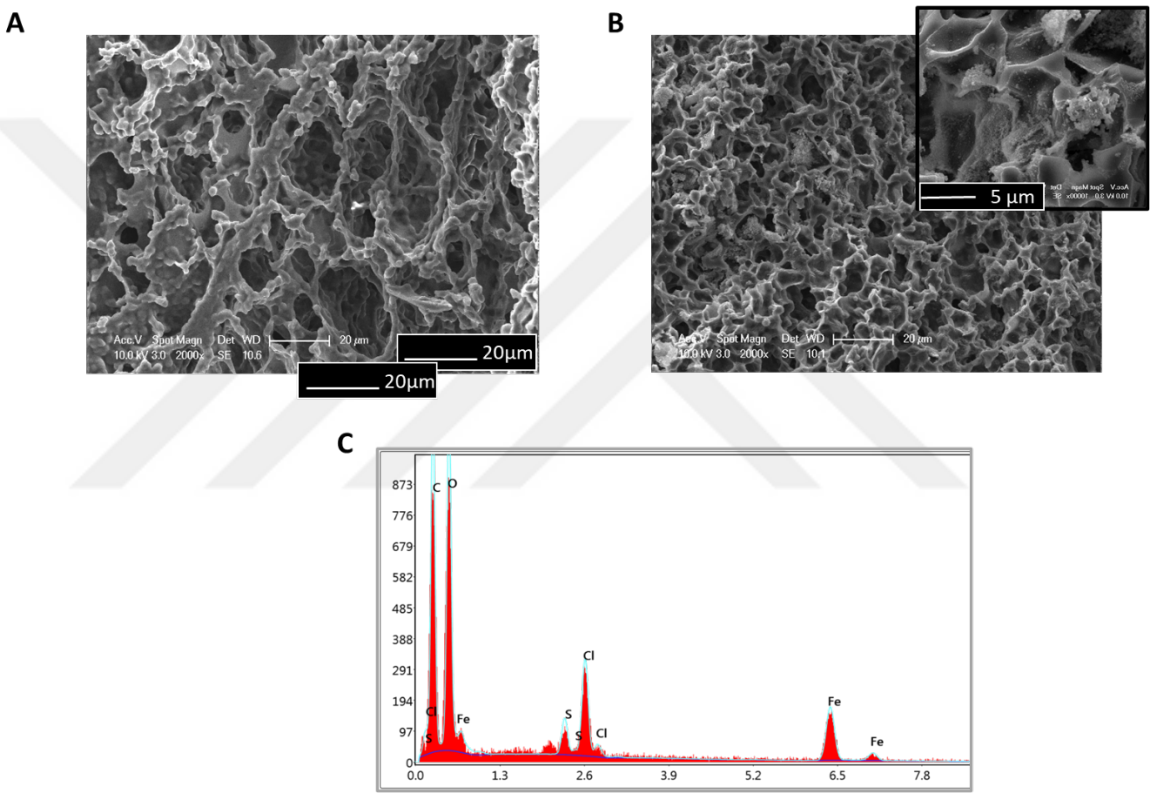

Figure 5.11. A) SEM image of H:PEG-DMSA/Na B) SEM image, C) EDX spectrum of H:PEG-DMSA/Na after swelling in 0.5 M $FeCl_3$ solution for 24 h.

Two of the macromers (PEG-DMSA/Na and PEG-DMSA/TEA) contain ester bonds, so degradation of the hydrogels crosslinked by these macromers will take place by hydrolysis of these bonds. Whereas the other two (MBA-DMSA/Na and MBA-DMSA/TEA) have amide linkages and the hydrogels prepared from these macromers will degrade through hydrolysis of amide bonds. Since the amide linkages are more stable, the hydrogels crosslinked with MBA-DMSA/Na and MBA-DMSA/TEA are expected to degrade more

slowly. The degradation behavior of the hydrogels was investigated in PBS solution at 37 °C and their weight loss was measured (Figure 5.12A). The PEG-DMSA/Na and PEG-DMSA/TEA crosslinked hydrogels lost 36 and 31 % of their initial mass during the 4-week time period. However, the percentage mass loss of the gels prepared from MBA-DMSA/Na and MBA-DMSA/TEA macromers was found to be lower, 23 and 19% during the same period. Moreover, it seemed that the degradation was affected by the relative hydrophobic/hydrophilic composition of the hydrogels. The hydrogels with PEG groups and/or Na^+ counterions have higher hydrophilicity, thus degrade faster than the ones with TEA counterions. These results demonstrate that the macromers can control degradation properties of the hydrogels [183].

The degradation mechanisms of two types of hydrogels, H:PEG-DMSA/TEA and H:MBA-DMSA/Na were examined by comparing the SEM images of the degraded and non-degraded hydrogels. The average pore size throughout the interior of the original H:PEG-DMSA/TEA, which was 55 µm (Figure 5.12B), had enlarged to 102 µm (Figure 5.12C) after 4 weeks degradation in PBS. After the same period, the average pore size of H:MBA-DMSA/Na had increased from 11 µm to 70 µm in PBS. Furthermore, many small pores of 2-7 µm in size appeared in the hydrogel surfaces. From these results, we can say that the hydrogels undergo both bulk and surface degradation [184].

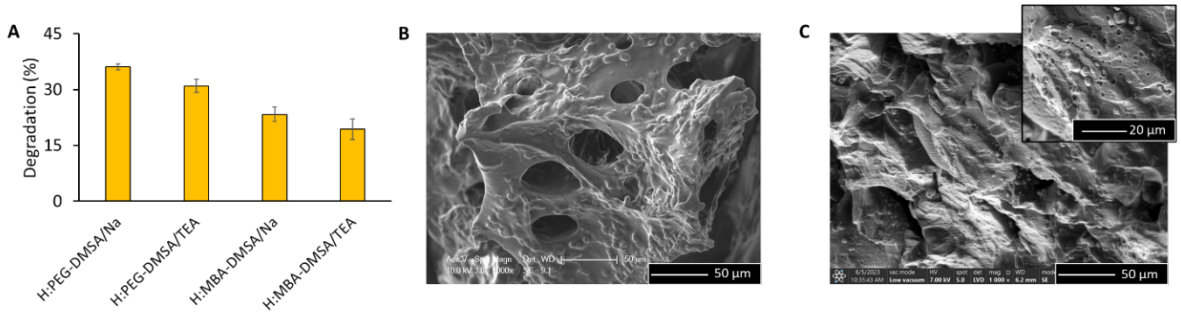

Figure 5.12. A) Degradation of HEMA hydrogels, SEM images of H:PEG-DMSA/TEA B) before degradation, C) after degradation in PBS (magnification x1000).

5.3.4. Complexing Capacities with Fe^{3+} Ion

The ability of DMSA to make complexes with heavy metals such as Hg and Pb is a well-studied subject [185]. The two thiol groups in DMSA are involved in coordination with metals [186]. In our work, these groups were used in thiol-ene reaction to form the macromers. However, the two carboxylic acid groups can provide the chelating sites for metal ions and form crosslinked structures. In order to find the amount of Fe^{3+} adsorbed by the hydrogels, o-phenanthroline method was used and the absorbance was measured at 512 nm. The maximum adsorption capacities of the hydrogels ranged from 20.5 to 13.9 mg/g in a solution with a total Fe^{3+} concentration of 47.72 mg/L, indicating that the macromers have an important role in Fe^{3+} adsorption (Figure 5.13). It was found that H:PEG-DMSA/Na and H:PEG-DMSA/TEA had a stronger adsorption capacity than H:MBA-DMSA/Na and H:MBA-DMSA/TEA. This was probably due to the more hydrophilic nature of the hydrogels prepared using PEG-based macromers, leading to accumulation of metal ions on the surface of the hydrogel and accelerating their diffusion from outside to the adsorption sites. The carboxyl groups of the hydrogels will provide adsorption sides. Also, these two hydrogels have more porous structure, which may enable high transport rates of metal ions. Since the adsorption of Fe^{3+} on the hydrogels is dependent on initial concentration of the solution, it was not possible to compare the adsorption capacity of our hydrogels with those of the literature.

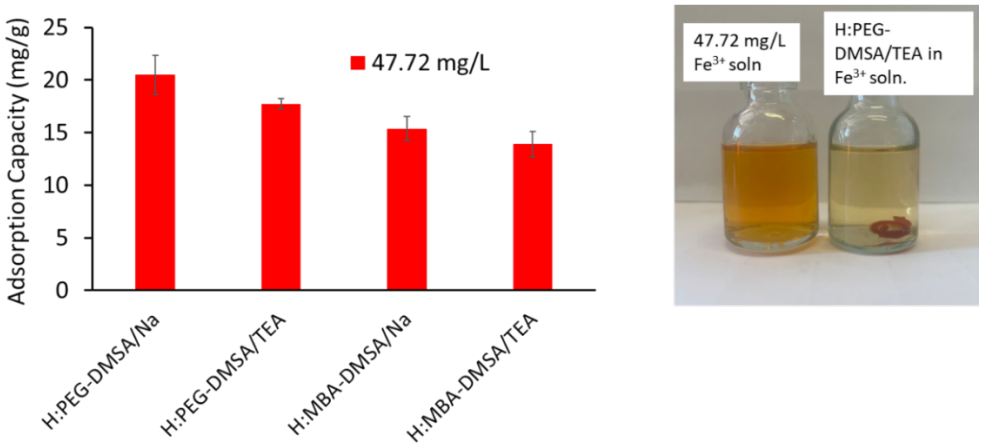

Figure 5.13. Fe^{3+} adsorption capacities of hydrogels.

5.3.5. Mechanical Properties

Mechanical properties of the gels in their equilibrium swollen states were investigated using uniaxial compression tests. Nominal stress (σ_{nom})-strain (ε) curves and Young's moduli E of hydrogels can be seen in Figure 5.14. Compression tests of the hydrogels were performed after the gels were kept in water, ethanol, pH 2 buffer and 0.5 M $FeCl_3$ solution for 12 hours. All of the hydrogels prepared with four different macromer contents showed the highest Young's modulus E when swollen in $FeCl_3$, the lowest modulus when swollen in H_2O.

When the gels were compared among themselves, apart from the solutions in which they immersed, it is seen that H:MBA-DMSA/Na has the highest modulus E, followed by H:PEG-DMSA/Na, H:MBA-DMSA/TEA, H:PEG-DMSA/TEA. For example, Young's modulus of H:MBA-DMSA/Na immersed in EtOH was found as 1.81 ± 0.09 MPa while H:PEG-DMSA/Na's modulus was 193 ± 2.4 kPa, H:MBA-DMSA/TEA's modulus was 135 ± 17 kPa and H:PEG-DMSA/TEA's modulus was 82 ± 3.5 kPa.

The modulus of the hydrogel prepared with the macromer of highest crosslink density, MBA-DMSA/Na, was much higher than the others, while the gel(s) prepared with the macromer of highest molecular weight (therefore lowest crosslink density), PEG-DMSA/TEA, showed the lowest modulus. The significant increase of the modulus of hydrogels when immersed in 0.5 M $FeCl_3$ solution indicates the formation of physical crosslinks between Fe^{3+} and hydrogels. Young's modulus of H:MBA-DMSA/Na increased to 4.83 ± 0.14 MPa when immersed in $FeCl_3$, while H:PEG-DMSA/Na's modulus increased to 2.9± 0.27 MPa, H:MBA-DMSA/TEA's modulus to 1.44 ± 0.15 MPa and H:PEG-DMSA/TEA's modulus to 1.55 ± 0.03 MPa. Also, it is observed that the fracture stress and the energy to break dramatically increased when hydrogels were immersed in $FeCl_3$ rather than other solvents (Figure 5.14B).

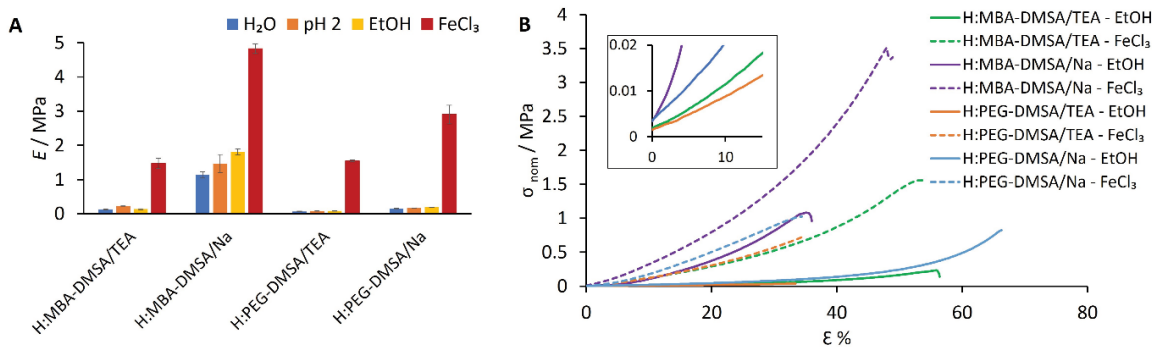

Figure 5.14. A) Young's moduli E of the gels swollen in different solutions B) Stress – strain curves of hydrogels swollen in EtOH (solid curves) and $FeCl_3$ (dashed curves).

5.3.6. *In vitro* Cytotoxicity of Macromers

In vitro cytotoxicity of the macromers was assessed in order to investigate the influence of their structures. U-2 OS and C2C12 cell viabilities were determined after exposure to macromers for 24 h using a calorimetric MTT assay. A dose dependent (5-100 µg/mL) study was performed to evaluate the influence of concentration of the macromers on the viability of the cell lines. Cell viability above 80% is defined as noncytotoxic according to ISO 10993–5 [147]. The PEG-DMSA macromers did not show any cytotoxicity, independent of their counterions, which is consistent with the well-known biocompatibility properties (limiting of antigenicity, immunogenicity, cell adhesion, and protein binding) of PEG [187]. On the other hand the MBA-DMSA macromers caused about 50% cytotoxicity in C2C12 cells in high concentrations. This might be explained with the higher cellular uptake due to the smaller size of these macromers.

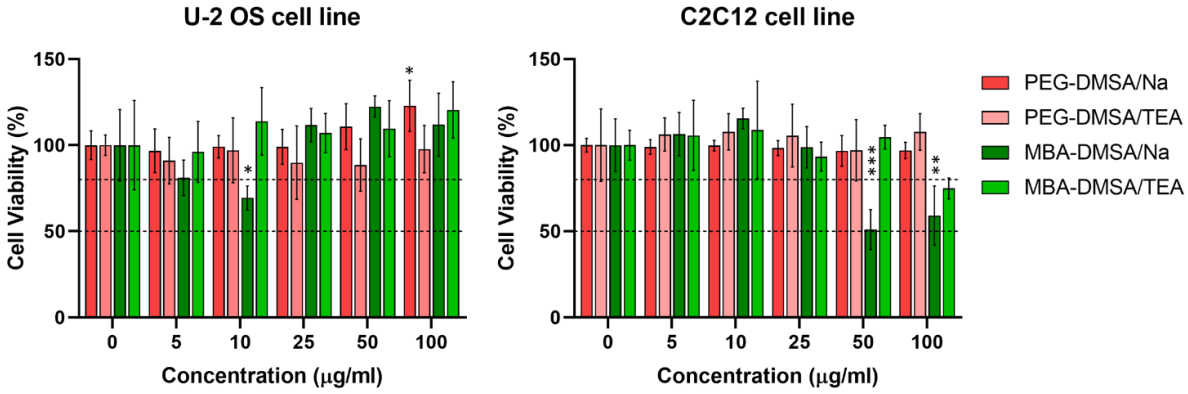

Figure 5.15. Viability of U-2 OS and C2C12 cell lines treated with macromers for 24 hours. Dashed lines show the 50 and 80% viabilities. Data were presented as mean ± SD of independent experiments (n = 5). $p < 0.0332$ (*), $p < 0.0021$ (**), $p < 0.0002$ (***).

5.4. Conclusion

In summary, four water-soluble diacrylate/diacrylamide macromers were prepared via thiol Michael addition reaction between PEGDA/MBA and DMSA. It was investigated how the changes in acrylate and acrylamide groups used in macromers as well as the utilization of various basic groups as counterions to the carboxylic acid groups derived from DMSA, affect the structures and polymerization properties of the macromers. These macromeric cross-linkers were used in the preparation of HEMA hydrogels. The degradability of the hydrogels can be adjusted by modifying the structures and concentrations of the macromers, due to the hydrophilicity and hydrogen bonding interactions of the amide and ester bonds within the macromer structures.

In addition, swelling properties of hydrogels were found to be highly dependent on pH of the swelling medium due to the carboxylic acid groups derived from DMSA in macromers. Moreover, the ability of carboxylic acid groups to bind to heavy metals was investigated using specifically Fe^{3+} ions. The study revealed that the hydrogels exhibited significant Fe^{3+} adsorption capabilities, and additionally, formation of physical crosslinking

between iron and hydrogel was observed to enhance the mechanical properties of the hydrogels. The cell studies showed that macromers, especially those containing the more hydrophilic PEG group, and macromers containing larger TEA group as counterion, do not show toxicity. Consequently, these hydrogels possess versatile biomaterial characteristics, namely high affinity for heavy metal adsorption, robust mechanical properties, and capability for controlled drug release via sequential swelling and degradation. Hence, these hydrogels exhibit potential applicability across diverse domains.

6. PHOSPHATE-FUNCTIONALIZED INTERPENATRATING NETWORK HYDROGELS FOR TISSUE ENGINEERING APPLICATIONS

6.1. Introduction

Although bone has unique regenerative capacity and most fractures heal without major treatment, in some cases, such as very large bone defects, surgical treatment can be needed. Current treatment, mostly bone grafting, works at a certain level, however problems such as the limited amount of bone available for grafting or the grafted bone not being accepted by the body and causing immune rejection and infection are frequently seen. In contrast to classic biomaterials approach, tissue engineering is based on tissue formation and regeneration, rather than just implanting tissue. For growing new bone tissues, bone tissue engineering (BTE) requires 3D porous scaffolds, mimicking bone structure, providing a system for cells to attach, proliferate, and form an extracellular matrix (ECM). Biocompatibility, biodegradability, mechanical strength, adjustable pore size, facility of cell adhesion and proliferation are the essential properties required for suitable scaffolds. To synthesize 3D scaffolds for tissue engineering applications, mostly biodegradable polymers are chosen to achieve compressive strength and porous structure similar to bones. Among these polymer-based bone scaffolds, hydrogels are especially promising candidates.

Hydrogels are highly hydrated three-dimensional polymer networks and present unique properties making them favorable for many clinical applications. They can exhibit behavior responsive to external stimuli such as pH, temperature, enzymes and redox state. Therefore, hydrogels have been tested for use in various biomedical fields such as drug delivery systems and tissue engineering, in addition to being used as wound dressings. Interpenetrating polymer networks (IPN) are hydrogels consisting of at least two non-covalently bonded polymer networks. IPN hydrogels show much higher mechanical strength compared to single component hydrogels. In this study, covalently bonded IPN hydrogels

are synthesized and their biomineralization properties are investigated for bone tissue engineering. The first network is produced by Michael addition reaction, while the second network polymer is obtained by photopolymerization of 10-methacryloyloxydecyl dihydrogen phosphate (MDP) which is a commercially used dental material, containing phosphate and methacrylate groups. The hydrogels were prepared and characterized, their swelling and degradation are still being studied. The biomineralization properties of the hydrogels were investigated by FTIR, other tests such as SEM, EDX, XRD and TGA were also performed to see the crystalline structure of mineralized hydrogels. Same hydrogels without MDP were synthesized as control hydrogels. Their biomineralization properties were investigated by FTIR, other properties such as swelling and degradation were studied.

6.2. Experimental

6.2.1. Materials and Methods

Poly(ethylene glycol) diacrylate (PEGDA), N,N′-methylene bisacrylamide (MBA), 1,4-diaminobutane, 2-hydroxy-4′-(2-hydroxyethoxy)-2-methylpropiophenone (Irgacure 2959), sodiumhydrogen carbonate, calcium chloride and all other chemicals and solvents were purchased at the highest quality from Sigma-Aldrich and used as received. Phosphate buffered saline (PBS) was obtained from Biomatik Corporation (Canada). 10-Methacryloyloxydecyl dihydrogen phosphate was a gift from Ivoclar Vivadent.

Fourier transform infrared spectrometer (FTIR) (Thermo Scientific Nicolet 380) equipped with a diamond ATR was used to characterize the hydrogels and analyze the mineralization of hydrogels. Swelling and degradation studies of hydrogels were done using an orbital shaker at 37 °C and 120 rpm. The morphologies of the hydrogels before and after mineralization were examined with scanning electron microscopy (SEM) (FEI-Philips XL30) with an accelerating voltage of 10.0 kV. The lyophilized hydrogel samples were sputter coated with a platinum layer and their internal fracture surface was examined. Also,

crystallographic properties of the apatite formed was analyzed by using X-ray powder diffraction (XRD) analysis (Rigaku-D/MAX-Ultima diffractometer).

6.2.2. Hydrogel Preparation

A stock solution containing MDP (21 mg, 0.065 mmol), 1,4-butanediamine (11.5 mg, 0.13 mmol), $NaHCO_3$ (10.2 mg, 0.12 mmol) and Irgacure 2959 (0.42 mg, 2 wt% of MDP) in 0.25 mL water was prepared. 0.25 mL of this solution was added onto the diacrylate PEGDA (150 mg, 0.26 mmol) or the diacrylamide MBA (40 mg, 0.26 mmol) placed into glass vials (diameter: 9 mm, thickness: 5 mm). Michael addition reaction between MBA or PEGDA and butanediamine was performed by shaking the mixture at 37 ºC, 180 rpm in an orbital shaker. When the mixture became viscous (for PEGDA containing mixtures 15 minutes, for MBA containing mixtures 3 hours), the vial was placed into the UV reactor ((Kerman UV/18) and exposed to UV light (365 nm) for 30 minutes. Then, unreacted gel precursors were removed by washing with ethanol for 3 hours and distilled water for one hour, and the gels were lyophilized. Same mixtures without MDP and $NaHCO_3$ were prepared and placed in orbital shaker, again after becoming viscous, they were exposed to UV light and washed in the same way and control hydrogels were obtained.

6.2.3. Swelling Studies

Swelling ratios of dry hydrogel samples (30 mg ± 10 mg) were investigated by immersing them in PBS (pH 7.4) and 0.5 M $CaCl_2$ solutions and placed into orbital shaker at 37 °C and 120 rpm. The hydrogels were removed after soaking in solution for 1 hour and 24 hours and the excess solution was removed with a tissue paper and the swollen weight was measured. The degree of swelling (Q) was calculated using the following equation;

$$Q = \frac{W_s - W_d}{W_d} \times 100, \quad (6.1)$$

where W_s and W_d refer to the weight of swollen and dry gel samples, respectively. The average data obtained from triplicate measurements were reported.

6.2.4. Degradation Studies

Degradation studies of the hydrogels were conducted by immersing dry hydrogels samples (30 mg ± 10 mg) (W_i) in 15 mL of PBS solution at 37 °C. Degradations of hydrogels were calculated by keeping the dry hydrogel samples (30 mg ± 10 mg) (W_i) in 15 mL of PBS solution at 37 °C for 1 day and also 1 week. After the time was up samples were taken out, rinsed with water, freeze-dried and re-weighed (W_f). The measurements were made in triplicate and the average data were reported. The degradation % was calculated as

$$Degradation\ (\%) = \frac{W_i - W_f}{W_i} \times 100. \quad (6.2)$$

6.2.5. Mechanical Studies

Mechanical properties of hydrogels in swollen state in H_2O and in 0.5 M $CaCl_2$ for 2 hours were investigated by uniaxial compression measurements on a Zwick Roell test machine with a 500 N load cell in a thermostated room at 25 °C. The tests were carried out at a constant cross-head speed of 5 mm min^{-1}. Before the tests, a complete contact between the gel specimen and the metal plate was provided by applying an initial compressive force of 0.05 N. The compressive stress is calculated as its nominal σ_{nom}, which is the force per cross-sectional area of the undeformed gel specimen, while strain is given by ε which is the change in the specimen length with respect to its initial length. Young's modulus E of the hydrogels was calculated from the slope of stress–strain curves between 5 and 15% compressions. Measurements were made with at least 3 hydrogels and the results were averaged.

6.2.6. Mineralization of Hydrogels

Four different hydrogels (PEGDA-MDP and MBA-MDP hydrogels and their control hydrogels) were immersed into 5 times concentrated simulated body fluid (5xSBF) and incubated at 37 °C for one day. In addition, these 4 hydrogel samples were immersed in 0.5 M $CaCl_2$ for 5 hours and then placed in 5xSBF and the effect of $CaCl_2$ on mineralization was examined. Then hydrogels were then taken out of the solution, rinsed with ultrapure water and freeze-dried to constant weight. The characterization of mineralized hydrogels was carried out by using FTIR.

6.3. Results and Discussion

6.3.1. Synthesis and Characterization of Hydrogels

In the MDP based interpenetrating network hydrogel, one network is formed through the Michael addition reaction, while the other network is created by the UV-initiated copolymerization of the excess diene with MDP's methacrylate group. The double crosslinked IPN hydrogels were synthesized by a one pot method via Michael addition and photopolymerization process (Figure 6.1). The first network was synthesized via Michael addition reaction between butanediamine and two different ene-containing groups (MBA and PEGDA). The secondary network of the IPN hydrogels was synthesized by photopolymerization of the methacrylate group of MDP, free dienes that did not participate in the Michael reaction also participate in this second network. The hydrogels are named MBA-MDP for methylene bisacrylamide containing hydrogels and PEGDA-MDP for polyethylene diacrylate containing hydrogels. MBA-control and PEGDA-control are the MDP free hydrogels.

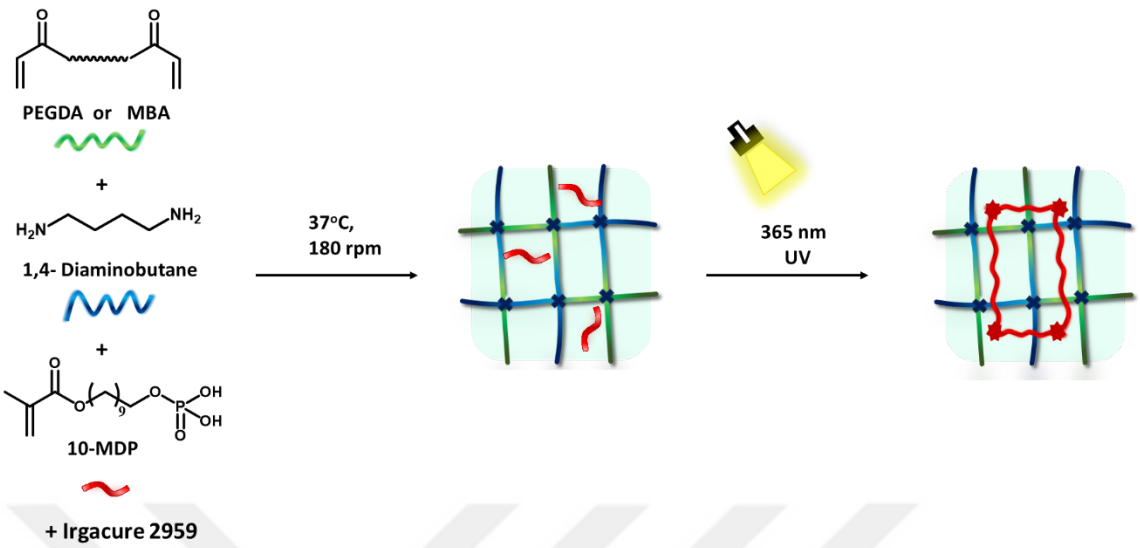

Figure 6.1. Hydrogel preparation.

The FTIR spectrum of the sodium salt of MDP shows strong peaks at 1716 cm^{-1} because of C=O stretching, and the small peak at 1639 cm^{-1} belongs to double bond of the methacrylate group of MDP. Moreover, the spectrum shows a peak at 1194 cm^{-1} due to P=O stretching and the strong bands at 1011 and 951 cm^{-1} in the FTIR spectrum of sodium salt of MDP correspond to the symmetric and asymmetric vibration of P-O. In the FTIR spectrum of the MBA-MDP hydrogel, in addition to the peaks of MDP, the peaks originating from MBA are seen as the strong peak at 1634 cm^{-1} due to C=O amide carbonyl stretching and the strong peak at 1531 cm^{-1} due to NH stretching. In the FTIR spectrum of PEGDA-MDP, the ester carbonyl peak appears at 1728 cm^{-1}, while the broad peak around 1090 cm^{-1} originates from symmetric and asymmetric vibrations of C−O (Figure 6.2).

The surface characteristics of the hydrogels were explored through scanning electron microscopy (SEM) analysis of freeze-dried hydrogels (Figure 6.3). The SEM images of the gel cross-sections before mineralization revealed the porous structures of the PEGDA-MDP and MBA-MDP hydrogels. The pore sizes of both gels were determined to be around 40 µm. Furthermore, the EDX outcomes for the non-mineralized gels were also evaluated,

confirming the presence of phosphorus atoms introduced into the gel through the incorporation of MDP (Figure 6.3C)

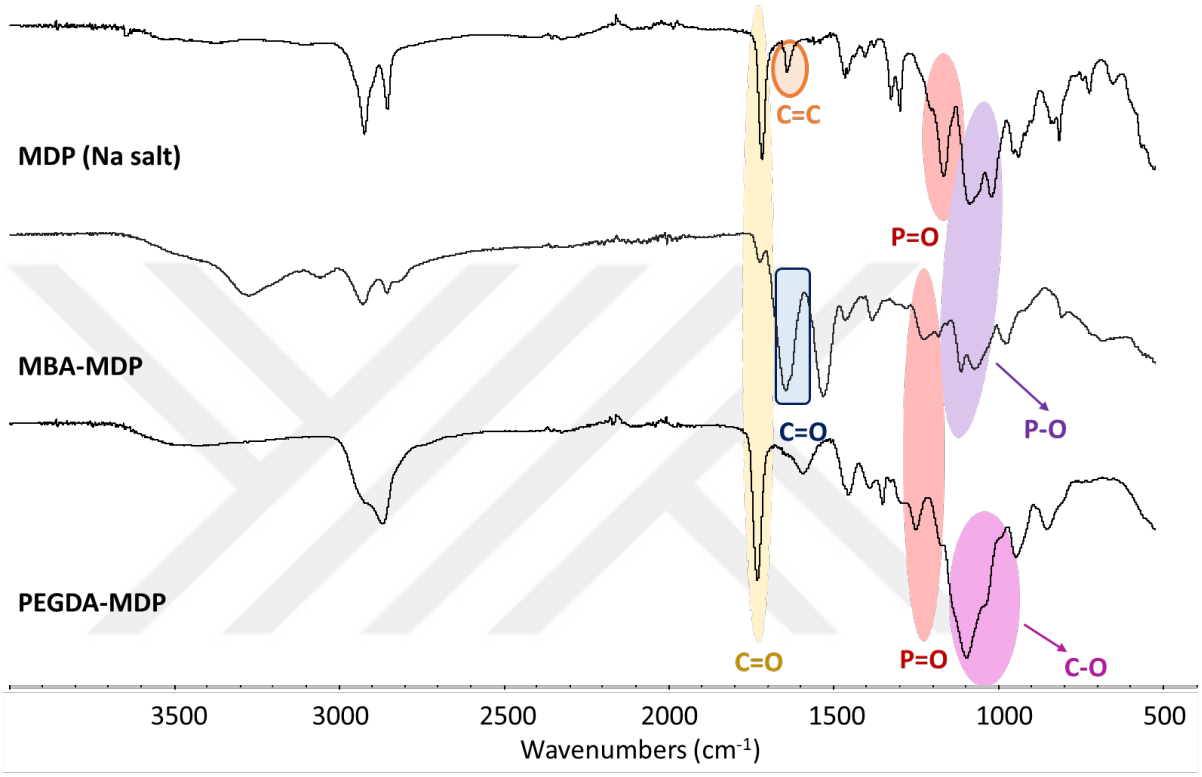

Figure 6.2. FTIR spectra of MDP and MDP containing hydrogels.

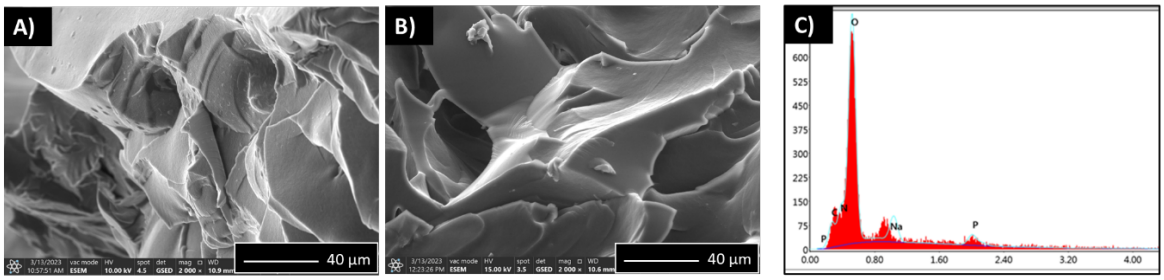

Figure 6.3. SEM images of A) PEGDA-MDP, B) MBA-MDP and C) EDX image of MBA-MDP hydrogels.

6.3.2. Swelling and Degradation Studies

The swelling ratios of the MDP containing hydrogel samples PEGDA-MDP and MBA-MDP, in PBS (pH 7.4) and $CaCl_2$ solution (0.5 M) were measured after 1 hour and 24 hours immersion in solvents (Figure 6.4). It is known that the swelling behavior of hydrogels depends on the hydrophilicity/hydrophobicity of the polymer, the crosslink density of the hydrogel, and the solvent. After being kept in PBS for one hour, the highest swelling ratio was observed in the PEGDA-MDP gel. The swelling ratios were ranked as follows: PEGDA-MDP > PEGDA-control > MBA-MDP > MBA-control. This expected result can be attributed to PEGDA's more hydrophilic nature compared to MBA, as well as the additional hydrophilicity provided by MDP, which contains phosphoric acid, to the gel.

Likewise, the MBA-MDP gel showed greater swelling capacity than the MBA-control hydrogel. After being kept in PBS for 24 hours, all gels showed a decrease in swelling ratio, with more significant reduction observed in PEGDA-containing gels, both PEGDA-MDP and PEGDA-control. These gels have a high degradation potential and some degradation within a 24-hour period results in a reduction in swelling rates. Additionally, the more hydrophilic nature of PEGDA resulted in a higher degree of degradation, hence causing a greater decrease in the swelling ratio compared to gels containing MBA.

When hydrogels were immersed for 1 hour in 0.5 M $CaCl_2$ solution instead of PBS, gels containing MDP appeared to swell much less than gels immersed in PBS which indicates interaction of phosphoric acid groups in MDP with Ca^{2+} ions forming physical crosslinking. Furthermore, when the gels were kept in a $CaCl_2$ solution for 24 hours, their swelling capacities were found to be very similar to their swelling capacities after being kept for 1 hour in $CaCl_2$. The presence of a third network in the form of $POO^{-}Ca^{2+}$ physical crosslinks contributed to the gels' rigid structure, resulting in reduced swelling capacities and decreased degradation rates, which maintained their swelling capacities unchanged.

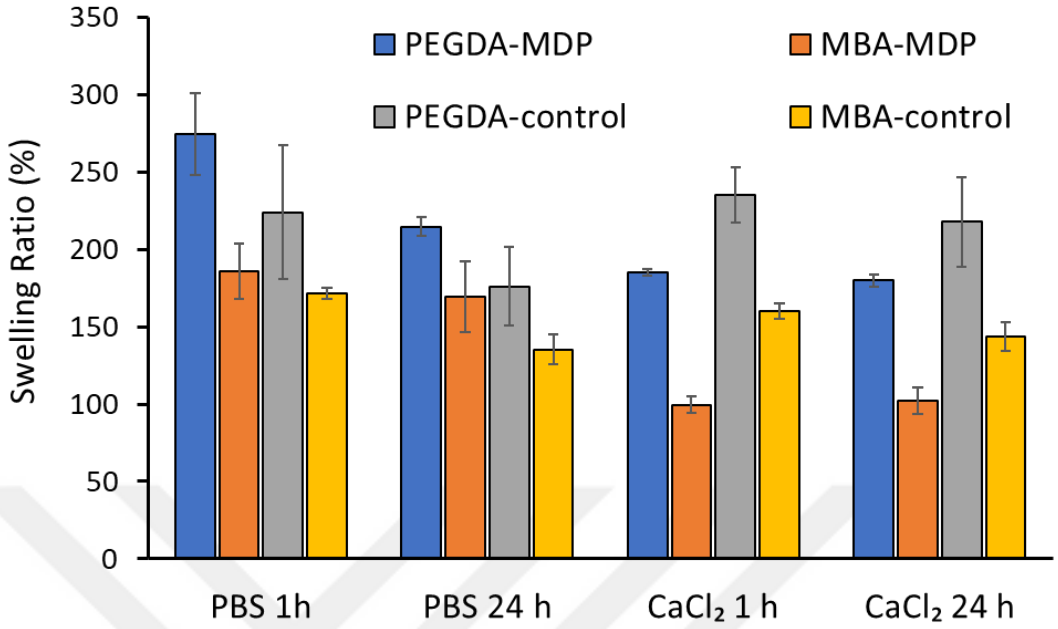

Figure 6.4. Swelling capacities of hydrogels.

The degradation behavior of the hydrogels was studied in PBS (pH 7.4) at 37 °C (Figure 6.5). Because MDP has groups of methacryloxy and phosphate ester, it is highly degradable in water. Again, since PEGDA with ester groups and MBA with amide bonds are degradable structures, the synthesized gels are expected to have extremely high degradation rates.

While the mass loss of PEGDA-MDP hydrogels increased from 22% at the end of 1 day to 36% at the end of 1 week, the mass loss in MBA-MDP gel was 9% at the end of 1 day and increased to 18% at the end of 1 week. While the degradation rates of these two MDP-containing gel compositions were very high, it was also observed that the PEGDA-MDP gel with ester bonds degraded faster than the MBA-MDP gel with amide bonds, as expected.

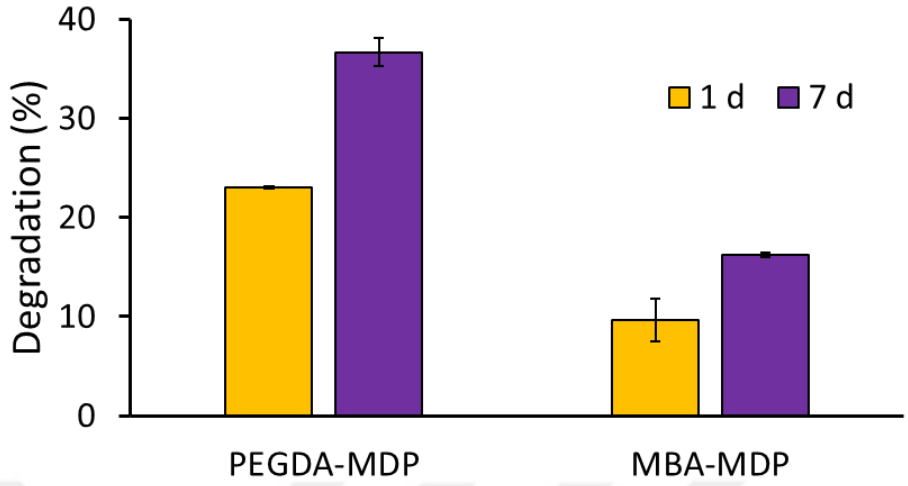

Figure 6.5. Degradation (%) of hydrogels.

6.3.3. Mechanical Properties of Hydrogels

The mechanical properties of gels in equilibrium swollen states were investigated by uniaxial compression tests. Figure 6.6 shows the nominal stress (σ_{nom}) - strain (ε) curves and Young's modulus *E* obtained from compression tests performed on four different gels: MBA-MDP, PEGDA-MDP, and their MDP-free control hydrogels, after being soaked in water. Hydrogels containing MBA exhibited both higher Young's moduli (*E*) and compressive strengths compared to hydrogels containing PEGDA. The PEGDA-MDP gel, which is more hydrophilic and has a higher swelling ratio, had a Young's modulus of 0.0972 MPa after swelling in water, whereas the MBA-MDP gel had a modulus of 0.175 MPa. While the modulus of PEGDA-control gel in water, which is more prone to degradation, was 0.0443 MPa, the modulus of MBA-control gel was calculated as 0.084 MPa. When the gels were swollen in 0.5 M $CaCl_2$ instead of water, a slight increase was observed in the moduli of the control gels, while a significant increase was observed in the moduli of the MDP-containing gels. The modulus of the MBA-MDP gel after swelling in $CaCl_2$ was calculated as 0.569 MPa, whereas the modulus of the PEGDA-MDP gel was 0.23 MPa. As expected, the physical interaction between MDP's phosphate groups and Ca^{2+} ions led to a notable increase in mechanical properties. The inset illustrates the change in the MBA-MDP

hydrogel after swelling in water and $CaCl_2$. It can be observed that the clear MBA-MDP gel turns opaque due to its interaction with Ca^{2+}.

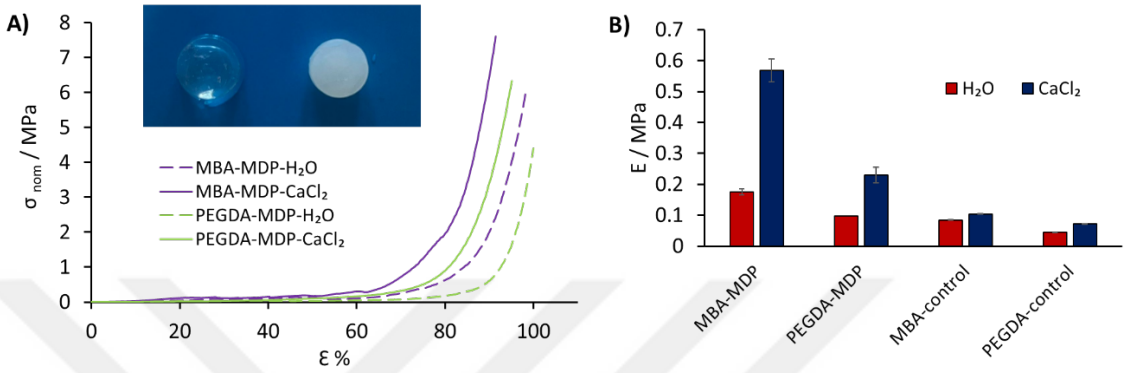

Figure 6.6. A) Stress – strain curves of hydrogels swollen in 0.5 M $CaCl_2$ (solid curves) and H_2O (dashed curves), The inset shows MBA-MDP hydrogel after being kept in H_2O and $CaCl_2$ solution, B) Young's moduli E of the hydrogels.

6.3.4. Mineralization of Hydrogels

The ability of hydrogels to form CaP phases at their surface similar to bone mineral is tested by immersing them in simulated body fluid (SBF), mimicking the ionic concentrations and pH typically observed in plasma. In this study, we used high concentrations of SBF (5xSBF) to increase the rate of biomineralization due to the rapid degradation of hydrogels. In order to assess the role of the phosphate group of MDP in the mineralization properties of the synthesized hydrogels, MDP-free PEGDA-control and MBA-control hydrogels were also prepared and used as reference. In addition, some of the gels were kept in 0.5 M $CaCl_2$ solution for 5 hours before being immersed in 5xSBF, with the expectation that the Ca^{2+} interaction of the MDP groups would form an induction point for mineralization. After hydrogels (PEGDA-MDP, MBA-MDP, PEGDA-control and PEGDA-control) were immersed in 5xSBF for 1 day and washed with deionized water for 3 hours with an hourly water change, they were freeze-dried. CaP minerals deposited were characterized by FTIR. The FTIR spectra obtained for mineralized MBA-MDP and PEGDA-MDP and their control

hydrogels were used to characterize mineral phases in the samples and compared with hydroxyapatite (HAP). As is known, there are four Raman and IR active vibrational modes for phosphate ions. O-P-O bending vibrations were indicated by the very intense ν_3PO mode between 1190-976 cm^{-1} and ν_4PO mode between 660-520 cm^{-1}. Also, the phosphate ν_1PO band is observed at 962 cm^{-1} and the ν_2PO band is observed in the region of 475 and 440 cm^{-1} as weak bands [162]. The spectra of the mineralized control hydrogels PEGDA-control showed no difference from the pre-mineralization hydrogels. Although C-O-C stretching bands of PEG are seen at 1100 cm^{-1} as a broad peak for PEGDA-containing gels, newly formed ν_3PO and ν_4PO vibration peaks can be seen around 1000 cm^{-1} and around 550 cm^{-1}, observed after immersion in 5xSBF. After immersing the PEGDA-MDP gels in $CaCl_2$ and then placing them in SBF for mineralization, it is observed in the FTIR spectra of these gels that the O-P-O peaks are increasing, indicating the process of mineralization (Figure 6.7).

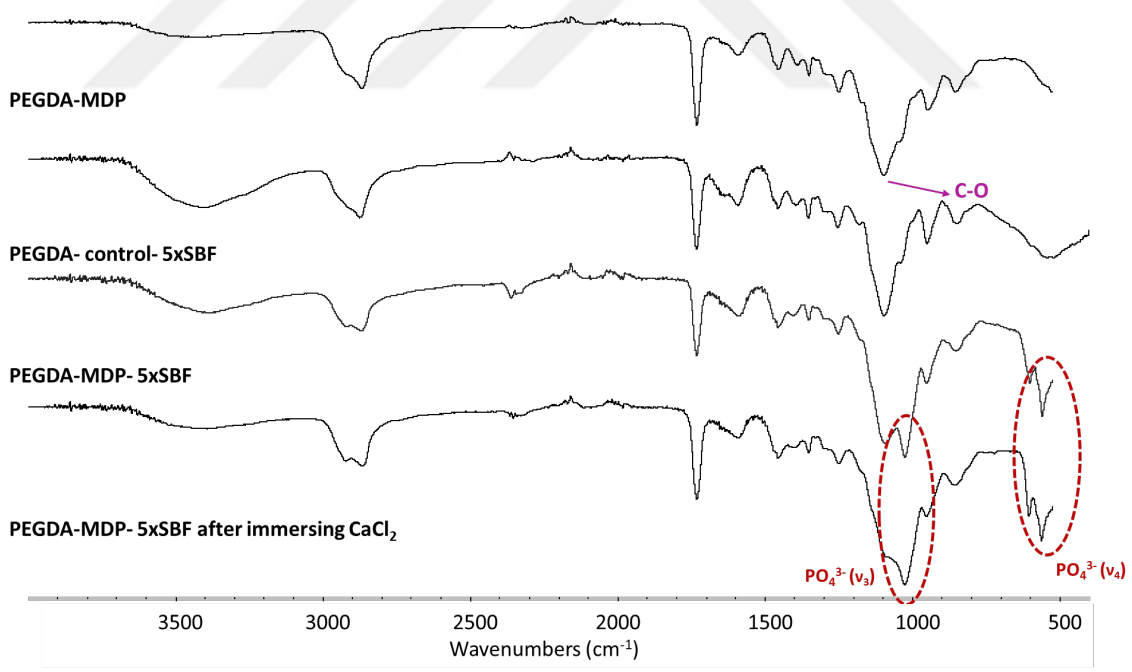

Figure 6.7. FTIR spectra of PEGDA-MDP and PEGDA-control hydrogels before and after mineralization.

On the other hand, similar to the PEGDA-control gel, there is no formation of any new peaks in the MBA-control gel after being immersed in 5xSBF. In the MBA-MDP gel mineralized in 5xSBF, two orthophosphate (O-P-O) absorption peaks are observed at 1190-976 cm^{-1} and 660-520 cm^{-1}. The gel with the highest mineralization is observed to be the MBA-MDP-$CaCl_2$-5xSBF gel, which was immersed in $CaCl_2$ and then mineralized in 5xSBF, showing the highest P-O vibration peak. Its spectrum largely overlaps with the HAP spectrum (Figure 6.8).

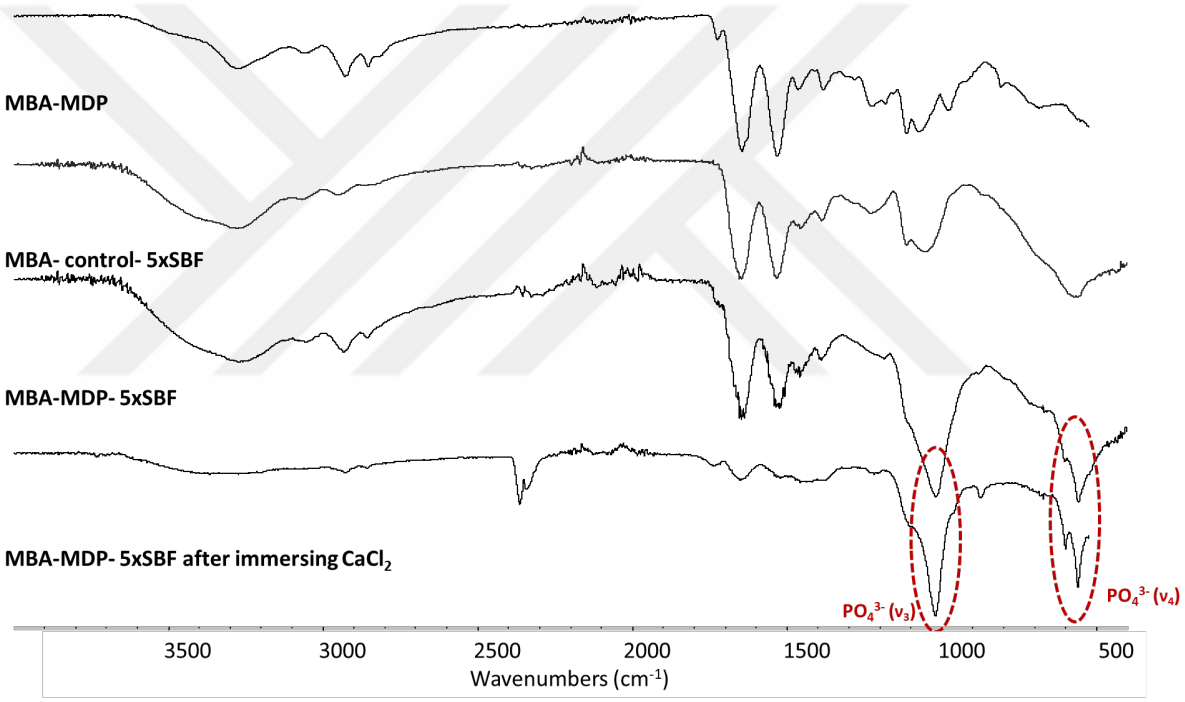

Figure 6.8. FTIR spectra of MBA-MDP and MBA-control hydrogels before and after mineralization.

The morphologies of the crystal structures accumulated on the hydrogels after mineralization in 5xSBF were examined using electron microscopy (SEM) analysis (Figure 6.9). The post-mineralization results validate the findings obtained from FTIR analysis. After immersing the PEGDA-MDP gel directly into 5xSBF for one day, minimal accumulation of CaP-like minerals was observed on its surface (Figure 6.9 A). The elemental analysis of the accumulated minerals was performed using EDX, revealing a Ca/P ratio of

1.18. On the other hand, when the PEGDA-MDP gel was first immersed in a 0.5M $CaCl_2$ solution for 5 hours and then placed in 5xSBF for a day, the SEM image showed a significantly greater amount of needle-like minerals resembling HAP on its surface (Figure 6.9 B). The Ca/P ratio was calculated as 1.35 using EDX (Figure 6.9 C). In the case of MBA-containing gels, both the gel immersed in $CaCl_2$ solution first and the gel directly immersed in 5xSBF exhibited needle-like crystals resembling HAP in SEM images. However, when the MBA-MDP gel was mineralized directly in 5xSBF, a lower amount of HAP-like minerals was observed compared to the gel that was immersed in $CaCl_2$ solution first and then placed in 5xSBF (Figure 6.9 D).

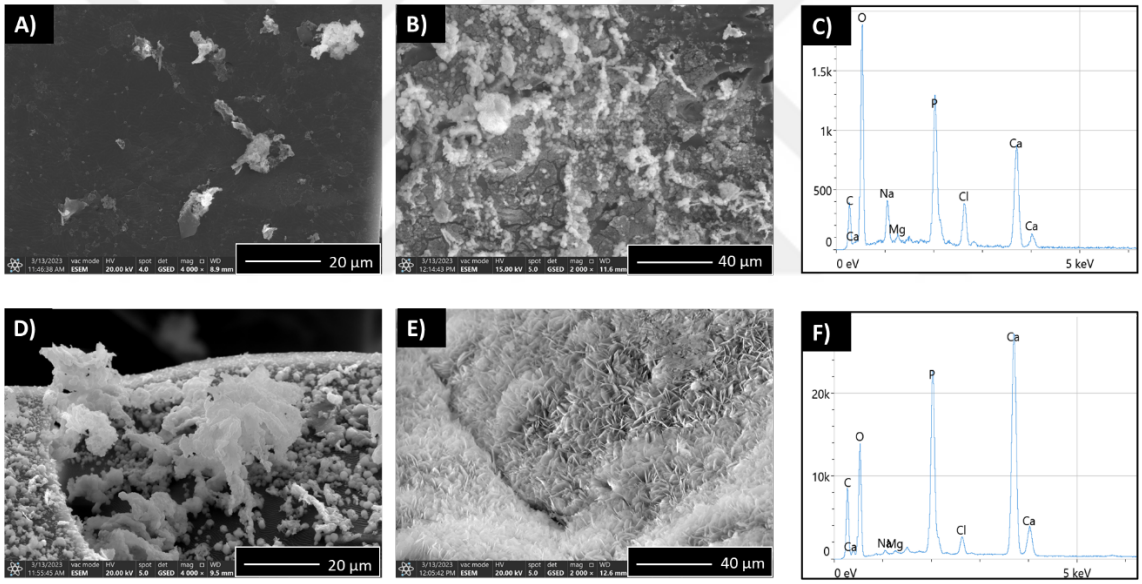

Figure 6.9. SEM images of PEG-MDP hydrogels A) after mineralization in 5xSBF, B) first immersing in $CaCl_2$ then mineralization in 5xSBF, C) EDX result of PEGDA-MDP-$CaCl_2$-5xSBF and MBA-MDP hydrogels D) after mineralization in 5xSBF, E) first immersing in $CaCl_2$ then mineralization in 5xSBF, F) EDX result of MBA-MDP-$CaCl_2$-5xSBF.

The Ca/P ratio was calculated as 1.35 using EDX. Additionally, after immersion in $CaCl_2$ and subsequent mineralization in 5xSBF, the entire gel surface was covered with HAP-like minerals, and the Ca/P ratio matched HAP at 1.67 (Figure 6.9 E and 6.9 F). It is known that the Ca/P ratios for HAP [$Ca_{10}(PO_4)_6(OH)_2$], calcium phosphate [$Ca_3(PO_4)_2$]

(amorphous), brushite [$(CaHPO_4)_3$-H_2O], and octacalcium phosphate [$Ca_8(PO_4)_6H_2$] are 1.67, 1.5, 1.0, and 1.33, respectively [163]. These results indicate that mineralization of the MBA-MDP gel in $CaCl_2$ followed by 5xSBF leads to the accumulation of amorphous HAP minerals, while in other gels, accumulation of apatite-like minerals and non-stoichiometric HAP is observed.

The crystal properties of the deposited minerals were analyzed by XRD measurements. The specific peaks of CaP apatite minerals in XRD are observed at 2θ = 26 and the other group is ranging from 2θ = 30-32 [188]. Additionally, the broad peak between 16° to 25° in PEG-containing gels is attributed to the PEG group [189].

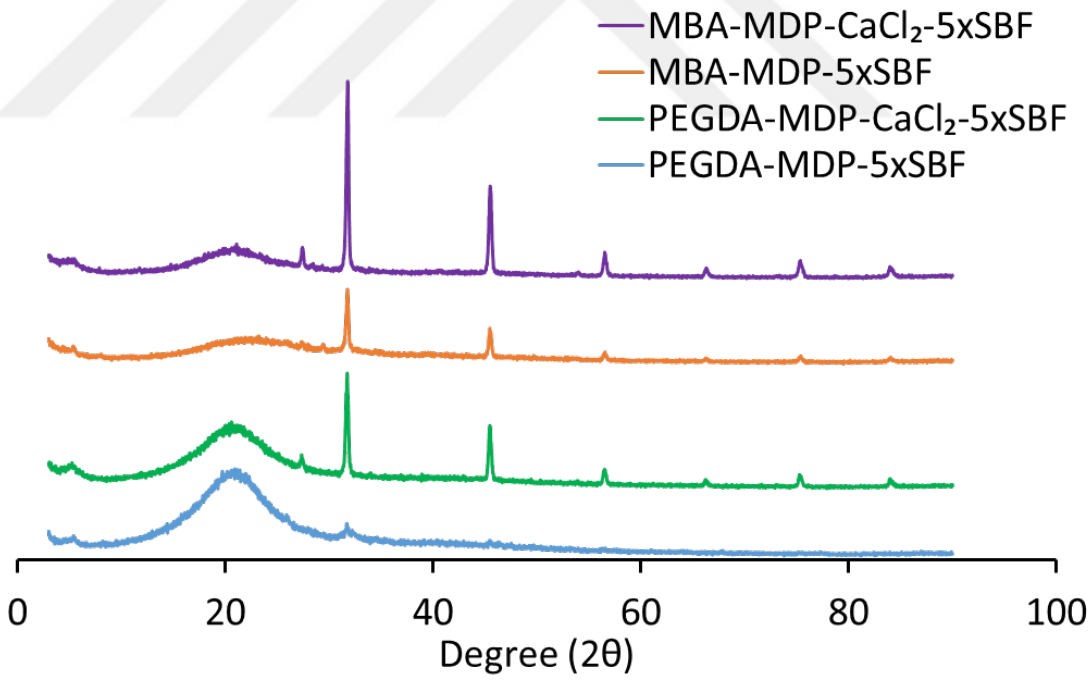

Figure 6.10. XRD spectra of mineralized hydrogels.

6.4. Conclusion

10-Methacryloyloxydecyl dihydrogen phosphate (MDP) which is a commercial dental material, was used to synthesize interpenetrating network hydrogels. One of the networks was obtained through the Michael addition reaction of MBA or PEGDA with 1,4-butanediamine, while the other network was formed by the UV-initiated copolymerization of the excess remaining diene with MDP's methacrylate group. The high hydrophilicity provided by the phosphate ester group of MDP was investigated for its impact on the swelling and degradation properties of the hydrogels, as well as its contribution to biomineralization due to its strong interaction potential with Ca^{2+}.

For comparison, hydrogels without MDP were also synthesized, and their properties were examined. It was observed that the MDP-containing hydrogels exhibited high swelling and degradation properties. Furthermore, it was demonstrated that the swelling and degradation properties of the hydrogels could be adjusted by using MBA and PEGDA. In addition, it has been observed that hydrogels containing MDP have better mechanical properties than control hydrogels and their mechanical properties have increased significantly as a result of their interaction with Ca^{2+}. The biomineralization study was conducted in 5xSBF. The hydrogels were mineralized by directly immersing them in 5xSBF or by first immersing them in a 0.5M $CaCl_2$ solution and then in 5xSBF. It was found that the initial immersion of the hydrogels in calcium served as a starting point for mineralization and increased the mineralization rate. Additionally, the hydrogels containing MBA, which were more hydrophobic, were observed to be coated with more HAP-like minerals in both mineralization methods.

7. CONCLUDING REMARKS

In this doctoral dissertation, polymers, macromers, and their crosslinked hydrogels and cryogels functionalized with phosphate, bisphosphonate, bisphosphonic acid, and carboxylic acid in various ways were synthesized. The potential use of these materials, with varying properties such as swelling, degradation, mineralization and binding ability, mechanical strength and cell adhesion, was investigated for various biomedical applications, in particular bone tissue engineering.

Two novel PAA macromers functionalized with ALE and AP, and a control macromer functionalized only with AP were synthesized via Michael addition reaction. Crosslinked cryogels were prepared through photopolymerization of these macromers. The swelling properties of these cryogels containing different amounts of ALE and the control cryogel with no ALE were investigated according to the macromer weight, the amount of ALE present, and the pH and ion content of the solution. Despite the increased hydrophilicity added by the ALE group, the degradation percentages of the cryogels were found to be more affected by their crosslink densities. The mineralization properties of the cryogels were examined, revealing that the control cryogel accumulated the highest amount of HAP-like mineral. Mechanical testing of the cryogels showed that cryogels made from all three macromers were highly durable and can be compressed up to about 97% without any crack formation. As the amount of ALE within the cryogels increased, both the Young's moduli and compression fracture stresses of the cryogels increased. After mineralization of the cryogels in SBF, a significant increase in the moduli of the cryogels was observed, attributed to the physical crosslinking of Ca^{2+} with the ALE groups. The toxicities of the degradation products of the cryogels were investigated, revealing that the degradation products of all cryogels were safe at concentrations of 25 μg/mL or lower. Overall, these three PAA cryogels have the potential to be used as s scaffold materials for applications in tissue engineering.

A novel PAA macromer functionalized with bisphosphonate (BP) was synthesized by using tetraethyl vinylidene bisphosphonate and named PAA-BP. The unfunctionalized form of this macromer with BP was also named PAA-NH_2 and used as the control macromer. These macromers were used for copolymerization with HEMA to create hydrogels, whose properties were investigated. It was observed that the hydrophilicity and hydrogen bond interaction provided by the macromers to the hydrogels thanks to the BP and NH_2 groups, increased the degradability of the hydrogels. Both hydrogels from the two distinct macromers exhibited pH sensitivity in terms of equilibrium swelling ratios. Additionally, due to physical crosslinks between BP groups and Ca^{2+} ions, the swelling behavior of the H:PAA-BP hydrogel was shown to be responsive to the ion concentration in the solution. Following mineralization in 5xSBF, both hydrogels accumulated HAP-like CaP minerals, which was verified by SEM and EDX analyses. It was seen that the gel containing BP had a higher mineral forming potential. Mechanical tests of the mineralized gels indicated an increase in Young's moduli and mechanical properties, with the BP-containing hydrogel showing a greater enhancement. Cell experiments demonstrated that the H:PAA-BP hydrogel facilitated cell attachment, proliferation, and growth after mineralization. Consequently, these materials, especially the novel H:PAA-BP hydrogel, hold significant potential for applications in tissue engineering.

Four macromers were synthesized through thiol Michael addition reactions between PEGDA/MBA and DMSA. In addition to the changes in the acrylate and acrylamide groups used in the macromers, two different base groups were employed as ion counterparts to carboxylic acid groups and the effect of this on the structures and polymerization properties of macromers was investigated. Hydrogels were prepared through copolymerization of these macromers with HEMA. Swelling and degradation properties of the hydrogels were found to be influenced by the hydrophilic disparity between amide and ester bonds within the macromer structures. Furthermore, it was discovered that the swelling behavior of the hydrogels was significantly dependent on the pH of the swelling medium, attributed to DMSA's carboxylic acid groups in the macromers. The metal binding capability of the carboxylic acid groups was investigated using Fe^{3+} ions. The hydrogels exhibited substantial Fe^{3+} adsorption, as determined by UV spectroscopy. Mechanical tests also demonstrated that the physical crosslinking between Fe^{3+} ions and the hydrogels enhanced their mechanical

properties. Toxicity studies indicated that the macromers, particularly those containing more hydrophilic PEG groups and larger TEA groups as counter ions, exhibited low toxicity. In conclusion, these hydrogels possess versatile biomaterial properties, including high affinity for heavy metal adsorption, strong mechanical characteristics, and the potential for controlled drug release through sequential swelling and degradation. Hence, these hydrogels display potential applicability across various domains.

In the MDP based interpenetrating network hydrogel, one network is formed through the Michael addition reaction of MBA/PEGDA with 1,4-butanediamine, while the other network is created by the UV-initiated copolymerization of the excess diene with MDP's methacrylate group. The hydrophilicities of the functional groups in the hydrogel backbones and their hydrogen bonding abilities were observed to impact the degradation and swelling properties of the hydrogels. Furthermore, the high hydrophilicity provided by MDP's phosphate ester group was found to enhance the swelling and degradation properties of the hydrogels. Control hydrogels not based on MDP exhibited lower swelling and degradation rates compared to those based on MDP. It was observed that the swelling ratio of the gels was influenced by the ion concentration of the solution due to the strong interaction potential of MDP's phosphate group with Ca^{2+}, and the gels swelled less in Ca^{2+} containing solutions. The young moduli and mechanical properties of the hydrogels improved after being immersed in a Ca^{2+} solution. After mineralization in 5x SBF, it was observed that hydrogels containing MBA had a higher mineral accumulation potential and immersing the gels in a Ca^{2+} solution prior to SBF immersion increased the mineralization rate. With their tailorable swelling, degradation, and mechanical properties, along with their ability to generate high levels of HAP-like minerals, these hydrogels are found to be suitable for bone tissue engineering applications.

REFERENCES

1. Ratner, B. D., and G. Zhang, *Biomaterials Science*, Fourth Edition, Academic Press, Cambridge, 2020.

2. Yaqub, K. M., and C. Min-Hua, "A Review on Role of Biomaterials in Biomedical Field", *International Journal of Bio-Pharma Research,* Vol. 8, No. 9, pp. 2788-2793, 2019.

3. Patel, N. R., and P. P. Gohil, "A Review on Biomaterials: Scope, Applications & Human Anatomy Significance", *International Journal of Emerging Technology and Advanced Engineering A*, Vol. 2, No. 4, pp. 91-101, 2012.

4. Ghasemi-Mobarakeh, L., D. Kolahreez, S. Ramakrishna, and D. Williams, "Key Terminology in Biomaterials and Biocompatibility", *Current Opinion in Biomedical Engineering*, Vol. 10, No. Jun. 01, pp. 45-50, 2019.

5. Silver, F. H., and D. L. Christiansen, *Biomaterials Science and Biocompatibility,* Springer New York, New York, 1999.

6. Todros, S., M. Todesco, and A. Bagno, "Biomaterials and Their Biomedical Applications: From Replacement to Regeneration", *Processes*, Vol. 9, No. 11, p. 1949, 2021.

7. Blaine, G., "The Uses of Plastics in Surgery", *The Lancet*, Vol. 248, No. 6424, pp. 525-528, 1946.

8. Griffith, L. G., "Polymeric Biomaterials", *Acta Materialia*, Vol. 48, No. 1, pp. 263-277, 2000.

9. Nair L. S., and C. T. Laurencin, "Biodegradable Polymers as Biomaterials", *Progress in Polymer Science*, Vol. 32, No. 8-9, pp. 762-798, 2007.

10. Nair L. S., and C. T. Laurencin, *Tissue Engineering I,* Springer Berlin, Heidelberg, 2005.

11. Anderson, J. M., A. Rodriguez, and D. T. Chang, “Foreign Body Reaction to Biomaterials”, *Seminars in Immunology*, Vol. 20, No. 2, pp. 86-100, 2008.

12. Banoriya, D. R. Purohit, and R. K. Dwivedi, “Advanced Application of Polymer Based Biomaterials”, *Materials Today Proceedings*, Vol. 4, No. 2, pp. 3534-3541, 2017.

13. Vroman, I., and L. Tighzert, “Biodegradable Polymers”, *Materials*, Vol. 2, No. 2, pp. 307-344, 2009.

14. Chandra, R., and R. Rustgi, “Biodegradable Polymers”, *Progress in Polymer Science*, Vol. 23, No. 7, pp. 1273-1335, 1998.

15. Sudha P. N., and M. H. Rose, “Beneficial Effects of Hyaluronic Acid”, *Advances in Food and Nutrition Research,* Vol. 72, No. 9, pp. 137-176, 2014.

16. Doppalapudi, S., A. Jain, W. Khan, and A. J. Domb, “Biodegradable Polymers-an Overview”, *Polymers for Advanced Technologies*, Vol. 25, No. 5., pp. 427-435, 2014.

17. Hofmann, D., M. Entrialgo-Castaño, K. Kratz, and A. Lendlein, “Knowledge-based Approach Towards Hydrolytic Degradation of Polymer-based Biomaterials”, *Advanced Materials*, Vol. 21, No. 32-33, pp. 3237-3245, 2009.

18. Hahn S., and D. Hennecke, “What Can We Learn from Biodegradation of Natural Polymers for Regulation?”, *Environmental Sciences Europe*, Vol. 35, No. 50, pp. 1-14, 2023.

19. Visan, A. I., G. Popescu-Pelin, and G. Socol, “Degradation Behavior of Polymers Used as Coating Materials for Drug Delivery - A Basic Review”, *Polymers*, Vol. 13, No. 8, p. 1272, 2021.

20. Ulery, B. D., L. S. Nair, and C. T. Laurencin, “Biomedical Applications of Biodegradable Polymers”, *Journal of Polymer Science, Part B: Polymer Physics*, Vol. 49, No. 12, pp. 832-864, 2011.

21. Nutan, B., A. K. S. Chandel, D. V. Bhalani, and S. K. Jewrajka, "Synthesis and Tailoring the Degradation of Multi-responsive Amphiphilic Conetwork Gels and Hydrogels of Poly(β-Amino Ester) and Poly(Amido Amine)", *Polymer,* Vol. 111, No. February, pp. 265-274, 2017.

22. Wang, X., Z. Zhang, and N. Hadjichristidis, "Poly(Amino Ester)s as an Emerging Synthetic Biodegradable Polymer Platform: Recent Developments and Future Trends" *Progress in Polymer Science*, Vol. 136, No. January, pp. 101634, 2023.

23. Katti, D. S., S. Lakshmi, R. Langer, and C. T. Laurencin "Toxicity, Biodegradation and Elimination of Polyanhydrides", *Advanced Drug Delivery Reviews*, Vol. 54, No. June, pp. 933-961, 2002.

24. Kannan, M. B., *Surface Modification of Magnesium and Its Alloys for Biomedical Applications*, Woodhead Publishing, Cambridge, 2015.

25. Kramschuster, A., and L. S. Turng, *Handbook of Biopolymers and Biodegradable Plastics: Properties, Processing and Applications*, Elsevier, Oxford, 2013.

26. Ferruti, P., M. A. Marchisio, and R. Duncan, "Poly(Amido-Amine)s: Biomedical Applications", *Macromolecular Rapid Communications*, Vol. 23, No. 5-6, pp. 332-355, 2002.

27. Lin, C., and J. F. J. Engbersen, "Effect of Chemical Functionalities in Poly(Amido Amine)s for Non-viral Gene Transfection", *Journal of Controlled Release*, Vol. 132, No. 3, pp. 267-272, 2008.

28. Mather, B. D., K. Viswanathan, K. M. Miller, and T. E. Long, "Michael Addition Reactions in Macromolecular Design for Emerging Technologies", *Progress in Polymer Science*, Vol. 31, No. 5, pp. 487-531, 2006.

29. Ferruti, P., "Poly(Amidoamine)s: Past, Present, and Perspectives", *Journal of Polymer Science Part A: Polymer Chemistry*, Vol. 51, No. 11, pp. 2319-2353, 2013.

30. Holden, C. A., P. Tyagi, A. Thakur, R. Kadam, G. Jadhav, U. B. Kompella, and H. Yang, "Polyamidoamine Dendrimer Hydrogel for Enhanced Delivery of Antiglaucoma Drugs", *Nanomedicine*, Vol. 8, No. 5, pp. 776-783, 2012.

31. Chen, S., J. Shi, X. Xu, J. Ding, W. Zhong, L. Zhang, M. Xing, and L. Zhang, "Study of Stiffness Effects of Poly(amidoamine)-poly(n-isopropyl acrylamide) Hydrogel on Wound Healing," *Colloids and Surfaces B: Biointerfaces*, Vol. 140, No. April, pp. 574-582, 2016.

32. Bahadir E. B., and M. K. Sezgintürk, "Poly(amidoamine) (PAMAM): An Emerging Material for Electrochemical Bio(sensing) Applications" *Talanta*, Vol. 148, No. February, pp. 427-438, 2016.

33. Jacchetti, E., E. Emilitri, S. Rodighiero, M. Indrieri, A. Gianfelice, C. Lenardi, A. Podestà, E. Ranucci, P. Ferruti and P. Milani, "Biomimetic Poly(amidoamine) Hydrogels as Synthetic Materials for Cell Culture", *Journal of Nanobiotechnology*, Vol. 6, No. 14, pp. 1-15, 2008.

34. Shi, J., J. Ouyang, Q. Li, L. Wang, J. Wu, W. Zhong, and M. M. Xing, "Cell-compatible Hydrogels Based on a Multifunctional Crosslinker with Tunable Stiffness for Tissue Engineering", *Journal of Materials Chemistry*, Vol. 22, No. 45, pp. 23952-23962, 2012.

35. Nutan, B., A. K. S. Chandel, D. V. Bhalani, and S. K. Jewrajka, "Synthesis and Tailoring the Degradation of Multi-responsive Amphiphilic Conetwork Gels and Hydrogels of Poly(β-amino ester) and Poly(amido amine)", *Polymer*, Vol. 111, No. February, pp. 265-274, 2017.

36. Ekenseair, A. K., K. W. M. Boere, S. N. Tzouanas, T. N. Vo, F. K. Kasper, and A. G. Mikos, "Structure-Property Evaluation of Thermally and Chemically Gelling Injectable Hydrogels for Tissue Engineering", *Biomacromolecules*, Vol. 13, No. 9, pp. 2821-2830, 2012.

37. Emilitri, E., F. Guizzardi, C. Lenardi, M. Suardi, E. Ranucci, and P. Ferruti, "Novel Poly(amidoamine)-Based Hydrogels as Scaffolds for Tissue Engineering", *Macromolecular Symposia*, Vol. 266, No.1, pp. 41-47, 2008.

38. Ferruti, P., S. Bianchi, E. Ranucci, F. Chiellini, and A. M. Piras, "Novel Agmatine-Containing Poly(amidoamine) Hydrogels as Scaffolds for Tissue Engineering", *Biomacromolecules*, Vol. 6, No. 4, pp. 2229-2235, 2005.

39. Yang, F., C. G. Williams, D. Wang, H. Lee, P. N. Manson, and J. Elisseeff, "The Effect of Incorporating RGD Adhesive Peptide in Polyethylene Glycol Diacrylate Hydrogel on Osteogenesis of Bone Marrow Stromal Cells" *Biomaterials*, Vol. 26, No. 30, pp. 5991-5998, 2005.

40. Martello, F., A. Tocchio, M. Tamplenizza, I. Gerges, V. Pistis, R. Recenti, M. Bortolin, M. Del Fabbro, S. Argentiere, P. Milani, and C. Lenardi, "Poly(amido-amine)-Based Hydrogels with Tailored Mechanical Properties and Degradation Rates for Tissue Engineering", *Acta Biomaterialia*, Vol. 10, No. 3, pp. 1206-1215, 2014.

41. Chen, C. K., P. K. Huang, W. C. Law, C. H. Chu, N. T. Chen, and L. W. Lo, "Biodegradable Polymers for Gene-delivery Applications", *International Journal of Nanomedicine*, Vol. 15, No. January, pp. 2131-2150, 2020.

42. Rai, R., S. Alwani, and I. Badea, "Polymeric Nanoparticles in Gene Therapy: New Avenues of Design and Optimization for Delivery Applications", *Polymers*, Vol. 11, No. 4, p. 745, 2019.

43. Santos-Carballal, B., E. F. Fernández, and F. M. Goycoolea, "Chitosan in Non-viral Gene Delivery: Role of Structure, Characterization Methods, and Insights in Cancer and Rare Diseases Therapies", *Polymers*, Vol. 10, No. 4, p. 444, 2018.

44. Lin C., and J. F. J. Engbersen, "Effect of Chemical Functionalities in Poly(amido amine)s for Non-viral Gene Transfection", *Journal of Controlled Release*, Vol. 132, No. 3, pp. 267-272, 2008.

45. Yellepeddi V. K., and H. Ghandehari, "Poly(amido amine) Dendrimers in Oral Delivery", *Tissue Barriers*, Vol. 4, No. 2, p. e1173773, 2016.

46. Jones, N. A., I. R. C. Hill, S. Stolnik, F. Bignotti, S. S. Davis, and M. C. Garnett, "Polymer Chemical Structure is a Key Determinant of Physicochemical and Colloidal Properties of Polymer-DNA Complexes for Gene Delivery", *Biochimica et Biophysica Acta,* Vol. 1517, No. 1, pp. 1-18, 2000.

47. Gosselin, M. A., W. Guo, and R. J. Lee, "Efficient Gene Transfer Using Reversibly Cross-Linked Low Molecular Weight Polyethylenimine", *Bioconjugate Chemistry*, Vol. 12, No. 6, pp. 989-994, 2001.

48. Richardson, S. C. W., N. G. Pattrick, Y. K. Stella Man, P. Ferruti, and R. Duncan, "Poly(Amidoamine)s as Potential Nonviral Vectors: Ability to Form Interpolyelectrolyte Complexes and to Mediate Transfection in Vitro," *Biomacromolecules*, Vol. 2, No. 3, pp. 1023-1028, 2001.

49. Ferruti, P., S. Manzoni, S. C. Richardson, R. Duncan, N. G. Pattrick, R. Mendichi, and M. Casolaro, "Amphoteric Linear Poly(amido-amine)s as Endosomolytic Polymers: Correlation between Physicochemical and Biological Properties", *Macromolecules*, Vol. 33, No. 21, pp. 7793-7800, 2000.

50. Demirci, G., M. N. Guven, S. Altuncu, Y. U. Konca, D. Avci, and H. Yagci Acar, "(Bis)phosphonic Acid-Functionalized Poly(ethyleneimine)-Poly(amido amine)s for Selective In Vitro Transfection of Osteosarcoma Cells", *ACS Applied Polymer Materials*, Vol. 3, No. 8, pp. 3776-3787, 2021.

51. Patel A., and K. Mequanint, *Biomedical Engineering - Frontiers and Challenges*, IntechOpen, Rijeka, 2011.

52. Dergunov S. A., and G. A. Mun, "γ-irradiated Chitosan-Polyvinyl Pyrrolidone Hydrogels as pH-Sensitive Protein Delivery System", *Radiation Physics and Chemistry*, Vol. 78, No. 1, pp. 65-68, 2009.

53. Amukarimi, S., S. Ramakrishna, and M. Mozafari, "Smart Biomaterials-A Proposed Definition and Overview of the Field", *Current Opinion in Biomedical Engineering*, Vol. 19, No. September, pp. 65-68, 2021.

54. Erol, O., A. Pantula, W. Li, and D. H. Gracias, “Transformer Hydrogels: A Review”, *Advanced Materials Technologies*, Vol. 4, No. 4, p. 1900043, 2019.

55. Kalia, S. (Editor), *Polymeric Hydrogels as Smart Biomaterials*, Springer Cham, Switzerland, 2016.

56. Mantha, S., S. Pillai, P. Khayambashi, A. Upadhyay, Y. Zhang, O. Tao, H. M. Pham, and S. D. Tran, “Smart Hydrogels in Tissue Engineering and Regenerative Medicine”, *Materials*, Vol. 12, No. 20, p. 3323, 2019.

57. Chakrapani, G., M. Zare, and S. Ramakrishna, “Intelligent Hydrogels and Their Biomedical Applications”, *Materials Advances*, Vol. 3, No. 21, pp. 7757-7772, 2022.

58. Lim, H. L., Y. Hwang, M. Kar, and S. Varghese, “Smart Hydrogels as Functional Biomimetic Systems”, *Biomaterials Science*, Vol. 2, No. 5, pp. 603-618, 2014.

59. Sikdar, P., M. M. Uddin, T. M. Dip, S. Islam, M. S. Hoque, A. K. Dhar, and S. Wu, “Recent Advances in the Synthesis of Smart Hydrogels”, *Materials Advances*, Vol. 2, No. 14, pp. 4532-4573, 2021.

60. Kopeček, J., “Hydrogel Biomaterials: A Smart Future?”, *Biomaterials*, Vol. 28, No. 34, pp. 5185-5192, 2007.

61. Bahram, M., N. Mohseni, and M. Moghtader, “*Emerging Concepts in Analysis and Applications of Hydrogels*”, InTechOpen, Rijeka, 2016.

62. Uhrich, K. E., S. M. Cannizzaro, R. S. Langer, and K. M. Shakesheff, “Polymeric Systems for Controlled Drug Release”, *Chemical Reviews*, Vol. 99, No. 11, pp. 3181-3198, 1999.

63. Drury J. L., and D. J. Mooney, “Hydrogels for Tissue Engineering: Scaffold Design Variables and Applications”, *Biomaterials*, Vol. 24, No. 24, pp. 4337-4351, 2003.

64. Wang, C., R. R. Varshney, and D. A. Wang, “Therapeutic cell delivery and fate control in hydrogels and hydrogel hybrids”, *Advanced Drug Delivery Reviews*, Vol. 62, No. 7-8, pp. 699-710, 2010.

65. Slaughter, B. V., S. S. Khurshid, O. Z. Fisher, A. Khademhosseini, and N. A. Peppas, “Hydrogels in Regenerative Medicine”, *Advanced Materials*, Vol. 21, No. 32-33, pp. 3307-3329, 2009.

66. Bae, J., J. Park, S. Kim, H. Cho, H. J. Kim, S. Park, and D. S. Shin, “Tailored Hydrogels for Biosensor Applications”, *Journal of Industrial and Engineering Chemistry*, Vol. 89, No. September, pp. 1-12, 2020.

67. Pakdel, P. M., and S. J. Peighambardoust, “A Review on Acrylic Based Hydrogels and Their Applications in Wastewater Treatment”, *Journal of Environmental Management*, Vol. 217, No. July, pp. 123-143, 2018.

68. Dhand, A. P., J. H. Galarraga, and J. A. Burdick, “Enhancing Biopolymer Hydrogel Functionality through Interpenetrating Networks”, *Trends in Biotechnology*, Vol. 39, No. 5, pp. 519-538, 2021.

69. Gong, J. P., Y. Katsuyama, T. Kurokawa, and Y. Osada, “Double-Network Hydrogels with Extremely High Mechanical Strength”, *Advanced Materials*, Vol. 15, No. 14, pp. 1155-1158, 2003.

70. Myung, D., W. Koh, J. Ko, Y. Hu, M. Carrasco, J. Noolandi, C. N. Ta, and C. W. Frank, “Biomimetic Strain Hardening in Interpenetrating Polymer Network Hydrogels”, *Polymer,* Vol. 48, No. 18, pp. 5376-5387, 2007.

71. Samanta, H. S., and S. K. Ray, “Synthesis, Characterization, Swelling and Drug Release Behavior of Semi-interpenetrating Network Hydrogels of Sodium Alginate and Polyacrylamide”, *Carbohydrate Polymers*, Vol. 99, No. January, pp. 666-678, 2014.

72. Matricardi, P., C. Di Meo, T. Coviello, W. E. Hennink, and F. Alhaique, “Interpenetrating Polymer Networks Polysaccharide Hydrogels for Drug Delivery and Tissue Engineering”, *Advanced Drug Delivery Reviews*, Vol. 65, No. 9, pp. 1172-1187, 2013.

73. Myung, D., D. Waters, M. Wiseman, P. E. Duhamel, J. Noolandi, C. N. Ta, and C. W. Frank, "Progress in the Development of Interpenetrating Polymer Network Hydrogels", *Polymers for Advanced Technologies*, Vol. 19, No. 6, pp. 647-657, 2008.

74. Banerjee, S., G. Chaurasia, D. Pal, A. K. Ghosh, A. Ghosh, and S. Kaity, "Investigation on Crosslinking Density for Development of Novel Interpenetrating Polymer Network (IPN) Based Formulation", *Journal of Scientific & Industrial Research*, Vol. 69, No. October, pp. 777-784, 2010.

75. Mandal, B. B., S. Kapoor, and S. C. Kundu, "Silk Fibroin/Polyacrylamide Semi-interpenetrating Network Hydrogels for Controlled Drug Release", *Biomaterials*, Vol. 30, No. 14, pp. 2826-2836, 2009.

76. Feig, V. R., H. Tran, M. Lee, and Z. Bao, "Mechanically Tunable Conductive Interpenetrating Network Hydrogels That Mimic the Elastic Moduli of Biological Tissue", *Nature Communications*, Vol. 9, No. 1, p. 2740, 2018.

77. Hebeish, A., S. Farag, S. Sharaf, and T. I. Shaheen, "Thermal Responsive Hydrogels Based on Semi Interpenetrating Network of Poly(NIPAm) and Cellulose Nanowhiskers", *Carbohydrate Polymers*, Vol. 102, No. 1, pp. 159-166, 2014.

78. Strong L. E., and J. L. West, "Thermally Responsive Polymer-Nanoparticle Composites for Biomedical Applications", *Wiley Interdisciplinary Reviews: Nanomedicine and Nanobiotechnology,* Vol. 3, No. 3, pp. 307-317, 2011.

79. Graisuwan, W., H. Zhao, S. Kiatkamjornwong, P. Theato and V. P. Hoven, "Formation of Thermo-Sensitive and Cross-Linkable Micelles by Self-Assembly of Poly(pentafluorophenyl Acrylate)-Containing Block Copolymer", *Journal of Polymer Science Part A Polymer Chemistry*, Vol. 53, No. 9, pp. 1103-1113, 2015.

80. Ward, M. A., and T. K. Georgiou, "Thermoresponsive Polymers for Biomedical Applications", *Polymers*, Vol. 3, No. 3, pp. 1215-1242, 2011.

81. Rafael, D., M. M. R. Melendres, F. Andrade, S. Montero, F. Martinez-Trucharte, M. Vilar-Hernandez, E. F. Durán-Lara, S. Schwartz Jr, and I. Abasolo, "Thermo-Responsive Hydrogels for Cancer Local Therapy: Challenges and State-of-art", *International Journal of Pharmaceutics*, Vol. 606, No. September, p. 120954, 2021.

82. Klouda, L., and A. G. Mikos, "Thermoresponsive Hydrogels in Biomedical Applications", *European Journal of Pharmaceutics and Biopharmaceutics*, Vol. 68, No. 1, pp. 34-45, 2008.

83. Ma, C., Y. Shi, D. A. Pena, L. Peng, and G. Yu, "Thermally Responsive Hydrogel Blends: A General Drug Carrier Model for Controlled Drug Release", *Angewandte Chemie - International Edition*, Vol. 54, No. 25, pp. 7376-7380, 2015.

84. Andrade, F., M. M. Roca-Melendres, E. F. Durán-Lara, D. Rafael, and S. Schwartz, "Review Stimuli-Responsive Hydrogels for Cancer Treatment: The Role of pH, Light, Ionic Strength and Magnetic Field", *Cancers*, Vol. 13, No. 5, pp. 1-17, 2021.

85. Kocak, G., C. Tuncer, and V. Bütün, "pH-Responsive Polymers", *Polymer Chemistry*, Vol. 8, No. 1, pp. 144-176, 2017.

86. Karoyo, A. H., and L. D. Wilson, "A Review on The Design and Hydration Properties of Natural Polymer-Based Hydrogels", *Materials*, Vol. 14, No. 5, pp. 1-36, 2021.

87. Emam, H. E., and T. I. Shaheen, "Design of a Dual pH and Temperature Responsive Hydrogel Based on Esterified Cellulose Nanocrystals for Potential Drug Release", *Carbohydrate Polymers,* Vol. 278, No. February, p. 118925, 2022.

88. Lavanya, K., S. V. Chandran, K. Balagangadharan, and N. Selvamurugan, "Temperature- and pH-Responsive Chitosan-Based Injectable Hydrogels for Bone Tissue Engineering", *Materials Science and Engineering C*, Vol. 111, No. June, p. 110862, 2020.

89. Han, Z., P. Wang, G. Mao, T. Yin, D. Zhong, B Yiming, X. Hu, Z. Jia, G. Nian, and W. Yang, "Dual pH-Responsive Hydrogel Actuator for Lipophilic Drug Delivery," *ACS Applied Materials and Interfaces*, Vol. 12, No. 10, pp. 12010-12017, 2020.

90. Xu, L., L. Qiu, Y. Sheng, Y. Sun, L. Deng, X. Li, M. Bradley, and R. Zhang, "Biodegradable pH-Responsive Hydrogels for Controlled Dual-Drug Release", *Journal of Materials Chemistry B*, Vol. 6, No. 3, pp. 510-517, 2018.

91. Kousar, F., J. Malmstrom, S. Swift, J. Ross, J. Perera, J., S. C. Moratti, "Protein-Resistant Behavior of Poly(ethylene glycol)-Containing Polymers with Phosphonate/Phosphate Units on Stainless Steel Surfaces", *ACS Applied Polymer Materials*, Vol. 3, No. 5, pp. 2785-2801, 2021.

92. Strasser P., and I. Teasdale, "Main-Chain Phosphorus-Containing Polymers for Therapeutic Applications", *Molecules*, Vol. 25, No. 7, p. 1716, 2020.

93. Monge, S., B. Canniccioni, A. Graillot, and J. J. Robin, "Phosphorus-Containing Polymers: A Great Opportunity for the Biomedical Field", *Biomacromolecules*, Vol. 12, No. 6. pp. 1973-1982, 2011.

94. Solimando, X., Y. Catel, N. Moszner, J. J. Robin, and S. Monge, "Smart Functionalized Phosphonic Acid Based Copolymers: New Structures for Old Purposes", *Polymer Chemistry*, Vol. 11, No. 18, pp. 3237-3250, 2020.

95. Bujoli, B., H. Roussière , G. F. Montavon , S. Laïb , P. Janvier , B. Alonso , F. Fayon , M. Petit, D. Massiot , J. M. Bouler, J. Guicheux , O. Gauthier , L. Sm , G. Nonglaton , M. Pipelier, J. Léger , Talham Dr , and C. Tellier "Novel Phosphate–Phosphonate Hybrid Nanomaterials Applied to Biology", *Progress in Solid State Chemistry*, Vol. 34, No. 2-4, pp. 257-266, 2005.

96. Tang, L., S, Gou, Y. He, L. Liu, S. Fang, W. Duan, and T. Liu, "An Efficient Chitosan-Based Adsorption Material Containing Phosphoric Acid and Amidoxime Groups for the Enrichment of Cu(II) and Ni(II) from Water", *Journal of Molecular Liquids*, Vol. 331, No. June, p. 115815, 2021.

97. Ossipov, D. A., "Bisphosphonate-Modified Biomaterials for Drug Delivery and Bone Tissue Engineering", *Expert Opinion on Drug Delivery*, Vol. 12, No. 9, pp. 1443-1458, 2015.

98. Fleisch, H., J. Maerki, and R. G. G. Russell, “Effect of Pyrophosphate on Dissolution of Hydroxyapatite and its Possible Importance in Calcium Homeostasis”, *Proceedings of the Society for Experimental Biology and Medicine*, Vol. 122, No. 2, pp. 317-320, 1966.

99. Van Acker, H. H., S. Anguille, Y. Willemen, E. L. Smits, E. L., and V. F. Van Tendeloo, “Bisphosphonates for Cancer Treatment: Mechanisms of Action and Lessons From Clinical Trials”, *Pharmacology & Therapeutics*, Vol. 158, No. February, pp. 24-40, 2016.

100. Walker, R. E., M. A. Lawson, C. H. Buckle, J. A. Snowden, and A. D. Chantry, “Myeloma Bone Disease: Pathogenesis, Current Treatments and Future Targets”, *British Medical Bulletin*, Vol. 111, No. 1, pp. 117-138, 2014.

101. Clézardin, P., I. Benzaïd, and P. I. Croucher, “Bisphosphonates in Preclinical Bone Oncology”, *Bone*, Vol. 49, No. 1, pp. 66-70, 2011.

102. Cattalini, J. P., A. R. Boccaccini, S. Lucangioli, and V. Mouriño, “Bisphosphonate-Based Strategies for Bone Tissue Engineering and Orthopedic Implants”, *Tissue Engineering Part B: Reviews*, Vol. 18, No. 5, pp. 323-340, 2012.

103. Xu, T., L. Zhang, Z. Cheng, and X. Zhu, “A Novel Methacrylate with a Bisphosphonate Group: RAFT Polymerization and Flame-Retardant Property of the Resultant Polymers”, *Polymer Chemistry*, Vol. 6, No. 12, pp. 2283-2289, 2015.

104. Shi, L., H. Carstensen, K. Hölzl, M. Lunzer, H. Li, J. Hilborn, A. Ovsianikov, and D. A. Ossipov, “Dynamic Coordination Chemistry Enables Free Directional Printing of Biopolymer Hydrogel”, *Chemistry of Materials*, Vol. 29, No. 14, pp. 5816-5823, 2017.

105. Giger, E. V., B. Castagner, and J. C. Leroux, “Biomedical Applications of Bisphosphonates”, *Journal of Controlled Release*, Vol. 167, No. 2, pp. 175-188, 2013.

106. Erezuma, I., I. Lukin, M. Desimone, Y. S. Zhang, A. Dolatshahi-Pirouz, and G. Orive, “Progress in Self-healing Hydrogels and Their Applications in Bone Tissue Engineering”, *Biomaterials Advances*, Vol. 146, No. March, p. 213274, 2023.

107. Mouriño, V. and A. R. Boccaccini, "Bone Tissue Engineering Therapeutics: Controlled Drug Delivery in Three-Dimensional Scaffolds", *Journal of the Royal Society Interface*, Vol. 7, No. 43, pp. 209-227, 2010.

108. Xue, X., Y. Hu, S. Wang, X. Chen, Y. Jiang, and J. Su, "Fabrication of Physical and Chemical Crosslinked Hydrogels for Bone Tissue Engineering", *Bioactive Materials*, Vol. 12, No. June, pp. 327-339, 2022.

109. Thula, T. T., F. Svedlund, D. E. Rodriguez, J. Podschun, L. Pendi, and L. B. Gower, "Mimicking the Nanostructure of Bone: Comparison of Polymeric Process-Directing Agents", *Polymers*, Vol. 3, No. 1, pp. 10-35, 2011.

110. Yuan, W., Z. Li, X. Xie, Z. Y. Zhang, and L. Bian, "Bisphosphonate-Based Nanocomposite Hydrogels for Biomedical Applications", *Bioactive Materials*, Vol. 5, No. 4. pp. 819-831, 2020.

111. S. Bose and S. Tarafder, "Calcium Phosphate Ceramic Systems in Growth Factor and Drug Delivery for Bone Tissue Engineering: A Review", *Acta Biomaterialia*, Vol. 8, No. 4, pp. 1401-1421, 2012.

112. Yang, X., S. Akhtar, S. Rubino, K. Leifer, J. Hilborn, and D. Ossipov, "Direct Click Synthesis of Hybrid Bisphosphonate-Hyaluronic Acid Hydrogel in Aqueous Solution for Biomineralization", *Chemistry of Materials*, Vol. 24, No. 9, pp. 1690-1697, 2012.

113. Cui, Y., T. Zhu, D. Li, Z. Li, Y. Leng, X. Ji, H. Liu, D. Wu, and J. Ding "Bisphosphonate-Functionalized Scaffolds for Enhanced Bone Regeneration", *Advanced Healthcare Materials*, Vol. 8, No. 23, p. 1901073, 2019.

114. Zhang, K., W. Yuan, K. Wei, B. Yang, X. Chen, Z. Li, Z. Zhang, and L. Bian "Highly Dynamic Nanocomposite Hydrogels Self-Assembled by Metal Ion-Ligand Coordination", *Small*, Vol. 15, No. 15, p. 1900242, 2019.

115. Oliveira, A. L., A. J., Pedro, C. S. Arroyo, J. F. Mano, G. Rodriguez, J. S. Roman, and R. L. Reis, "Biomimetic Ca-P Coatings Incorporating Bisphosphonates Produced on Starch-Based Degradable Biomaterials", *Journal of Biomedical Materials Research Part B: Applied Materials*, Vol. 92, No. 1, pp. 55-67, 2009.

116. Nejadnik, M. R., X. Yang, M. Bongio, H. S. Alghamdi, J. J. J. P. van den Beucken, M. C. Huysmans, J. A. Jansen, J. Hilborn, D. Ossipov and S. C. G. Leeuwenburgh, "Self-Healing Hybrid Nanocomposites Consisting of Bisphosphonated Hyaluronan and Calcium Phosphate Nanoparticles", *Biomaterials*, Vol. 35, No. 25, pp. 6918-6929, 2014.

117. Hirabayashi, H., and J. Fujisaki, "Bone-Specific Drug Delivery Systems Approaches via Chemical Modification of Bone-Seeking Agents", *Clinical Pharmacokinetics*, Vol. 42, No. September, pp. 1319-1330, 2003.

118. Rudnick-Glick, S., E. Corem-Salkmon, I. Grinberg, and S. Margel, "Targeted Drug Delivery of Near IR Fluorescent Doxorubicin-Conjugated Poly(ethylene glycol) Bisphosphonate Nanoparticles for Diagnosis and Therapy of Primary and Metastatic Bone Cancer in a Mouse Model", *Journal of Nanobiotechnology,* Vol. 14, No. 1, pp. 1-11, 2016.

119. Carmona-Sarabia, L., G. Q. Vélez, D. Mojica-Vázquez, A. M. Escalera-Joy, S. Esteves-Vega, E. A. Peterson-Peguero, and V. López-Mejías, "High-Affinity Extended Bisphosphonate-Based Coordination Polymers as Promising Candidates for Bone-Targeted Drug Delivery", *ACS Applied Material Interfaces*, Vol. 15, No. 28, pp. 33397-33412, 2023.

120. Cole, L. E., T. Vargo-Gogola, and R. K. Roeder, "Targeted Delivery to Bone and Mineral Deposits Using Bisphosphonate Ligands", *Advanced Drug Delivery Reviews*, Vol. 99, No. April, pp. 12-27, 2016.

121. Li, Z., H. Wang, K. Zhang, B. Yang, X. Xie, Z. Yang, L. Kong, P. Shi, Y. Zhang, Y. Ho, Z. Zhang, G. Li, and L. Bian, "Bisphosphonate-Based Hydrogel Mediates Biomimetic Negative Feedback Regulation of Osteoclastic Activity to Promote Bone Regeneration", *Bioactive Materials*, Vol. 13, No. July, pp. 9-22, 2022.

122. Fujisaki, J., Y. Tokunaga, T. Takahashi, F. Shimojo, S. Kimura, and T. Hata, "Osteotropic Drug Delivery System (ODDS) Based on Bisphosphonic Prodrug. IV Effects of Osteotropic Estradiol on Bone Mineral Density and Uterine Weight in Ovariectomized Rats", *Journal of Drug Targeting*, Vol. 5, No. 2, pp. 129-138, 1998.

123. Morioka, M., A. Kamizono, H. Takikawa, A. Mori, H. Ueno, S. Kadowaki, Y. Nakao, K. Kato, and K. Umezawa, "Design, Synthesis, and Biological Evaluation of Novel Estradiol–Bisphosphonate Conjugates as Bone-Specific Estrogens", *Bioorganic & Medicinal Chemistry*, Vol. 18, No. 3, pp. 1143-1148, 2010.

124. Pan, H., M. Sima, P. Kopečková, K. Wu, S. Gao, J. Liu, D. Wang, S. C. Miller and J. Kopeček, "Biodistribution and Pharmacokinetic Studies of Copolymer-Alendronate Conjugates", *Molecular Pharmaceutics*, Vol. 5, No. 4, pp. 548-558, 2008.

125. Guven, M. N., G. Demirci, S. Altuncu, U. Gulyuz, O. Okay, H. Yagci Acar, and D. Avci, "Alendronate-functionalized Poly(amido amine) Cryogels of High-toughness for Biomedical Applications", *Polymer*, Vol.190, p. 122248, 2020.

126. Kokubo, T. and H. Takadama, "How Useful Is SBF in Predicting in Vivo Bone Bioactivity?", *Biomaterials*, Vol. 27, No. 15, pp. 2907-2915, 2006.

127. Chou, Y. F., W. A. Chiou, Y. Xu, J. C. Y. Dunn and B. M. Wu, "The Effect of pH on The Structural Evolution of Accelerated Biomimetic Apatite", *Biomaterials*, Vol. 25, No. 22, pp. 5323-5331, 2004.

128. Argun, A., V. Can, U. Altun, and O. Okay, "Nonionic Double and Triple Network Hydrogels of High Mechanical Strength," *Macromolecules*, Vol. 47, No. 18, pp. 6430-6440, 2014.

129. Sunshine, J. C., M. I. Akanda, D. Li, K. L. Kozielski, and J. J. Green, "Effects of Base Polymer Hydrophobicity and End-Group Modification on Polymeric Gene Delivery", *Biomacromolecules*, Vol. 12, No. 10, pp. 3592-3600, 2011.

130. Wang, R., L. Zhou, Y. Zhou, G. Li, X. Zhu, H. Gu, X. Jiang, H. Li, J. Wu, L. He, X. Guo, B. Zhu, and D. Yan, "Synthesis and Gene Delivery of Poly(amido amine)s with Different Branched Architecture", *Biomacromolecules*, Vol. 11, No. 2, pp. 489-495, 2010.

131. Manfredi, A., E. Ranucci, M. Suardi and P. Ferruti, "Polymerization Kinetics of Poly(amidoamine)s in Different Solvents", *Journal of Bioactive and Compatible Polymers*, Vol. 22, No. 2, pp. 219-231, 2007.

132. Mateos-Timoneda, M. A., M. C. Lok, W. E. Hennink, J. Feijen, and J. F. Engbersen, "Poly (amido amine) s as Gene Delivery Vectors: Effects of Quaternary Nicotinamide Moieties in the Side Chains", *ChemMedChem: Chemistry Enabling Drug Discovery*, Vol. 3, No. 3, pp. 478-486, 2008.

133. Lin, C., and J. F. J. Engbersen, "PEGylated Bioreducible Poly(amido amine)s for Non-Viral Gene Delivery", *Material Science and Engineering C*, Vol. 31, No. 7, pp. 1330-1337, 2011.

134. Song, W., Z. Tang, M. Li, S. Lv, H. Yu, L. Ma, X. Zhuang, Y. Huang, and X. Chen, "Tunable pH-Sensitive Poly(β-amino ester)s Synthesized from Primary Amines and Diacrylates for Intracellular Drug Delivery", *Macromolecular Bioscience*, Vol. 12, No. 10, pp. 1375-1383, 2012.

135. Ke, J., H. Dou, X. Zhang, D. S. Uhagaze, X. Ding, and Y. Dong, "Determination of pKa Values of Alendronate Sodium in Aqueous Solution by Piecewise Linear Regression Based on Acid-Base Potentiometric Titration", *Journal of Pharmaceutical Analysis,* Vol. 6, No. 6, pp. 404-409, 2016.

136. Hamai, R., Y. Shirosaki and T. Miyazaki, "Apatite-Forming Ability of Vinylphosphonic Acid-Based Copolymer in Simulated Body Fluid: Effects of Phosphate Group Content", *Journal of Materials Science: Materials in Medicine,* Vol. 27, No. 10, pp. 1-8, 2016.

137. Phadke, A., C. Zhang, Y. Hwang, K. Vecchio, and S. Varghese, "Templated Mineralization of Synthetic Hydrogels for Bone-Like Composite Materials: Role of Matrix Hydrophobicity", *Biomacromolecules*, Vol. 11, No. 8, pp. 2060-2068, 2010.

138. Oyane, A., H. M. Kim, T. Furuya, T. Kokubo, T. Miyazaki, and T. Nakamura, "Preparation and Assessment of Revised Simulated Body Fluids", *Journal of Biomedical Materials Research Part A*, Vol. 65A, No. 2, pp. 188-195, 2003.

139. Costa, D. O., B. A. Allo, R. Klassen, J. L. Hutter, S. J. Dixon, and A. S. Rizkalla, "Control of Surface Topography in Biomimetic Calcium Phosphate Coatings", *Langmuir*, Vol. 28, No. 8, pp. 3871-3880, 2012.

140. Sauer, G. R., and R. E. Wuthier, “Fourier Transform Infrared Characterization of Mineral Phases Formed During Induction of Mineralization by Collagenase-Released Matrix Vesicles in Vitro”, *Journal of Biological Chemistry*, Vol. 263, No. 27, pp. 13718-13724, 1988.

141. Harding, J. L., and M. D. Krebs, “Controlled and Tunable Biomimetic Apatite Mineralization of Synthetic Hydrogels”, *Macromolecular Materials and Engineering*, Vol. 301, No. 10, pp. 1172-1180, 2016.

142. Shkilnyy, A., A. Friedrich, B. Tiersch, S. Schöne, M. Fechner, J. Koetz, C.-W. Schläpfer, and A. Taubert, “Poly(ethylene imine)-Controlled Calcium Phosphate Mineralization”, *Langmuir*, Vol. 24, No. 25, pp. 2102-2109, 2008.

143. Shkilnyy, A., S. Schöne, C. Rumplasch, A. Uhlmann, A. Hedderich, C. Günter, and A. Taubert, “Calcium Phosphate Mineralization with Linear poly(ethylene imine): A Time-Resolved Study”, *Colloid and Polymer Science*, Vol. 289, No. 8, pp. 881-888, 2011.

144. Li, Y., X. Chen, A. Fok, J. C. Rodriguez-Cabello, and C. Aparicio, “Biomimetic Mineralization of Recombinamer-Based Hydrogels toward Controlled Morphologies and High Mineral Density”, *ACS Applied Materials and Interfaces*, Vol. 7, No. 46, pp. 25784-25792, 2015.

145. Ak, F., Z. Oztoprak, I. Karakutuk, and O. Okay, “Macroporous Silk Fibroin Cryogels,” *Biomacromolecules*, Vol. 14, No. 3, pp. 719-727, 2013.

146. Yetiskin, B., and O. Okay, “High-Strength and Self-Recoverable Silk Fibroin Cryogels with Anisotropic Swelling and Mechanical Properties”, *International Journal of Biological Macromolecules,* Vol. 122, No. February, pp. 1279-1289, 2019.

147. Wallin, R. F., and E. Arscott, “A Practical Guide to ISO 10993–5: Cytotoxicity” *Medical Device and Diagnostic Industry*, Vol. 20, No. April, pp. 96-98, 1998.

148. Cheng, Y. Y., L. Huang, K. M. Lee, K. Li, and S. M. Kumta, “Alendronate Regulates Cell Invasion and MMP-2 Secretion in Human Osteosarcoma Cell Lines”, *Pediatric Blood & Cancer*, Vol. 42, No. 5, pp. 410-415, 2004.

149. Xin, Z. F., Y. K. Kim, and S. T. Jung, "Risedronate Inhibits Human Osteosarcoma Cell Invasion", *Journal of Experimental & Clinical Cancer Research*, Vol. 28, No. 1, p. 105, 2009.

150. Guven, M. N., B. Balaban, G. Demirci, H. Yagci Acar, O. Okay, and D. Avci, "Bisphosphonate-functionalized Poly(amido amine) Crosslinked 2-Hydroxyethyl Methacrylate Hydrogel as Tissue Engineering Scaffold", *European Polymer Journal,* Vol.159, p. 110732, 2021.

151. Degenhardt, C. R., and D. C. Burdsall, "Synthesis of Ethenylidenebis(phosphonic acid) and Its Tetraalkyl Esters", *The Journal of Organic Chemistry*, Vol. 51, No. 18, pp. 3488-3490, 1986.

152. Liu, M., J. Chen, Y. P. Cheng, Y. N. Xue, R. X. Zhuo, and S. W. Huang, "Novel Poly(amidoamine)s with Pendant Primary Amines as Highly Efficient Gene Delivery Vectors", *Macromolecular Bioscience*, Vol. 10, No. 4, pp. 384-392, 2010.

153. Lin, C., C. J. Blaauboer, M. M. Timoneda, M. C. Lok, M. van Steenbergen, W. E. Hennink, Z. Zhong, J. Feijen, and J. F. J. Engbersen, "Bioreducible Poly(amido amine)s with Oligoamine Side Chains : Synthesis, Characterization, and Structural Effects on Gene Delivery", *Journal of Controlled Release*, Vol. 126, No. 2, pp. 166-174, 2008.

154. Bailly, T., R. Burgada, T. Prangé, and M. Lecouvey, "Synthesis of Tetradentate Mixed Bisphosphonates - New Hydroxypyridinonate Ligands for Metal Chelation Therapy", *Tetrahedron Letters*, Vol. 44, No. 1, pp. 189-192, 2003.

155. Chen, J., S. W. Huang, M. Liu, and R. X. Zhuo, "Synthesis and Degradation of Poly(beta-aminoester) with Pendant Primary Amine", *Polymer,* Vol. 48, No. 3, pp. 675-681, 2007.

156. Mastrogiacomo, M., S. Scaglione, R. Martinetti, L. Dolcini, F. Beltrame, R. Cancedda, and R. Quarto, "Role of Scaffold Internal Structure on in Vivo Bone Formation in Macroporous Calcium Phosphate Bioceramics", *Biomaterials*, Vol. 27, No. 17, pp. 3230-3237, 2006.

157. Wang, Q. Z., X. G. Chen, N. Liu, S. X. Wang, C. S. Liu, X. H. Meng, and C. G. Liu, "Protonation Constants of Chitosan with Different Molecular Weight and Degree of Deacetylation", *Carbohydrate Polymers*, Vol. 65, No. 2, pp. 194-201, 2006.

158. Kepa, K., R. Coleman, and L. Grøndahl, "In Vitro Mineralization of Functional Polymers", *Biosurface and Biotribology*, Vol. 1, No. 3, pp. 214-227, 2015.

159. Rehm, I., and W. Bonfield, "Characterization of Hydroxyapatite and Carbonated Apatite by Photo Acoustic FTIR Spectroscopy", *Journal of Materials Science: Materials in Medicine*, Vol.8, No. January, pp. 1-4, 1997.

160. Suzuki, S., M. R. Whittaker, L. Grøndahl, M. J. Monteiro, and E. Wentrup-Byrne, "Synthesis of Soluble Phosphate Polymers by RAFT and Their in Vitro Mineralization", *Biomacromolecules*, Vol. 7, No. 11, pp. 3178-3187, 2006.

161. Mayer, I., R. Schlam, and J. D. B. Featherstone, "Magnesium-Containing Carbonate Apatites", *Journal of Inorganic Biochemistry*, Vol. 66, No. 1, pp. 1-6, 1997.

162. Zhai, Y., and F. Z. Cui, "Recombinant Human-Like Collagen Directed Growth of Hydroxyapatite Nanocrystals", *Journal of Crystal Growth*, Vol. 291, No. 1, pp. 202-206, 2006.

163. Rusu, V. M., C. H. Ng, M. Wilke, B. Tiersch, P. Fratzl, and M. G. Peter, "Size-Controlled Hydroxyapatite Nanoparticles as Self-Organized Organic-Inorganic Composite Materials", *Biomaterials*, Vol. 26, No. 26, pp. 5414-5426, 2005.

164. Tan, J., R. A. Gemeinhart, M. Ma, and W. Mark Saltzman, "Improved Cell Adhesion and Proliferation on Synthetic Phosphonic Acid-Containing Hydrogels", *Biomaterials*, Vol. 26, No. 17, pp. 3663-3671, 2005.

165. Hulsart-Billström, G., P. K. Yuen, R. Marsell, J. Hilborn, S. Larsson and D. Ossipov, "Bisphosphonate-Linked Hyaluronic Acid Hydrogel Sequesters and Enzymatically Releases Active Bone Morphogenetic Protein-2 for Induction of Osteogenic Differentiation", *Biomacromolecules*, Vol. 14, No. 9, pp. 3055-3063, 2013.

166. George, M. N., X. Liu, A. L. Miller, H. Xu, and L. Lu, "Phosphate Functionalization and Enzymatic Calcium Mineralization Synergistically Enhance Oligo[poly(ethylene glycol) fumarate] Hydrogel Osteoconductivity for Bone Tissue Engineering", *Journal of Biomedical Materials Research - Part A*, Vol. 108, No. 3, pp. 515-527, 2020.

167. Zhang, X., Y. He, P. Huang, G. Jiang, M. Zhang, F. Yu, W. Zhang, G. Fu, Y. Wang, W. Li, and H. Zeng, "A Novel Mineralized High Strength Hydrogel for Enhancing Cell Adhesion and Promoting Skull Bone Regeneration in Situ", *Composites Part B: Engineering*, Vol. 197, No. September, p. 108183, 2020.

168. Nuttelman, C. R., M. C. Tripodi, and K. S. Anseth, "Synthetic Hydrogel Niches that Promote hMSC Viability", *Matrix Biology*, Vol. 24, No. 3, pp. 208-218, 2005.

169. Guven, M.N., G. Demirci, H. Yagci. Acar, and D. Avci, "Meso-2,3-dimercaptosuccinic Acid-Based Macromers for pH-Sensitive Degradable Hydrogels", *ACS Applied Polymer Journal,* Vol. 5, No. 11, pp. 9147-9158, 2023.

170. Ali, A. E., H. A. Shawky, H. A. Abd El Rehim, and E. A. Hegazy, "Synthesis and Characterization of PVP/AAc Copolymer Hydrogel and Its Applications in the Removal of Heavy Metals from Aqueous Solution", *European Polymer Journal*, Vol. 39, No. 12, pp. 2337-2344, 2003.

171. Sinha, V., and S. Chakma, "Advances in the Preparation of Hydrogel for Wastewater Treatment: A Concise Review", *Journal of Environmental Chemical Engineering*, Vol. 7, No. 5, pp. 103295, 2019.

172. Gong, J. P., Y. Katsuyama, T. Kurokawa, and Y. Osada, "Double-Network Hydrogels with Extremely High Mechanical Strength", *Advanced Materials*, Vol. 15, No. 14, pp. 1155-1158, 2003.

173. Wu, X., H. Sun, Z. Qin, P. Che, X. Yi, Q.Yu, H. Zhang, X. Sun, F. Yao, and J. Li, "Fully Physically Crosslinked Pectin-Based Hydrogel with High Stretchability and Toughness for Biomedical Application", *International Journal of Biological Macromolecules*, Vol. 149, No. April, pp. 707-716, 2020.

174. Wang, X. H., F. Song, D. Qian, Y. D. He, W. C. Nie, X. L. Wang, and Y. Z. Wang, "Strong and Tough Fully Physically Crosslinked Double Network Hydrogels with Tunable Mechanics and High Self-healing Performance", *Chemical Engineering Journal*, Vol. 349, No. October, pp. 588-594, 2018.

175. Li, D., H. Gao, M. Li, G. Chen, L. Guan, M. He, J. Tian, and R. Cao, "Nanochitin/Metal Ion Dual Reinforcement in Synthetic Polyacrylamide Network-based Nanocomposite Hydrogels", *Carbohydrate Polymers*, Vol. 236, No. May, p. 116061, 2020.

176. Yang, Z., Y. Yan, A. Yu, B. Pan, and J. J. Pignatello, "Revisiting the Phenanthroline and Ferrozine Colorimetric Methods for Quantification of Fe(II) in Fenton Reactions", *Chemical Engineering Journal*, Vol. 391, No. July, p. 123592, 2020.

177. Tesfaldet, Z. O., J. F. Van Staden, and R. I. Stefan, "Sequential Injection Spectrophotometric Determination of Iron as Fe(II) in Multi-Vitamin Preparations Using 1,10-Phenanthroline as Complexing Agent", *Talanta*, Vol. 64, No. 5, pp. 1189-1195, 2004.

178. Guo, X., D. Xu, H. Yuan, Q. Luo, S. Tang, L. Liu, and Y. Wu, "A Novel Fluorescent Nanocellulosic Hydrogel Based on Carbon Dots for Efficient Adsorption and Sensitive Sensing in Heavy Metals", *Journal of Materials Chemistry A*, Vol. 7, No. 47, pp. 27081-27088, 2019.

179. Gennari, A., J. Wedgwood, E. Lallana, N. Francini, and N. Tirelli, "Thiol-Based Michael-Type Addition. A Systematic Evaluation of Its Controlling Factors", *Tetrahedron*, Vol. 76, No. 47, p. 131637, 2020.

180. Sun, Y., H. Liu, L. Cheng, S. Zhu, C. Cai, T. Yang, L. Yang, and P. Ding, "Thiol Michael Addition Reaction: A Facile Tool for Introducing Peptides into Polymer-Based Gene Delivery Systems", *Polymer International*, Vol. 67, No. 1, pp. 25-31, 2018.

181. Walter, R. I., E. C. A. Ojadi, and H. Linschitzll, "A Proton NMR Study of the Reactions with Acid of meso-Tetraphenylporphyrins with Various Numbers of 4-(dimethylamino) Groups", *The Journal of Physical Chemistry*, Vol. 97, No.50, pp. 13308-13312, 1993.

182. Suhail, M., C. W. Fang, I. H. Chiu, M. C. Hung, Q. L. Vu, I. L. Lin, and P. C. Wu, "Designing and In Vitro Characterization of pH-Sensitive Aspartic Acid-Graft-Poly(Acrylic Acid) Hydrogels as Controlled Drug Carriers", *Gels*, Vol. 8, No. 8, p. 521, 2022.

183. Buwalda, S. J., P. J. Dijkstra, L. Calucci, C. Forte, and J. Feijen, "Influence of Amide Versus Ester Linkages on the Properties of Eight-Armed PEG-PLA Star Block Copolymer Hydrogels", *Biomacromolecules*, Vol. 11, No. 1, pp. 224-232, 2010.

184. He, B., E. Wan, and M. B. Chan-Park, "Synthesis and Degradation of Biodegradable Photo-Cross-Linked Poly(α,β-malic acid)-Based Hydrogel", *Chemistry of Materials*, Vol. 18, No. 17, pp. 3946-3955, 2006.

185. Crisponi, G., F. Cristiani, V. M. Nurchi, R. Pinna, and M. J. Tapia Estevez, "Equilibrium Study on Pd(II) Chelates of Mercapto Carboxylic Acids", *Polyhedron*, Vol. 18, No. 25, pp. 3257-3262, 1999.

186. Radosz, M., and Y. Shen, "Degradable Thermoresponsive Poly(ethylene glycol) Analogue Materials", U.S. Patent 0177592 Al, May 30, 2007. https://patents.google.com/patent/US20120177592A1/en, accessed on July 12, 2012.

187. Nazli, C., T. I. Ergenc, Y. Yar, H. Yagci Acar, and S. Kizilel, "RGDS-Functionalized Polyethylene Glycol Hydrogel-Coated Magnetic Iron Oxide Nanoparticles Enhance Specific Intracellular Uptake by HeLa Cells", *International Journal of Nanomedicine*, Vol. 7, No. April, pp. 1903-1920, 2012.

188. Lara-Ochoa, S., W. Ortega-Lara, and C. E. Guerrero-Beltrán, "Hydroxyapatite Nanoparticles in Drug Delivery: Physicochemistry and Applications", *Pharmaceutics*, Vol. 13, No. 10, p. 1642, 2021.

189. Chieng, B., N. Ibrahim, W. Yunus, and M. Hussein, “Poly(lactic acid)/Poly(ethylene glycol) Polymer Nanocomposites: Effects of Graphene Nanoplatelets”, *Polymers,* Vol. 6, No. 1, pp. 93-104, 2013.

APPENDIX A: SUPPLEMENTARY DATA

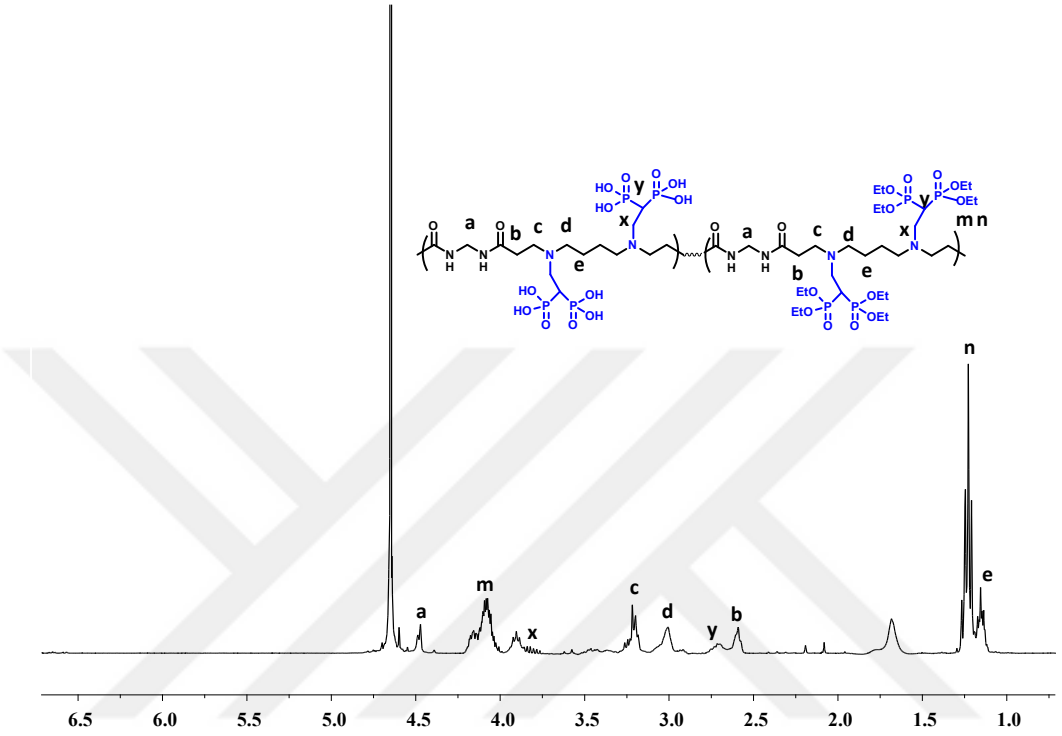

Figure A.1. ^{1}H NMR of PAA3

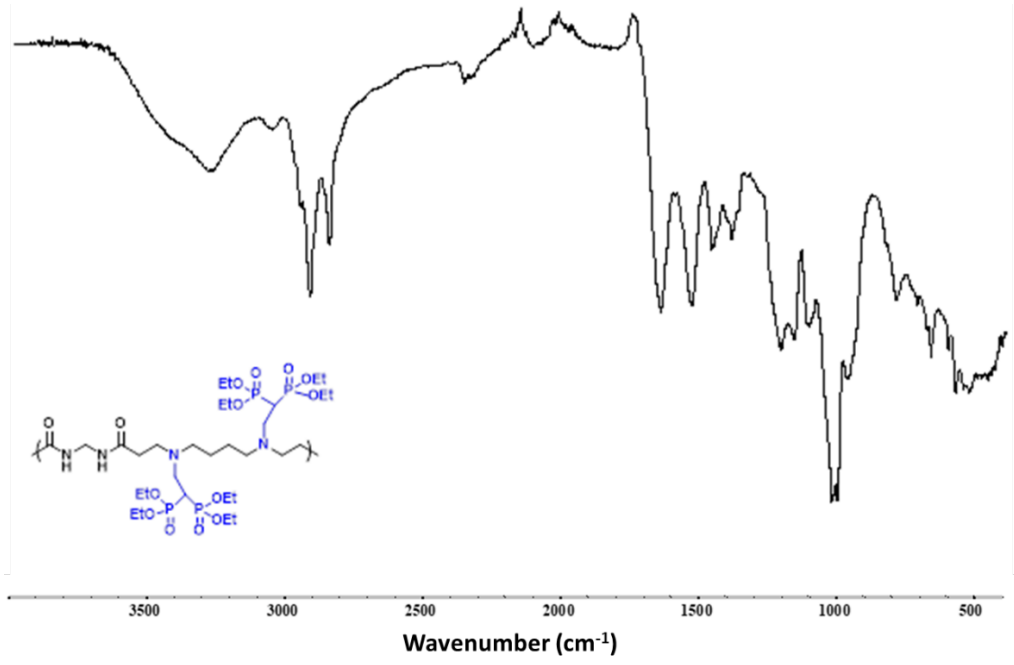

Figure A.2. FTIR spectrum of PAA2

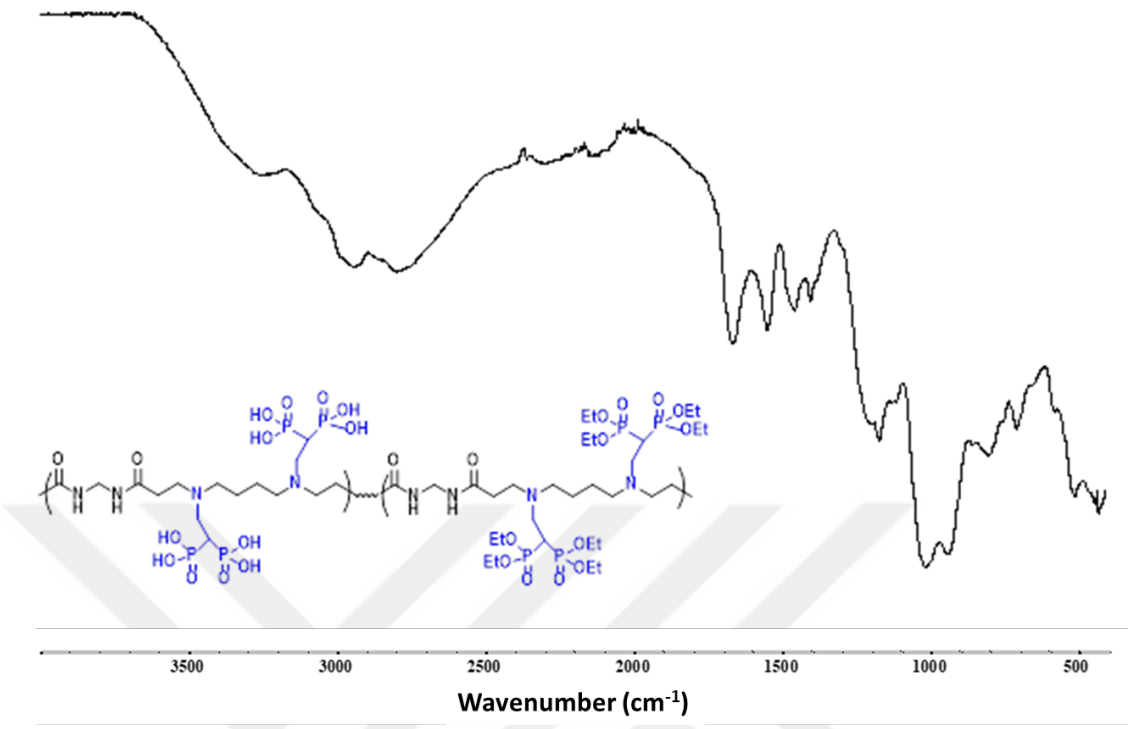

Figure A.3. FTIR spectrum of PAA3

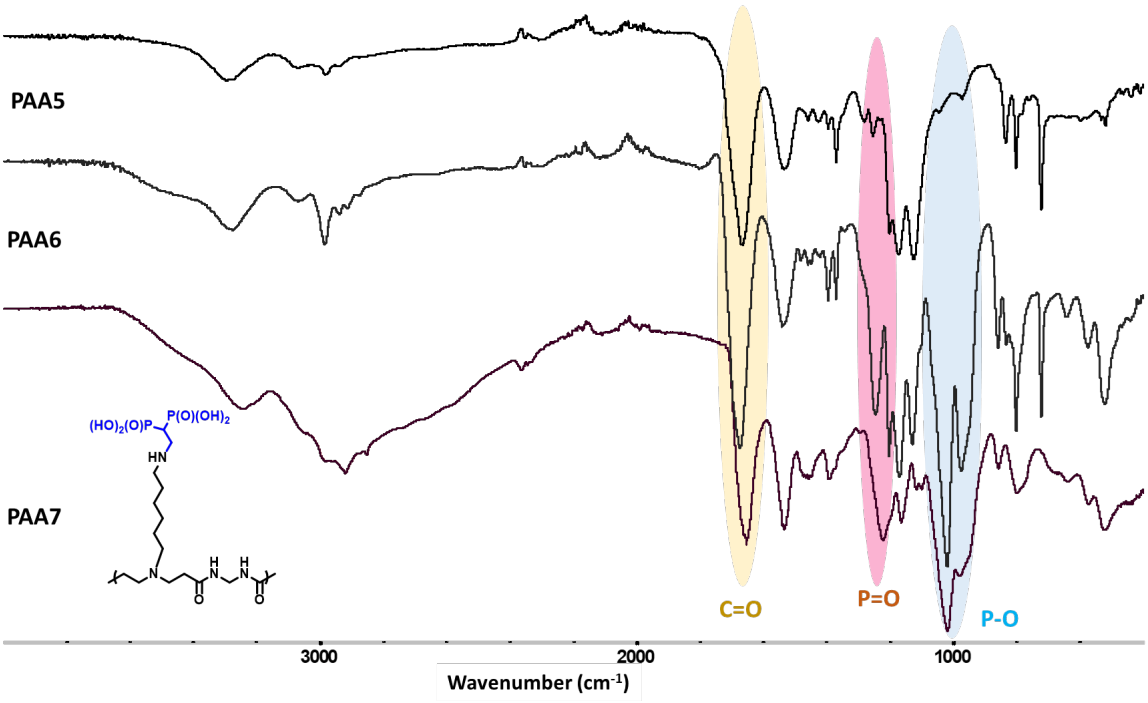

Figure A.4. FTIR spectra of PAA5, PAA6 and PAA7

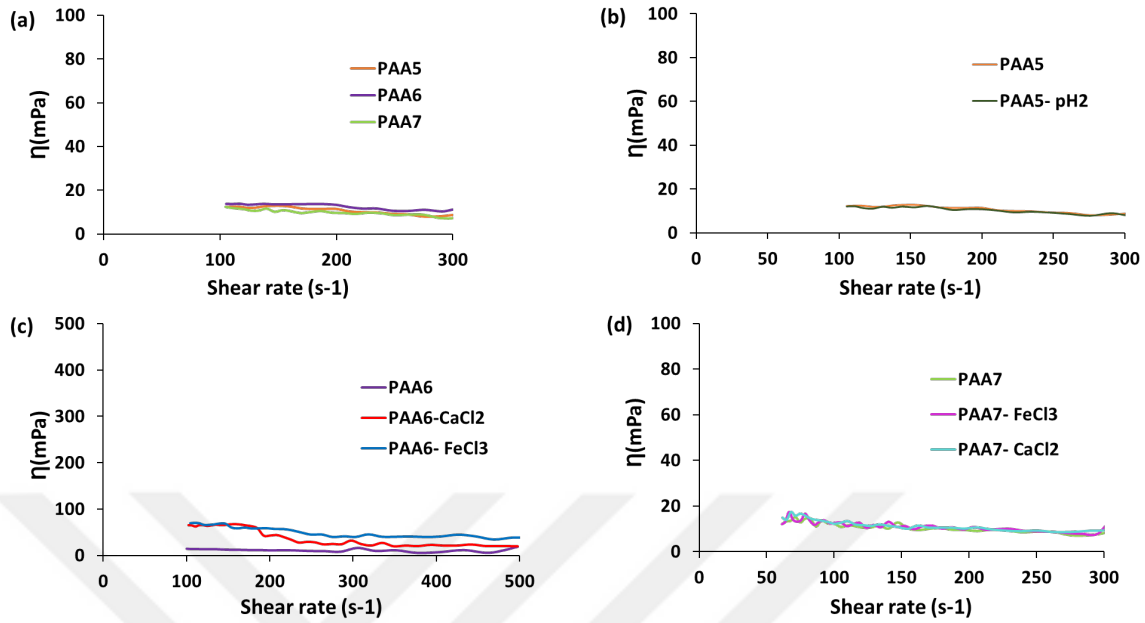

Figure A.5. A) The viscosities of the solutions of PAA5, PAA6, and PAA7 polymers at a concentration of 10%. B) The viscosities of the original form of PAA5 and its solutions at pH 2. C) The viscosities of the solutions of PAA6 and PAA6 in $CaCl_2$ and $FeCl_3$. D) The viscosities of the solutions of PAA7 and PAA7 in $CaCl_2$ and $FeCl_3$

APPENDIX B: COPY RIGHT LICENCES

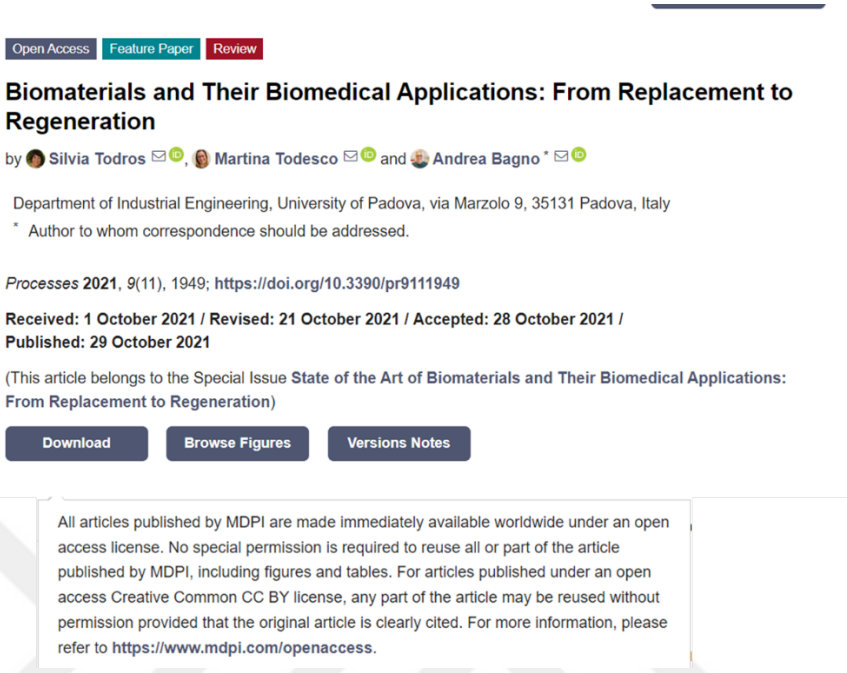

Open Access Feature Paper Review

Biomaterials and Their Biomedical Applications: From Replacement to Regeneration

by Silvia Todros, Martina Todesco and Andrea Bagno *

Department of Industrial Engineering, University of Padova, via Marzolo 9, 35131 Padova, Italy

* Author to whom correspondence should be addressed.

Processes **2021**, *9*(11), 1949; **https://doi.org/10.3390/pr9111949**

Received: 1 October 2021 / Revised: 21 October 2021 / Accepted: 28 October 2021 / Published: 29 October 2021

(This article belongs to the Special Issue **State of the Art of Biomaterials and Their Biomedical Applications: From Replacement to Regeneration**)

Download Browse Figures Versions Notes

All articles published by MDPI are made immediately available worldwide under an open access license. No special permission is required to reuse all or part of the article published by MDPI, including figures and tables. For articles published under an open access Creative Common CC BY license, any part of the article may be reused without permission provided that the original article is clearly cited. For more information, please refer to **https://www.mdpi.com/openaccess**.

Figure B.1. Permission from [6] Elsevier, Copyright (2013).

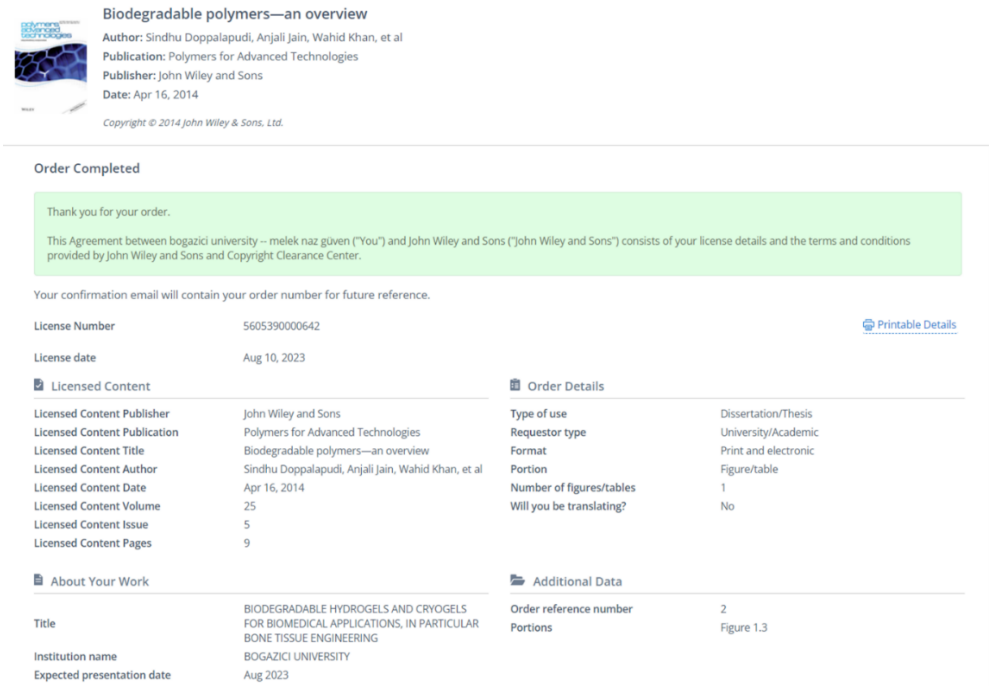

Biodegradable polymers—an overview

Author: Sindhu Doppalapudi, Anjali Jain, Wahid Khan, et al
Publication: Polymers for Advanced Technologies
Publisher: John Wiley and Sons
Date: Apr 16, 2014

Copyright © 2014 John Wiley & Sons, Ltd.

Order Completed

Thank you for your order.

This Agreement between bogazici university -- melek naz güven ("You") and John Wiley and Sons ("John Wiley and Sons") consists of your license details and the terms and conditions provided by John Wiley and Sons and Copyright Clearance Center.

Your confirmation email will contain your order number for future reference.

Printable Details

License Number	5605390000642
License date	Aug 10, 2023

Licensed Content

Licensed Content Publisher	John Wiley and Sons
Licensed Content Publication	Polymers for Advanced Technologies
Licensed Content Title	Biodegradable polymers—an overview
Licensed Content Author	Sindhu Doppalapudi, Anjali Jain, Wahid Khan, et al
Licensed Content Date	Apr 16, 2014
Licensed Content Volume	25
Licensed Content Issue	5
Licensed Content Pages	9

Order Details

Type of use	Dissertation/Thesis
Requestor type	University/Academic
Format	Print and electronic
Portion	Figure/table
Number of figures/tables	1
Will you be translating?	No

About Your Work

Title	BIODEGRADABLE HYDROGELS AND CRYOGELS FOR BIOMEDICAL APPLICATIONS, IN PARTICULAR BONE TISSUE ENGINEERING
Institution name	BOGAZICI UNIVERSITY
Expected presentation date	Aug 2023

Additional Data

Order reference number	2
Portions	Figure 1.3

Figure B.2. Permission from [16] John Wiley and Sons, Copyright (2014).

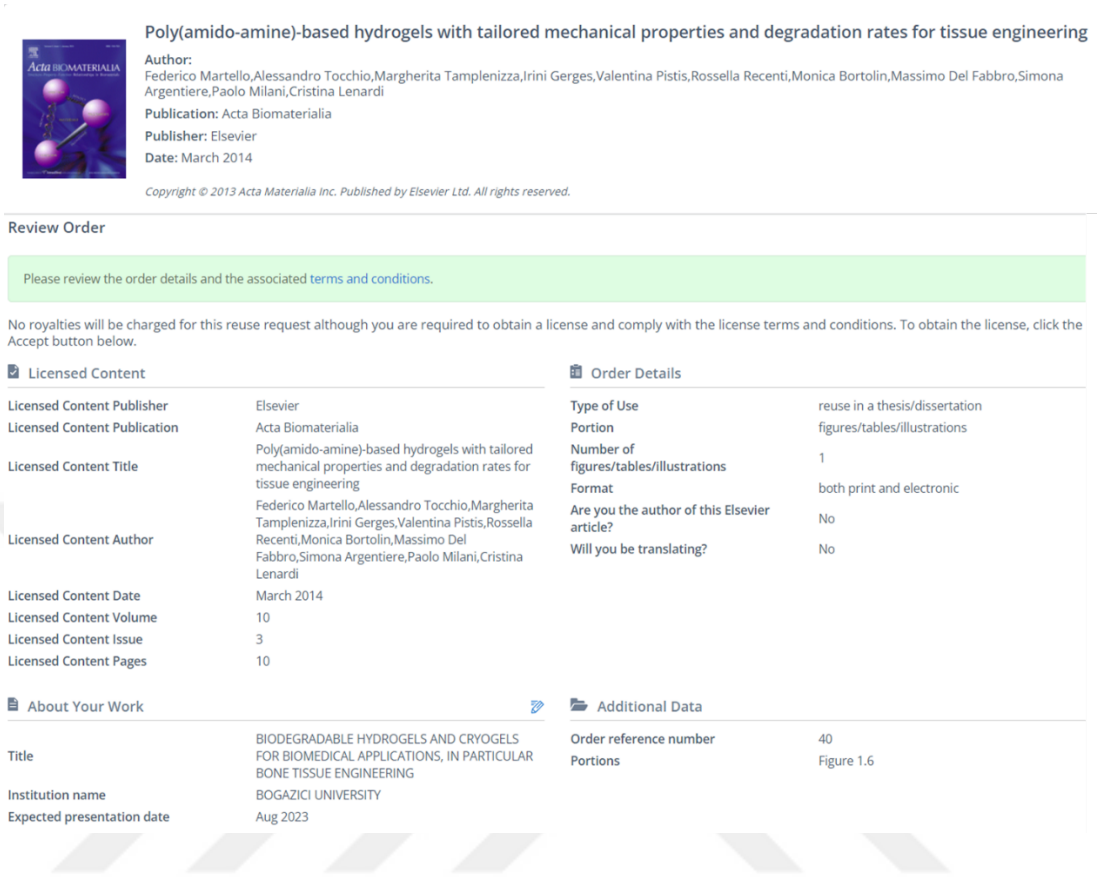

Poly(amido-amine)-based hydrogels with tailored mechanical properties and degradation rates for tissue engineering

Author:
Federico Martello,Alessandro Tocchio,Margherita Tamplenizza,Irini Gerges,Valentina Pistis,Rossella Recenti,Monica Bortolin,Massimo Del Fabbro,Simona Argentiere,Paolo Milani,Cristina Lenardi

Publication: Acta Biomaterialia

Publisher: Elsevier

Date: March 2014

Copyright © 2013 Acta Materialia Inc. Published by Elsevier Ltd. All rights reserved.

Review Order

Please review the order details and the associated terms and conditions.

No royalties will be charged for this reuse request although you are required to obtain a license and comply with the license terms and conditions. To obtain the license, click the Accept button below.

Licensed Content

Licensed Content Publisher	Elsevier
Licensed Content Publication	Acta Biomaterialia
Licensed Content Title	Poly(amido-amine)-based hydrogels with tailored mechanical properties and degradation rates for tissue engineering
Licensed Content Author	Federico Martello,Alessandro Tocchio,Margherita Tamplenizza,Irini Gerges,Valentina Pistis,Rossella Recenti,Monica Bortolin,Massimo Del Fabbro,Simona Argentiere,Paolo Milani,Cristina Lenardi
Licensed Content Date	March 2014
Licensed Content Volume	10
Licensed Content Issue	3
Licensed Content Pages	10

Order Details

Type of Use	reuse in a thesis/dissertation
Portion	figures/tables/illustrations
Number of figures/tables/illustrations	1
Format	both print and electronic
Are you the author of this Elsevier article?	No
Will you be translating?	No

About Your Work

Title	BIODEGRADABLE HYDROGELS AND CRYOGELS FOR BIOMEDICAL APPLICATIONS, IN PARTICULAR BONE TISSUE ENGINEERING
Institution name	BOGAZICI UNIVERSITY
Expected presentation date	Aug 2023

Additional Data

Order reference number	40
Portions	Figure 1.6

Figure B.3. Permission from [40] Acta Materialia by Elsevier, Copyright (2013).



Review

Biodegradable Polymers for Gene-Delivery Applications

Chih-Kuang Chen, Ping-Kuan Huang, Wing-Cheung Law, Chia-Hui Chu, Nai-Tzu Chen & Leu-Wei Lo

Pages 2131-2150 | Published online: 05 Jan 2023

Download citation

Check for updates

Taylor & Francis Group
an informa business

Our Ref: dijn/03305532

8/10/2023

Dear Requester,

Thank you for your correspondence requesting permission to reproduce content from a Taylor & Francis Group journal content in your thesis to be posted on your university's repository.

We will be pleased to grant free permission on the condition that your acknowledgement must be included showing article title, author, full Journal title, and **© copyright # [year]**, reprinted by permission of Informa UK Limited, trading as Taylor & Taylor & Francis Group, http://www.tandfonline.com

Figure B.4. Permission from [41] Taylor & Francis Group, Copyright (2023).

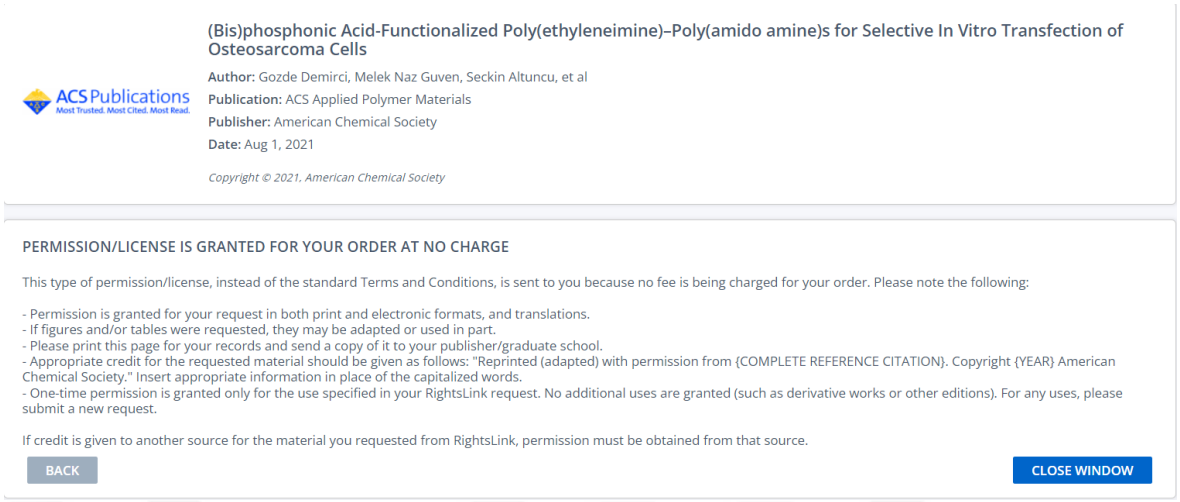

(Bis)phosphonic Acid-Functionalized Poly(ethyleneimine)–Poly(amido amine)s for Selective In Vitro Transfection of Osteosarcoma Cells

Author: Gozde Demirci, Melek Naz Guven, Seckin Altuncu, et al
Publication: ACS Applied Polymer Materials
Publisher: American Chemical Society
Date: Aug 1, 2021

Copyright © 2021, American Chemical Society

PERMISSION/LICENSE IS GRANTED FOR YOUR ORDER AT NO CHARGE

This type of permission/license, instead of the standard Terms and Conditions, is sent to you because no fee is being charged for your order. Please note the following:

- Permission is granted for your request in both print and electronic formats, and translations.
- If figures and/or tables were requested, they may be adapted or used in part.
- Please print this page for your records and send a copy of it to your publisher/graduate school.
- Appropriate credit for the requested material should be given as follows: "Reprinted (adapted) with permission from {COMPLETE REFERENCE CITATION}. Copyright {YEAR} American Chemical Society." Insert appropriate information in place of the capitalized words.
- One-time permission is granted only for the use specified in your RightsLink request. No additional uses are granted (such as derivative works or other editions). For any uses, please submit a new request.

If credit is given to another source for the material you requested from RightsLink, permission must be obtained from that source.

BACK CLOSE WINDOW

Figure B.5. Permission from [50] American Chemical Society, Copyright (2021).

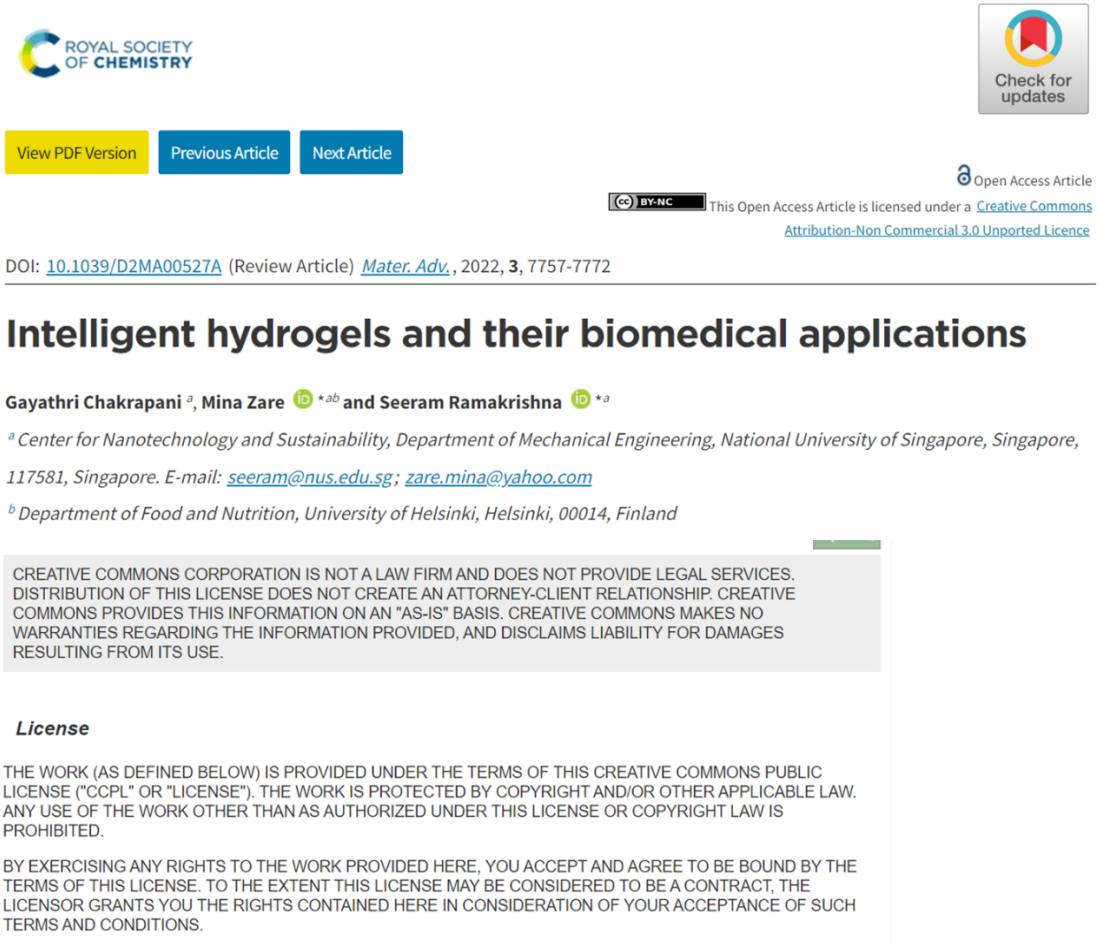

ROYAL SOCIETY OF CHEMISTRY

Check for updates

View PDF Version Previous Article Next Article

Open Access Article

This Open Access Article is licensed under a Creative Commons Attribution-Non Commercial 3.0 Unported Licence

DOI: 10.1039/D2MA00527A (Review Article) *Mater. Adv.*, 2022, **3**, 7757-7772

Intelligent hydrogels and their biomedical applications

Gayathri Chakrapani [a], **Mina Zare** [ab] **and Seeram Ramakrishna** [a]

[a] *Center for Nanotechnology and Sustainability, Department of Mechanical Engineering, National University of Singapore, Singapore, 117581, Singapore. E-mail: seeram@nus.edu.sg; zare.mina@yahoo.com*

[b] *Department of Food and Nutrition, University of Helsinki, Helsinki, 00014, Finland*

CREATIVE COMMONS CORPORATION IS NOT A LAW FIRM AND DOES NOT PROVIDE LEGAL SERVICES. DISTRIBUTION OF THIS LICENSE DOES NOT CREATE AN ATTORNEY-CLIENT RELATIONSHIP. CREATIVE COMMONS PROVIDES THIS INFORMATION ON AN "AS-IS" BASIS. CREATIVE COMMONS MAKES NO WARRANTIES REGARDING THE INFORMATION PROVIDED, AND DISCLAIMS LIABILITY FOR DAMAGES RESULTING FROM ITS USE.

License

THE WORK (AS DEFINED BELOW) IS PROVIDED UNDER THE TERMS OF THIS CREATIVE COMMONS PUBLIC LICENSE ("CCPL" OR "LICENSE"). THE WORK IS PROTECTED BY COPYRIGHT AND/OR OTHER APPLICABLE LAW. ANY USE OF THE WORK OTHER THAN AS AUTHORIZED UNDER THIS LICENSE OR COPYRIGHT LAW IS PROHIBITED.

BY EXERCISING ANY RIGHTS TO THE WORK PROVIDED HERE, YOU ACCEPT AND AGREE TO BE BOUND BY THE TERMS OF THIS LICENSE. TO THE EXTENT THIS LICENSE MAY BE CONSIDERED TO BE A CONTRACT, THE LICENSOR GRANTS YOU THE RIGHTS CONTAINED HERE IN CONSIDERATION OF YOUR ACCEPTANCE OF SUCH TERMS AND CONDITIONS.

Figure B.6. Permission from [57] Royal Society of Chemistry, Copyright (2022).

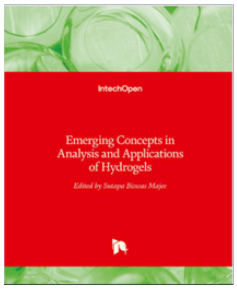

Chapter 2

An Introduction to Hydrogels and Some Recent Applications

Morteza Bahram, Naimeh Mohseni and Mehdi Moghtader

Additional information is available at the end of the chapter

http://dx.doi.org/10.5772/64301

INTECH
open science | open minds

© 2016 The Author(s). Licensee InTech. This chapter is distributed under the terms of the Creative Commons Attribution License (http://creativecommons.org/licenses/by/3.0), which permits unrestricted use, distribution, and reproduction in any medium, provided the original work is properly cited. CC BY

Figure B.7. Permission from [61] IntechOpen, Copyright (2016).



Enhancing Biopolymer Hydrogel Functionality through Interpenetrating Networks

Author: Abhishek P. Dhand,Jonathan H. Galarraga,Jason A. Burdick
Publication: Trends in Biotechnology
Publisher: Elsevier
Date: May 2021

© 2020 Elsevier Ltd. All rights reserved.

Review Order

Please review the order details and the associated terms and conditions.

No royalties will be charged for this reuse request although you are required to obtain a license and comply with the license terms and conditions. To obtain the license, click the Accept button below.

Licensed Content

Licensed Content Publisher	Elsevier
Licensed Content Publication	Trends in Biotechnology
Licensed Content Title	Enhancing Biopolymer Hydrogel Functionality through Interpenetrating Networks
Licensed Content Author	Abhishek P. Dhand,Jonathan H. Galarraga,Jason A. Burdick
Licensed Content Date	May 2021
Licensed Content Volume	39
Licensed Content Issue	5
Licensed Content Pages	20

Order Details

Type of Use	reuse in a thesis/dissertation
Portion	figures/tables/illustrations
Number of figures/tables/illustrations	1
Format	both print and electronic
Are you the author of this Elsevier article?	No
Will you be translating?	No

About Your Work

Title	BIODEGRADABLE HYDROGELS AND CRYOGELS FOR BIOMEDICAL APPLICATIONS, IN PARTICULAR BONE TISSUE ENGINEERING
Institution name	BOGAZICI UNIVERSITY
Expected presentation date	Aug 2023

Additional Data

Order reference number	1
Portions	Figure 1. 11

Figure B.8. Permission from [68] Elsevier, Copyright (2020).

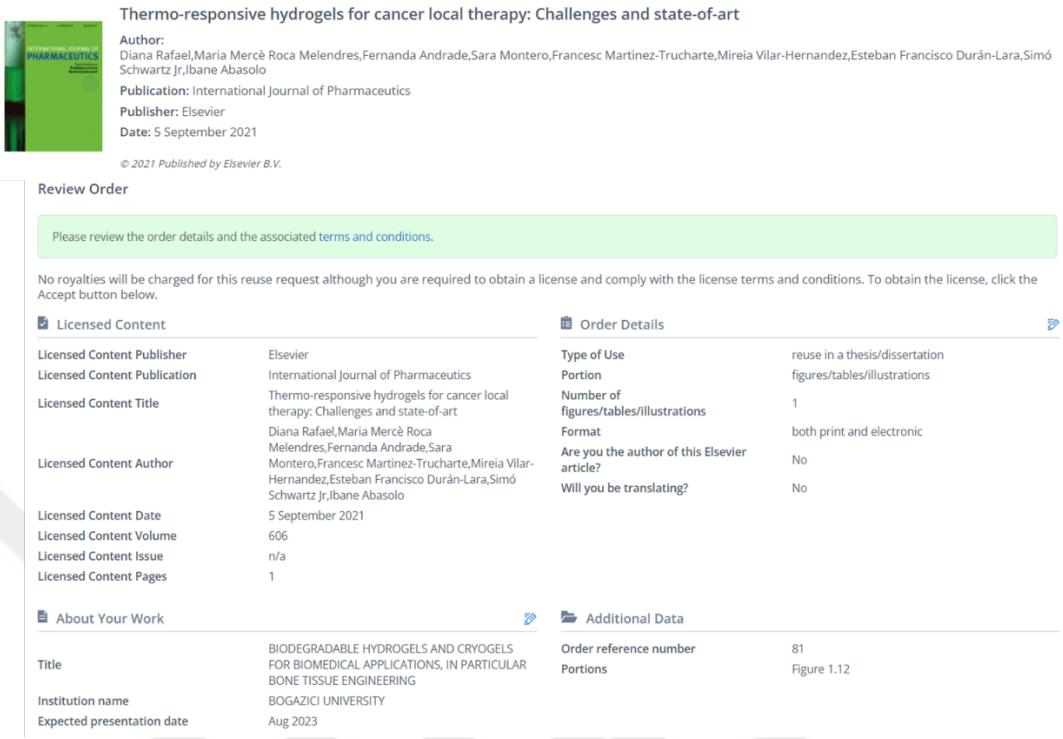

Thermo-responsive hydrogels for cancer local therapy: Challenges and state-of-art

Author:
Diana Rafael,Maria Mercè Roca Melendres,Fernanda Andrade,Sara Montero,Francesc Martinez-Trucharte,Mireia Vilar-Hernandez,Esteban Francisco Durán-Lara,Simó Schwartz Jr,Ibane Abasolo

Publication: International Journal of Pharmaceutics
Publisher: Elsevier
Date: 5 September 2021

© 2021 Published by Elsevier B.V.

Review Order

Please review the order details and the associated terms and conditions.

No royalties will be charged for this reuse request although you are required to obtain a license and comply with the license terms and conditions. To obtain the license, click the Accept button below.

Licensed Content

Licensed Content Publisher	Elsevier
Licensed Content Publication	International Journal of Pharmaceutics
Licensed Content Title	Thermo-responsive hydrogels for cancer local therapy: Challenges and state-of-art
Licensed Content Author	Diana Rafael,Maria Mercè Roca Melendres,Fernanda Andrade,Sara Montero,Francesc Martinez-Trucharte,Mireia Vilar-Hernandez,Esteban Francisco Durán-Lara,Simó Schwartz Jr,Ibane Abasolo
Licensed Content Date	5 September 2021
Licensed Content Volume	606
Licensed Content Issue	n/a
Licensed Content Pages	1

Order Details

Type of Use	reuse in a thesis/dissertation
Portion	figures/tables/illustrations
Number of figures/tables/illustrations	1
Format	both print and electronic
Are you the author of this Elsevier article?	No
Will you be translating?	No

About Your Work

Title	BIODEGRADABLE HYDROGELS AND CRYOGELS FOR BIOMEDICAL APPLICATIONS, IN PARTICULAR BONE TISSUE ENGINEERING
Institution name	BOGAZICI UNIVERSITY
Expected presentation date	Aug 2023

Additional Data

Order reference number	81
Portions	Figure 1.12

Figure B.9. Permission from [81] Elsevier, Copyright (2021).



Order Article Reprints

Open Access Review

A Review on the Design and Hydration Properties of Natural Polymer-Based Hydrogels

by Abdalla H. Karoyo and Lee D. Wilson *

Department of Chemistry, University of Saskatchewan, 110 Science Place, Saskatoon, SK S7N 5C9, Canada
* Author to whom correspondence should be addressed.

Materials **2021**, *14*(5), 1095; **https://doi.org/10.3390/ma14051095**

Received: 5 January 2021 / Revised: 7 February 2021 / Accepted: 17 February 2021 / Published: 26 February 2021

(This article belongs to the Special Issue **Research Advances in Natural Polymer-Based Hydrogels**)

Download | Browse Figures | Review Reports | Versions Notes

Open Access Review

All articles published by MDPI are made immediately available worldwide under an open access license. No special permission is required to reuse all or part of the article published by MDPI, including figures and tables. For articles published under an open access Creative Common CC BY license, any part of the article may be reused without permission provided that the original article is clearly cited. For more information, please refer to **https://www.mdpi.com/openaccess**.

Figure B.10. Permission from [86] MDPI, Copyright (2021).

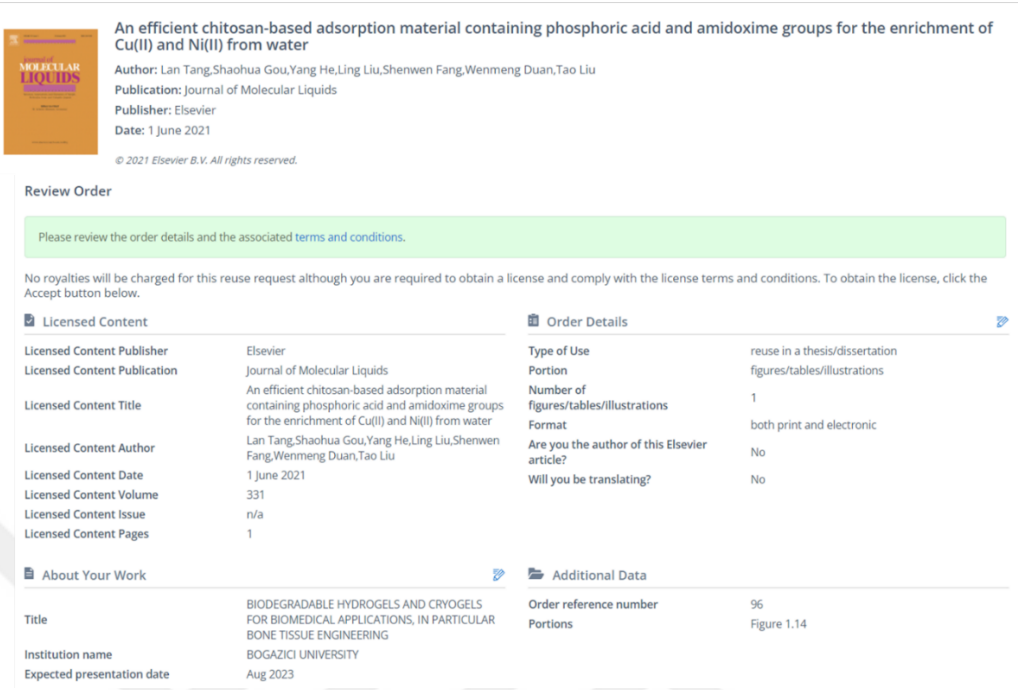

An efficient chitosan-based adsorption material containing phosphoric acid and amidoxime groups for the enrichment of Cu(II) and Ni(II) from water

Author: Lan Tang,Shaohua Gou,Yang He,Ling Liu,Shenwen Fang,Wenmeng Duan,Tao Liu
Publication: Journal of Molecular Liquids
Publisher: Elsevier
Date: 1 June 2021

© 2021 Elsevier B.V. All rights reserved.

Review Order

Please review the order details and the associated terms and conditions.

No royalties will be charged for this reuse request although you are required to obtain a license and comply with the license terms and conditions. To obtain the license, click the Accept button below.

Licensed Content

Licensed Content Publisher	Elsevier
Licensed Content Publication	Journal of Molecular Liquids
Licensed Content Title	An efficient chitosan-based adsorption material containing phosphoric acid and amidoxime groups for the enrichment of Cu(II) and Ni(II) from water
Licensed Content Author	Lan Tang,Shaohua Gou,Yang He,Ling Liu,Shenwen Fang,Wenmeng Duan,Tao Liu
Licensed Content Date	1 June 2021
Licensed Content Volume	331
Licensed Content Issue	n/a
Licensed Content Pages	1

Order Details

Type of Use	reuse in a thesis/dissertation
Portion	figures/tables/illustrations
Number of figures/tables/illustrations	1
Format	both print and electronic
Are you the author of this Elsevier article?	No
Will you be translating?	No

About Your Work

Title	BIODEGRADABLE HYDROGELS AND CRYOGELS FOR BIOMEDICAL APPLICATIONS, IN PARTICULAR BONE TISSUE ENGINEERING
Institution name	BOGAZICI UNIVERSITY
Expected presentation date	Aug 2023

Additional Data

Order reference number	96
Portions	Figure 1.14

Figure B.11. Permission from [96] Elsevier, Copyright (2021).

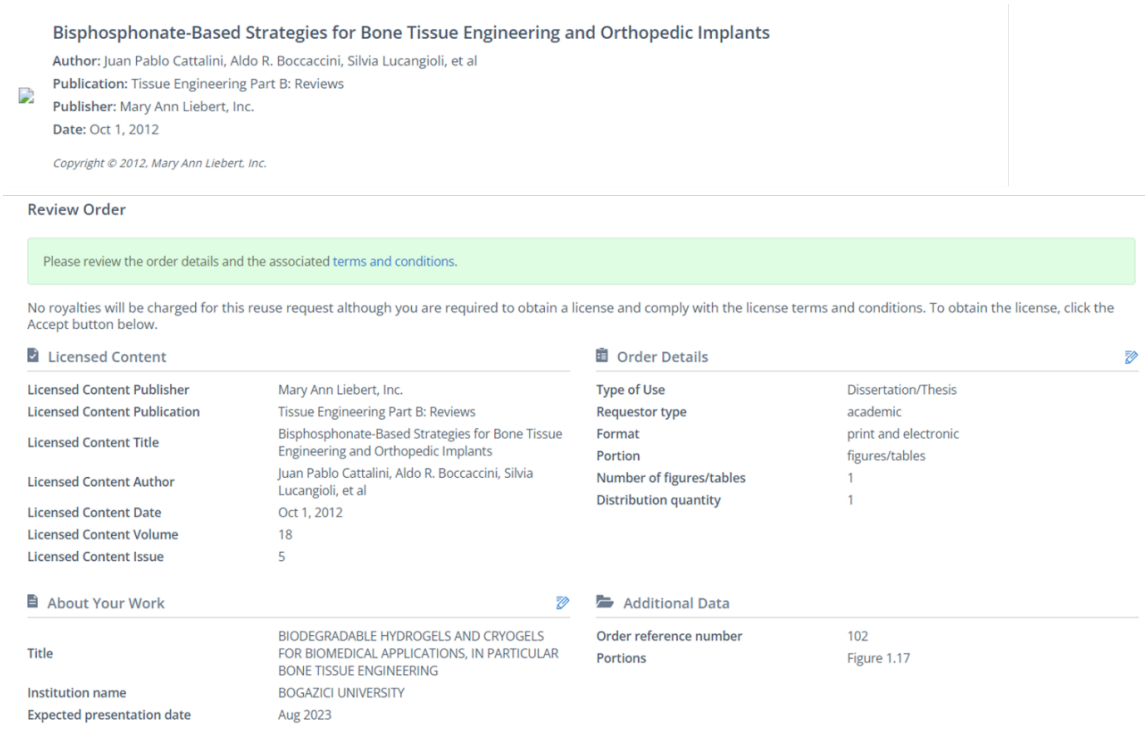

Bisphosphonate-Based Strategies for Bone Tissue Engineering and Orthopedic Implants

Author: Juan Pablo Cattalini, Aldo R. Boccaccini, Silvia Lucangioli, et al
Publication: Tissue Engineering Part B: Reviews
Publisher: Mary Ann Liebert, Inc.
Date: Oct 1, 2012

Copyright © 2012, Mary Ann Liebert, Inc.

Review Order

Please review the order details and the associated terms and conditions.

No royalties will be charged for this reuse request although you are required to obtain a license and comply with the license terms and conditions. To obtain the license, click the Accept button below.

Licensed Content

Licensed Content Publisher	Mary Ann Liebert, Inc.
Licensed Content Publication	Tissue Engineering Part B: Reviews
Licensed Content Title	Bisphosphonate-Based Strategies for Bone Tissue Engineering and Orthopedic Implants
Licensed Content Author	Juan Pablo Cattalini, Aldo R. Boccaccini, Silvia Lucangioli, et al
Licensed Content Date	Oct 1, 2012
Licensed Content Volume	18
Licensed Content Issue	5

Order Details

Type of Use	Dissertation/Thesis
Requestor type	academic
Format	print and electronic
Portion	figures/tables
Number of figures/tables	1
Distribution quantity	1

About Your Work

Title	BIODEGRADABLE HYDROGELS AND CRYOGELS FOR BIOMEDICAL APPLICATIONS, IN PARTICULAR BONE TISSUE ENGINEERING
Institution name	BOGAZICI UNIVERSITY
Expected presentation date	Aug 2023

Additional Data

Order reference number	102
Portions	Figure 1.17

Figure B.12. Permission from [102] Mary Ann Liebert, Copyright (2012).

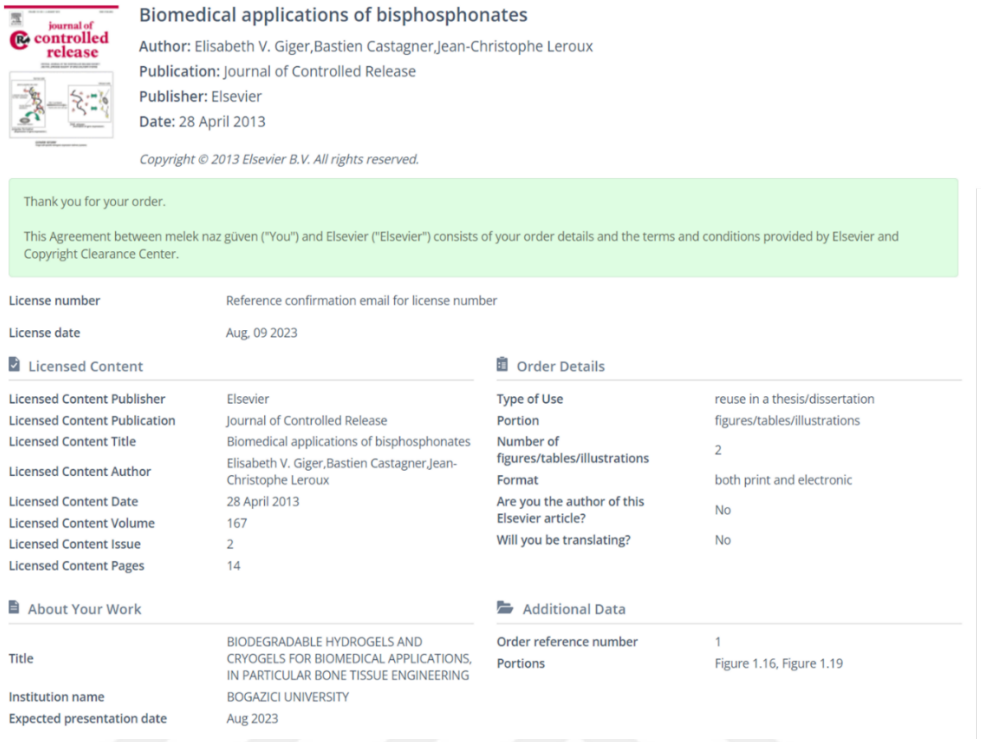

Biomedical applications of bisphosphonates

Author: Elisabeth V. Giger,Bastien Castagner,Jean-Christophe Leroux
Publication: Journal of Controlled Release
Publisher: Elsevier
Date: 28 April 2013

Copyright © 2013 Elsevier B.V. All rights reserved.

Thank you for your order.

This Agreement between melek naz güven ("You") and Elsevier ("Elsevier") consists of your order details and the terms and conditions provided by Elsevier and Copyright Clearance Center.

License number	Reference confirmation email for license number
License date	Aug. 09 2023

Licensed Content

Licensed Content Publisher	Elsevier
Licensed Content Publication	Journal of Controlled Release
Licensed Content Title	Biomedical applications of bisphosphonates
Licensed Content Author	Elisabeth V. Giger,Bastien Castagner,Jean-Christophe Leroux
Licensed Content Date	28 April 2013
Licensed Content Volume	167
Licensed Content Issue	2
Licensed Content Pages	14

Order Details

Type of Use	reuse in a thesis/dissertation
Portion	figures/tables/illustrations
Number of figures/tables/illustrations	2
Format	both print and electronic
Are you the author of this Elsevier article?	No
Will you be translating?	No

About Your Work

Title	BIODEGRADABLE HYDROGELS AND CRYOGELS FOR BIOMEDICAL APPLICATIONS, IN PARTICULAR BONE TISSUE ENGINEERING
Institution name	BOGAZICI UNIVERSITY
Expected presentation date	Aug 2023

Additional Data

Order reference number	1
Portions	Figure 1.16, Figure 1.19

Figure B.13. Permission from [105] Elsevier, Copyright (2013).



Self-healing hybrid nanocomposites consisting of bisphosphonated hyaluronan and calcium phosphate nanoparticles

Author:
M. Reza Nejadnik,Xia Yang,Matilde Bongio,Hamdan S. Alghamdi,Jeroen J.J.P. van den Beucken,Marie C. Huysmans,John A. Jansen,Jöns Hilborn,Dmitri Ossipov,Sander C.G. Leeuwenburgh
Publication: Biomaterials
Publisher: Elsevier
Date: August 2014

Copyright © 2014 Elsevier Ltd. All rights reserved.

Review Order

Please review the order details and the associated terms and conditions.

No royalties will be charged for this reuse request although you are required to obtain a license and comply with the license terms and conditions. To obtain the license, click the Accept button below.

Licensed Content

Licensed Content Publisher	Elsevier
Licensed Content Publication	Biomaterials
Licensed Content Title	Self-healing hybrid nanocomposites consisting of bisphosphonated hyaluronan and calcium phosphate nanoparticles
Licensed Content Author	M. Reza Nejadnik,Xia Yang,Matilde Bongio,Hamdan S. Alghamdi,Jeroen J.J.P. van den Beucken,Marie C. Huysmans,John A. Jansen,Jöns Hilborn,Dmitri Ossipov,Sander C.G. Leeuwenburgh
Licensed Content Date	August 2014
Licensed Content Volume	35
Licensed Content Issue	25
Licensed Content Pages	12

Order Details

Type of Use	reuse in a thesis/dissertation
Portion	figures/tables/illustrations
Number of figures/tables/illustrations	1
Format	both print and electronic
Are you the author of this Elsevier article?	No
Will you be translating?	No

About Your Work

Title	BIODEGRADABLE HYDROGELS AND CRYOGELS FOR BIOMEDICAL APPLICATIONS, IN PARTICULAR BONE TISSUE ENGINEERING
Institution name	BOGAZICI UNIVERSITY
Expected presentation date	Aug 2023

Additional Data

Order reference number	116
Portions	Figure 1.18

Figure B.114. Permission from [116] Elsevier, Copyright (2014).